NEHRP Recommended Seismic Provisions for New Buildings and Other Structures

Volume II: Part 3 Resource Papers

FEMA P-2082-2/ September 2020

FEMA

nehrp

Veterans Administration Puget Sound Mental Health and Research Building located in Seattle, Washington and opened in 2019. The six-story buckling restrained steel braced frame was designed as a Risk Category IV structure.

Credit: © Benjamin Benschneider. Used with permission.

NEHRP (National Earthquake Hazards Reduction Program)

Recommended Seismic Provisions

for New Buildings and Other Structures (FEMA P-2082-2)

2020 Edition

Volume II: Part 3 Resource Papers

NOTICE: Any opinions, findings, conclusions, or recommendations expressed in this publication do not necessarily reflect the views of the Federal Emergency Management Agency. Additionally, neither FEMA nor any of its employees make any warranty, expressed or implied, nor assume any legal liability or responsibility for the accuracy, completeness, or usefulness of any information, product, or process included in this publication.

2020 NEHRP RECOMMENDED SEISMIC PROVISIONS FOR NEW BUILDINGS AND OTHER STRUCTURES

PART 3, RESOURCE PAPER

This part of the 2020 *NEHRP Provisions* consists of a series of Part 3 resource papers. They introduce new concepts and procedures for trial use by the design community, researchers, and standards-development and code-development organizations. They also represent Issue Team efforts on substantive proposals for topics that require further consideration by the seismic design community and additional research before being considered for Parts 1 and 2 provisions. In some cases, the resource papers provide additional information and background for the recommended changes and commentary in Parts 1 and 2. Like Parts 1 and 2 of the provisions, these resource papers have been approved for inclusion in this volume by both the 2020 Provisions Update Committee and the BSSC member organizations. These resource papers are self-contained and not written in standards language format. Feedback from these users is encouraged.

CONTENTS

RESOURCE PAPER 1 RESILIENCE-BASED DESIGN AND THE NEHRP PROVISIONS

RP1-1 SUMMARY

This paper addresses the potential relationship between future NEHRP *Provisions* and resilience-based earthquake design, especially in the context of definitions and priorities established in federal law by the 2018 NEHRP reauthorization. It extends concepts proposed in Resource Paper 1 in Part 3 of the 2015 *Provisions*. Federal policy now calls for increasing earthquake resilience at the community scale and identifies building codes and standards as tools for doing so. Resilience relies on the timely recovery of the built environment. Building codes and standards can therefore serve a resilience goal, at any scale, by providing design criteria based on functional recovery time. The current code-and-standard model is adaptable to resilience-based design, with the standard providing technical definitions and design criteria, and the code setting policy goals. The NEHRP *Provisions* can support resilience-based design by providing source material for a functional recovery standard. Specific design strategies and criteria would be required for different functional recovery times, much in the same way that the current *Provisions* set specific criteria for different seismic design categories. While many questions remain to be answered through research, the current *Provisions* suggest a set of requirements that might be used in the short term.

RP1-2 BACKGROUND AND CURRENT FEDERAL POLICY

Federal policy now calls for increasing earthquake resilience at the community scale and identifies building codes and standards as tools for doing so.

Resilience, especially at the community scale, is broad and complex. The NEHRP *Provisions*, historically, address the design of new buildings and building-like structures for earthquake loads. Because community resilience also involves existing buildings, infrastructure, and multiple hazards, as well as societal issues tangential to performance of the built environment, the *Provisions'* contribution to resilience will be limited. The purpose of this paper, given both the opportunities and the limits, is to consider what role the *Provisions* might play as stakeholders embrace concepts of community resilience.

Since the last edition of the NEHRP *Provisions*, the topic of earthquake resilience has emerged as newly compelling, if not entirely new. Since 2015, government agencies at all levels, non-governmental organizations, academia, and industry stakeholders have all published on the need for resilience, how to identify or measure it, and how it might be achieved. While there is no industry-wide consensus on the details, some basic concepts are now accepted widely enough to be referenced in federal policy (Public Law 115-307, 2018; Thune, 2018).

Of particular interest is *community resilience*, now defined in federal regulations by the 2018 NEHRP reauthorization as "the ability of a community to prepare and plan for, absorb, recover from, and more successfully adapt to adverse seismic events" (42 U.S.C. 7703). With the NEHRP reauthorization act, increasing community resilience is now a stated purpose of the program (42 U.S.C. 7702).

In addition, the act charges NIST to conduct research "to improve community resilience through building codes and standards" (42 U.S.C. 7704(b)(5)), linking the holistic concept of resilience with the specific subject of the NEHRP *Provisions*.

The link between community resilience and building codes and standards is not new. In 2016, a presidential Executive Order encouraged federal agencies to go "beyond [current] codes and standards," noting that "to achieve true resilience against earthquakes, ... new and existing buildings may need to exceed [current] codes and standards to ensure ... that the buildings can continue to perform their essential functions following future earthquakes" (Federal Register, 2016). The White House later extended the idea to privately owned and locally regulated buildings with a conference "to highlight the critical role of building

codes in furthering community resilience and the importance of incorporating resilience ... in the codes and standards development process" (The White House, 2016).

More recently, discussion of community resilience and earthquake design has begun to focus on the merits of codes and standards based on a building's *functional recovery*, as discussed in the next section.

RP1-3   KEY CONCEPTS

A functional recovery standard is necessary for resilience-based earthquake design. Resilience relies on the timely recovery of the built environment. Building codes and standards can therefore serve a resilience goal by providing design criteria based on functional recovery time. The current code-and-standard model is adaptable to resilience-based design, with the standard providing technical definitions and design criteria, and the code setting policy goals.

To understand the potential relationship between future NEHRP *Provisions* and resilience, it is useful to review key terms and concepts.

RP1-3.1   Resilience

Though now ubiquitous, the term *resilience* is still not consistently used or defined. The definition of *community resilience* given above is necessary, but it is not sufficient for purposes of building code or standard development, as it does not relate clearly to the tasks of seismic evaluation or design of buildings. That said, a review of proposed definitions of resilience from the last ten years (see the Appendix) reveals four common themes that should inform any efforts to develop a resilience-based code or standard:

- Resilience is an attribute of human organizations, not of physical buildings or structures. Earthquake resilience thus makes sense for any organization – a region, a neighborhood, a campus, a corporation, an industry, a business, or even a household – that comprises more than just its physical assets. As noted above, however, the organization of interest to NEHRP is the community, which is consistent with the role of a building code as public policy. This fundamental idea, that resilience is an attribute of organizations, conveys its holistic nature, but it also implies limits to what a building code or standard can achieve in resilience terms; this is further discussed below.
- Resilience is about the preservation and recovery of functionality, not just safety. In the context of building codes and standards, this means that resilience-based design criteria must consider not only structural and nonstructural components, but also certain building contents and even some externalities normally ignored by a code or standard, such as the functionality of infrastructure systems, the availability of repair contractors, or the performance of other facilities supporting related functions. Further, the focus on functionality suggests that resilience-based design criteria should vary with a facility's specific use and occupancy.
- Resilience incorporates an element of time. Unlike earthquake safety, which is gauged by the immediate and direct effects of structural response, and unlike design of emergency facilities already expected to be immediately functional, resilience-based design might contemplate the return of any lost functionality over hours, days, weeks, or even months. In resilience-based design, the emphasis is on the timely return to normal conditions, not just the performance during the emergency phase (which current codes already consider).
- Resilience implies an event from which the organization must recover. For earthquake resilience, the event is obvious. Outside the NEHRP context, the event might be another natural hazard, a natural event exacerbated by human activity (such as climate change), a socio-economic event related to natural causes (such as a power outage), or an entirely human-caused event (such as terrorism).

Given these four themes, *community resilience*, even as defined above, can be related to the timely post-earthquake recovery of certain community functions that rely on the built environment, such as

housing, healthcare, commerce, culture, or government services. This understanding has been developed by NIST in its *Community Resilience Planning Guide for Buildings and Infrastructure Systems*, or CRPG (NIST, 2016).

As noted, however, the concept of resilience is applied to smaller organizations as well. The resilience of a business, for example, relies on the timely recovery of its essential parts, which might include a workforce, supply chain, customer base, facilities, and community services. To the extent that a business relies on its physical facilities, its resilience is linked to the functional recovery of buildings – even if only a single structure.

RP1-3.2   Functional Recovery

Though resilience is not an attribute of physical buildings, it is related to building performance as measured by the time it takes to recover basic functionality. This, too, is now reflected in the 2018 NEHRP reauthorization, which charges NIST and FEMA to convene a committee of experts to "assess and recommend options for improving the built environment and critical infrastructure to reflect performance goals stated in terms of post-earthquake reoccupancy and functional recovery time" (42 U.S.C. 7705b). The charge is to be completed with a report to Congress by June 30, 2020.

Functional recovery is not yet formally defined, though the term has been used informally in the context of earthquake design (especially regarding infrastructure) since at least 1980. Unlike resilience, functional recovery is widely understood to refer to the performance and capacity of a distinct piece of the built environment, such as an individual building or infrastructure network.

Tentative definitions have been proposed to align with established concepts in earthquake engineering.[1] On its face, functional recovery is related to the third major category of potential earthquake losses – downtime – as used in FEMA P-58 and its source documents (ATC, 2018a, Section 1.5). Functional recovery is also related to the ASCE 41 performance levels Immediate Occupancy, which involves a structure safe enough to occupy with essentially no interruption, and Operational, which adds the uninterrupted performance of critical nonstructural systems (ASCE, 2017b). Functional recovery is similar to Operational performance, but as discussed below, with the allowance of a time delay and possibly with a relaxed set of necessary functions.

SEAONC BRC (2015) described functional recovery to mean "the owners' and tenants' ability to resume normal pre-earthquake operations, which can vary with occupancy," positioning it as the second of three post-earthquake milestones. Functional recovery comes after "reoccupancy, at which time the building may be safely occupied," if not usable, and before "full recovery, at which time even cosmetic damage is repaired and even non-essential functions are restored."

NIST (2018) also recognized multiple recovery milestones or functionality levels and, consistent with the CRPG, tied functional recovery to a desired or acceptable time: "[When] developing criteria ..., multiple functional levels that may differ in terms of the acceptable recovery time should be considered, depending on the building's role in the community, the services it provides, and the hazard level."

As for functional recovery itself, NIST (2018) describes it as the state in which "damage to the building's structural system is controlled, limited, and repairable while the building remains safe to occupy. The building's ability to function at full or minimally reduced capacity is also affected by the damage state of the non-structural systems of the building (e.g., building envelope, equipment, interior utilities), as well as the infrastructure that connects the building to its surrounding community."[2]

---

[1] Precedents outside of earthquake engineering also exist but are not as specific as those cited in the text. For example, NFPA (2018) includes a generic "Mission Continuity" objective involving "continued function" for "buildings that provide a public welfare role for the community," and ASCE (2019) contemplates an "Operational" performance level, paired with relatively frequent wind loads, for design of new buildings.
[2] NIST (2018) uses the term immediate occupancy, or IO, instead of functionality because of legislative language,

Perhaps the most formal definition has been provided by a bill introduced to the California Legislature. Anticipating the 2020 NIST-FEMA report, the bill defined a functional recovery standard as:

> [A] set of enforceable building code provisions and regulations that provide specific design and construction requirements intended to result in a building for which post-earthquake structural and nonstructural capacity are maintained or can be restored to support the basic intended functions of the building's pre-earthquake use within an acceptable time, where the maximum acceptable time may differ for various uses or occupancies (Assembly Bill 393, 2019).

The definition, while it describes a design standard as opposed to a building condition, covers all of the key ideas discussed above: consideration of structural and nonstructural performance, a focus on functionality, and acceptability measured by recovery time, allowing different times for different building uses. Importantly, designing for functional recovery does not imply that the building must recover immediately.

The AB 393 definition does two things. First, it describes a post-earthquake condition that might now be taken as the definition of functional recovery:

> Functional recovery is a post-earthquake state in which capacity is maintained or restored to support the basic intended functions of the pre-earthquake use.

For a building, "capacity" means that of the structural and nonstructural systems, as in the AB 393 definition. But, as NIST (2018) notes, it should also mean the capacity of contents, infrastructure, and even certain services external to the building, as needed "to support the basic intended functions."

Second, the AB 393 definition contemplates that "maximum acceptable" recovery times will be assigned to different buildings. With these two ideas, the AB 393 definition is combining the familiar roles of design standards (which establish objective technical criteria) and building codes (which set policy regarding minimum requirements).

RP1-3.3 The role of codes and standards

If resilience is an attribute of the whole community, and if community resilience is only partly a function of building design, how would the NEHRP *Provisions* contribute? After all, the *Provisions* are explicitly about the design of individual buildings.

Figure 1 describes the broad scope of the resilience movement and illustrates how apparently disparate ideas, documents, programs, etc. can all play a role. The "resilience field" is a two-dimensional space in which any resilience-related concept can be located in terms of whether it addresses more technical topics (like structural engineering) or more holistic ideas (like a company's mission statement or the well-being of a family) and in terms of whether it is meant to apply to an individual physical facility (like a typical architectural commission) or to the whole organization in question.

Consider the definition of community resilience from the 2018 NEHRP reauthorization: "the ability of a community to prepare and plan for, absorb, recover from, and more successfully adapt to adverse seismic events." The concept is explicitly about the whole organization – the community – and the broad tasks of planning, preparing, recovering, and adapting go well beyond the technical design of its physical assets. Thus the NEHRP concept of community resilience is located in the lower right quadrant of Figure 1.

By contrast, the *Provisions*, together with the codes and standards based on them, would be located in the upper left quadrant of Figure 1. They are technical, packed with specialized terminology about physical

---

explaining, "The term IO is used for general reference to a potential range of functional levels for consistency with the congressional language."

components, and they are written with the understanding that they will be applied one building, structure, or project at a time.

Though technical and applied to individual facilities, a building code can still be resilience-*based*, serving holistic, organization-wide resilience goals. Indeed, a functional recovery standard (using the AB 393 definition above) is necessary, if not sufficient, for resilience-based earthquake design.[3] The challenge is to conceive, write, and implement the code so that when it is applied by technical experts to individual facilities, it reflects the larger holistic goals of the community. Over time, as resilience-based codes and policies are applied to individual new and existing buildings, the aggregate effect should improve community resilience.

This idea, that technical provisions, narrowly applied, might improve an organization's earthquake resilience, is perhaps easier to grasp when applied to a smaller organization. It is not difficult to see, for example, how a corporation might serve its shareholders by applying a careful seismic due diligence policy to the office space it builds or leases. Similarly, by setting high design criteria, a campus can better protect its research funding and serve its educational mission (Comerio, 2000). Resilience-based codes and standards, written to address functional recovery time explicitly, will help such organizations.

(Figure 1 also shows how the NIST CRPG might provide a bridge between holistic thinking about community resilience and technical design of individual buildings to support resilience goals. The CRPG breaks the built environment into building "clusters" based on their use and occupancy, not their structural systems or materials, and it contemplates recovery goals for whole groups, not for individual facilities.)

---

[3] To be sure, a community could avoid the need for a separate functional recovery-based design standard by setting very lax recovery goals (which the current safety-based code would already satisfy), by stipulating that certain provisions of the current code are deemed to comply with various recovery goals (an approach that has been suggested as an interim strategy), or by taking an entirely different approach to resilience and recovery, for example through comprehensive insurance and planning schemes. The presumption of the NEHRP *Provisions*, however, is that earthquake *design* involves engineering with defined, repeatable procedures, and for that approach to work, a standard is needed.
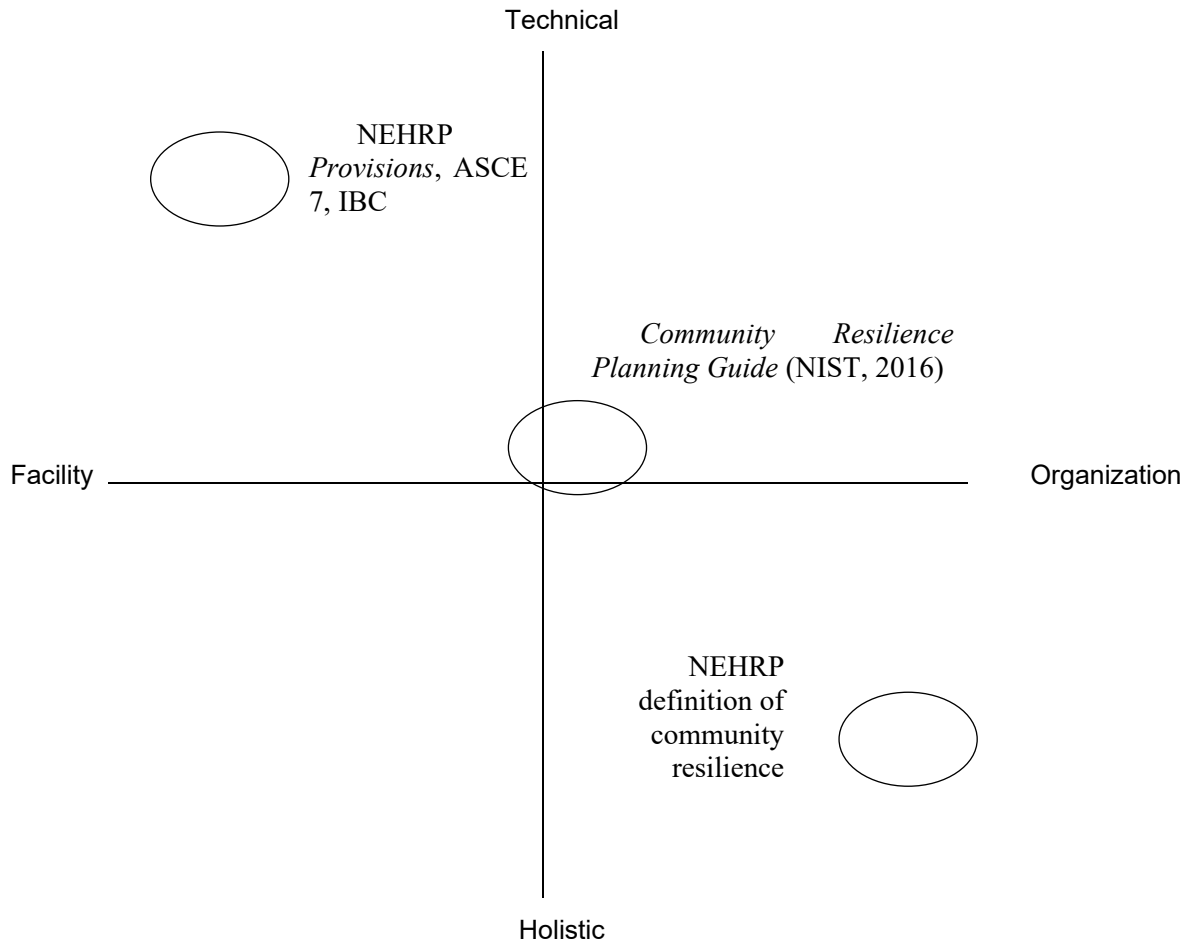
Figure 1 The Resilience Field (after Meister Consultants Group, 2017)

While a building code can be resilience-*based*, Figure 1 also confirms that there are important limits to what a code or standard can do to affect an organization's resilience. Because it is applied to individual buildings, a code has little impact on its neighborhood (or its city) or even on its own functional cohort (housing, schools, etc.) unless applied consistently over time. Even then, separate codes or mitigation programs are generally needed to address resilience risks posed by the vast existing building stock. Separate design standards and policies are also needed to address new and existing infrastructure, which the *Provisions* do not address. Most significantly, a building code cannot address most socio-economic externalities that affect community resilience.

Like the current building code, a functional recovery code would address the design of structural systems and bracing for nonstructural components. The scope would likely be expanded to consider contents bracing and adjacent buildings, two issues not far from the code's traditional scope. To begin to address socio-economic externalities, resilience-based codes and standards might be expanded further with provisions that think of the building in a more holistic way. For example, on-site backup utilities, reoccupancy plans, continuity of operations plans, retainers for repair contractors, and even insurance, while not traditional building code topics, are strategies related to building design that might be considered for a future resilience-based design standard, or at least for related building regulations (ATC, 2018d).

Ultimately, however, even if we rewrite our building codes as functional recovery standards, they would contribute to community resilience only in the way that the current safety-based codes and standards contribute to a holistic view of community safety and vitality. Our current codes limit collapse and fire –

two sources of earthquake deaths and injuries – but a building code does not consider broader questions regarding the supply of clean water, food, sanitation, or medical services.

RP1-3.4   The code-and-standard model

To implement resilience-based earthquake design, we need a policy tool and a technical tool. The building code is the policy tool, setting performance objectives by assigning buildings to risk categories based on their use and the implications of damage. With a resilience-based code, each building would be assigned to a category representing a desired functional recovery time. As discussed above, the assignments would be made by considering the aggregate effect of applying the code over time.

Policy questions are normative; they consider desired outcomes, asking what the functional recovery time of a given building *should* be. In the long term, these preferences, together with benefit-cost analysis, should be informed by social science research linking objectively measurable recovery time to more holistic measures of organizational resilience. In the short term, absent the critical research, these policy decisions are likely to be influenced primarily by stakeholder estimates regarding perceived benefits and immediate costs (NIST, 2016). In either case, the policy questions, which include a jurisdiction's decision to adopt a recovery-based code as mandatory, voluntary, or applicable only in certain cases, are outside the scope of the *Provisions*.

The design standard (along with the *Provisions* as its resource document) is the technical tool. A functional recovery standard would provide the definitions and criteria estimated to achieve a given functional recovery time, independent of any policy about what time limit *should* be selected.

The code-and-standard model, familiar to users of the *International Building Code* and its adopted standard, ASCE 7, should be adaptable to resilience-based earthquake design. With reference to the NIST-FEMA committee charge, the code-and-standard model is one "option" for "improving the built environment and critical infrastructure to reflect performance goals stated in terms of post-earthquake reoccupancy and functional recovery time."

RP1-4   A FRAMEWORK FOR NEHRP *PROVISIONS* FOR RESILIENCE-BASED DESIGN

The NEHRP *Provisions* can support resilience-based design by providing source material for a functional recovery standard. Specific design strategies and criteria would be required for different functional recovery times, much in the same way that the current *Provisions* set specific criteria for different seismic design categories. While many questions remain to be answered through research, the current *Provisions* suggest a set of requirements that might be used in the short term.

Using a code-and-standard model, the NEHRP *Provisions* would be the basis for a functional recovery standard, which would then be cited by, or incorporated into, a resilience-based code. The code would assign desired or target recovery times. As discussed above, the scope of the *Provisions* would likely need to be expanded to cover topics like contents bracing and backup utilities.

The idea of adapting the *Provisions* to address functional recovery is not entirely new. In the 2015 *Provisions*, Resource Paper 1 built on work by NIST to propose assigning an explicit "function loss" performance objective to Risk Category IV (BSSC, 2015; NEHRP CJV, 2012). Design criteria for Risk Category IV had been assumed to deliver some measure of post-earthquake functionality, but the expectation was never quantified or clearly stated (ASCE, 2017a, Sec. C1.3.3). Using the Operational terminology of ASCE 41, the proposal would have aligned the criteria for Risk Category IV to provide a 10% probability of less-than-Operational performance in a Function-Level Earthquake, analogous to the 10% probability of collapse in a Maximum Considered Earthquake expected for buildings assigned to Risk Category II.

There are two main differences between that 2015 proposal and the concept of functional recovery presented here. With the 2015 proposal, functionality would only have been considered for buildings

already assigned to Risk Category IV because of their "essential" nature, and meeting the objective would mean the building remains functional "immediately following" the earthquake shaking (ASCE, 2017a). That is, where functionality is considered important, immediate functionality (or Operational performance, in ASCE 41 terms) would be sought; otherwise, no attention would be paid to functionality. Here, every new building would be assigned a desired or target functional recovery time, and different building uses would have different assignments, from hours to days to weeks to months, consistent with concepts from the NIST CRPG.

The concept presented here would make functional recovery a supplemental (or perhaps primary) basis for earthquake design of all buildings, as opposed to a special objective only for "essential" facilities. This is not to say, however, that all buildings would need to be designed like hospitals and fire stations. On the contrary, by allowing functional recovery times as long as weeks or months, it is likely that many buildings would be designed and detailed just as they are now; the only difference would be that their estimated (or desired) recovery time would be explicitly stated, providing transparency to all stakeholders and facilitating resilience planning.

RP1-4.1   Definitions

As source material for a functional recovery standard, the *Provisions* would mostly address technical questions regarding demand, capacity, detailing, and acceptability criteria. Before that, however, they would also need to address questions inherent in the definition of functional recovery given above: What are a given building's "basic intended functions"?

The 2015 *Provisions* Resource Paper anticipated this question as well: "[A] framework is needed for determining what constitutes functionality following the earthquake. ... Significant study and likely additional provisions development is required to quantitatively define these performance states. ... [I]t is not known what various stakeholders will deem tolerable damage and still be 'functional' (sic)."

A plain reading of the definition suggests that functional recovery could be achieved with cosmetic damage still in place. Similarly, partial functional loss (for example, one restroom in a house with two), or the loss of one use in a mixed-use building (for example, the parking levels in an office building or the ground floor retail space in an apartment house) might be deemed acceptable. Beyond this, however, the possibilities quickly get into questions of habitability and even law. Are boarded windows acceptable? Or the loss of an accessible entry or an elevator in a low-rise building? Researchers have begun to study these questions (NIST, 2018; Center for Risk-Based Community Resilience Planning; Soga et al, 2019) but in the short term the gaps will surely need to be filled by consensus judgment, perhaps starting with the current building code's nonstructural bracing scope for Risk Category IV as a benchmark.

RP1-4.2   Demand

Among the issues that will need to be resolved in the course of developing a functional recovery standard is the selection of a design ground motion.

The 2015 *Provisions*, and NIST before it, defined a Function-Level Earthquake, FLE_R, analogous to the risk-targeted MCE_R (NEHRP CJV, 2012). These new spectral acceleration values would be set to ensure a uniform 10% probability of failing to achieve Operational performance. A similar approach could be taken for the functional recovery concept described here, but at least two new considerations would be needed. First, defining a risk-targeted ground motion this way presumes a known set of design criteria. But, as the 2015 *Provisions* noted, "current story drift limits of Table 12.12-1 of ASCE/SEI 7-10 do not provide adequate damage control to meet functional and/or economic loss objectives and would require substantial revision." Further, functional recovery is more closely tied to the performance of nonstructural components than safety is, but design criteria relating nonstructural performance to recovery time are far from robust. So if it is unclear what counts as functional (as discussed above), or what the acceptability criteria will be, then the FLE_R cannot yet be defined.

Second, the FLE_R corresponds to a performance level achieved immediately after the earthquake. If functional recovery is now going to be defined as a suite of target recovery times ranging from hours to months, a separate map of ground motions will be needed for each limit state, complicating the normal design procedures.

Adopting a risk-targeted demand for the functional recovery standard would help maintain at least philosophical consistency within the *Provisions*. That said, the non-uniform variation between expected FLE_R and MCE_R values is certain to cause some confusion. In the short term, and certainly until the definitional questions are addressed, it might be preferable to use the MCE_R or the Design Earthquake (or some specified fraction thereof) as the demand, if only to simplify the procedures. Though theoretically incorrect, this simplification would be entirely consistent with current practice, which uses the DE even for Risk Category IV facilities where functionality is expected to be preserved.

Complicating the issue further, if the functional recovery criteria are really meant to be linked to a community-wide resilience goal, then the use of site-specific ground motion data might itself be incorrect. For resilience planning, a scenario event is often more appropriate.

RP1-4.3   Capacity and Acceptability

In theory, the functional recovery design criteria would follow basic principles of performance-based engineering. For the current safety-based *Provisions*, the criteria for a new building assigned to Risk Category II should ensure that the probability of collapse is less than 10%, given the site-specific MCE_R ground motion: P(Collapse) < 10%, given MCE_R.

By analogy, it should be simple to state the functional recovery objective. The probability of *not* achieving functional recovery is small, say less than Y%, given the appropriate demand. With functional recovery defined in terms of a target time, T_{target}, this would be stated as:

$$P(T_{FR} > T_{target}) < Y\%, \text{ given } D_{FR},$$

where:

- D_{FR} is the ground motion deemed appropriate for functional recovery, discussed above.
- Y is tentatively set at 10%, matching the Risk Category II safety criteria, consistent with the reasoning of the 2015 *Provisions* Resource Paper.
- T_{target} is the target recovery time for the building's use and occupancy, assigned as a policy matter by a resilience-based code.
- T_{FR} is the estimated functional recovery time, given the building's design and forthcoming consensus regarding requirements for functional recovery.

Each of those four values deserves its own research program. The first three, however, can be set by default or by consensus judgment. The last, T_{FR}, can be estimated with the FEMA P-58 methodology. FEMA P-58, however, predicts repair time, which is not the same as functional recovery time (ATC, 2018a, Section 3.9.2; ATC, 2018c, Section 3.2.2.3). The commentary to ASCE 7 acknowledges that "the fragilities of structural systems to ensure function are not well established" (ASCE, 2017, Section C1.3.3). Most important, the few studies that have been done show wide variation in repair or recovery times of code-designed buildings as functions of the lateral system, Site Class, and other factors (ATC, 2018b; ATC 2018d, Part 3; Haselton et al., 2018). So until a consensus standard is available, FEMA P-58 might be supplemented with user-defined inputs and appropriate adjustments of its repair time results.

Absent a consensus method of calculating T_{FR} for a specific new building design, another approach suitable to a first generation functional recovery standard might be to presume a value of T_{FR} by reference to a consensus checklist of design features or strategies associated with different recovery times. This appears feasible (and perhaps no less reliable at this stage than a calculation) because the range of estimated functional recovery times for a new code-designed building is already bounded in part by the nature of the

current code. That is, the current building code (and the *Provisions* and ASCE 7) contains a set of design strategies and requirements already associated with different risk categories and seismic design categories. Criteria for a recovery-based design would likely use some or all of these available strategies, and in the worst case, a building with no special recovery goal would still be subject to the current safety-based code.

Regardless of how T_{FR} is determined, its value will certainly involve substantial uncertainty. Given our current state of knowledge, factors including variability in ground motion, quality of design, quality of construction, and post-construction use, alteration, and maintenance can be expected to add even more uncertainty regarding recovery time than they do regarding safety. In addition, actual recovery time will be influenced by the availability of skilled inspectors, repair contractors, and suppliers, regulatory decisions accounting for conditions outside the building itself, the decisions of affected stakeholders, and other externalities.

Table 1 shows – in a hypothetical or conceptual way only – how current earthquake design requirements could be adapted into a functional recovery standard by assigning them to target functional recovery times. If one assumes that a building designed with the current code would reliably achieve functional recovery within a month (given the recovery-based demand, discussed above), then few additional requirements would be imposed for a building assigned a target functional recovery time of "1 Month" or longer. Where a shorter recovery time is desired or assigned, additional design strategies or tighter acceptability criteria would be "Required."

The list of potential requirements could come from the current *Provisions*, specifically from the set of design strategies and provisions already used for Risk Category IV. Supplemental requirements, shown in concept at the bottom of Table 1, could introduce non-traditional strategies to address building contents, backup utilities, and even reoccupancy or recovery planning. Building contents would be expected to affect recovery of buildings or tenant spaces containing manufacturing, retail, broadcasting, out-patient medical services and other uses involving specialty equipment. Reoccupancy and recovery planning is expected to cut the functional recovery time significantly in large or complex buildings (ATC, 2018d, Part 3). However, as shown at the bottom of the Figure, even these strategies might be ineffective, and therefore "Moot," where a very short target recovery time is assigned.

The designer would need to satisfy only the requirements indicated for the target functional recovery time set by the resilience-based code, T_{target}. Requirements would continue to vary by structural system and material if, for example, higher drifts are deemed repairable within a given time for some systems but not for others. All of the table entries would be subject to adjustment as new research and reconnaissance data becomes available, but the broad categories of target times – 1 Day v. 1 Week, as opposed to 24 hours v. 48 hours, for example – will help keep the provisions stable and are appropriate to our current level of knowledge.

Of course, the challenge lies in deriving consensus regarding the set of requirements to be associated with each value of T_{target}, without defaulting to the most conservative recommendations in every case.

Table 1 Hypothetical prescriptive design requirements for a range of functional recovery times

Functional Recovery Design Requirement	Target Functional Recovery Time, T_{target}			
	1 Hour	1 Day	1 Week	1 Month
Structural				
Limits on lateral system selection	Required	Required	Required	–
Limits on drift	Required	Required	Required	–
Factor on required strength	Required	Required	–	–
etc.	...	...	...	...
Nonstructural				
Increased bracing scope	Required	Required	Required	–
Reliability factors on design strength	Required	Required	–	–
Ruggedness certification	Required	Required	–	–
etc.	...	...	...	...
Recovery-critical contents				
To be determined by user groups	Required	Required	...	...
etc.	...	...	...	...
Utility service				
Electricity backup	Required	Required	Required	–
Potable water backup	Required	Required	Required	Required
Wastewater alternative	Required	–	–	–
Telecommunications	Required	–	–	–
etc.	...	...	...	...
Reoccupancy and recovery planning				
Repair services on retainer	Moot	Required	Required	–
Pre-determined safety evaluation	Moot	Required	–	–
Business continuity plan	Required	Required	–	–
Pre-defined permit application	Moot	Required	Required	–
etc.	...	...	...	...

RP1-5   REFERENCES

ASCE, 2017a. *Minimum Design Loads and Associated Criteria for Buildings and Other Structures* [ASCE/SEI 7-16]. American Society of Civil Engineers.

ASCE, 2017b. *Seismic Evaluation and Retrofit of Existing Buildings* [ASCE/SEI 41-17]. American Society of Civil Engineers

ASCE, 2019. *Prestandard for Performance-Based Wind Design.* American Society of Civil Engineers.

Assembly Bill 393, 2019. "An act to add Section 18941.11 to the Health and Safety Code, relating to building standards." California Legislature – 2019-20 Regular Session. Introduced by Assembly Member Nazarian, February 6; Amended in Assembly, March 21.

ATC, 2018a. *Seismic Performance Assessment of Buildings, Volume 1 – Methodology* [FEMA P-58-1]. Federal Emergency Management Agency, December.

ATC, 2018b. *Seismic Performance Assessment of Buildings, Volume 5 – Expected Seismic Performance of Code-Conforming Buildings* [FEMA P-58-5]. Federal Emergency Management Agency, December.

ATC, 2018c. *Guidelines for Performance-Based Seismic Design of Buildings* [FEMA P-58-6]. Federal Emergency Management Agency, December.

ATC, 2018d. *San Francisco Tall Buildings Study*. City and County of San Francisco, Office of Resilience and Capital Planning, December.

Bonowitz, 2018. "Performance-Based Design for Community Resilience: Obstacles and Opportunities." Presentation to the PEER 2018 Annual Meeting, Berkeley, January 18.

Bonowitz, 2018. "Designing for Resilience: The Role of the Structural Engineer." ICC-SKGA, May 1.

BSSC, 2015. "Resource Paper 1: New Performance Basis for the Provisions," in *NEHRP Recommended Seismic Provisions for New Buildings and Other Structures, Volume II: Part 3 Resource Papers* [FEMA P-1050-2]. Building Seismic Safety Council, Washington.

Center for Risk-Based Community Resilience Planning. http://resilience.colostate.edu/index.shtml

Comerio, M., 2000. "The Economic Benefits of a Disaster Resistant University: Earthquake Loss Estimation for UC Berkeley." Institute of Urban & Regional Development.

Federal Register, 2016. "Executive Order 13717 of February 2, 2016: Establishing a Federal Earthquake Risk Management Standard." V.84, n.24, February 5.

Haselton, C., Hamburger, R., and Baker, J., 2018. "Resilient Design and Risk Assessment using FEMA P-58 Analysis," in *Structure Magazine*, March.

Meister Consultants Group, 2017. *Voluntary Resilience Standards: An Assessment of the Emerging Market for Resilience in the Built Environment*. Energy, Kresge and Barr Foundations, May.

MitFLG, 2019. *National Mitigation Investment Strategy*. Prepared by the Mitigation Framework Leadership Group and published by the Department of Homeland Security, August.

NEHRP CJV, 2012. *Tentative Framework for Development of Advanced Seismic Design Criteria for New Buildings* [NIST GCR 12-917-20]. National Institute of Standards and Technology, November.

NFPA, 2000. *NFPA 5000: Building Construction and Safety Code*. National Fire Protection Association.

NIST, 2016. *Community Resilience Planning Guide for Buildings and Infrastructure Systems* [NIST Special Publication 1190]. U.S. Department of Commerce, National Institute of Standards and Technology, May.

NIST, 2017. *Implementation Guidelines for Executive Order 13717: Establishing a Federal Earthquake Risk Management Standard* [ICSSC Recommended Practice (RP) 9]. U.S. Department of Commerce, National Institute of Standards and Technology, January.

NIST, 2018. *Research Needs to Support Immediate Occupancy Building Performance Objective Following Natural Hazards Events* [NIST Special Publication 1224]. U.S. Department of Commerce, National Institute of Standards and Technology, August.

Public Law 115-307, 2018. "National Earthquake Hazards Reduction Program Reauthorization Act of 2018" [132 Stat. 4408]. December 11.

SEAONC BRC, 2015. *Earthquake Performance Rating System: User's Guide*. Structural Engineers Association of Northern California, Building Ratings Committee, February 2.

Soga, K., et al., 2019. "City-scale Multi-infrastructure Network Resilience Simulation Tool." https://peer.berkeley.edu/sites/default/files/peer-multi-infrastructure-simulation-tool-soga-20190408.pdf

Thune, J., 2018. "National Earthquake Hazards Reduction Program Reauthorization Act of 2017: Report of the Committee on Commerce, Science, and Transportation on S.1768 [Report 115-336]." U.S. Government Publishing Office, September 6.

White House, The, 2013. "Presidential Policy Directive – Critical Infrastructure Security and Resilience [PPD-21]." The White House, Office of the Press Secretary, February 12.

White House, The, 2016. "Fact Sheet: Obama Administration Announces Public and Private Sector Efforts to Increase Community Resilience through Building Codes and Standards." The White House, Office of the Press Secretary, May 10.

RP1-6   APPENDIX: DEFINITIONS OF RESILIENCE

There is no standard (i.e. formal, consensus) definition of resilience. Recent federal law charges FEMA with defining the term "resilient" by April 2020 for purposes of implementing disaster assistance programs (42 U.S.C. 5172(e)). Meanwhile, the following working definitions from other groups are useful because they have common themes, as shown by the underlining:

- UNISDR (2009): The ability of a system, community or society exposed to hazards to resist, absorb, accommodate to and recover from the effects of a hazard in a timely and efficient manner, including through the preservation and restoration of its essential basic structures and functions.
- FEMA NDRF (2011): Ability to adapt to changing conditions and withstand and rapidly recover from disruption due to emergencies.
- NRC (2011): A disaster-resilient nation is one in which its communities, through mitigation and pre-disaster preparation, develop the adaptive capacity to maintain important community functions and recover quickly when major disasters occur.
- National Academies (2012): The ability to prepare and plan for, absorb, recover from, or more successfully adapt to actual or potential adverse events.
- Presidential Policy Directive 21 (The White House, 2013; cited similarly in NIST, 2016, Section 1.3, and MitFLG, 2019, Appendix B): The ability to prepare for and adapt to changing conditions and to withstand and recover rapidly from disruptions. Resilience includes the ability to withstand and recover from deliberate attacks, accidents, or naturally occurring threats or incidents.
- US GAO (2014): The term resilience refers to the ability to prepare and plan for, absorb, recover from, and more successfully adapt to actual or potential adverse events.
- 100 Resilient Cities: Urban resilience is the capacity of individuals, communities, institutions, businesses, and systems within a city to survive, adapt, and grow no matter what kinds of chronic stresses and acute shocks they experience.
- AIA NRI (2016): Resilience is achieved when systems remain adaptable and functioning when faced with major disruptions.

The new definition of *community resilience* provided in the 2018 NEHRP reauthorization is nearly identical to the National Academies and GAO definitions.

Comparing these definitions reveals four common themes:

- Resilience is an attribute of human organizations, not of physical buildings or structures. Key words from the foregoing definitions include *institutions, businesses, communities, city, nation, society*. One might add *household, campus, corporation,* etc. The organization of interest depends on one's perspective. For the practicing engineer, the organization of interest might be that of the client. From the perspective of the building code, which represents public policy, the key organization is probably the entire jurisdiction, perhaps even the region if the building code is linked to policy like a local hazard mitigation plan (LHMP).
- Resilience is primarily about recovery of functionality, not safety. Key words include *basic functions, important functions, institutions, businesses, systems*. From the terminology of our current codes and standards, one might add *use, occupancy, habitability, operational, essential facility.*
- With its emphasis on recovery, resilience incorporates an element of time. Key words include *timely and efficient, quickly, rapidly.* One might add *immediate*.
- Resilience implies an event from which the organization must recover. Key words include *hazard, emergency, disaster, adverse event, attacks, accidents, incidents, acute shocks, major disruptions*. One might add current code categories of design load such as *earthquake, wind, snow, rain, flood.* The focus is mostly, but not exclusively, on natural hazards characterized by discrete events. An earthquake is a perfect example. More generally, however, the broader

precedents consider a wider range of shocks, and even what the 100 Resilient Cities program calls stressors. Shocks or events considered by some resilience initiatives have included:

- o Natural hazard events not considered in the building code: Wildfire, drought, heat, tsunami.
- o Natural hazard events exacerbated by humans: Climate change, species extinction, urban heat, wildland-urban interface fire, urban flooding.
- o Socio-economic events related to natural causes: Famine, power outage, dam failure, pandemic.
- o Human-made events: Terrorism, war.
- o Human-made stressors, as opposed to shocks: Poverty, sprawl, blight, economic depression.

The themes suggest some definitions that might be useful from the perspective of building codes and standards. Each definition proposed here is certain to require elaboration as needed to cover specific situations. Traditionally, that specificity is provided through a standards process.

- **Resilience** is the ability of an organization to recover its essential functionality in a timely fashion after a potentially damaging natural hazard event.
- A **resilience objective** is, for an organization, a combination of a desired or acceptable recovery time with a presumed hazard level.
  - o The pairing of a resilience level with a hazard is borrowed from performance-based earthquake design.
- **Resilience-based design** is any design process or method intended to satisfy a specified resilience objective.
  - o The emphasis is on having the elements of a defined objective, not on the methodology or even the discipline (architecture, engineering, financial planning, etc.).
  - o Thus, a resilience-based code or standard is simply one that explicitly references the elements of a resilience objective. Consistent with the idea that resilience-based design is multi-disciplinary, a resilience-based design methodology can be one that deals with any aspect of the organization in question.
- **Resilience-based structural engineering** is the intersection of structural engineering with resilience-based design.
  - o Similarly, resilience-based earthquake design is the intersection of earthquake design (or structural engineering considering earthquake loading) with resilience-based design.

With resilience and related terms defined, other concepts used in building evaluation, design, and regulation can be distinguished from resilience-related work. Importantly, not every good idea needs to be about resilience, and resilience need not encompass every good idea. In particular, the following practices and priorities are all valuable, though their relationship to resilience-based design is often at most tangential:

- Performance-based design, especially of individual projects or structures
- Building code adoption and enforcement
- Reduced property losses and repair costs (including "PML" analysis)
- Retrofit, especially safety-based retrofit
- Building rating
- New or advanced materials, systems, or analysis techniques
- Sustainability
- Economic recovery
- Baseline community functionality.

RESOURCE PAPER 2 RISK-BASED ALTERNATIVES TO DETERMINISTIC GROUND MOTION CAPS

RP2-1   INTRODUCTION

Structures designed according to modern building codes are targeted to have a low probability of collapse when strong earthquakes occur. If seismic design provisions are targeted to a goal of zero probability of collapse, construction costs could be so high as to discourage development. If design forces are too low, strong earthquakes would cause large number of collapses with appurtenant loss of life and resources, which is also clearly unacceptable. A critical function of committees that draft procedures used in seismic design codes is finding a middle ground between these conflicting considerations. There are no clear ground rules for this.

The expected level of seismic performance for most (Risk Level I and II) buildings designed according to the ASCE 7-16 standard is that if the maximum considered ground motion were to occur, the probability of collapse should not exceed 10%. This expectation has its origins in the ATC-63 project (FEMA 2009), which was conducted to derive procedures to establish design coefficients for structural systems. This project included extensive reliability analyses of then code-conforming structural systems and determined that for the ground motion levels then defined (2% in 50-year probability of exceedance), only the best performing structural systems then permitted by code could be shown to provide this level of reliability. A higher reliability might have been selected if it could have been demonstrated for common structural types without extensive revision of contemporary design procedures and requirements.

This performance expectation directly informs the process by which design ground motions are computed, which follows a risk-based framework (Luco et al. 2007). The concept behind this framework is illustrated in Figure 1. Part (a) shows a ground motion hazard curve, which expresses the time rates with which ground motions of different amplitudes (i.e., variable intensity measures - *IMs*) are exceeded, ν_{IM}. Part (b) of the Figure depicts a collapse fragility curve for the structure, which represents the dependence of collapse probability on ground motion amplitude *IM*. A *risk integral* is used to combine the hazard and fragility curves to compute the time rate of structural collapse.

Since the 2010 version of the ASCE 7 standard, the primary objective of seismic design for buildings has been based on a uniform risk target of 1% probability of collapse in 50 years. The horizontal position of the fragility curve is adjusted in an iterative manner until the target risk level is achieved. As shown in Figure 1(b), the ground motion for design, which in turn controls the strength of the structure, is then established from the value of *IM* at a 10% collapse probability, per the aforementioned performance expectation. The ground motion established using this process is referred to as a probabilistic risk-targeted maximum considered earthquake ground motion (MCE_R). The actual design ground motion is reduced from MCE_R using a two-thirds factor that was introduced in Project 97 for reasons described subsequently (Leyendecker et al. 2000; BSSC 1997).
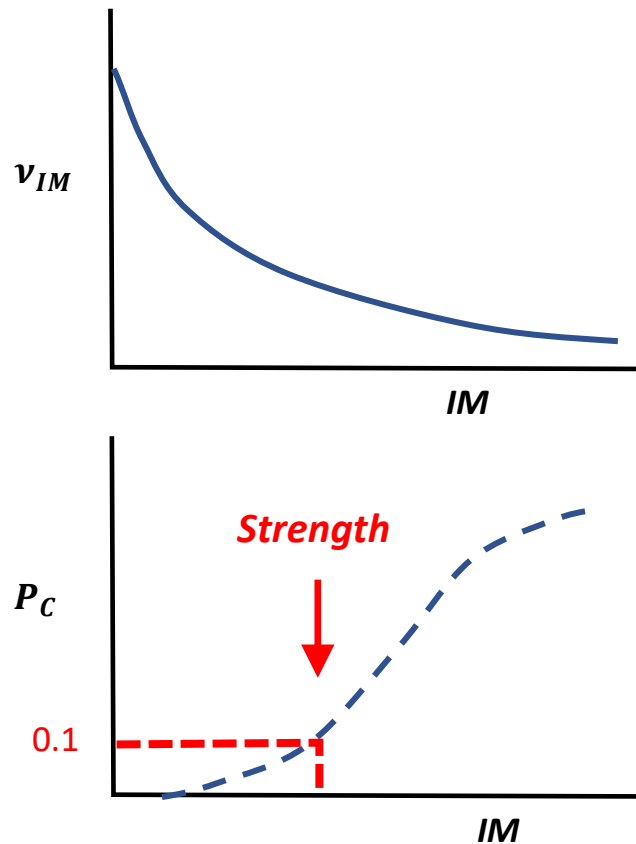
Figure 1 (a) Schematic ground motion hazard curve; (b) schematic structure fragility curve showing how structural strength is established at the 10% collapse probability

The target risk level of 1% probability of collapse in 50 years was established by the Project 07 team, as approximately representing the risk level that could be demonstrated for code-conforming structures designed to the requirements of the 2003 NEHRP Provisions. This target was recently revisited in Project 17 (BSSC 2018) and reconfirmed as appropriate, given considerations of cost, safety, and our ability to adequately characterize collapse safety.

The costs associated with increases in seismic demands were an important consideration in Project 17 and other review bodies. The costs associated with providing additional resistance for seismic loads has been investigated for the Memphis area (ATC 2013). An approximate 50% increase in seismic resistance was shown to increase the total construction cost by about 1%. However, four of the six buildings studied had inherently strong lateral force systems as a result of their architecture (the walls provided the resistance, rather than building columns), thus the added cost in those buildings was mainly in details of connections. The cost increase was substantially greater for buildings in which the lateral force resistance did not come from walls. Furthermore, the level of seismic demand, even with the 50% increase, was moderate. This increase in cost cannot be extrapolated *pro rata* to higher levels of seismic demand. For example, demands on foundations begin to influence the cost. As a result, the cost increases associated with increases in seismic resistance in higher seismic regions (like coastal California), while not formally studied in the manner undertaken for Memphis, are known to be higher.

Regarding the target seismic risk level (1% probability of exceedance in 50 years), it should be recognized that this target is more than one order of magnitude higher than what is used for other common loadings, including wind, snow, and occupancy live loads for Risk Category II (ordinary occupancy)

structures (ASCE 2016). The large discrepancy between target risk targets has its roots in the different committees and processes used to develop criteria for the different loads, the large demand created by strong ground motions, and, at least in part, the cost of providing higher resistance to strong ground motion.

This NEHRP Part 3 paper addresses the use of deterministic caps on the ground motions used in seismic design. Where they are applied, deterministic caps produce ground motions that increase risk. The following section will describe how these caps are applied in current practice, the rationale for their use, and the issues generated by their incorporation into design ground motion maps. As part of Project 17, two alternative procedures were developed that would allow for the elimination of deterministic caps. These procedures are described in subsequent sections. This paper is concluded by presenting the outcomes of Project 17 deliberations, describing the rationales for not supporting alternatives to deterministic caps, and discussing a path forward for future code cycles.

RP2-2 DETERMINISTIC CAPS

RP2-2.1 Application

Risk-targeted ground motions are used in most of the United States, but exceptions are applied near highly active faults, which are mostly located in California, where deterministic caps are applied to limit the ground motions to the 84th percentile level, given the occurrence of a characteristic earthquake on nearby active fault. Deterministic caps were introduced in Project 97 and the 1997 NEHRP Provisions (Leyendecker et al. 2000; BSSC 1997), at which time the general basis for design ground motions was uniform hazard ground motions computed using probabilistic seismic hazard analyses (PSHA). The practice has continued since then for reasons described here, but was reconsidered in Project 17, as described in subsequent sections.

To compute deterministic ground motions, the PUC defines rules for what constitutes an active fault, what magnitude should be considered for a particular fault (which is taken as the characteristic magnitude), and what ground motion level should be applied when the specified earthquake occurs. Lowering (or not raising) of design ground motions is ensured by comparing deterministic ground motions to probabilistic MCER ground motions, and taking the lower of the two spectral ordinates. Figure 2 schematically depicts this process. Part (a) of the Figure shows a case where deterministic ground motions are lower than probabilistic MCER at all periods, whereas Part (b) shows a case where deterministic motions are lower only for a certain period range. The selected spectrum envelopes the lowest ordinates in both cases (referred to subsequently as the "site MCER spectrum").
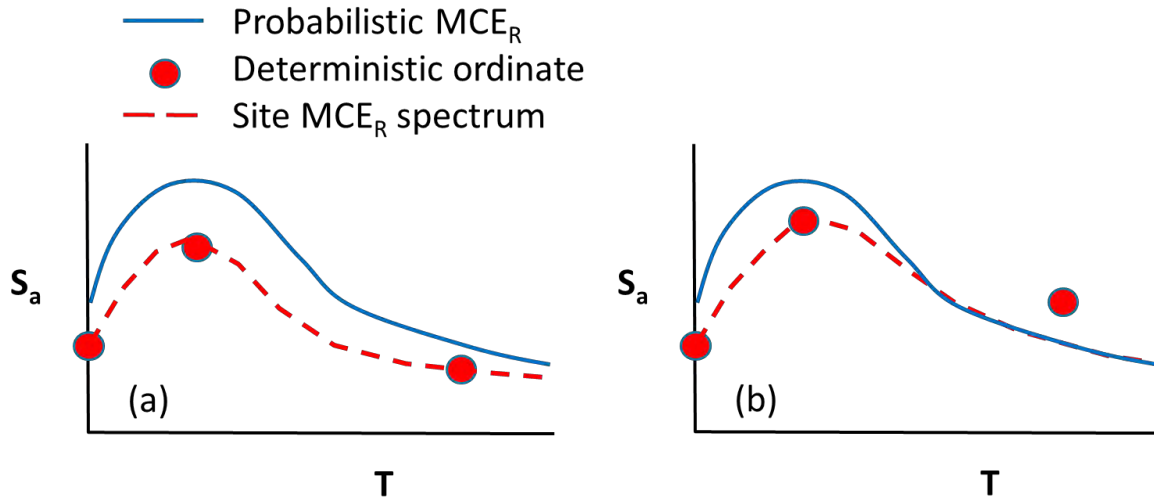
Figure 2 Schematics showing probabilistic risk-targeted response spectra (MCE$_R$), spectral ordinates computed using deterministic procedures, and selected site MCE$_R$ spectrum, which is taken as the lower of the two for cases of: (a) deterministic spectra control of design spectra at all periods and (b) hybrid of deterministic ordinates and probabilistic MCE$_R$ control for different period ranges.

A procedure introduced in Project 97 that has continued stipulates that deterministic spectral ordinates computed as 84th percentile ground motions from selected deterministic events are compared to the *deterministic lower limit spectrum*, and the larger of the two is used for comparison to the probabilistic MCE$_R$ spectrum. The deterministic lower limit spectrum is defined, since 1997, as the 1994 Uniform Building Code Zone 4 design response spectrum × 1.5. The rationale for application of the deterministic lower limit spectrum at the time was that it served as a convenient transition from the probabilistic MCE$_R$ to the 84th percentile deterministic response spectrum in the near field.

RP2-2.2   Argument in Favor of Deterministic Caps and Reasons for their Persistence

During Project 17 deliberations, the rationale put forward in support of deterministic caps was:

- Deterministic caps are only used for faults that produce frequent, large magnitude earthquakes, which can be readily identified (e.g., San Andreas and Hayward faults).

- These faults have been the subject of extensive investigation and the characteristic magnitude of future large (i.e., full segment rupturing) earthquakes can be established with reasonable certainty.

- Under the assumption that the specified characteristic event occurs, we can ensure that site MCE$_R$ ground motions are large enough to avoid catastrophic consequences by taking deterministic spectral ordinates at the 84th percentile (meaning that if the event occurs, there is an 84% chance that the actual ground motions at a particular site, and for a given period, will be smaller than the deterministic ordinate).

Logic gaps in the above arguments are elaborated on in Section 2.3. Because these gaps are well understood, it is difficult for many earthquake professionals to understand why the use of deterministic caps has persisted since 1997. To help understand their persistence, it is useful to recognize (1) the circumstances under which deterministic caps were introduced and (2) the inherent conservatism of code writing committees, meaning that substantive changes in design ground motions over time tend to be avoided unless there is overwhelming justification, and hence once procedures are incorporated into seismic provisions, they are more likely to persist than to be changed.

Before the 1997 NEHRP Provisions (BSSC 1997), design ground motions were based on uniform hazard spectra from PSHA. The return period of design-basis uniform hazard spectra was taken as 475 years and deterministic caps were not applied. Starting in 1997, the return period was increased to 2475 years for reasons elaborated on in Section 3. This increase in the return period increased ground motions in active regions like California where seismic loads are controlling in structural design. In keeping with the conservative posture of code writing committees, this increase was considered problematic.

In parallel with discussions to increase return period, the PUC considered the question – *In the event of a design-level earthquake on a known fault, how much larger can the shaking be at the location of a code-conforming building before we would anticipate a significant likelihood of collapse?* The collective judgment of the PUC at that time was 1.5, meaning that design ground motions could be increased by 1.5 to obtain MCE ground motions. The two-thirds factor (inverse of 1.5) was thus created to scale MCE ground motions to design motions. It was fortuitous, and perhaps not accidental, that the two-thirds factor approximately retained pre-1997 design ground motions in active regions like California.

Deterministic caps were also introduced in 1997 in combination with the return period increase and introduction of the two-thirds factor. The motivation for introducing deterministic caps was that two-thirds of probabilistically derived ground motions was considered impractical and unjustifiably costly for engineering design near active faults. As indicated previously (Section 1), the cost implications of ground motion increase (from potentially removing deterministic caps, while retaining the current risk targets) are anticipated to be higher in high-seismic regions like California than a similar increase in lower seismicity regions (ATC 2013).

RP2-2.3   Issues with Use of Deterministic Caps

The rationale put forward in support of deterministic caps does not account for challenges that are faced in specifying the attributes of future earthquakes. In particular:

- The identification of major active faults is non-trivial

- The magnitude of future earthquakes on 'deterministic' sources has a significant degree of variability

- Ground motions from future earthquake will have a wide range of intensities, including realizations beyond the 84th percentile.

These points are elaborated below.

Identification of faults: While the San Andreas and Hayward faults clearly belong in this category, the situation is less clear for active but lower slip-rate faults such as the Concord and Santa Monica faults. This requires the PUC to exercise judgment on which faults to include in use of deterministic caps, usually relying on fault dimensions and slip rates. There is necessarily a certain degree arbitrariness in how these choices are made.

Magnitude of earthquakes: The San Andreas fault is often cited by proponents of deterministic methods as having "known" characteristic magnitudes. Figure 3 shows the probability mass function of earthquake magnitudes for a site in San Bernardino, a few kilometers from the San Andreas fault. The probable magnitude range is approximately 7.5 to 8.4 (established from disaggregation of hazard using at 2475-year return period). While it may be tempting to assume that the next earthquake will match the last one (**M** ~7.8 in 1680 in this case[4]), that outcome, while certainly possible, is in fact unlikely. As an analogy, if a dice roll produces a particular outcome (e.g., 4), the next roll could again be 4 but that specific outcome is improbable. Moreover, the choice of a deterministic event within the range is consequential. For 1 sec

---

[4] The last great earthquake on the southern San Andreas fault was the **M** ~ 7.9 1857 Ft. Tejon earthquake (Sieh, 1978). The southern terminus of this rupture was near Wrightwood. The 1680 earthquake is the last event to have ruptured past San Bernardino (Sieh et al. 1989).

spectral acceleration, the expected change in ground motion over the 7.5 to 8.4 magnitude range in Figure 3 is about a factor of 1.5 (becomes about 3.0 for 3 sec spectral acceleration). Compounding these difficulties is that whereas this example of a site near the San Andreas fault is relatively 'easy', selection of a characteristic magnitude becomes even more challenging for sources that are relatively poorly understood.

Ground motions: Earthquakes produce ground motions with a high degree of variability, which is quantified by standard deviation terms. The deterministic procedure specifies the ground motion at a fixed 84th percentile (one standard deviation above the mean). This assumption is one of many that could be made, and ground motions at higher percentiles are routinely observed in well-recorded earthquakes.

The San Bernardino example shows that selection of the deterministic event and ground motion is non-trivial, will necessarily require specific judgements to be made within seismic source and ground motion models, and has significant consequence for design ground motions. PSHA procedures were developed in the 1960s – 1970s to overcome these issues, by considering all known seismic sources, a wide range of future earthquakes along with their relatively likelihoods of occurring, and the full range of possible shaking intensities for each earthquake realization.
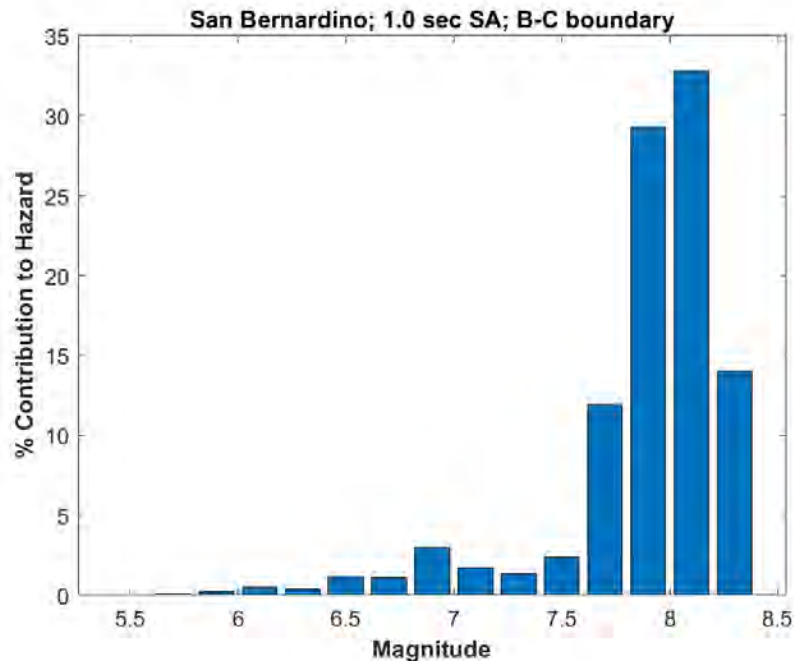
Figure 3 Relative contribution of earthquakes of different magnitudes to ground motion hazard for 1.0 sec spectral acceleration at a 2475-year return period for a site in San Bernardino. The controlling magnitudes in the range of 7.5 to 8.4 are mostly from earthquakes on the San Andreas fault (the San Jacinto fault also contributes to a lesser degree)

RP2-2.4   Impact of Applying Deterministic Caps

Figure 4 shows the risk level that corresponds with site MCE$_R$ ground motions in California and Nevada. For most of the mapped region, and the remainder of the United States outside the limits of the Figure, the risk level is 1% probability of exceedance in 50 years, consistent with the probabilistic MCE$_R$ definition (Luco et al. 2017).
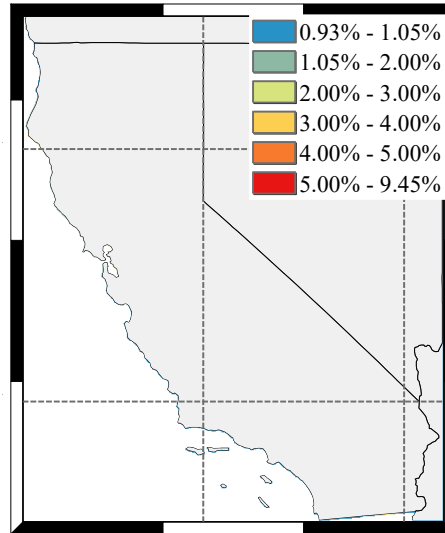
Figure 4 Risk levels provided by site MCER ground motions, expressed as a probability of structural collapse in 50 years. Regions with risk levels elevated from 1% are affected by deterministic caps. From Luco et al. (2017)

Near major active faults in California, the risk level is higher by factors ranging from approximately 1 to 10. The amount of surface area in the conterminous United States subject to capped design motions is ~1%, but it contains about 11-12 million people (~3.6% of the US population), including major urban centers. The reason for these different risk levels is fundamentally related to the lack of consideration of earthquake and ground motion exceedance rates in deterministically capped zones, and basing ground motions on those rates outside of deterministic zones.

Because the basis for the deterministic ground motions has several elements for which judgment must be exercised (assumed segment ruptures, magnitude, and realized ground motion) and the rate of the characteristic earthquake is not considered, the levels of risk that are produced are not controlled and are highly spatially variable, as shown in Figure 4. Deterministic capped ground motions are problematic for three basic reasons:

- The non-uniform risk that results is not understood by the public, and is difficult to explain to building owners. While design professionals can state that the design of a building within a deterministically capped zone is 'for a particular earthquake', questions such as *Why was that particular earthquake selected?*; *Why was that particular ground motion selected?*; or *What level of performance will my building have?* are difficult to answer. In contrast, when a risk level is targeted, these source and ground motion modelling decisions are not required. While any specific risk target could also be considered as arbitrary, risk is a more effective means by which the PUC (and the public) can quantify performance expectations for code-designed buildings.

- An outcome of non-uniform risk is that different levels of seismic protection are enforced in the design process for different regions. For example, short period (0.2 sec) structures on a reference site condition (site class B/C boundary) in San Jose CA, Reno NV, and Salt Lake City UT all have site MCE_R ground motions of about 1.5 g, but different risk levels of 3% probability of collapse in 50 years in San Jose and 1% in the other locations. Engineers outside of California, who were consulted during Project 17 deliberations, raised concerns regarding the inconsistency of these different seismic requirements.

- Deterministically capped ground motions increase risk by an unspecified amount, and hence there is a lack of transparency in the level of seismic protection provided by design ground motions in capped areas.

An objective of Project 17 was to revisit the risk levels provided by design ground motions. As part of that assessment, we identified options to the current use of deterministic caps. Two such options were identified as described in the following sections.

RP2-3   ALTERNATIVE 1: MODIFIED UNIFORM RISK

As described in Section 2.4, current procedures for evaluating design ground motions (ASCE 7-16) provide spatially non-uniform levels of seismic protection. Figure 4 illustrates this in the form of elevated collapse risk probabilities in zones where deterministic caps are applied. This section describes procedures developed in Project 17 to provide uniform risk levels, while also approximately preserving design ground motions at the regional level.

To understand the rationale for the proposed procedures, it is useful to consider the ground motion hazard levels that are provided by the site MCE_R design ground motions currently in use. Figure 5 shows a map of these hazard levels in the form of return periods for 0.2 sec spectral acceleration for the contiguous United States. In the 99% of the country with uniform risk, ground motion return periods range from about 1500 to 2500 years. Much lower return periods (as low as 200 years) occur in the deterministically capped regions.

2750 - 3781
2250 - 2750
1750 - 2250
1250 - 1750
750 - 1250
250 - 750
181 - 250
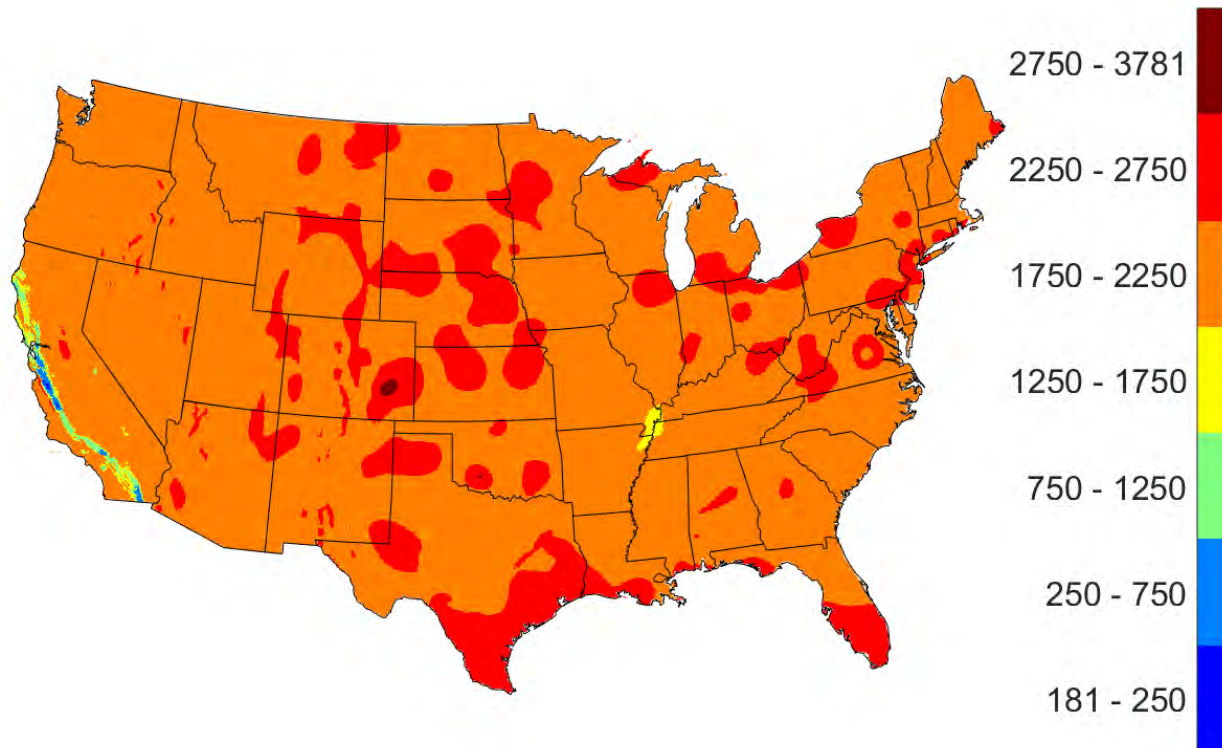
Figure 5 Map of ground motion return period associated with site MCER ground motions provided by risk-based and deterministic procedure, based on procedures in the 2015 NEHRP Provisions. The scale bar indicates return period in years.

RP2-3.1   Earthquake Recurrence for Central and Eastern North America Sources

At the time of Project 97 and the 1997 NEHRP Provisions, the return period of large earthquakes in the New Madrid seismic zone was taken as approximately 1000 years in the contemporaneous seismic hazard maps published by the US Geological Survey (Frankel et al. 1996). As arguably the most significant seismic source in central and eastern North America, this return period significantly influenced selection of the 2475 year ground motion return period that was adopted.

To understand why the ground motion return period exceeds the earthquake return period, consider the relationship between the corresponding rates for the case of a single source,

$$\nu_{IM} = \lambda P \tag{1}$$

where ν_{IM} is the rate of exceedance of a ground motion intensity level, λ is the rate of earthquakes on the fault (if the problem is simplified such than only large-magnitude, or characteristic, earthquakes are considered, λ would be the rate of those events), and P is the probability of exceeding the selected ground motion intensity level when an earthquake occurs. Eq. (1) indicates that ground motion return period $1/\nu_{IM}$ exceeds earthquake return period $1/\lambda$, with a factor of 2 being required for a median conditional ground motion ($P = 0.5$). Accordingly, the ground motion return period of 2475 years that was selected in 1997 can be recognized as providing reasonable assurance that when the characteristic New Madrid event occurs, the resulting ground motions are likely to be somewhat less than the design-basis ground motion used to set structural strength.

Since the late 1990s, additional work on seismic sources in central and eastern North America has generally shown lower earthquake return periods than was used to develop the 1996 maps. Figure 6 shows faults and seismic source zones, which act in combination with background seismicity to produce earthquakes in recent USGS models (e.g., Petersen et al. 2015). Table 1 lists earthquake return periods ($1/\lambda$) used in the 2014 USGS source models for the source zones in Figure 6. Since 1997, the New Madrid return period has shortened by approximately a factor of 2, and the Charleston return period has also been reduced (from about 650 years to 530 years). Following the logic applied in 1997, these changes allow for reduced ground motion return periods in central and eastern North America, which is discussed next.
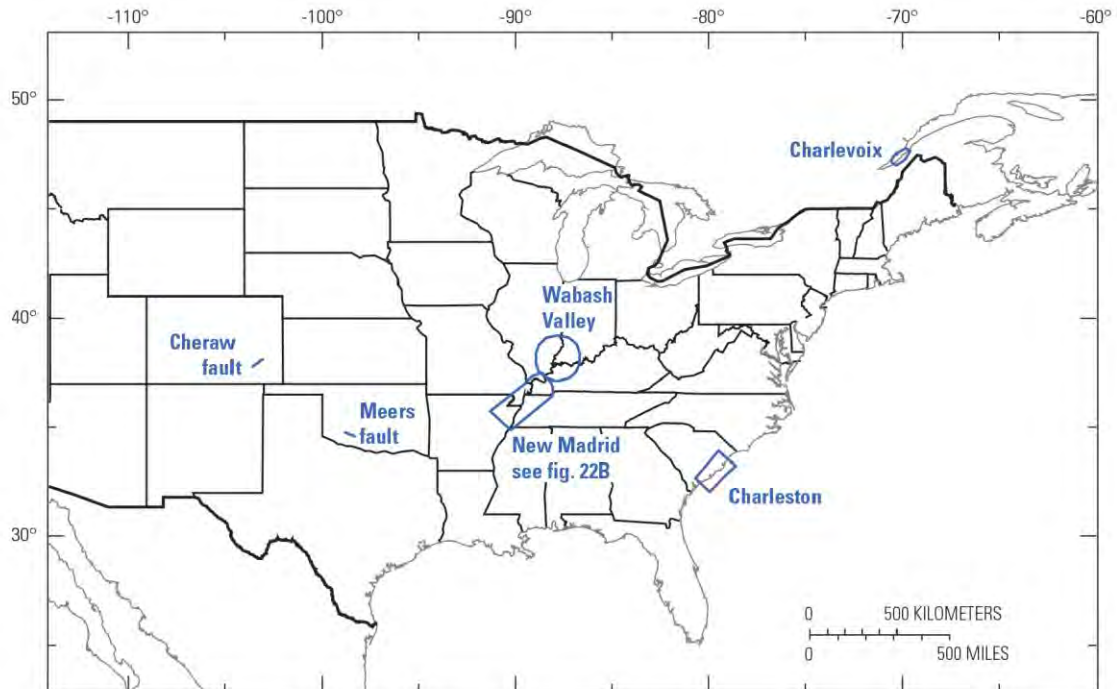
Figure 6 Faults and source zones in central and eastern North America considered in USGS seismic hazard modeling (Petersen et al. 2015).

Table 1 Approximate maximum magnitudes and corresponding earthquake return periods for faults and source zones in Figure 6 (Petersen et al. 2014).

Fault or Source Zone	Maximum Magnitude	Return Period, $1/\lambda$ (yrs)
New Madrid	7.5	~500
Charleston	7.1	530
Charlevoix	7	730
Meers	6.9	2100
Wabash	7.5	5900
Cheraw	7	9500

RP2-3.2   Suggested Framework for Developing Uniform National Risk Targets

The process of selecting a target rate of structural collapse for buildings designed using code-derived strengths can be undertaken with these steps:

1. Select seismic sources from tectonically stable regions (central and eastern US) that exert a critical influence on seismic demands in population centers. Evaluate return periods of large characteristic earthquakes on those sources.

2. Select target ground motion hazard levels (i.e., return periods) that adequately exceed the earthquake rates from (1).

3. Define an initial risk level that provides a spatial pattern of ground motion that is roughly consistent with the target hazard levels from (2).

4. Disaggregate the hazard for critical locations at the hazard levels provided by the initial risk levels from (3). Judge the effectiveness of the risk levels on the basis of the percentile levels of ground motion that are provided.

5. Adjust the factor applied to probabilistic MCE_R ground motions if it is desired to minimize changes in design ground motions from a previous code cycle. While there were multiple motivations behind development of the current two-thirds factor, its effect is to scale MCE_R ground motions in this manner, and it was originally developed through collective judgment of the PUC. Judgement could similarly be exercised again. If the risk target was increased (i.e., higher collapse probability), the resulting decreases in ground motions could be mitigated for a target region by increasing the factor.

These steps are intended to facilitate the exercising of informed judgment in a systematic manner by decision-making bodies like the PUC. As demonstrated in Section 3.3 below, application of this process with contemporary earthquake rates results in an increased risk target, decreasing ground motions. As a result, the perceived need for deterministic capping in active regions is reduced.

In Step 4, the disaggregation of hazard provides the earthquake magnitudes, site-to-source distances, and ground motion epsilon (ε) levels that contribute most strongly to the hazard. Epsilon is defined as:

$$\varepsilon = \frac{ln(IM) - \mu_{ln}}{\sigma_{ln}} \qquad (2)$$

where *IM* is a ground motion intensity measure (in this case, corresponding to the selected hazard level), and μ_{ln} and σ_{ln} are the natural log mean and standard deviation of *IM* from ground motion prediction equations for a given magnitude, distance, and other parameters. As a result, ε provides information on how rare is the ground motion controlling the hazard. A median ground motion corresponds to $\varepsilon = 0$, and an 84th percentile ground motion corresponds to $\varepsilon = 1$.

RP2-3.3   Recommended Risk Target

The approach in Section 3.2 was preliminarily implemented in Project 17, although the final steps were not completed due to lack of support from Project 17. Here we describe this preliminary development of a proposal for uniform risk across the US, which represents the first of two alternative methods developed in Project 17.

For *Step 1*, we focused mainly on the New Madrid and Charleston source zones, due to their proximity to major population centers (e.g., Memphis, Charleston). We also considered Charlevoix. In the case of the other source zones shown in Table 1, hazard in their vicinity is mostly is low and is mostly controlled by background seismicity. Per Table 1, the event return periods for these sources range from 500-700 years. Accordingly, in *Step 2*, target ground motion return periods should be approximately 1000 to 1500 years to maintain a minimum ε of zero.

For *Step 3*, we initially considered two approaches to define alternate risk levels:

- Same performance expectation (10% probability of collapse if maximum considered earthquake ground motion occurs), but different risk target

- Different performance expectation (≠ 10%), generally consistent with recent studies of the seismic performance of code-conforming buildings (e.g., Goulet et al. 2007), and same risk target

We ultimately chose the first approach, so as to maintain the precedent of 10% collapse probability given the probabilistic MCE_R ground motion, per ASCE 7-10 and 7-16. Following some iteration, we found that a risk target of 1.5% probability of collapse in 50 years, with the 10% collapse probability, provides ground motion return periods reasonably consistent with those of *Step 2*. This is shown in Figure 7 for the case of 0.2 sec spectral acceleration as the intensity measure; return periods are approximately 1500 years in most of the US, with lower values (about 1100 years) in the most active regions (California and the New Madrid seismic zone). These are consistent with the 1000-1500 year targets.
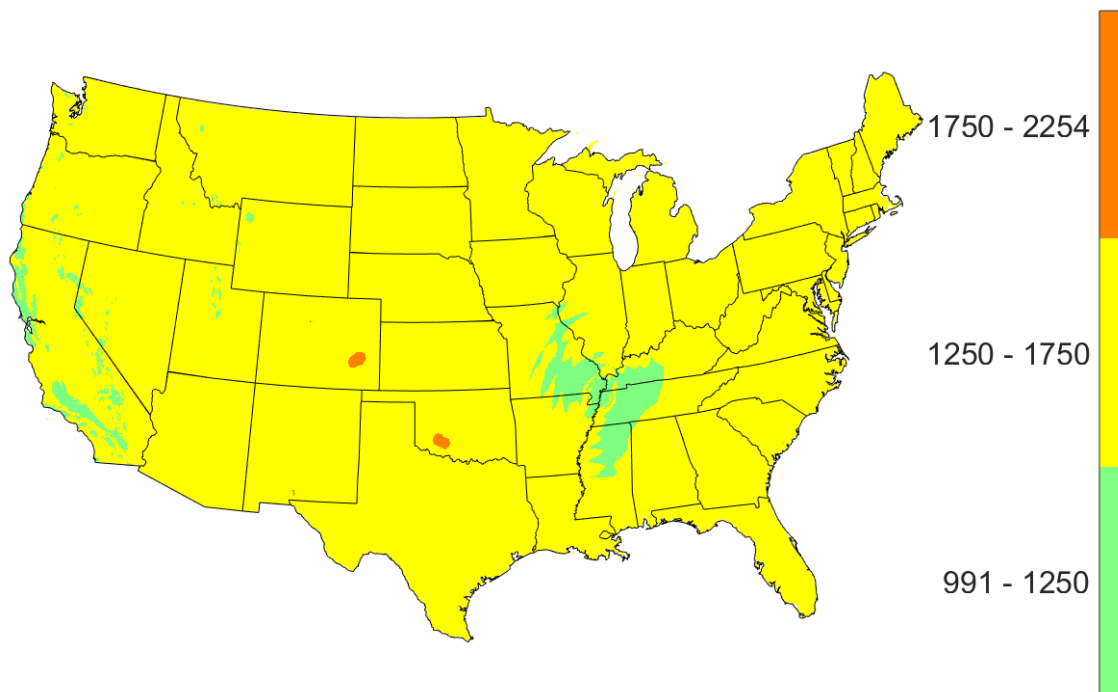
Figure 7 National map of ground motion return period (0.2 sec spectral acceleration) for risk-targeted maximum considered earthquake ground motion computed using a 1.5% probability of collapse in 50 years target risk level. The scale bar indicates return period in years.

For *Step 4*, disaggregation was performed for 29 locations in the western US (details in Table 1 of Petersen et al. 2014), and five central and eastern US locations (Charleston, Chicago, Memphis, New York, St. Louis). Figure 8 plots the variation of ε with the risk target probability for 0.2 sec and 1.0 sec spectral accelerations. For the western US, at a 1.5% risk target, ε averages about 1.0, corresponding to about an 84th percentile ground motion. For most central and eastern US locations, the same 1.5% risk target provides an ε of approximately 0.5 (69th percentile). This includes areas, such as Chicago, with strong contributions from background seismicity relative to contributions from specific fault sources. For a few locations (New York and Charleston), ε is approximately zero (50th percentile). Some Project 17 members expressed concern that the modified risk target would provide inadequate seismic protection for such locations. To address this concern, there was discussion of possibly implementing a deterministic floor, which would

consist of a source, magnitude and ε for a given region, to define levels of ground motion that maximum considered ground motions should not fall below.

Figure 9 shows the impact on deterministically capped regions if the modified risk target were adopted. The maps in the Figure shade only those regions where deterministic caps apply, using the current framework in which deterministic ground motions are adopted if they are less than probabilistic MCE$_R$ ground motions. The shading indicates the ground motion return period as marked in the legend. The left and right sides of the Figure show the capped regions under the current and modified risk targets, respectively. The modification reduces significantly the area subject to caps, but does not eliminate it. Caps are eliminated in several important locations, including most of Los Angeles and surrounding urbanized areas, the San Francisco peninsula, and most of Silicon Valley. Most of the areas where deterministic caps would remain under current 'rules' are sparsely populated (an exception being portions of the east San Francisco Bay Area; approximately Fremont to Oakland). As a result, were this proposal to be adopted, deterministic caps would no longer be needed to reduce ground motions for most populated areas, and therefore could likely be eliminated.

If the risk target were increased in a manner similar to what is described here, deterministic caps were eliminated, and the two-thirds factor was retained, there would be several impacts:

- The levels of seismic protection provided for code-designed structures would be uniform nation-wide, increasing transparency.

- Ground motions would be lowered in areas not previously governed by deterministic caps. Luco et al. (2017) (their Figure 4) show the lowering of 0.2 sec MCE$_R$ ground motions for different risk target levels at 34 locations across the U.S. -- at a 1.5% risk target, reductions range from about 12 to 24% relative to current levels, with the largest reductions in central and eastern North America and the intermountain west.

- For engineers who wish to describe the earthquake controlling design ground motions in a deterministic manner (i.e., specific fault, magnitude, and distance), this information would no longer be pre-determined by PUC 'rules'. Instead, it would be derived using disaggregation that is specific to a site location and the selected ground motion parameter (i.e., spectral acceleration for a given period).
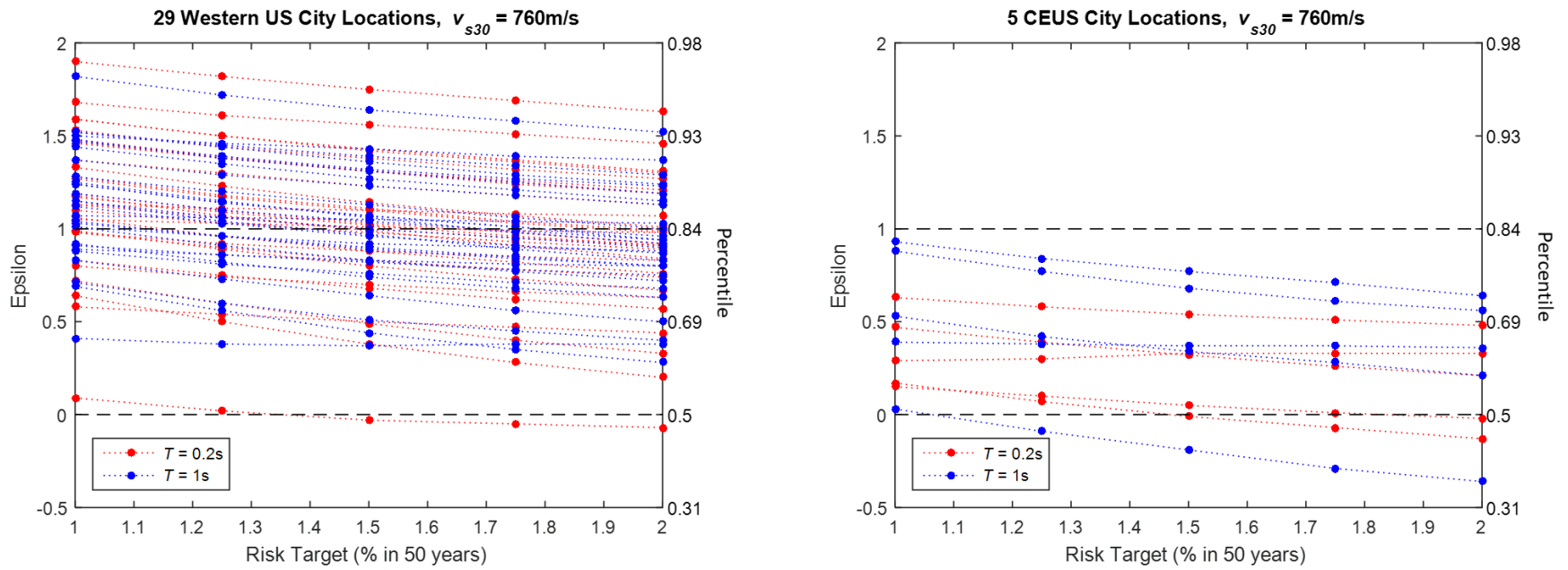
Figure 8 Variation of mean epsilon as a function of risk target percentage (1% being the default, current value) for 0.2 and 1.0 sec spectral accelerations at various locations in the western and central/eastern US.

Current MCE_R (1% prob. collapse in 50 yr.) _____ *Modified MCE_R (1.5% prob. collapse in 50 yr.)*
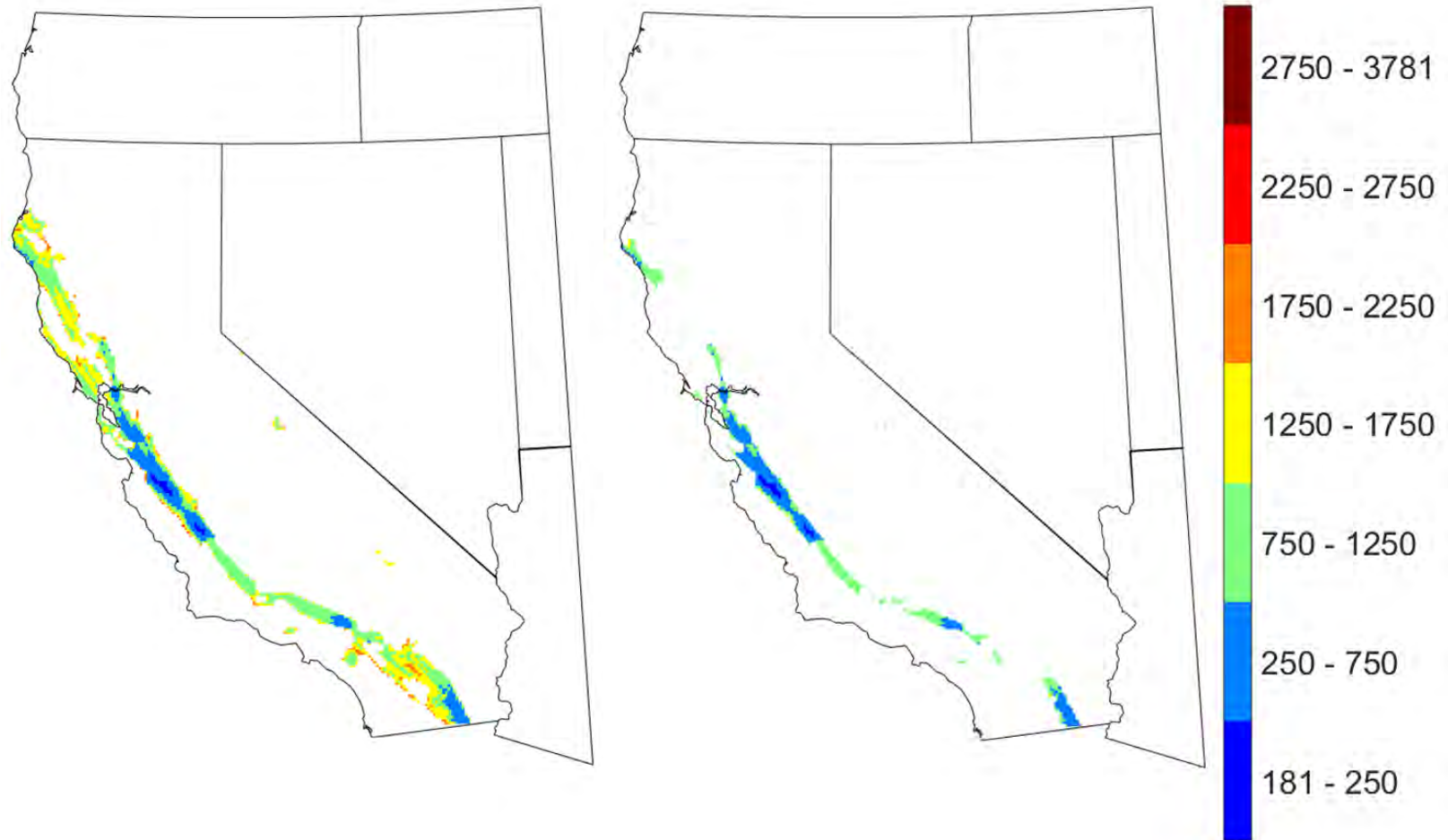
Figure 9 Shading of deterministically capped regions in California according to ground motion return period provided by current and modified risk targets. The scale bar indicates return period in years. The ground motion parameter is 0.2 sec spectral acceleration.

RP2-4 ALTERNATIVE 2: SPECIFIED LEVELS OF NON-UNIFORM RISK

Current procedures for deriving site MCE_R ground motions provide spatially non-uniform levels of risk in areas near major active faults (Figure 4). For most deterministically capped regions, Figure 4 shows that risk levels currently provided range from about 1% to 4% probability of collapse in 50 years. However, for some locations (e.g., Parkfield), the risk level is almost 10% collapse probability. Hence, risk levels in California vary by up to a factor of 10.

While Alternative 1 (Section 3.3) removes this spatial non-uniformity, in the course of deliberations, it became evident that such non-uniformity is considered to be acceptable to some Project 17 team members in order to reduce design ground motions near active faults (Section 2.2). Viewed from this perspective, the problem with current procedures is not that the risk is non-uniform, but that levels of non-uniform risk in deterministically capped zones are substantial and uncontrolled.

The premise of Alternative 2 is that while non-uniform risk is established practice in California, levels of elevated risk near active faults should be specified. Figure 10 illustrates the concept. Part (a) shows that beyond some fault distance, the risk target is unchanged (1% probability of collapse in 50 years). Parts (b) and (c) show that within a zone of uniform width along the fault, one or more elevated collapse probabilities are used. Ground motions within the elevated risk zones are computed in the same manner as done currently for the probabilistic MCE_R, but with the elevated risk targets in lieu of 1%.

Implementation of Alternative 2 requires answers to three questions:

1. What faults would be subject to elevated risk?

2. What zone width would be used around faults?

3. What levels of elevated risk would be applied?
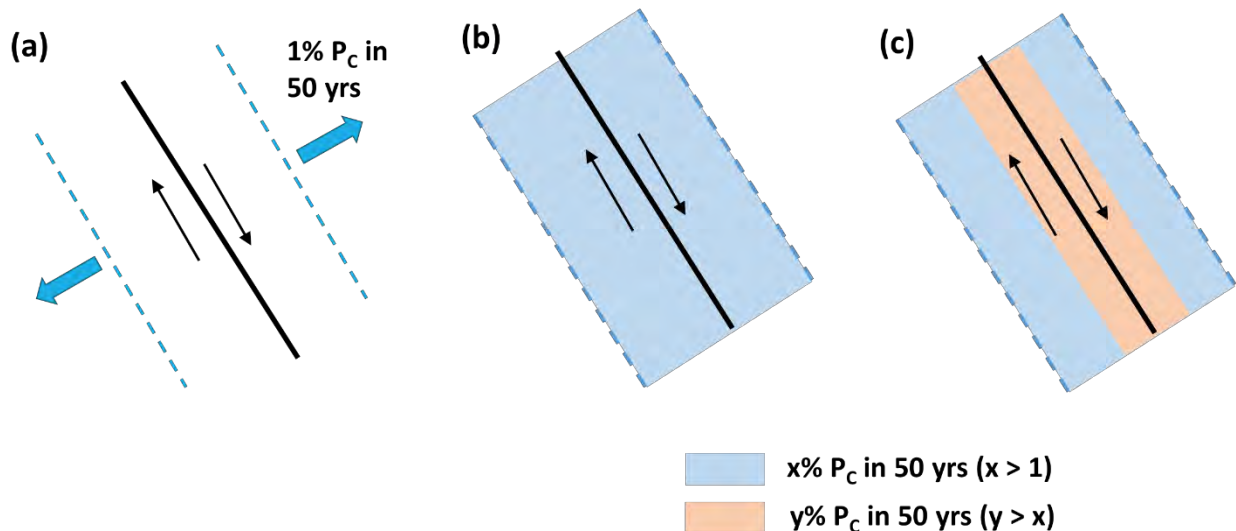
Figure 10 Schematic illustration of Alternative 2 risk targets as function of position relative to active fault. (a) standard 1% probability of collapse (PC) in 50 years, which applies beyond some fault distance (indicated by dotted lines); (b) single zone of elevated risk near active fault; (c) two zones of elevated risk, with risk target increasing at closer fault distances

Answers to these questions were not developed in Project 17 deliberations. However, presumably the targeted faults would be the same as those used currently for deterministic caps. A specific recommendation for zone width was not developed, but it would likely be nominally less than the width of deterministically capped zones, which is generally about 50 km for major strike-slip faults. Based on Figure 4, if elevated target risk levels of about 2-3% collapse probability were selected, design ground motions in urban areas would not change appreciably from current levels. Because avoiding change of design ground motions over time influences PUC decision making (Section 2.2), risk levels in the range of 2-3% collapse probability would likely be used if Alternative 2 were implemented. A similar alternative that selects elevated risk targets based only on the levels of hazard, such that locations of higher hazard use higher risk targets, was proposed in Luco et al. (2017).

If near-fault elevated risk targets were to be implemented, there would be several impacts:

- Deterministic procedures would no longer be used to derive design ground motions.

- Regions near large, active faults in California would have elevated risk levels, but those levels would be specified in the NEHRP Provisions. Moreover, by applying elevated risk targets in a uniform manner, the uncontrolled risk levels provided currently in deterministically capped zones would be eliminated.

- While design ground motions would change at individual sites, when viewed more broadly at regional scales, the changes could be made to be minimal relative to current levels.

RP2-5   CONCLUSIONS AND PATH FORWARD

This Part 3 paper describes the application of deterministic caps in the derivation of design ground motions, issues associated with the use of such caps, and two alternative procedures for deriving ground motions that were developed in Project 17. Both alternative procedures allow elimination of deterministic methods. Alternative 1 increases the risk target at a national level. Alternative 2 maintains the current national risk target, but elevates risk targets near large, active faults in California.

Adoption of either option would require substantive deliberation and judgment by the PUC. The central issue that would face the PUC for either option is the appropriate level of collapse risk that should be used in the derivation of design ground motions. While we recognize the difficulty and significance of developing such recommendations, this matter is fundamental to PUC's charge. What adoption of either option would replace is the exercise of judgment by the PUC in the application of seismic source and ground motion models. As a deliberative body, the PUC is arguably better equipped to apply judgement that is quantified in the form of collapse risk than judgment quantified with respect to details of seismological models.

The topics addressed in this paper, including the two alternative procedures, were discussed in detail as part of Project 17 (BSSC, 2018). Both alternatives were rejected. The primary reasons for rejection were:

- Alternative 1: Some Project 17 members were not willing to adopt changes to the design ground motions that would result from changes to the risk target. Potential changes to the two-thirds factor to mitigate changes to design ground motions were not discussed. Because changes in design ground motions over time tend to be avoided (Section 2.2), this caused Alternative 1 to not be supported. It was not balloted.

- Alternative 2: There was discomfort with clearly delineating non-uniform levels of risk for sites near major, active faults in California. The preference of some Project 17 members was to exercise judgement not at the risk level, but at the level of seismic source and ground motion models, and for elevated risk in these regions to be a relatively opaque outcome of deterministic calculations. Alternative 2 was balloted and failed with a slight majority of Project 17 members.

By rejecting these alternatives, Project 17 endorsed continued use of deterministic capping of design ground motions. Some adjustments in the means by which deterministic faults are selected and earthquake magnitudes are chosen have been made, which brings somewhat more rigor and computational efficiency to the process. These changes are described in the 2020 NEHRP Commentary.

It is possible that PUCs formed for future code cycles might revisit this topic. Given the significance of this issue, a systematic, consensus-building approach is needed. Such an approach could include the following steps:

1. Form an issue team (IT) to address this issue, composed of ground motion and risk experts, practicing structural and geotechnical engineers, and building department officials;

2. IT undertakes work, ideally starting prior to the start of the next code cycle, to move towards consensus on the following points:

   a. Is a uniform risk framework (Alternative 1) or specified non-uniform risk framework (Alternative 2) preferred?

   b. For Alternative 1, what risk target should be selected? What modification of the resulting ground motions, if any, is most appropriate? Should the two-thirds factor be adjusted to mitigate changes in design ground motions in targeted regions?

   c. For Alternative 2, answers to the three questions posed in Section 4 could be developed.

3. Sensitivities to different answers would be documented prior to, or in the early stages of, the next cycle so that the IT has sufficient time to work out the final details with the PUC.

RP2-6   REFERENCES

ASCE, 2016. *Minimum Design Loads for Buildings and Other Structures, ASCE/SEI 7-16*. American Society of Civil Engineers, Reston, Virginia.

Applied Technology Council, ATC, 2013. Cost Analysis and Benefit Studies for Earthquake-Resistant Construction in Memphis Tennessee, *NIST GCR 14-917-26*, National Institute of Standards and Technology, Gaithersburg, MD.

BSSC, 1997. NEHRP Recommended Provisions for Seismic Regulations for New Buildings and Other Structures, Part 1: Provisions and Part 2: Commentary, Building Seismic Safety Council, FEMA 303, Washington, D.C., 362 pp.

BSSC, 2018. Project 17 Final Report, National Institute of Building Sciences, Building Seismic Safety Council, Project 17 Committee, Chair Ronald O. Hamburger. Draft

Federal Emergency Management Agency, FEMA, 2009. Quantification of Building Seismic Performance Factors, FEMA P-695, Washington DC.

Frankel A., Mueller, C., Barnhard, T., Perkins, D., Leyendecker, E.V., Dickman, N., Hanson, S., and Hopper, M., 1996. National seismic hazard maps: Documentation June 1996, U.S. Geological Survey, Open File Report 96-532, Denver, CO.

Goulet, C.A., Haselton, C.B., Mitrani-Reiser, J., Beck, J.L., Deierlein, G.G., Porter, K.A., and Stewart, J.P. 2007. Evaluation of the seismic performance of a code-conforming reinforced-concrete frame building – from seismic hazard to collapse safety and economic losses, *Earthquake Engineering and Structural Dynamics*, 36 (13), 1973-1997.

Leyendecker, E.V., Hunt, R.J., Frankel, A.D., and Rukstales, K.S., 2000. Development of maximum considered earthquake ground motion maps. Earthquake Spectra, 16 (1), 21-40.

Luco, N., Ellingwood, B. R., Hamburger, R. O., Hooper, J. D., Kimball, J. K., and Kircher, C. A., 2007. Risk-targeted versus current seismic design maps for the conterminous United States, *Proc. Struct. Engineers Assoc. of California 76th Annual Convention*, Lake Tahoe, CA.

Luco, N., Liu, T.J., and Rukstales, K.S., 2017. A risk-targeted alternative to deterministic capping of maximum considered earthquake ground motion maps. *Proceedings of the 16th World Conference on Earthquake Engineering*, Santiago, Chile.

Petersen, M.D., Moschetti, M.P., Powers, P.M., Mueller, C.S., Haller, K.M., Frankel, A.D.,, Zeng, Y., Rezaeian, S., Harmsen, S.C., Boyd, O.S., Field, E., Chen, R., Rukstales, K.S., Luco, N., Wheeler, R.L., Williams, R.A., and Olsen, A.H., 2015. The 2014 United States National Seismic Hazard Model. Earthquake Spectra, 31 (S1), S1-S30.

Sieh, K.E., 1978. Slip along the San Andreas fault associated with the great 1857 earthquake, Bull. Seismol. Soc. Am., 68 (5), 1421–1448.

Sieh, K.E., Stuiver, M., and Brillinger, D., 1989. A more precise chronology of earthquakes produced by the San Andreas fault in southern California. J. Geophy. Res.: Solid Earth, 94(B1), 603-623.

RESOURCE PAPER 3 DESIGN OF ISOLATED AND COUPLED SHEAR WALLS OF CONCRETE, MASONRY, STRUCTURAL STEEL, COLD-FORMED STEEL AND WOOD

PREFACE

IT4 was formed with the broad mandate of identifying possible areas of improvement in current design practices for shear walls of concrete, masonry, steel, and wood, and of formulating specific improvements.

IT4 developed two Part 1 proposals for modifications to ASCE 7-16 Table 12.2-1 (ASCE 2016). The first one adds line items on Bearing Wall Systems, Building Frame Systems, and Dual Systems (with Special Moment Frames) featuring Reinforced Concrete Ductile Coupled Shear Walls. The second proposal adds line items on Building Frame Systems and Dual Systems (with Special Moment Frames) featuring Steel and Concrete Coupled Composite Plate Shear Walls. In addition, IT4 developed this Part 3 Resource Paper.

This Resource Paper was developed to help practitioners understand how the design of shear walls of various materials is approached; what the common elements are, and what the differences are.

This Resources Paper also discusses topics of particular concern to practitioners dealing with the design of shear walls of a particular material or construction. Some of this topical discussion goes beyond current building code provisions and provides guidance on issues facing the practitioner. This resource paper also provides technical background to the two Part 1 proposals developed by IT4. One of the proposals on reinforced concrete ductile coupled shear walls utilized changes in shear wall design and detailing made in ACI 318-19. The background to these changes is explained.

RP3-1 OVERVIEW OF DESIGN OF SHEAR WALLS OF VARIOUS MATERIALS

RP3-1.0 Introduction

This chapter discusses seismic force-resisting systems featuring shear wall types that are addressed in ASCE 7. Seismic design forces for shear walls, as given in ASCE 7, depend on response modification factors, R, listed in ASCE 7 Table 12.2-1. This chapter deals with the strength and ductility of shear

walls. Included is a general treatment of issues regarding shear walls.

This chapter addresses basic behavior modes and design principles for shear walls of a wide range of materials. Included for each material are: shear wall system (construction) description; preferred energy-dissipation mechanisms; design concepts, methods, and details; and approaches to analytical modeling.

Detailed discussions of shear walls of various materials follow in later chapters.

RP3-1.1 Seismic Force-Resisting Structural Systems

The basic structural systems that may be used to resist earthquake forces are listed in ASCE 7 Table 12.2-1 (ASCE 2016). Included in the table are the response modification factors R to be used in determining the base shear V, the overstrength factor Ω_o to be used in determining maximum element design forces, and the deflection amplification factor C_d to be used in determining design story drift. Also given in the table are height limits for the various structural systems, which depend on the Seismic Design Category (SDC). It is the height limits portion of the table that indicates that when it comes to concrete moment frames, for instance, ordinary detailing is permitted only for SDC B (and, of course, A); intermediate or special detailing is required for SDC C; and special detailing is the minimum requirement for SDC D, E, or F. Also included in Table 12.2-1 is a column that lists ASCE 7 sections where detailing requirements for the various structural systems are specified. This column is not particularly useful because most of the references are to ASCE 7 Chapter 14 section numbers. For all reinforced concrete systems, reference is made to ASCE 7-16 Section 14.2. That section references ACI 318-14 (ACI 2014), which is where the actual detailing requirements are found. A general description of each major category of seismic force-resisting systems featuring shear walls is given below.

For structural members within a building assigned to SDC D, E, or F that are not proportioned to resist forces induced by earthquake motions, the deformation compatibility requirements of ASCE 7-16 Section 12.12.5 must be satisfied. In short, every structural component not included in the seismic force-resisting system in the direction under consideration must be designed to be adequate for vertical load-carrying capacity and the induced bending moments and shear forces resulting from the design story drift. Note that reinforced concrete frame members not designed as part of the seismic force-resisting system are deemed to satisfy deformation compatibility requirements if they comply with Section 18.14 of ACI 318-14.

RP3-1.1.1 Bearing wall systems

The moment-resisting frame system, shown in Figure 1.1-1(a), is not discussed here because it does not contain shear walls. The bearing wall system depicted in Figure 1.1-1(b) is a structural system without an essentially complete space frame that provides support for the gravity loads. Bearing walls provide support for all or most of the gravity loads. Resistance to lateral forces is provided by the same bearing walls acting as shear walls. See ASCE 7 Table 12.2-1 Row A for bearing wall systems of various materials specifically recognized by ASCE 7-16.
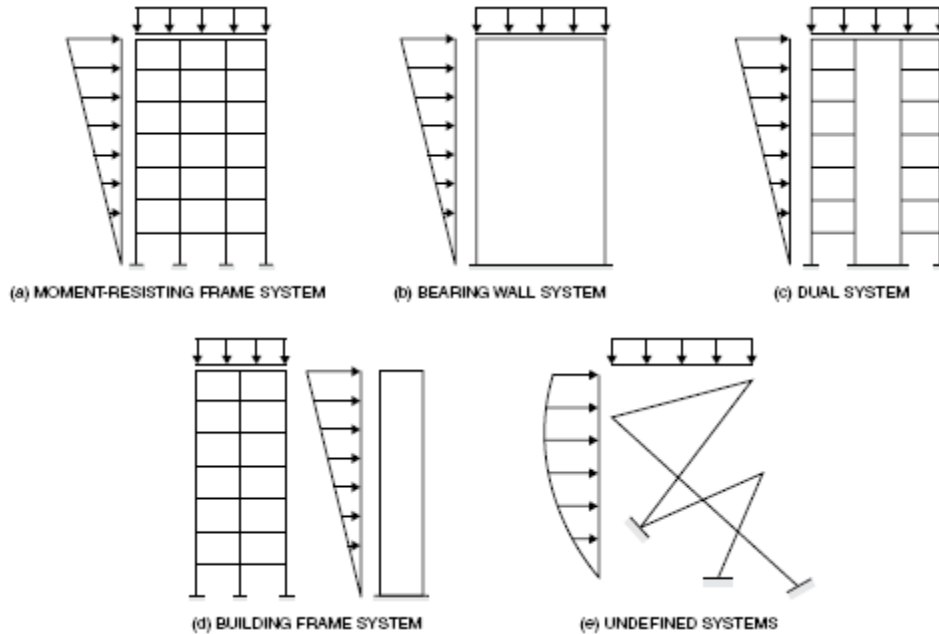
Figure 1.1-1: Seismic force-resisting structural systems

RP3-1.1.2   Dual Systems

A dual system, depicted in Figure 1.1-1(c), is a structural system with the following essential features:

1. An essentially complete space frame provides support for gravity loads;

2. Resistance to lateral forces is provided by moment-resisting frames capable of resisting at least 25% of the design base shear and by shear walls or braced frames (ASCE 7-16 Section 12.2.5.1); and

3. The two subsystems (moment-resisting frames and shear walls) are designed to resist the design base shear in proportion to their relative rigidities (ASCE 7-16 Section 12.2.5.1).

ASCE 7-16 separately recognizes dual systems in which the moment-resisting frame consists of special moment frames (ASCE 7 Table 12.2-1 Row D) and dual systems in which the moment-resisting frame consists of intermediate moment frames (ASCE 7 Table 12.2-1 Row E).

The concept of the dual system loses its validity in buildings assigned to SDC A and B, since it is questionable whether the moment frames, which are required to have only ordinary detailing, can act as a back-up to the ordinary reinforced concrete shear walls (the inelastic deformability of both systems are comparable). In areas of low seismicity, utilizing a **Shear Wall-Frame Interactive System** (ASCE 7 Table 12.2-1 Row F) is more logical. In this system, defined in ASCE 7-16 Section 12.2.5.10, the shear walls and frames resist the lateral forces in proportion to their rigidities, considering interaction between the two subsystems at all levels. In addition, the shear strength of the shear walls must be at least 75% of the design story shear at each story. The frames of the shear wall-frame interactive system must be capable of resisting at least 25% of the design story shear in every story.

RP3-1.1.3   Building Frame Systems

A building frame system is depicted in Figure 1.1-1(d). This is a structural system with an essentially complete space frame that supports the gravity loads. Resistance to lateral forces is provided by shear walls or braced frames. No interaction between the shear walls or braced frames and the moment frames

is considered in the lateral load analysis; all of the lateral forces are allocated to the walls. Deformation compatibility between the gravity frame and the seismic force-resisting shear walls or braced frames must be maintained.

Similar to dual systems, the concept of the building frame system loses its appeal for structures assigned to SDC A or B, since there is little to be gained from assigning the entire lateral resistance to the shear walls in the absence of any special detailing requirements for the frames. As noted above, a Shear Wall-Frame Interactive System may be more practical and economical in such cases.

RP3-1.1.4   Undefined Structural Systems

ASCE 7 Table 12.2-1 also defines Cantilever Column Systems and Steel Systems Not Specifically Detailed for Seismic Resistance. These systems are not discussed here. Undefined structural systems are any systems not listed in ASCE 7 Table 12.2-1. ASCE 7 Section 12.2.1.1 provides for alternative structural systems.

RP3-1.2   Mechanics of Shear Walls

Shear walls provide resistance to horizontal accelerations of the building mass through shear forces and overturning moments that are transmitted to the building foundation. The internal mechanisms for resisting the shear and moment differ between shear wall types, configurations, materials, and construction. The shear forces may be resisted in elements idealized to be in pure shear (as in plywood shear walls), in a compression strut (concrete and masonry shear walls), or in a diagonal tension field (thin-web steel-plate shear walls).

The overturning moments similarly are resisted by different elements or mechanisms in different wall types. Wood shear walls typically have posts at each end that resist the overturning moment as a force couple, with special hardware providing tension splices and uplift restraint. Concrete shear walls may have designated wall-end boundary elements working in both tension and compression, or may resist overturning moments without special boundary element over the entire wall length at lower strains. The compression component of the overturning moment in concrete walls is not completely distinct from the diagonal compression that resists shear. Additionally, wall "flanges" (typically large segments of perpendicular walls) may provide overturning resistance. Masonry shear walls are similar to concrete shear walls, although masonry walls rarely have special boundary elements and the overturning moment is resisted over the entire wall length at lower strains. In steel-plate shear walls the overturning moment is resisted by means of compression in one of the columns and tension in the other (combined with the diagonal web tension that resists shear).

The preferred yielding mechanism for each type of wall is the one that provides the most reliable inelastic drift capacity. For wood shear walls it is shear deformation, provided largely through bending of nails and deformation of nail holes. For concrete and masonry shear walls it is flexural yielding of the under-reinforced section, with crack formation and elongation of the vertical reinforcement. In steel-plate shear walls it is tension yielding of the steel web plate. Design provisions for these systems generally require proportioning such that the preferred yield mechanism is ensured or made more likely to occur.

RP3-1.3   Design of Concrete Shear Walls

RP3-1.3.1   Cast-in-Place, Non-Prestressed

RP3-1.3.1.1   Ordinary and Special

Cast-in-place shear walls can be designed and detailed as ordinary shear walls by Chapter 11 of ACI 318 (ACI 2014) or as special shear walls by Section 18.10 of ACI 318. There are no intermediate shear walls of cast-in-place concrete. Ordinary shear walls are permitted in buildings assigned to Seismic Design Categories up to C. Special shear walls are required to be used in buildings assigned to SDC D, E, or F.

RP3-1.3.1.2   Squat versus Slender

As clearly indicated in NIST Tech Brief No.6 (Moehle et al. 2011, Revised 2012), "Expected behavior of walls depends partly on wall aspect ratio. Slender walls ($h_w/\ell_w \geq 2.0$) tend to behave much like flexural cantilevers. The preferred inelastic behavior mode of slender walls is ductile flexural yielding, without shear failure. In contrast, walls with very low aspect ratios ($h_w/\ell_w \leq 0.5$) tend to resist lateral forces through a diagonal strut mechanism in which concrete and distributed horizontal and vertical reinforcement resist shear. Wall behavior transitions between these extremes for intermediate aspect ratios. Shear yielding of slender walls generally is considered unacceptable because it reduces inelastic deformation capacity below expected values. Shear yielding of very squat walls is often accepted because such walls tend to have high inherent strength and low ductility demands."

Special shear walls need to be slender, because flexural yielding preceding shear failure is anticipated. That does not necessarily require $h_w/\ell_w \geq 2.0$. $h_w/\ell_w \geq 1.5$ is typically sufficient. To have flexural yielding preceding shear failure becomes more and more of a challenge for lower height to horizontal length ratios.

RP3-1.3.1.3   Design for Shear

A shear wall is designed first for shear and then for combined flexure and axial load. Shear design is essentially the same for ordinary as well as special shear walls, but a couple of important details are different. The required shear strength, V_u, for both ordinary and special shear walls is equal to the factored shear at the critical section, typically at the base of the shear wall (wall-foundation interface) obtained from elastic analysis of the structure containing the shear wall under code-prescribed seismic forces. This has changed drastically for special shear walls in ACI 318-19 (ACI 2019), as indicated in Sections RP3-3.8.2 and RP3-3.8.5.

For ordinary shear walls, the shear-resisting area is the web thickness, h, times be effective depth, which can be taken equal to $0.8\ell_w$ where ℓ_w is the total horizontal length of the shear wall. For special shear walls, the shear resisting area is the web thickness b_w times the total length ℓ_w. In both ordinary and special shear walls, the shear is resisted partly by concrete and partly by horizontal shear reinforcement. In an ordinary shear wall, the concrete contribution, V_c, can be taken equal to $2\sqrt{f_c'}hd$ for walls subject to axial compression or can be calculated by Table 11.5.4.6, where V_c is dependent on the axial compression or tension on the wall. In a special shear wall, V_c is $2\sqrt{f_c'}b_wd$ for $h_w/\ell_w \geq 2.0$, it is $3\sqrt{f_c'}b_wd$ for $h_w/\ell_w \leq 1.5$, and is linearly interpolated between $3\sqrt{f_c'}b_wd$ and $2\sqrt{f_c'}b_wd$ for h_w/ℓ_w between 2.0 and 1.5.

RP3-1.3.1.4   Design for Flexure and Axial Loads

The basic design for flexure and axial loads is the same for ordinary as well as special shear walls. A shear wall cross-section is designed like a column section, with the entire cross-section being effective. The (P_u, M_u) demands from various load combinations must be within the design strength interaction diagram.

RP3-1.3.1.5   Detailing

For ordinary shear walls, detailing the requirements are fairly minimal and are given in ACI 318-14 Sections 11.6 and 11.7.

In a special shear wall, those parts of the shear wall cross-section that are in significant compression must be specially confined. There are two ways of determining whether any part of a shear wall is under significant compression. There is a displacement-based approach for cantilever shear walls hinging at the base, with $h_w/\ell_w \geq 2.0$. Under this approach, the neutral axis depth, c, under the axial load P_u from the counteractive seismic load combination and the corresponding φV_n, is compared against a critical neutral axis depth c_{cr}. If the calculated neutral axis depth is larger than or equal to c_{cr}, the length of specially confined boundary zone at each end must be equal to $c/2$ or $c - 0.1\ell_w$, whichever is larger. The vertical extent of the confined boundary zone above the critical section must be ℓ_w or $M_u/4P_u$, whichever is larger.

Where the displacement based approach is not applicable, if the stress $P_u/A_g + (M_u/I_g)(\ell_w/2)$ at the critical section exceeds $0.2f_c$', a length equal to $c/2$ or $c - 0.1\ell_w$, as in the displacement based approach, must be specially confined. The specially confined boundary zone can be discontinued at the height about the critical section where the above stress falls below $0.15\,f_c$'.

Where special confinement is not required, if the local reinforcement ratio at the ends of a shear wall exceeds $400/f_y$, non-special confinement, as specified in ACI 318-14 Section 18.10.6.5 (a) must be provided.

ACI 318-14 also has provisions to prevent out-of-plane buckling of shear walls under significant compression in Sections 18.10.6.4 (b) and (c).

RP3-1.3.1.6   References for RP3-1.3.1

ACI Committee 318, *Building Code Requirements for Structural Concrete* (ACI 318-14) *and Commentary* (ACI 318R-14), American Concrete Institute, Farmington Hills, MI.

Moehle, J., Ghodsi, T., Hooper, J., Fields, D., and Gedhada, R. (2011, Revised 2012)). *Seismic Design of Cast-in-Place Concrete Special Structural Walls and Coupling Beams: A Guide for Practicing Engineers*, NEHRP Seismic Design Technical Brief 6, NIST GCR 11-917-11REV-1, National Institute of Standards and Technology, Gaithersburg, MD.

RP3-1.3.2   Cast-in-Place, Post-tensioned

Extensive research since the 1990s has shown that the use of unbonded post-tensioning (PT) can result in highly-ductile primary seismic force-resisting structural systems with large self-centering capability and reduced damage. In comparison with precast concrete shear walls (discussed in the following section), previous research on the application of unbonded PT in monolithic cast-in-place (CIP) concrete walls has been limited. An especially successful configuration for high seismic performance has been the special "hybrid" shear wall system where elastic unbonded PT steel for self-centering is combined with yielding mild-steel reinforcement for energy dissipation. Through an analytical investigation, Srivastava (2013) developed closed-form expressions for estimating the lateral load behavior of hybrid-CIP concrete walls with bonded or debonded longitudinal mild steel reinforcement and investigated the effects of design parameters on the lateral load behavior of the walls. Pakiding et al. (2015) conducted a subsequent experimental study on two walls with different amounts of PT strands and mild steel bars crossing the critical base joint with the foundation. The experimental results, which were compared with numerical models, demonstrated the self-centering, energy dissipation, and lateral displacement capacity of the walls. Case studies, real-world applications, conceptual background, and basic guidelines for the design and construction of hybrid-CIP concrete walls for seismic resistance can be found in Panian et al. (2007a,b) and Stevenson et al. (2008). Most recently, Xilin et al. (2017) tested 8 walls with different amounts of mild steel and PT steel crossing the base joint. Different from the other previous studies, these walls utilized steel plates over a predetermined length of the base joint to facilitate the development of a crack, and therefore concentrated rotations, at this location, so as to reduce cracking over the wall height.

RP3-1.3.2.1   References for RP3-1.3.2

Pakiding, L., Pessiki, S., Sause, and Rivera, M. (2015). "Lateral load response of unbonded post-tensioned cast-in-place concrete walls," *Proceedings*, Structures Congress 2015, pp. 1891–1902, Portland, Oregon, USA.

Panian, L., Steyer, M., and Tipping, S. (2007a). "An innovative approach to earthquake safety and concrete construction in buildings." *Journal Post-Tensioning Institute*, 5(1), 7–16.

Panian, L.; Steyer, M.; Tipping, S., "Post-Tensioned Shotcrete Shearwalls," *Concrete International*, October 2007b, Vol. 29, number 10, American Concrete Institute, Farmington Hills, Michigan.

Srivastava, S., Sause, R., Pessiki, S. (2003). "Analytical Lateral Load Response of Unbonded Post-Tensioned Cast-in-Place Concrete Special Structural Walls with Bonded or Debonded Longitudinal Mild Steel Reinforcement," *Department of Civil and Environmental Engineering*, Lehigh University, Bethlehem, PA.

Stevenson, M., Panian, L., Korolyk,M., and Mar, D. (2008). "Post-tensioned concrete walls and frames for seismic-resistance: A case study of the David Brower Center." *Proceedings*, SEAOC Annual Convention, SEAOC, Sacramento, CA.

Xilin, L., Xiangliang, D., Jiang, Q., Ying, Z. (2017). "Experimental Study of Self-Centering Shear Walls with Horizontal Bottom Slits," *Journal of Structural Engineering*, Volume: 143.

RP3-1.3.3   Precast

Precast concrete shear walls can be constructed using single or multiple rectangular wall panels with "emulative" or "jointed" connections. Emulative connections are detailed to result in a precast wall with lateral strength, stiffness, and energy dissipation similar to those of an equivalent monolithic cast-in-place special reinforced concrete wall (Ericson and Warnes 1990). These connections can be designed to undergo flexural yielding (i.e., "ductile" connections) or remain elastic ("i.e., "strong" connections). Walls with ductile connections develop plastic hinges in the connections, while walls with strong connections develop plastic hinges away from the connections. In either case, capacity-design principles are used to ensure that locations other than the selected plastic hinges remain essentially linear-elastic.

According to ACI 318-14 Section 18.11.2.1, special emulative precast walls are required to satisfy ACI 318-14 Sections 18.10 and 18.5.2. 2018 IBC (ICC 2017) Section 1905.1.3 imposes additional requirements to ensure adequate lateral displacement capacity. Emulative precast walls can be constructed by stacking the wall panels on top of each other, with the necessary connections made using deformed reinforcing bars, bonded prestressing steel, or mechanical connectors. Early studies investigated "platform-type" horizontal strong connections (Martin and Korkosz 1982; ACI 550R-96 2001; Oliva et al. 1989, 1990; Armouti 1993), where the floor slab is placed in between the wall panels above and below. Systems where the wall panels directly support each other without the floor slab in between result in simpler horizontal connections (ACI 550R-96 2001; CAE 1999; Park 1995; Seifi et al. 2016) than the platform-type system. Both systems require the use of concrete confinement reinforcement or other special detailing at the wall toes (similar to that used in cast-in-place monolithic wall construction) to ensure that the large compressive strain demands can be sustained in these regions under seismic loading.

In contrast with emulative systems, jointed precast walls are intended to behave differently from monolithic cast-in-place special reinforced concrete walls under lateral loads by allowing the opening of a large concentrated gap at the base joint with the foundation. This gap opening behavior results in rocking-type concentrated rotations of the wall at the base. However, previous research has shown that jointed walls with solely mild steel reinforcing bars grouted across the base joint (Crisafulli et al. 2002; Smith et al. 2013) can suffer from excessive uplift, shear slip, and lateral strength and stiffness degradation due to the accumulation of residual tensile strains in the connection reinforcement under reversed-cyclic loading. In comparison, extremely ductile behavior with large self-centering capability but little energy dissipation develops in the case of walls with solely unbonded PT steel crossing the base joint (Kurama et al. 1999a,b, 2002; Galusha 1999; Allen and Kurama 2002a,b; Holden et al. 2003; Perez et al. 2007, 2013; Erkmen and Schultz 2009; Henry et al. 2012; Belleri et al. 2014a). Practical real-world applications of unbonded PT-

precast concrete walls can be found in the Dominican Republic, New Zealand and Chile (Pampanin et al. 2011; Ghosh and Cleland 2012).

Due to the low energy dissipation capacity associated with unbonded PT connections, a number of researchers have investigated the use of supplemental energy dissipation components in precast concrete walls (Kurama 2000, 2001; Ajrab et al. 2004; Restrepo and Rahman 2007; Marriott et al. 2008). The most successful jointed precast shear wall system to-date is the "hybrid" system, where unbonded PT steel is supplemented with mild steel reinforcement crossing the base joint, as applied to hybrid precast concrete moment frames in Priestley et al. (1999) and Nakaki et al. (1999). The unbonded PT steel is designed to remain elastic and provide self-centering capability while the mild steel reinforcement is designed to yield and provide energy dissipation, resulting in a superior "special" reinforced concrete shear wall system. Hybrid-precast concrete shear walls have been investigated extensively (Rahman and Restrepo 2000; Holden et al. 2001, 2003; Kurama 2002, 2005; Restrepo 2003). Importantly, the system has been shown to satisfy ACI 318-14 Section 18.11.2.2 based on validation testing (Smith et al. 2011, 2013, 2015) according to ACI ITG 5.1-07 (2007) and accompanying design guidelines in ACI ITG 5.2-09 (2009). Full seismic design and detailing recommendations can be found in Smith and Kurama (2014) to ensure that the walls satisfy ACI 318-14 and ACI ITG 5.1-07 requirements for special RC structural walls.

RP3-1.3.3.1   Design of Precast Concrete Walls

Precast concrete shear walls can be designed and constructed as efficient and high-performing primary seismic force-resisting elements in building structures. Individual wall panels are produced (prefabricated) in a manufacturing facility, transported to the building site, and erected and connected in the field, resulting in cost-effective, rapid, and high-quality construction. The following sections provide a general overview of the types of precast wall configurations, as well as their construction, behavior, design, and analysis.

RP3-1.3.3.2   Shear Wall System Description, Construction, and Performance

Precast concrete shear walls can be constructed using single or multiple rectangular (uniform-thickness) wall panels. Possible wall configurations are shown in Figure 1.3-1. Walls can be uncoupled or coupled, with each pier consisting of single or multiple panels connected along horizontal joints. Coupling of piers can be developed using connectors along vertical joints or coupling beams at floor levels.
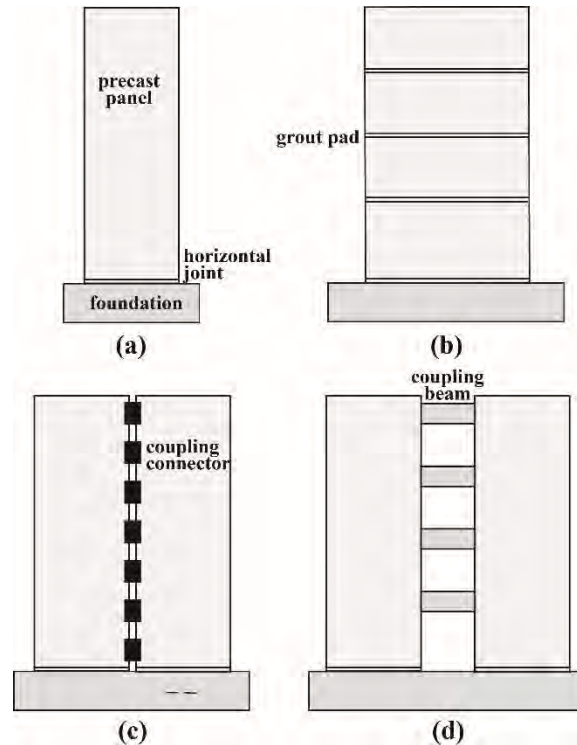
Figure 1.3-1 Precast walls (reinforcement note shown): (a) single panel wall; (b) multi panel wall; (c) coupled wall with vertical joint; (d) coupled wall with coupling beams

The regions of a wall where adjacent precast panels are erected against each other or against the foundation are generally referred to as "joints," while the term "connection" generally refers to the hardware and reinforcement components that provide stiffness and strength across a joint. A small construction space is incorporated at each joint to allow for tolerances and alignment of the panel; this space is then filled with non-shrink fiber-reinforced grout. Connections between the precast panels and between the base panel and the foundation are the most critical components of a precast concrete shear wall and require special attention to detailing for load path, strength, stiffness, and ductility. Connections are typically completed in the field during erection; and thus, quality control during the erection process is also of utmost importance. Bolted or welded embedded mechanical hardware (e.g., steel plates and proprietary inserts), embedded or grouted deformed steel bars, and/or bonded or unbonded post-tensioning steel (PCI 2010; PTI 2006) are typical components used in the connections of different types of precast concrete shear walls.

Precast shear walls can be detailed and constructed as "emulative" or "jointed" walls. Emulative walls are designed to have lateral strength, stiffness, and energy dissipation similar to those of an equivalent monolithic cast-in-place special reinforced concrete shear wall (Ericson and Warnes 1990), as depicted in Figure 1.3-2. As such, the nonlinear lateral load behavior of an emulative precast wall occurs through the yielding of the reinforcement and associated extensive cracking of the concrete. The axial-flexural nonlinear behavior can be designed as plastic hinges at the panel-to-panel and panel-to-foundation horizontal connections. These connections are referred to as "ductile" connections. Conversely, in the case of "strong" connections, the connections remain essentially linear-elastic while the plastic hinging occurs adjacent to or away from the joints. Connections for emulative walls are typically made using deformed steel reinforcing bars, bonded post-tensioning steel, and/or mechanical hardware, with specific details that can be found in ACI 550R-96 (ACI 2001). While early studies investigated emulative walls using "platform-type" strong horizontal connections (Martin and Korkosz 1982; ACI 550R-96 2001; Oliva et al. 1989, 1990; Armouti 1993), where the floor slab is placed in between the wall panels above and below,

systems where the wall panels are directly stacked without the floor slab in between result in simpler details (ACI 550R-96 2001; CAE 1999; Park 1995; Seifi et al. 2016).
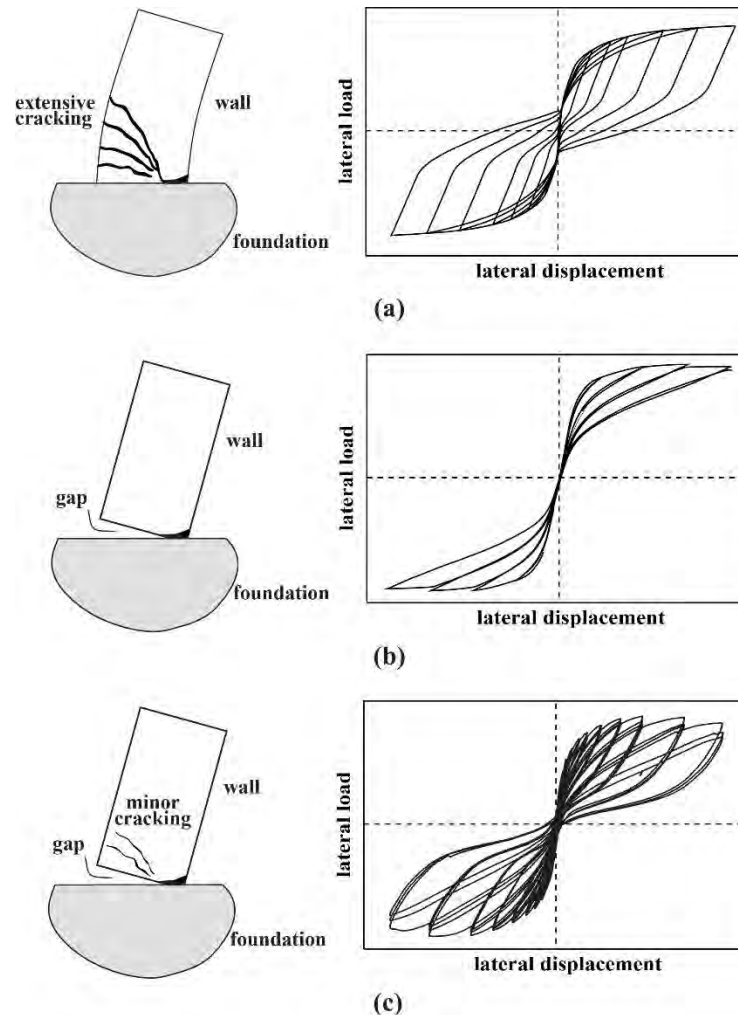
Figure 1.3-2 Lateral load behaviors: (a) monolithic cast-in-place wall; (b) unbonded post-tensioned jointed (rocking) wall; (c) hybrid jointed (rocking) wall

Jointed precast walls (also referred to as "non-emulative" walls) are designed to behave differently than emulative precast walls, and therefore differently than monolithic cast-in-place special reinforced concrete shear walls. Specifically, in jointed precast walls, most of the nonlinear axial-flexural deformations are concentrated through a controlled rocking mechanism (i.e., concentrated rotational mechanism) at a selected critical joint (usually the base joint above the foundation). This rocking behavior develops by the opening (during lateral loading) and subsequent closing (upon unloading) of a gap at the selected joint, taking advantage of the unique discrete nature of precast construction. As a major advantage, the concentrated gap opening rotations allow the wall to undergo large nonlinear lateral displacements with little damage to the precast panels.

The critical gap opening joint in a jointed wall needs to be reinforced using a ductile connection for adequate lateral strength, stiffness, and energy dissipation. Tests of jointed walls with only deformed steel reinforcing bars across the gap opening joint (Crisafulli et al. 2002; Smith et al. 2013) have shown large energy dissipation, like that of an emulative wall, but premature failure can occur from excessive uplift,

shear slip, and lateral strength and stiffness degradation of the wall due to the accumulation of residual tensile strains in the bars under reversed-cyclic lateral loading. Conversely, fully post-tensioned jointed walls (Kurama et al. 1999a,b, 2002; Galusha 1999; Allen and Kurama 2002a,b; Holden et al. 2003; Perez et al. 2007, 2013; Erkmen and Schultz 2009; Henry et al. 2012; Belleri et al. 2014a) with only unbonded post-tensioning (PT) steel (usually in the form of multi-strand tendons) have extremely ductile, nearly nonlinear-elastic behavior (Figure 1.3-2b) with little or no damage to the wall panels or yielding of the PT steel. However, as a major disadvantage, the hysteretic energy dissipation of a fully post-tensioned wall is low, which may result in increased seismic displacement demands (Priestley and Tao 1993; Farrow and Kurama 2003; Seo and Sause 2005).

Thus, to satisfy the energy dissipation requirements of current building design codes, jointed precast concrete shear walls need to be designed with supplemental energy dissipation components (Kurama 2000, 2001; Ajrab et al. 2004; Restrepo and Rahman 2007; Marriott et al. 2008). Out of the jointed precast walls tested to-date, the "hybrid" system has been the most successful (Rahman and Restrepo 2000; Holden et al. 2001, 2003; Kurama 2002, 2005; Restrepo 2003), where unbonded multi-strand PT tendons are supplemented with deformed steel reinforcing bars crossing the critical gap opening joint. The unbonded PT steel is designed to remain elastic and provide self-centering (restoring) capability to the wall, while the deformed steel reinforcement is designed to yield and provide energy dissipation, resulting in a superior system with an efficient combination of large energy dissipation and large self-centering capability (Figure 1.3-2c). As a critical detail, a predetermined length of each energy dissipation (ED) bar is unbonded from the concrete (by wrapping the bar inside a plastic sleeve) to ensure that the maximum tension strains of the steel remain within an allowable range.

The deliberate unbonding of the PT steel in jointed walls allows the steel to remain linear-elastic by distributing the elongations of the steel (upon gap opening) uniformly over the entire unbonded length (often over the entire wall height), rather than being concentrated at the rocking joint. As an added benefit, no significant tension stresses are transferred to the concrete from the elongation of the PT steel during gap opening, thereby reducing the cracking of the concrete. Up until the initiation of gap opening (which occurs when the lateral load moment at the joint overcomes the precompression from the PT force and gravity loads), the initial lateral stiffness of a jointed wall is similar to that of a comparable emulative wall. Stiffness reduction (and thereby nonlinear behavior) is initiated and dominated by the opening of a discrete gap, which reduces the wall cross-section in contact at the joint and provides geometry-based (rather than material yielding-based) nonlinearity. Upon unloading, the PT and gravity forces provide a restoring (self-centering) effect that pulls the wall back to its original undisplaced position, closing the gap and reducing the residual (i.e., plastic) lateral displacements. By keeping the PT steel elastic, the initial prestress force is maintained when the wall returns to zero lateral displacement after being subjected to large nonlinear cyclic displacements.

RP3-1.3.3.3   Shear Wall Design

Governing design requirements for precast concrete shear walls are given by the 2018 IBC (ICC 2017), ASCE/SEI 7-16 (ASCE 2016), and ACI 318-14 (ACI 2014). Additional important resource documents for wall design are the National Earthquake Hazards Reduction Program (NEHRP) *Provisions* (BSSC 2015), PCI Design Handbook (PCI 2010), and PCI Seismic Design Manual (Cleland and Ghosh 2012).

In general, the design of emulative special precast concrete shear walls is subject to the following requirements:

- According to ACI 318-14 Section 18.11.2.1, emulative special precast concrete shear walls shall satisfy all requirements of ACI 318-14 Section 18.10 for special monolithic cast-in-place reinforced concrete shear walls.

- In general, capacity-design principles shall be used to ensure that strong connections and locations other than the selected plastic hinges remain essentially linear-elastic.
- There shall be compliance with ACI Section 18.5.2, where yielding in the connections is restricted to steel components or reinforcement, and connection components that are not intended to yield are designed for at least 1.5 times the strength of the yielding components (based on capacity design principles).
- The design of connection components shall include adequate anchorage to concrete according to Chapter 17 of ACI 318-14.
- According to the 2018 IBC (ICC 2017) Section 1905.1.3, "*connections that are designed to yield shall be capable of maintaining 80% of their design strength at the deformation induced by the design displacement or shall use Type 2 mechanical splices.*" ACI 318-14 Section 18.2.7.1 requires Type 2 splices to be "*capable of developing the specified tensile strength of the spliced bars*", and according to Section 18.2.7.2 of ACI 318-14, Type 2 splices are permitted at any location of a wall, including yielding regions. However, Type 2 grouted splices of ED bars in jointed precast walls have experienced failure due to bond pullout of the bars under cyclic loading (Smith and Kurama 2014) tested according to ACI ITG 5.1-07 (2007). Thus, Type 2 grouted splices should not be used for the ED bars, including yielding bars in plastic hinges of emulative special precast concrete shear walls.

Seismic provisions for jointed special precast concrete shear walls are given in ACI 318-14 Section 18.11.2.2, which specifies acceptance criteria based on satisfactory validation testing subjected to a prescribed displacement procedure and validation drift amplitude according to ACI ITG 5.1-07 (ACI 2007). Additionally, the commentary to ACI 318-14 Section 18.11.2.2 refers to ACI ITG 5.2-09 (ACI 2009), which provides design requirements for wall satisfying ACI ITG-5.1. Based on testing according to ACI ITG 5.1-07 (2007), the hybrid precast wall system has been validated as a special reinforced concrete shear wall system (Smith et al. 2011, 2013, 2015). Seismic design and detailing recommendations can be found in Smith and Kurama (2014) to ensure that the walls satisfy ACI ITG 5.1-07 performance requirements as follows:

- Capacity-design principles shall be used to ensure that no significant gap opening or nonlinear material behavior occurs at joints other than the critical gap opening joint.
- There shall be adequate restoring force from post-tensioning and gravity loads to ensure that the gap at the critical joint fully closes upon unloading. Prestress losses from cycling of the wall at the validation drift shall be considered when determining the available restoring force.
- There shall be no significant shear slip at the horizontal joints.
- The post-tensioning steel shall be in the essentially linear-elastic range, with strains not exceeding 0.01 mm/mm through the validation drift.
- The energy-dissipating bars shall undergo significant yielding to satisfy the minimum energy-dissipation requirements of ACI ITG 5.1-07 (2007), but shall not fracture through cycling of the wall up to the validation drift.
- Adequate concrete confinement reinforcement shall be designed adjacent to the gap opening joint to prevent crushing of the confined concrete through cycling of the wall up to the validation drift.
- The PT tendons and the energy dissipation bars shall be adequately anchored to the concrete.
- The wall panels shall be adequately reinforced and detailed for the maximum moment and shear demands at the validation drift. Additionally, reinforcement shall be placed along the edge of the panel undergoing the concentrated gap opening rotation.

RP3-1.3.3.4   Shear Wall Analytical Modeling

Because of comparable wall behavior and mechanisms, the analytical modeling of emulative walls generally follows similar procedures as the modeling of monolithic cast-in-place reinforced concrete shear walls. In comparison, modeling of jointed walls require special techniques necessary to analyze the effects of the concentrated gap opening. Three different modeling tools, as depicted in Figure 1.3-3, that can be

used in the seismic design and analysis of hybrid precast concrete shear walls can be found in Smith and Kurama (2012): (1) a linear-elastic effective stiffness model; (2) a simplified nonlinear finite element model; and (3) a fiber element model. These analytical models intentionally incorporate several simplifying assumptions appropriate for the design office and have been validated based on the results from the experimental program.

The linear-elastic effective stiffness model can be used as part of the equivalent lateral force procedure in ASCE 7 (2016). Some of the important model features are:

- The effective flexural stiffness of the wall after gap opening but before significant material nonlinearity can be modeled using an effective moment of inertia of the wall cross-section that accounts for the extent of gap opening.
- Shear deformations are incorporated using an effective shear area. For perforated walls, the effective shear area is significantly reduced.

The finite element model is a simplified tool intended for the design of panels with perforations as well as to conduct nonlinear pushover analyses. Some of the important model features are:

- "Hard contact" surfaces are used at the horizontal joints to model for gap opening. These surfaces are defined with "rough" friction, which prevents joint slip when the surfaces are in contact.
- The wall panel concrete is modeled using linear-elastic properties in tension. The reinforcement contained within each panel is not modeled explicitly. This major simplification is possible because the tension deformations of the wall are concentrated as gap opening, with little cracking in the panels.
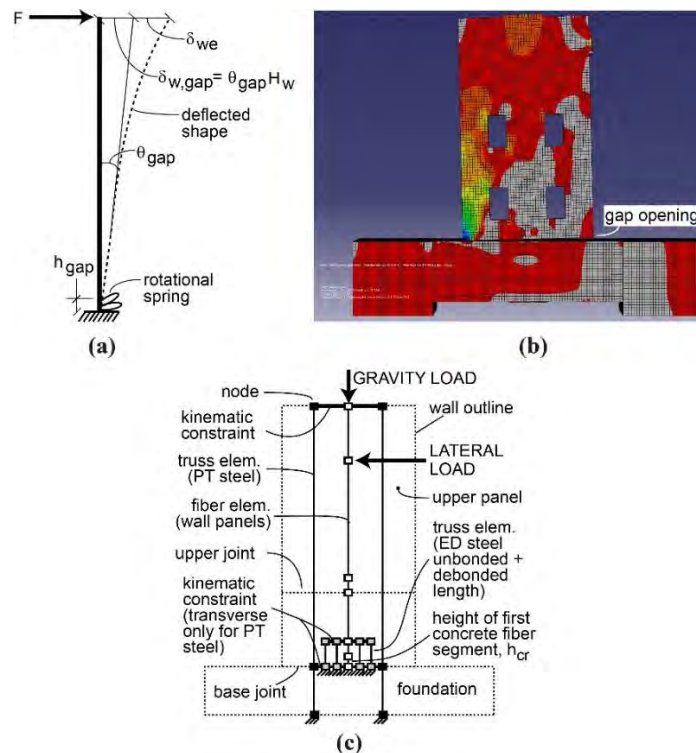- Elements modeling the ED bars are partitioned into bonded and unbonded regions.

Figure 1.3-3 Analytical modeling of hybrid walls: (a) linear-elastic effective stiffness model; (b) nonlinear finite element model; (c) fiber element model

The fiber element model is an effective tool to conduct nonlinear reversed-cyclic and dynamic response history analyses of hybrid walls under seismic loading. The goal is to accurately reproduce the hysteretic behavior of the structure including gap opening/closing at the horizontal joints and hysteretic stress-strain behaviors for the materials. Some of the important model features are:

- Fiber beam-column elements are used to represent the axial-flexural behavior of the precast wall panels. The shear stiffness of the panels is assumed to remain constant at the effective stiffness given by the linear-elastic effective stiffness model.
- To simulate the effect of gap opening, the tension strength of the concrete fibers at the bottom of the panel undergoing gap opening rotation is set to zero over a critical height.
- Outside the gap-opening joint region, the wall panel concrete is modeled as linear-elastic in tension (i.e., similar to the finite element model, the cracking of the concrete is ignored and the deformed steel reinforcement contained within each wall panel is not modeled explicitly).
- The bonded lengths of the ED bars are not modeled explicitly but represented through kinematic constraints to corresponding fiber element nodes for the wall panels at the same elevation (the actual bonded lengths of the ED bars are not modeled).
- The unbonded lengths of the ED bars are modeled using discrete steel elements separate from the fiber beam-column elements modeling the wall panels.
- The deformed steel bars across joints designed not to open a significant gap can be modeled using linear-elastic steel fibers over a short height of the fiber elements modeling the wall panels. The effect of any gap opening (albeit small) in these regions can be modeled by using "compression-only" material properties for the concrete fibers (i.e., the tension strength of the concrete is taken as zero), similar to the critical gap opening joint. Concrete with linear-elastic tension properties is used to model the remaining height of each wall panel.
- The stiffness of the PT steel should be reduced to account for the localized concrete and anchorage deformations at the tendon ends, since these local deformations cannot be captured by the fiber elements modeling the wall panels.

The finite element and fiber element models also share the following common features:

- The total unbonded length of the ED bars includes an additional length of "debonding," which is assumed to occur as a result of cyclic loading. This increased unbonded length is assumed to remain constant throughout the analysis.
- The concrete confinement reinforcement in the wall panels is not modeled explicitly but rather represented by incorporating the effect of the confinement on the nonlinear stress-strain relationship of the concrete in compression.
- The grout pads at the horizontal joints are not modeled explicitly. Instead, the grout thickness is modeled as part of the wall panels assuming that the grout and panel concrete behave similarly.
- In modeling the hysteretic behavior of the ED bars crossing the gap opening joint, Bauschinger effect of the steel should be included so as not to over-estimate the energy dissipation of the wall.

Shear Wall System Additional Resources: Extensive research conducted since the 1980s has led to the development of the precast concrete shear wall systems described above. An overview of the state of the art of these advances, including code developments and practical applications, can be found in Kurama et al. (2018).

RP3-1.3.3.5   References for RP3-1.3.3

ACI (American Concrete Institute). (2001). "Design recommendations for precast concrete structures (reapproved 2001)." *ACI 550R-96*, Farmington Hills, MI.

ACI (American Concrete Institute). (2007). "Acceptance criteria for special unbonded post-tensioned precast structural walls based on validation testing and commentary." *ACI ITG 5.1-07*, Farmington Hills, MI.

ACI (American Concrete Institute). (2009). "Requirements for design of a special unbonded post-tensioned precast shear wall satisfying ACI ITG-5.1 and commentary." *ACI ITG 5.2-09*, Farmington Hills, MI.

ACI (American Concrete Institute). (2014). "Building code requirements for structural concrete and commentary." *ACI Committee 318-14*, Farmington Hills, MI.

Ajrab, J., Pekcan, G., and Mander, J. (2004). "Rocking wall-frame structures with supplemental tendon systems." *Journal of Structural Engineering*, ASCE, 130(6), 895–903.

Allen, M., and Kurama, Y. (2002a). "Design of rectangular openings in precast walls under combined vertical and lateral loads." *PCI Journal*, 47(2), 58–83.

Allen, M., and Kurama, Y. (2002b). "Design of rectangular openings in precast walls under vertical loads." *PCI Journal*, 47(1), 50–67.

Armouti, N. (1993). "Seismic performance of precast concrete structural walls." Ph.D. dissertation, Lehigh Univ., Bethlehem, PA.

ASCE. (2010). "Minimum design loads for buildings and other structures." *ASCE/SEI 7-10*, Reston, VA.

Belleri, A., Brunesi, E., Nascimbene, R., Pagani, M., and Riva, P. (2014a). "Seismic performance of precast industrial facilities following major earthquakes in the Italian territory." *Journal of Performance of Constructed Facilities*, ASCE, 29(5).

BSSC (Building Seismic Safety Council). (2015). *NEHRP recommended seismic provisions for new buildings and other structures*, Washington, DC.

CAE (Centre for Advanced Engineering). (1999). *Guidelines for the use of structural precast concrete in buildings*, Christchurch, New Zealand.

Cleland, N. and Ghosh, S. K. (2012). *Seismic design of precast/prestressed concrete structures* (MNL-140-12), Second Edition, Precast/Prestressed Concrete Institute, Chicago, IL.

Crisafulli, F. J., Restrepo, J. I., and Park, R. (2002). "Seismic design of lightly reinforced precast concrete rectangular wall panels." *PCI Journal*, 47(4), 104–121.

Ericson, A. C., and Warnes, C. E. (1990). *Seismic technology for precast concrete systems*, Concrete Industry Board, Inc., Kew Gardens, NY.

Erkmen, B., and Schultz, A. E. (2009). "Self-centering behavior of unbonded, post-tensioned precast concrete shear walls." *Journal of Earthquake Engineering*, 13(7), 1047–1064.

Farrow, K. T., and Kurama, Y. C. (2003). "SDOF demand index relationships for performance-based seismic design." *Earthquake Spectra*, 19(4), 799–838.

Galusha, J. G. (1999). "Precast, post-tensioned concrete walls designed to rock." M.S.C.E. thesis, Univ. of Washington, Seattle.

Henry, R. S., Brooke, N. J., Sritharan, S., and Ingham, J. M. (2012). "Defining concrete compressive strain in unbonded post-tensioned walls." *ACI Structural Journal*, 109(1), 101–112.

Holden, T., Restrepo, J., and Mander, J. (2001). "A comparison of the seismic performance of precast wall construction: Emulation and hybrid approaches." *Report No. 2001-4*, Univ. of Canterbury, Christchurch, New Zealand.

Holden, T., Restrepo, J., and Mander, J. B. (2003). "Seismic performance of precast reinforced and prestressed concrete walls." *Journal of Structural Engineering*, ASCE, 129(3), 286–296.

IBC (International Building Code). (2015). "2015 international building code." *IBC-15*, International Code Council, Country Club Hills, IL.

Kurama, Y. (2000). "Seismic design of unbonded post-tensioned precast walls with supplemental viscous damping." *ACI Structural Journal*, 97(4), 648–658.

Kurama, Y. (2001). "Simplified seismic design approach for friction-damped unbonded post-tensioned precast walls." *ACI Structural Journal*, 98(5), 705–716.

Kurama, Y. (2002). "Hybrid post-tensioned precast concrete walls for use in seismic regions." *PCI Journal*, 47(5), 36–59.

Kurama, Y. (2005). "Seismic design of partially post-tensioned precast concrete walls." *PCI Journal*, 50(4), 100–125.

Kurama, Y., Pessiki, S., Sause, R., and Lu, L. W. (1999a). "Seismic behavior and design of unbonded post-tensioned precast concrete walls." *PCI Journal*, 44(3), 72–89.

Kurama, Y., Sause, R., Pessiki, S., and Lu, L. W. (1999b). "Lateral load behavior and seismic design of unbonded post-tensioned precast concrete walls." *ACI Structural Journal*, 96(4), 622–632.

Kurama, Y., Sause, R., Pessiki, S., and Lu, L.W. (2002). "Seismic response evaluation of unbonded post-tensioned precast walls." *ACI Structural Journal*, 99(5), 641–651.

Kurama, Y., Sritharan, S., Fleischman, R., Restrepo, J., Henry, R., Cleland, N., Ghosh, S.K., and Bonelli, P. (2018). "Seismic-Resistant Precast Concrete Structures: State of the Art," *Journal of Structural Engineering*, ASCE, 144(4).

Marriott, D., Pampanin, S., Bull, D., and Palermo, A. (2008). "Dynamic testing of precast, post-tensioned rocking wall systems with alternative dissipating solutions." *Bulletin of the New Zealand Society for Earthquake Engineering*, 41(2), 90–103.

Martin, L., and Korkosz, W. (1982). "Connections of precast prestressed concrete buildings, including earthquake resistance." *Technical Report No. 2*, Prestressed Concrete Institute, Chicago.

Oliva, M., Clough, R., and Malhas, F. (1989). "Seismic behavior of large panel precast concrete walls: Analysis and experiment." *PCI Journal*, 34(5), 42–66.

Park, R. (1995). "A perspective on the seismic design of precast concrete structures in New Zealand." *PCI Journal*, 40(3), 40–60.

PCI (Precast/Prestressed Concrete Institute). (2010). *PCI design handbook*, 7th Ed., Chicago.

Perez, F. J., Pessiki, S., and Sause, R. (2013). "Experimental lateral load response of unbonded post-tensioned precast concrete walls." *ACI Structural Journal*, 110(6), 1045–1055.

Perez, F. J., Sause, R., and Pessiki, S. (2007). "Analytical and experimental lateral load behavior of unbonded posttensioned precast concrete walls." *Journal of Structural Engineering*, ASCE, 133(11), 1531–1540.

Priestley, M., and Tao, J. (1993). "Seismic response of precast prestressed concrete frames with partially debonded tendons." *PCI Journal*, 38(1), 58–69.

PTI (Post-Tensioning Institute). (2006). *Post-tensioning manual*, 6th Ed., Farmington Hills, MI.

Rahman, A., and Restrepo, J. (2000). "Earthquake resistant precast concrete buildings: Seismic performance of cantilever walls prestressed using unbonded tendons." *Report No. 2000-5*, Univ. of Canterbury, Christchurch, New Zealand.

Restrepo, J. I. (2003). "Self-centering precast post-tensioned cantilever walls: Theory and experimental work." *Structures Congress*, ASCE, Seattle.

Restrepo, J. I., and Rahman, A. (2007). "Seismic performance of self-centering structural walls incorporating energy dissipators." *Journal of Structural Engineering*, ASCE, 133(11), 1560–1570.

Seifi, P., Henry, R. S., and Ingham, J. M. (2016). "Panel connection details in existing New Zealand precast concrete buildings." *Bulletin of the New Zealand Society for Earthquake Engineering*, 49(2), 190–199.

Seo, C., and Sause, R. (2005). "Ductility demands on self-centering systems under earthquake loading." *ACI Structural Journal*, 102(2), 275–285.

Smith, B. J., and Kurama, Y. C. (2012). "Seismic Design Guidelines for Special Hybrid Precast Concrete Shear Walls." *Research report NDSE-2012-02*, University of Notre Dame, Notre Dame, IN,, 88 pp.

Smith, B., and Kurama, Y. (2014). "Seismic design guidelines for solid and perforated hybrid precast concrete shear walls." *PCI Journal*, 59(3), 43–59.

Smith, B., Kurama, Y., and McGinnis, M. (2011). "Design and measured behavior of a hybrid precast concrete wall specimen for seismic regions." *Journal of Structural Engineering*, ASCE, 137(10), 1052–1062.

Smith, B., Kurama, Y., and McGinnis, M. (2013). "Behavior of precast concrete shear walls for seismic regions: Comparison of hybrid and emulative specimens." *Journal of Structural Engineering*, ASCE, 139(11), 1917–1927.

Smith, B., Kurama, Y., and McGinnis, M. (2013). "Behavior of precast concrete shear walls for seismic regions: Comparison of hybrid and emulative specimens." *Journal of Structural Engineering*, ASCE, 139(11), 1917–1927.

Smith, B., Kurama, Y., and McGinnis, M. (2015). "Perforated hybrid precast shear walls for seismic regions." *ACI Structural Journal*, 112(3), 359–370.

RP3-1.4 Design of Masonry Shear Walls

RP3-1.4.1 Introduction

Masonry shear walls provide the lateral force resisting system for masonry buildings. Unreinforced masonry shear walls can be used in low seismic areas, Seismic Design Categories A and B. Reinforced masonry shear walls are required in Seismic Design Category C and higher, with special reinforced masonry shear walls required in Seismic Design Category D and higher. The focus of the topics in this Resource Paper will be on reinforced masonry shear walls.

There are two types of reinforced masonry shear walls, partially grouted and solidly grouted. In partially grouted construction, only the vertical cells and horizontal courses containing reinforcement are grouted. The advantage of partial grouting is that it saves on material, and a partially grouted wall has a mass of approximately half that of a solidly grouted wall, thus reducing the seismic demand, particularly for out-of-plane loads.

The overturning moment in a reinforced masonry shear wall is resisted by vertical reinforcement. Shear is resisted by a combination of masonry and shear reinforcement. Shear reinforcement in a masonry shear wall is horizontal reinforcement that is placed in bond beams.

RP3-1.4.2 Design Methods

The current TMS 402 Building Code Requirements for Masonry Structures (TMS 2016) has two methods for the design of reinforced masonry shear walls: allowable stress design and strength design. Three failure modes need to be considered, which are overturning (combination of flexural and axial load), shear, and sliding.

Strength design results in much more efficient designs for overturning for walls with distributed reinforcement. This is due to almost all of the intermediate reinforcement having yielded at the nominal strength, while in allowable stress design, the behavior is considered to be linear elastic and intermediate reinforcement is at lower stress than the outermost, or jamb, reinforcement. Figure 1.4-1 provides a comparison of the interaction diagrams for two 16 ft long masonry shear walls, one designed by allowable stress design and one by strength design. The shear wall designed using strength design has No. 4 bars at 48 inches, for a total of five No. 4 bars. The shear wall designed using allowable stress design has No. 5 bars with a spacing at the end of 32 inches, and an intermediate spacing of 40 inches, for a total of six No. 5 bars. For comparison, the strength design interaction diagram is reduced to an allowable stress level by multiplying the nominal strength by the strength reduction factor, and multiplying by the allowable stress seismic load factor of 0.7. As can be seen, allowable stress design requires almost twice the reinforcement as strength design to give the same capacity.
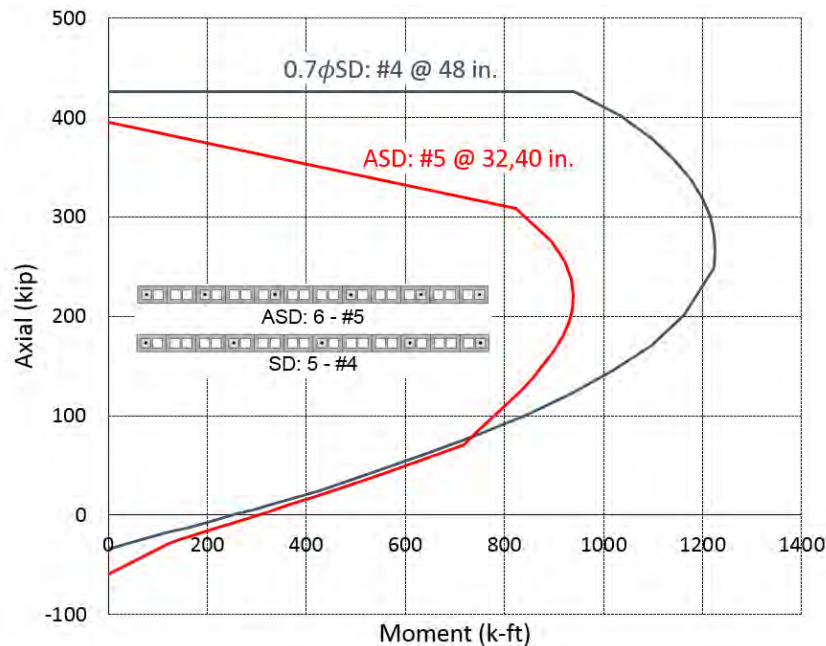
Figure 1.4-1 Comparison of Shear Wall Designed by Allowable Stress and Strength Design

The allowable shear stresses for masonry shear walls were recalibrated in the 2011 TMS 402 masonry standard (TMS 2011). The strength design provisions were converted to allowable stress provisions by dividing by area to go from nominal strength to stress and using a factor of safety of approximately 2. Thus, allowable stress and strength design will give approximately the same design. The shear strength is determined as the sum of the shear strength due to the masonry and the shear strength due to shear reinforcement.

Shear walls that have a low axial compressive load and a low shear-span ratio are vulnerable to shear sliding, which normally occurs at the base. To account for this, shear friction provisions were added in the 2016 TMS 402 masonry standard (TMS 2016). The provisions were developed so that allowable stress design and strength design give approximately the same design.

Two sources for information on the design of masonry shear walls are the Reinforced Masonry Engineering Handbook (2017) and the Masonry Designers Guide (2016).

RP3-1.4.3 Seismic Design

With respect to seismic design, there are three types of reinforced masonry shear walls: ordinary reinforced shear walls, intermediate reinforced shear walls, and special reinforced shear walls. Special reinforced shear walls are required in Seismic Design Category D and higher. The prescriptive reinforcement requirements for ordinary reinforced shear walls and intermediate reinforced shear walls are similar, with reinforcement being required around openings, at the corners and ends of the wall, at control joints, at diaphragm levels and at the top of the wall. The only difference in prescriptive reinforcement for an ordinary reinforced masonry shear wall and an intermediate reinforced masonry shear wall is that vertical reinforcing bars have to be at a maximum of 4 ft with intermediate reinforced masonry shear walls, but can have a spacing of up to 10 ft with ordinary reinforced masonry shear walls.

There are four requirements for special reinforced masonry shear walls. First, there is a minimum reinforcement ratio of 0.0007 in each direction and the sum of the vertical and horizontal reinforcement ratios has to be at least 0.002. This prescriptive reinforcement is often sufficient to provide the needed flexural and shear strength of the shear wall. The second requirement is a limitation on spacing of the reinforcement. The third requirement is a maximum reinforcement limitation to prevent toe crushing, and is discussed later. The fourth requirement is a capacity design requirement for shear. In both allowable stress design and strength design, the requirements effectively amount to the design shear being approximately doubled to prevent a brittle shear failure of the wall, and promote the formation of a ductile plastic hinge.

The maximum reinforcement requirements for special reinforced shear walls designed using allowable stress design are not very stringent, and typically do not control the design. The maximum reinforcement requirements in strength design can be met by either using boundary elements, or limiting the reinforcement. Boundary element provisions are not fully developed for masonry and are typically not used except that for low axial loads and low shear demand, the boundary element requirements are waived, thus allowing any amount of reinforcement to be used. For higher axial loads and/or higher shear demands, the reinforcement is limited based on a strain gradient of the maximum useable compressive strain in the extreme compression fiber of the masonry and a strain in the reinforcement of four times the yield strain. If the shear span ratio (factored moment divided by a quantity equal to the factored shear times the length of the wall) is less than one, which is a squat wall, the strain gradient is based on a strain in the reinforcement of 1.5 times the yield strain.

A final method of design is a limit design method, which was added as an appendix in the 2013 TMS 402 masonry standard (TMS 2013). This method is based on a yielding mechanism, and requires checking not only the mechanism strength but also the mechanism deformation. The limit design method does not have any maximum reinforcement limitations and is useful for shear walls with openings.

A source of information specific to special reinforced masonry shears walls is Seismic Design of Special Reinforced Masonry Shear Walls, A Guide for Practicing Engineers (2009).

RP3-1.4.4   References for RP3-1.4

Kingsley, G.R., Shing, P.B., and Gangel, T. (2014). *Seismic Design of Special Reinforced Shear Walls, A Guide for Practicing Engineers*, NEHRP Seismic Design Technical Brief No. 9, National Institute of Standards and Technology, Gaithersburg, MD..

MIA (2017). *Reinforced Masonry Engineering Handbook*, 8th edition, Masonry Institute of America, Torrance, CA.

TMS (2011). *Building Code Requirements for Masonry Structures* (TMS 402-11/ACI 530-11/ASCE 5-11). The Masonry Society, Longmont, CO.

TMS (2013). *Building Code Requirements for Masonry Structures* (TMS 402-13/ACI 530-13/ASCE 5-13). The Masonry Society, Longmont, CO.

TMS (2016). *Building Code Requirements for Masonry Structures* (TMS 402-16). The Masonry Society, Longmont, CO.

TMS (2016). *Masonry Designers Guide*, The Masonry Society, Longmont, CO.

RP3-1.5   Design of Steel Plate Shear Walls

RP3-1.5.1   Basic terminology, behavior, and modeling

Steel plate shear walls used as modern seismic force-resisting systems in the U.S., and denoted Special Plate Shear Walls (SPSWs) in AISC 341-16 (note that this summary will refer largely to the 2016 version of the AISC Seismic Provisions for Steel Building, AISC 341-16) (AISC 2016), consist of a moment frame of beams and columns infilled with thin steel plates as illustrated in Figure 1.5-1. AISC 341 refers to infill plates as web plates, columns as vertical boundary elements (VBEs) and beams as horizontal boundary elements (HBEs). SPSWs are assigned a seismic force modification factor, *R*, of 7 in ASCE 7-16 (ASCE 2016).
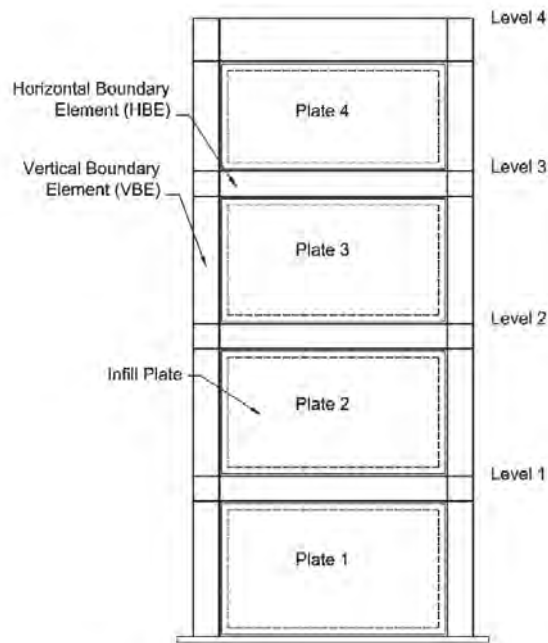
Figure 1.5-1 Special Plate Shear Wall (Berman and Bruneau, 2004)

Steel plate shear walls have been used around the world with both stiffened and unstiffened web plates. Sabelli and Bruneau (2006) provide an excellent summary of the research and thinking that went into the first development of the AISC 341 provisions for SPSW design which appeared in 2005. In the U.S., and specifically in AISC 341, unstiffened web plates that resist the design shear forces through the development of a post-buckling diagonal tension field are required as they have been found to have superior ductility. Figure 1.5-2 shows diagonal tension field action occurring in a test of a thin web plate. SPSWs can be thought of as analogous to vertically cantilevered plate girders, where the VBEs act as the flanges and carry the overturning moment while the web plates carry the story shear forces and the HBEs act as intermediate web stiffeners. A key difference is that the VBEs in SPSWs provide considerable stiffness and help develop

a complete tension field in the web plate as opposed to the partial tension field that occurs in plate girders.

Figure 1.5-2 Diagonal Tension Field in Thin Web Plate (Webster, 2013)

The thin web plates used in SPSWs have small buckling capacity, and the lateral force-deformation behavior of the web plate alone under cyclic lateral loading is pinched as shown in Figure 1.5-3 and not unlike tension-only braces. Thus, to meet the requirements for SPSW in AISC 341, the thin web plates must be used inside a moment resisting frame meeting selected requirements for ordinary, intermediate, and special moment frames (OMF, IMF, and SMF). Figure 1.5-4 shows the hysteretic behavior of a steel plate shear test specimen with fully restrained HBE-to-VBE connections (in this case RBS connections were used). Note the maximum story drift obtained was nearly 5% before the HBE-to-VBE connection failed, illustrating the exceptional deformation capacity of the SPSW system. Considering the full system response, there are three sources of yielding and ductility in SPSWs: the web plates in tension field action, the HBEs in flexure, and the VBEs in flexure. Note that the HBEs and VBEs can have large axial and shear forces in addition to moment.

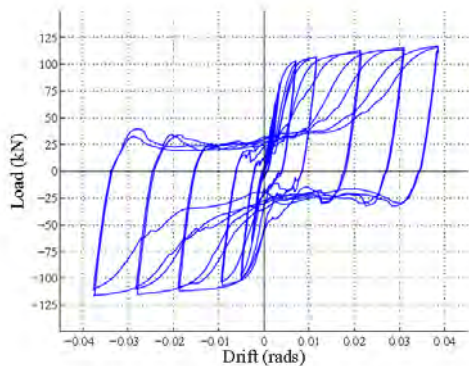**Figure 1.5-3 Pinched Lateral Force-Deformation Behavior Typical of Thin Web Plates (Webster, 2013)**
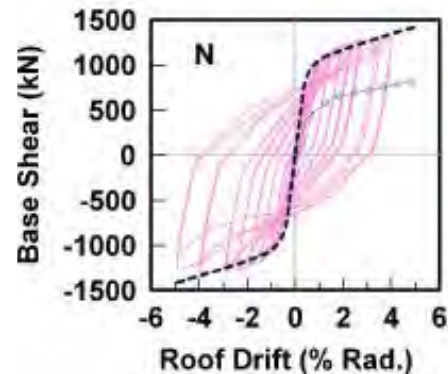

Figure 1.5-4 Lateral Force-Deformation Behavior of Typical SPSW with Fully Restrained Frame Connections (Li et al., 2009)

Several methods for computationally modeling SPSWs are available in the literature. However, the most widely used method is to model the tension field action of the web plate using inclined tension-only

truss elements as illustrated in Figure 1.5-5. A minimum of 10 elements is generally recommended for representing the web plate and web plate tension field yielding can be easily modeled through the material properties applied to the inclined truss elements. The surrounding HBEs and VBEs can be modeled with typical beam-column elements with the potential for yielding included for nonlinear analyses. Notably, shear deformations may be significant in HBEs or VBEs and caution should be used to select appropriately formulated elements.
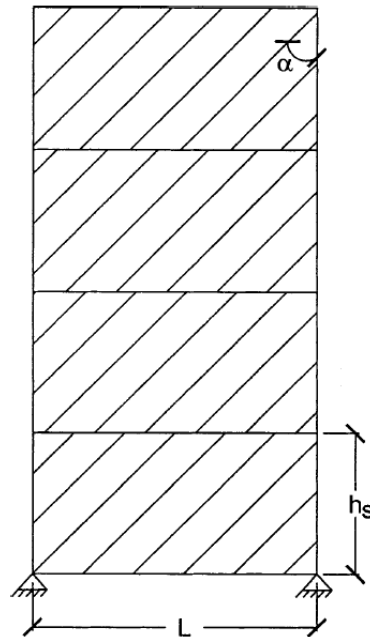
Figure 1.5-5 Typical Model for SPSWs with Truss Elements Representing Tension Field Action (Berman and Bruneau, 2003)

RP3-1.5.2   Design philosophy and concepts

The design philosophy for SPSWs in AISC 341 follows the capacity design principles used for most other ductile steel seismic force-resisting systems. The primary yield mechanism is the tension field yielding of the web plate with secondary yielding allowed at the ends of HBEs and at the base of VBEs. Figure 1.5-6 shows a steel plate shear wall after testing to nearly 5% drift where the tension field of the web plate and yielding of the HBEs and VBEs is evident. To accomplish the intended yield hierarchy, the web plate is designed for the full story shear force. Then, the HBEs and VBEs are designed for forces and moments at tension field yield of the web plate. Calculating the corresponding forces for design of the HBEs and VBEs is difficult as they have forces and moments from tension field action of the web plate, frame action, and overturning. The commentary of AISC 341 describes several methods for this calculation, the most accurate and conceptually simple of those methods is to use nonlinear pushover analysis. Note that the HBEs at story levels have tension field action acting on them from the stories above and below, which generally counteract each other, resulting in HBE demands that are due to the difference in web plate thickness above and below the story HBEs and frame action. At the roof, the HBE demands can be very large as it has to anchor the tension field action over the full width of the wall.

Figure 1.5-6 SPSW After Testing to Nearly 5% Drift (Li et al., 2009)

In order to properly develop the tension field yielding of the web plates it is not sufficient that the HBEs and VBEs have the required strength; they also must have sufficient stiffness. This is particularly important for VBEs and the HBE at the roof level. Insufficient stiffness at these locations has been shown in experiments to result in large VBE or HBE deformations, P-Delta buckling of the VBEs, and failure to develop the full web plate tension field strength. Figure 1.5-7 shows a schematic of the deformed shape of a SPSW with insufficient VBE stiffness from Sabelli and Bruneau (2006).
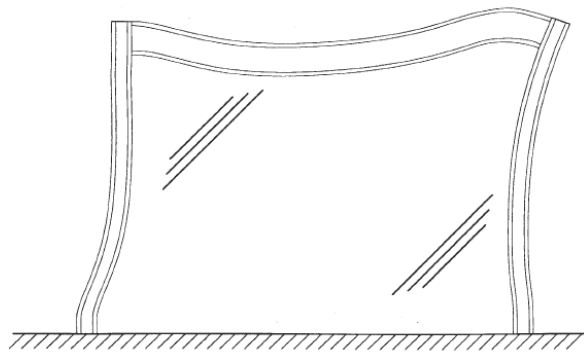

Figure 1.5-7 Schematic of HBE and VBE Deformations (Sabelli and Bruneau, 2006)

RP3-1.5.3   Detailed design requirements

Many of the detailed design requirements for SPSWs in AISC 341 are intended to ensure the desired yield hierarchy and that the web plate can fully develop tension field action. Some of the key points are listed below:

- The web plates must be designed to resist 100% of the design story shear and the HBEs and VBEs alone must be able to resist at least 25% of the design story shear.
- HBEs, VBEs and connections should be designed for forces corresponding to the expected yield stress of the web plates, assuming full tension field development, and the expected flexural strength of the HBEs, assuming development of plastic hinges at their ends.
- HBEs and VBEs must satisfy requirements for minimum moments of inertia that are functions of the web plate thickness attached to those elements.
- At HBE and VBE intersections the moment capacity ratio for special moment resisting frames must be met to guard against the development of soft-story mechanisms.
- Panel zones at HBE and VBE intersections must meet the requirements for special moment resisting frames, which allows only limited panel zone yielding.
- Web plate perforations are allowed to weaken the web plates (they often have larger strength than necessary due to limitations in available plate thickness) or allow pass-through of utilities. Means of calculating effective web plate strength and effective expected tension stress for capacity design are provided.
- Requirements for allowing and reinforcing corner cutouts in SPSW web plates are also provided.

Following the requirements of AISC 341 has generally been shown to produce SPSWs with ductile response but may also produce somewhat conservative designs in terms of overall steel weight.

RP3-1.5.4   References for RP3-1.5

AISC (2016). Seismic Provisions for Structural Steel Buildings. ANSI/AISC 341-16. American Institute of Steel Construction. Chicago, IL.

ASCE (2016), Minimum Design Loads and Associated Criteria for Buildings and Other Structures (ASCE/SEI 7-16)

Berman, J. and Bruneau, M. (2003). "Plastic Analysis and Design of Steel Plate Shear Walls." *Journal of Structural Engineering*, ASCE, Vol. 129, No. 11, pp. 1148-1156.

Berman, J.W. and Bruneau, M. (2004). "Steel Plate Shear Walls are Not Plate Girders," *Engineering Journal*, AISC, Vol.41, No.3, pp.95-106.

Li C., Tsai K., Lin C., Tsai C., Chen P. (2009). "Cyclic tests of four two-story narrow steel plate shear walls. Part 2: Experimental results and design implications". Earthquake Engineering and Structural Dynamics, No. 39, 801-826.

Sabelli, R., Bruneau, M. (2006). Steel Design Guide 20: Steel Plate Shear Walls. American Institute of Steel Construction, Inc., Chicago, IL.

Webster, D. (2013). "The Inelastic Seismic Response of Steel Plate Shear Wall Web Plates and Their Interaction with the Vertical Boundary Members." Ph.D. Dissertation, University of Washington, Seattle, WA.

RP3-1.6   Design of Composite Steel Plate Shear Walls

RP3-1.6.1   Introduction

ASCE 7-16 refers to "Composite Plate Shear Walls" (C-PSW) as seismic-force resisting systems whose detailing requirements are specified in AISC 341-16 Sections H6 and H7. The scope of H6 in AISC 341 addresses walls having steel plates with reinforced concrete encasement on one or both sides of the plate, termed "Composite Plate Shear Walls—Concrete Encased (C-PSW/CE)", while H7 is for walls having steel plates on both sides of reinforced concrete infill, called "Composite Plate Shear Walls—Concrete Filled (C-PSW/CF)". This section provides an overview of the latter system, including a description of the system and construction, system design, and anticipated seismic behavior. Additional guidance on behavior and design of C-PSW/CF has been provided in the extensive commentary included in Part 2 of the 2020 NEHRP *Provisions*.

Also included in the section is a brief introduction to coupled composite plate shear walls. Additional guidance on behavior and design of CC-PSW/CF has also been provided in the extensive commentary included in Part 2 of the 2020 NEHRP *Provisions*.

RP3-1.6.2   Shear Wall System and Construction

In concrete filled composite plate shear walls, the steel faceplates are connected to each other using tie bars that are embedded in the concrete infill (and, in some instances, additional steel headed stud anchors), as shown in Figure 1.6-1. The tie bars also provide stability during transportation and construction activities. After casting, the tie bars become embedded in the concrete infill and provide composite action between the steel and concrete. The steel faceplates serve as the primary reinforcement for the concrete infill, and they also serve as stay-in-place formwork during construction. The concrete infill prevents the inwards local buckling of the steel faceplates thus improving their stability. C-PSW/CF are assigned a seismic force modification factor, *R*, of 6.5 in ASCE 7-16.

The appeal of C-PSW/CF is that they are highly ductile, redundant, of high strength, and easy and rapid to construct (overcoming the congestion of reinforcement details that can be encountered in ordinary reinforced concrete walls, and because the steel shell can be used as formwork). In a 58-story high-rise where this structural system is being implemented, construction time is reduced by many months compared to a traditional design (AISC 2018, ENR 2019).
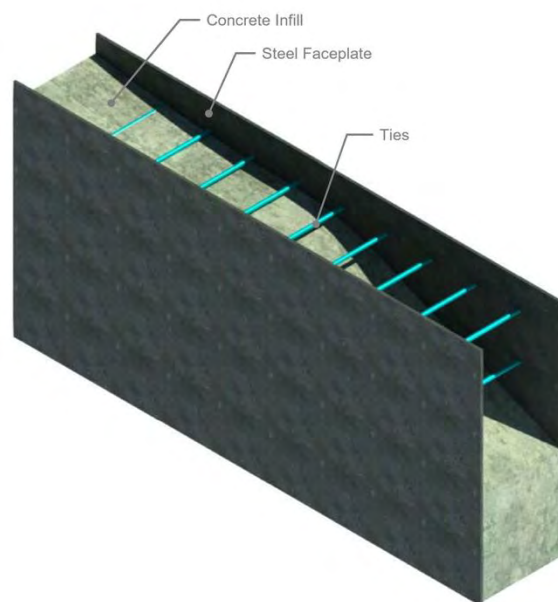
Figure 1.6-1 Components of C-PSW/CF

RP3-1.6.3   Shear Wall System Design

AISC 341-16 H7 currently provides design requirements for flexural walls having circular or semi-circular boundary elements, with resulting cross-sections as shown in Figure 1.6-2. These walls are detailed to be able to develop their plastic moment, which can be calculated as schematically illustrated in Figure 1.6-2, by yielding of the entire skin plate and the concrete attaining its compressive strength. On the strength of recent experimental results (Shafaei et al. 2019), it is foreseen that AISC-341 H7 will be expanded to also include planar (rectangular) cross-sections.

The detailed design requirements for C-SPW/CF in AISC 341 are intended to ensure development of the desired flexural ductile composite behavior described above. Some of the key requirements are summarized below:

- A maximum spacing between the ties, and slenderness limit for the circular elements are provided to ensure yielding of the steel prior to the development of local bucking.
- Design requirements are provided to ensure that the ties will not fail prior to development of the wall ductile flexural behavior.
- Per capacity design principles, the connection between the wall and its foundation is required to be to transfer the base shear force and the axial force acting together with an overturning moment corresponding to 1.1 times the plastic composite flexural strength of the wall.
- A shear strength equation is provided to verify that shear yielding is not the controlling limit state.

RP3-1.6.4   Shear Wall System Performance and Mechanisms

The ductile behavior of a C-PSW/CF is developed by flexural yielding of the wall; bucking of the faceplates between one or multiple levels of ties eventually develops, and more significantly in a localized location. Ultimately, fracture will initiate and progressively propagate across the cross-section, with a corresponding

reduction in flexural capacity. Note that the shear strength of C-PSW/CF is quite high, due to the presence of steel faceplates, and is generally not a governing design factor.

Bhardwaj and Varma (2017) provide an excellent summary of the research and thinking that went into the development this structural system (although this document was written for nuclear facilities). C-PSW/CF have been the subject of extensive research over the past few decades, with an emphasis on their potential application in nuclear power plants or high-rises (e.g., Oduyemi and Wright 1989, Wright et al. 1991a, b; Xie and Chapman 2006; Eom et al. 2009; Ramesh 2013; Zhang et al. 2014; Sener and Varma 2014; Varma et al. 2014; Epackachi et al. 2014; Sener et al. 2015; Epackachi et al. 2015; Booth et al. 2015; Kurt et al. 2016; Seo et al. 2016; Alzeni and Bruneau 2014, 2017; Polat and Bruneau, 2017). Experimental research has demonstrated that CFSSP-Walls can be highly ductile in flexure (e.g., Eom et al. 2009; Alzeni and Bruneau, 2014), as long as the ties that connect the steel plates are properly designed (Bowerman et al. 1999; Ramesh 2013) and plate yielding occurs before local buckling and does not hinder the development of plastic moment.

In well-designed C-PSW/CF walls with circular or semi-circular boundary elements, buckling initiates during the $2\Delta_y$ cycles, fracture initiates at 2.5% drift, and flexural strength degradation by 20% from peak values (due to fracture propagation) occurs at approximately 3.5% drift (Alzeni and Bruneau 2014, 2017). Typical hysteretic response of such a C-PSW/CF designed per AISC-341 H7 is shown in Figure 1.6-3.

In well-designed C-PSW/CF rectangular (planar) walls with closure plates: (i) yielding of the closure plates occurs during the $1\Delta_y$ cycles, (ii) local buckling of the closure plates initiated during the $2\Delta_y$ cycles, (iii) maximum lateral load is reached during the $3\Delta_y$ cycles, (iv) local buckling of the web plates occurs during the $4\Delta_y$ cycles, and (v) fracture failure occurs in the 5 to $6\Delta_y$ cycles depending on axial load ratio. Typical hysteretic response of such a specimen is shown in Figure 1.6-4.
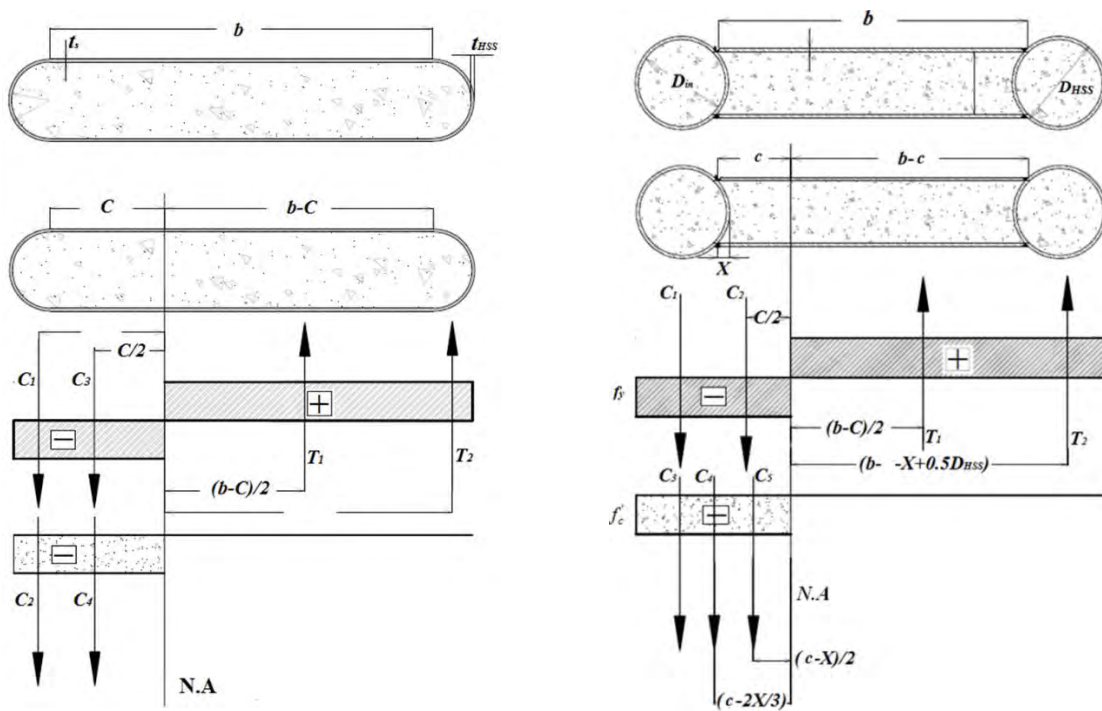

Figure 1.6-2 C-SPW/CF cross-sections and schematic diagram for stress distribution used to calculate M_p
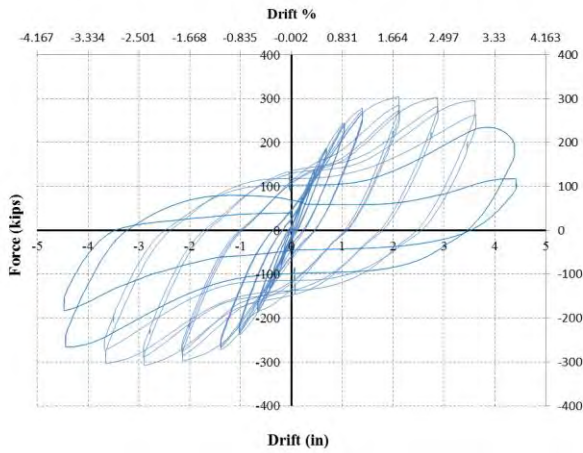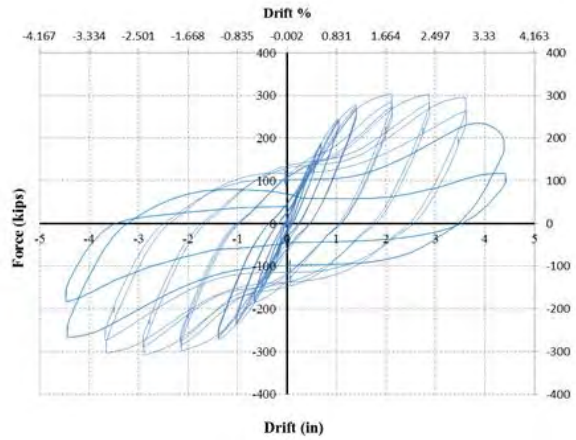
(a) CFSSP-NB1   (b) CFSSP-NB2
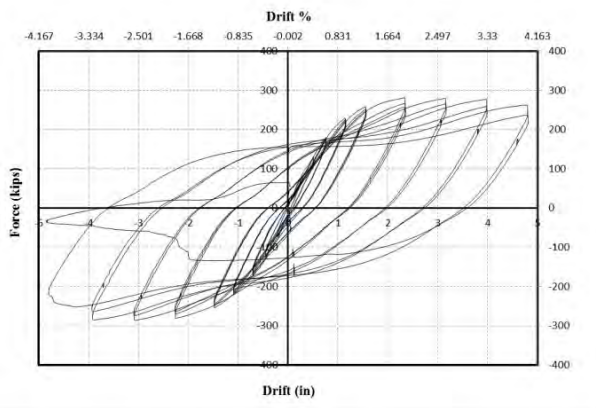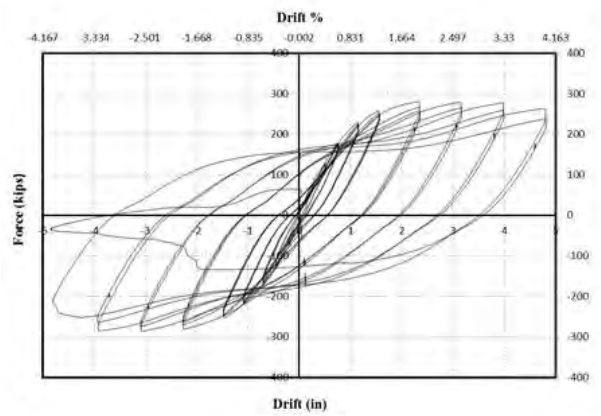
(c) CFSSP-B1   (d) CFSSP-B2

Figure 1.6-3 Force displacement relationships of tested specimens (Alzeni and Bruneau 2014)
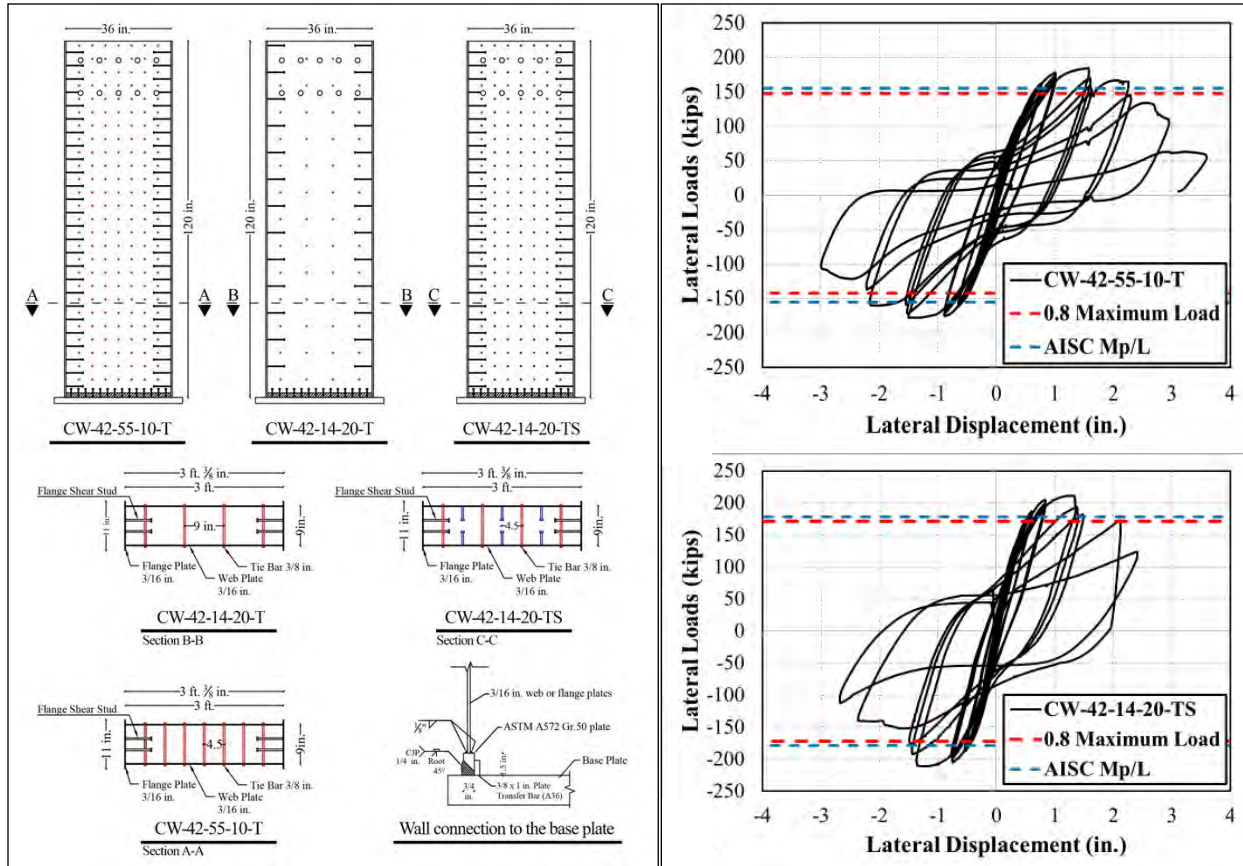
Figure 1.6-4 Force-displacement relationships of tested specimens (Shafaei et al. 2019)

RP3-1.6.5   Coupled Composite Plate Shear Walls(CC-PSW)

A coupled composite plate shear wall - concrete-filled (CC-PSW/CF) is a coupled-wall system comprised of composite walls and composite coupling beams, for which both walls and beams consists of a concrete core sandwiched between two steel plates. CC-PSW/CF are foreseen to become an efficient option in high-rise buildings having a core-wall system with coupled beams. Coupled C-PSW/CFs can also be beneficial in lower-rise buildings. In coupled walls, hysteretic energy dissipation of the coupled beams adds to the overall ability of the structural system to dissipate seismic energy. As such, coupled systems are more ductile and have more redundancy. ASCE currently does not assign them higher *R*-factors, but a research study co-funded by the AISC and the Charles Pankow Foundation has used the FEMA P-695 methodology to substantiate the use of an *R*-factor equal to 8 for such Coupled-C-PSW/CF structures (Kizilarslan et al. 2019).

RP3-1.6.6   References for RP3-1.6

AISC (2015), *Specification for Safety-Related Steel Structures for Nuclear Facilities*, including Supplement No. 1, ANSI/AISC N690-12 and ANSI/AISC N690s1-15, American Institute of Steel Construction, Chicago, IL.

AISC (2016). AISC-341 *Seismic Provisions for Structural Steel Building,* American Institute of Steel Construction, Chicago, Illinois.

AISC (2018). "Rainier Square Tower Uses Revolutionary Composite Steel Frame", *Modern Steel Construction*   news,   retrieved   1/18/2018   from

https://www.aisc.org/modernsteel/news/2018/january/rainier-square-tower-uses-revolutionary-composite-steel-frame/#.WmDKQzdG2Uk

Alzeni, Y., and Bruneau, M. (2014). *Cyclic Inelastic Behavior of Concrete Filled Sandwich Panel Walls Subjected to In-Plane Flexure*, *Technical Report* MCEER-14-0009, Multidisciplinary Center for Earthquake Engineering Research. State University of New York at Buffalo, Buffalo, NY.

Alzeni, Y., and Bruneau, M. (2017). "In-plane Cyclic Testing of Concrete Filled Sandwich Steel Panel Walls with and Without Boundary Elements." *Journal of Structural Engineering*, 143 (9).

Bhardwaj, S.R, Varma, A.H., (2017). *AISC design guide Design Guide 32: Design of Modular Steel-Plate Composite Walls for Safety-Related Nuclear Facilities*, American Institute of Steel Construction, Chicago, Il, 150p.

Booth, P. N., Varma, A. H., Sener, K. C., and Malushte, S. R. (2015). "Flexural behavior and design of steel-plate composite (SC) walls for accident thermal loading." *Nuclear Engineering and Design*, 295, 817-828.

Bowerman, H., Gough, M., and King, C. (1999). *Bi-Steel design and construction guide,* British Steel Ltd, Scunthorpe, U.K..

Epackachi, S., Nguyen, N.H.,Whittaker, A.S.,and Varma, A.H.(2014)."In-plane seismic behavior of rectangular steel-plate composite wall piers" *Journal of Structural Engineering*, 141 (7).

Epackachi, S., Whittaker, A. S., Varma, A. H., and Kurt, E. G. (2015). "Finite element modeling of steel-plate concrete composite wall piers." *Engineering Structures*, 100, 369-384.

Eom, T.-S., Park, H.-G., Lee, C.-H., Kim, J.-H., and Chang, I.-H. (2009). "Behavior of double skin composite wall subjected to in-plane cyclic loading." *Journal of Structural Engineering*, 135(10), 1239-1249.

Kizilarslan, E., Seo, J., Broberg, M., Shafaei, S., Varma, A.H., Bruneau., M., (2019). *Seismic Design Coefficients and Factors for Coupled Composite Plate Shear Walls—Concrete Filled (Coupled-C-PSW/CF)*, Final Report, Charles Pankow Foundation (to be published).

Kurt, E. G., Varma, A. H., Booth, P., and Whittaker, A. S. (2016). "In-Plane Behavior and Design of Rectangular SC Wall Piers without Boundary Elements." *Journal of Structural Engineering*, 142(6).

Oduyemi, T., and Wright, H. (1989). "An Experimental Investigation into the Behavior of double-Skin Sandwich Beams." *Journal of Constructional Steel Research*, 14(3), 197-220.

Polat, E., and Bruneau, M. (2017). " Modeling Cyclic Inelastic In-Plane Flexural Behavior of Concrete Filled Sandwich Steel Panel Walls." *Engineering Structures*, Vol.148, pp.63-80,

Post, N, (2019). "Erector proves speed prediction for radical steel frame of Seattle's Rainier Square Tower", *Engineering News Record*, January 14, 2019.

Ramesh, S. (2013). *Behavior and design of earthquake-resistant dual-plate composite shear wall systems*. P.hd. Thesis, Purdue University, West Lafayette, IN.

Sener, K., and Varma, A.H. (2014). "Steel-Plate Composite SC Walls: Experimental Database and Design for Out-of-Plane Shear." *Journal of Constructional Steel Research*, Elsevier Science, Vol. 100, pp. 197-210.

Sener, K., Varma, A.H., and Ayhan, D. (2015). "Steel-Plate Composite SC Walls: Experimental Database and Design for Out-of-Plane Flexure." *Journal of Constructional Steel Research*, Vol. 108, May, pp. 46-59, Elsevier Science.

Shafaei, S., Varma, A.H., Seo, J., and Morgen, B. (2019) "In-Plane Flexural Behavior of Planar Composite Plate Shear Walls." *Journal of Structural Engineering*, (in preparation for submission).

Seo, J., Varma, A. H., Sener, K., and Ayhan, D. (2016). "Steel-plate composite (SC) walls: In-plane shear behavior, database, and design." *Journal of Constructional Steel Research*, 119, 202-215.

Varma, A. H., Malushte, S. R., Sener, K. C., and Lai, Z. (2014). "Steel-plate composite (SC) walls for safety related nuclear facilities: Design for in-plane forces and out-of-plane moments." *Nuclear Engineering and Design*, 269, 240-249.

Wright, H., et al. (1991a). "The design of double skin composite elements." *Journal of Constructional Steel Research* 19(2): 111-132.

Wright, H., Oduyemi, T., and Evans, H. (1991b). "The experimental behaviour of double skin composite elements." *Journal of Constructional Steel Research*, 19(2), 97-110.

Xie, M., and Chapman, J. (2006). "Developments in Sandwich Construction." *Journal of Constructional Steel Research*, 62(11), 1123-1133.

Zhang, K., Varma, A. H., Malushte, S. R., and Gallocher, S. (2014). "Effect of Shear Connectors on Local Buckling and Composite Action in Steel Concrete Composite Walls." *Nuclear Engineering and Design*, 269, 231-239.

RP3-1.7   Cold-Formed Steel Shear Walls – Cardin

RP3-1.7.1   Introduction

The purpose of Section RP3-1.7 is to provide a discussion of cold-formed steel framed shear wall assemblies used to resist wind and seismic forces, with the intent is to help facilitate the understanding of shear wall design. This discussion is limited to steel sheet and wood structural panel (plywood or OSB) sheathed shear wall assemblies. This section provides a general introduction to this shear wall type. The shear wall system and construction are introduced, and an overview is provided of: design concepts, methods, and details; system seismic performance and intended energy-dissipating mechanisms; and approaches to analytical modeling.

The following discussion on cold-formed steel light-frame construction includes discussion drawn from Chapter 1 of AISI D113-19 (AISI, 2019), Cold-Formed Steel Shear Wall Design Guide. Printed in 2019, the design guide provides background on cold-formed steel light-frame shear wall design along with examples illustrating the use of the provisions to determine the shear wall strength in accordance with AISI S240-15, North American Standard for Cold-Formed Steel Structural Framing and AISI S400-15w/S-16, North American Standard for Seismic Design of Cold-Formed Steel Structural System with Supplement 1.

RP3-1.7.2   Shear Wall System Description and Construction

A typical light-frame shear wall resists lateral loads in the plane of the wall through sheathing that is attached with mechanical fasteners to the framing members. The in-plane shear loads are transferred from the shear wall to the floor framing or foundation below with connections along the length of the bottom horizontal member (bottom track). The induced overturning forces are transferred through the vertical boundary members (chord studs) and overturning restraint system (hold-downs) at the ends of the wall (Figure 1.7-1).

RP3-1.7.3   Shear Wall System Design

Design of steel sheet and wood structural panel sheathed, cold-formed steel framed shear walls is based upon the 2018 *International Building Code* (IBC) (ICC 2018), AISI S240-15, *North American Standard for Cold-Formed Steel Structural Framing* (AISI 2015) and AISI S400-15w/S1-16, *North American Standard for Seismic Design of Cold-Formed Steel Structural Systems* with Supplement 1 (AISI 2016). The 2018 IBC Section 2211 (ICC 2018) requires that the design of light-frame cold-formed shear walls be in accordance with AISI S240-15 and AISI S400-15w/S1-16. Previous editions of the IBC, including 2012

(ICC 2012) and 2015 (ICC 2015), referenced AISI S213-07w/S1-09, *North American Standard for Cold-Formed Steel Framing —Lateral Design* with Supplement 1, (AISI 2009). However, the current editions of AISI S400-15w/S1-16 and AISI S240-15 are used here.

For seismic design, there are additional requirements beyond what is typical for wind design. For example, capacity-protected components must be designed to ensure that shear walls can dissipate energy without sudden failure. Capacity-protected components pertinent to shear wall design include collectors, chord studs, hold-downs and anchorage, and all other components and connections that are not part of the designated energy-dissipating mechanism. AISI S400 (AISI 2016) defines the designated energy dissipating mechanism for cold-formed steel shear walls sheathed with wood structural panels or steel sheet sheathing as "The structural member-to-sheathing connection and the wood structural panel sheathing itself..."
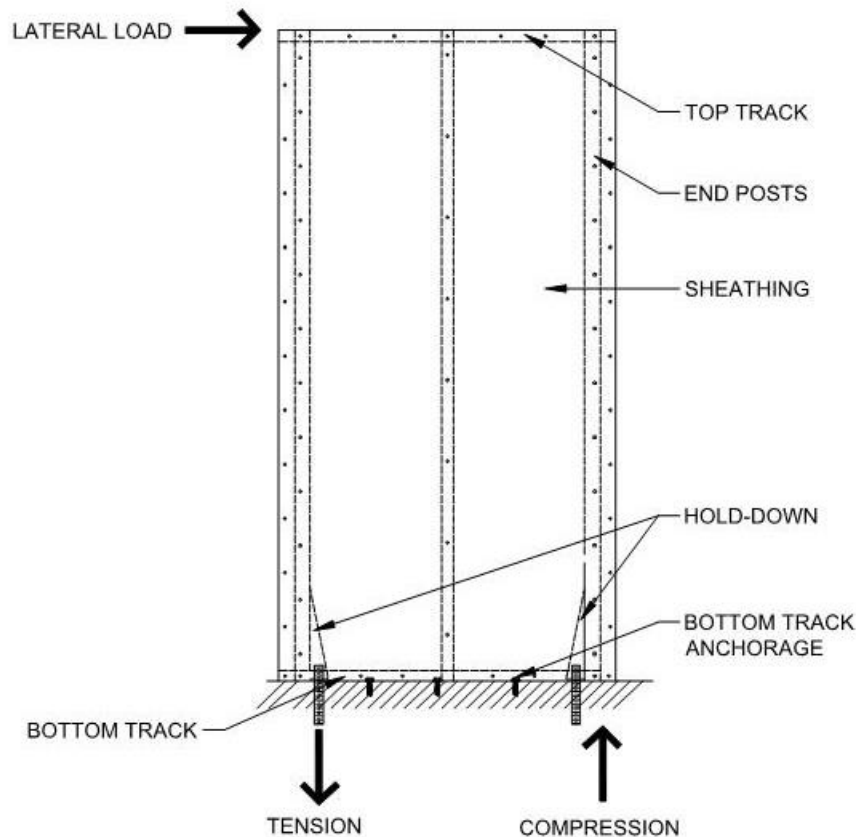
Figure 1.7-1 Typical Type I CFS Framed Shear Walls

RP3-1.7.3.1   Shear Wall Types

AISI S240 (AISI 2015) and AISI S400 (AISI 2016) recognize two basic types of cold-formed steel-framed shear walls: Type I and Type II. A Type I shear wall is defined as a "wall designed to resist in-plane lateral forces that is fully sheathed and that is provided with hold-downs at each end of the wall segment." Type I shear walls sheathed with steel sheet sheathing or wood structural panels are permitted to have openings where details are provided to account for force transfer around openings [AISI S400, B5.2.1].

Both AISI S240 and AISI S400 limit the aspect ratio (the shear wall height, *h*, divided by shear wall width, *w*) of Type I shear walls to 2:1 or 4:1, depending on the limits of testing for the particular assembly.

For some assemblies, when the aspect ratio exceeds 2:1, a strength reduction of $2w/h$ is required. In AISI S240, nominal shear strength and aspect ratio limits for steel sheet sheathed and wood structural panel shear walls are provided in Tables B5.2.2.3-1 and B5.2.2.3-2, respectively. In AISI S400, nominal shear strength and aspect ratio limits for wood structural panel shear walls are in Table E1.3-1, while these values for steel sheet sheathed shear walls are found in Table E2.3-1.

A Type II shear wall is defined as a "wall designed to resist in-plane lateral forces that is sheathed with wood structural panels or steel sheet sheathing that contains openings, but which has not been specifically designed and detailed for force transfer around wall openings. Hold-downs and anchorage for Type II shear walls are only required at the ends of the wall."

The nominal shear strength of Type II shear walls is based on the tabulated strength for Type I shear walls reduced by a shear resistance adjustment factor, C_a. The shear resistance factor, C_a, is tabulated in AISI S240 and AISI S400 based on the percent of full-height sheathing and the maximum opening height ratio. Additional limitations are imposed on Type II shear walls in AISI S240 and AISI S400. Figure 1.7-2 illustrates Type I shear walls with and without force transfer around openings, and a Type II shear wall.

Typical Type II Shear Wall
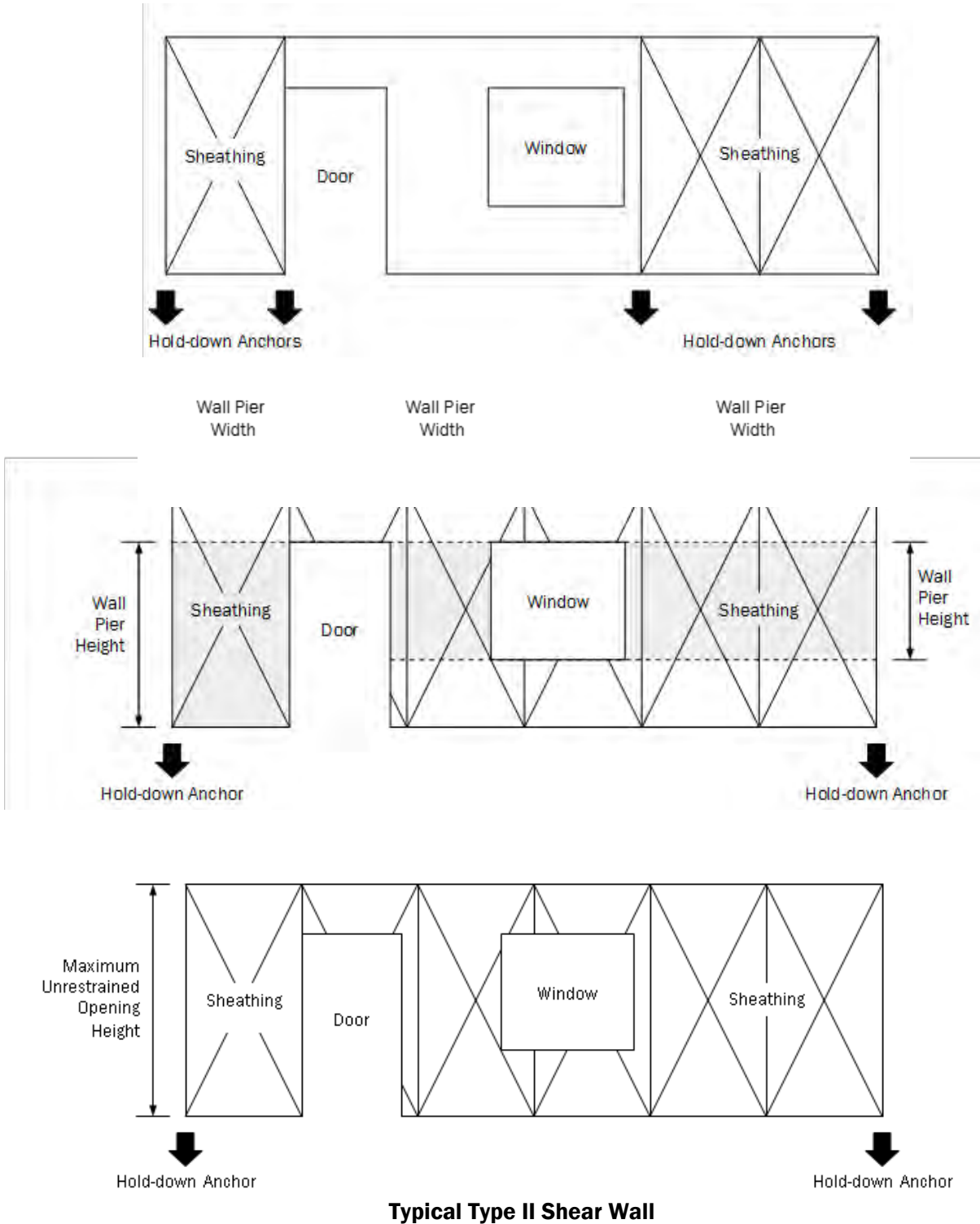
Figure 1.7-2 Figures from AISI S240-C

RP3-1-7.3.2   Sheathing Attachment to Framing

Fastener spacing and minimum sheathing screw size are specified in the nominal shear strength tables of AISI S400 and AISI S240. These tables do not specify the placement of screws for conditions where multiple (e.g. boxed or back-to-back) chord studs are used. Research at the University of North Texas (Yu, 2007) has found that when back-to-back chord studs are specified, a slight increase in shear wall strength and a reduction in boundary stud damage are observed when the sheathing fasteners at the chord studs are distributed evenly between the two chord members.

RP3-1.7.3.3   Chord Studs

The required axial strength of chord studs can be determined based on principles of mechanics using the shear wall loads from the applicable building code and the shear wall geometry in combination with other applicable axial forces such as dead and live loads. Chord studs may also be subject to bending moments from wind, seismic or eccentric gravity forces. For seismic designs based on AISI S400, the required strength of chord studs is based on the expected strength of the shear wall but need not exceed the seismic load effects determined from the applicable load combinations including overstrength. Basic combinations with seismic load effects including overstrength or expected strength are given in ASCE 7-16, *Minimum Design Loads and Associated Criteria for Buildings and Other Structures,* (ASCE 2016), Section 2.4.5.

RP3-1.7.3.4   Overturning Restraint and Shear Transfer

AISI S240 and S400 require that hold-downs and anchorage be used at each end of Type I shear walls and at the ends of Type II shear walls. For designs based on AISI S400, the required strength of hold-downs and anchorage is based on the expected strength of the shear wall but need not exceed the seismic load effect determined from the applicable load combinations including overstrength. The available strength of the hold-downs and anchorage must be greater than or equal to the required strength.

For Type II shear walls, in addition to designing for the concentrated uplift forces at the ends of the shear wall, AISI S240 and AISI S400 require that bottom tracks at full-height sheathing locations be anchored for a uniform uplift force equal to the unit shear force in the wall. For designs based on AISI S400, these forces are required to be increased to expected strength or overstrength level forces.

While dead load may be used to resist uplift forces at Type I and Type II shear wall ends with the appropriate load combination factors, care should be taken to not overestimate the dead load that is capable of contributing to uplift resistance. It is not appropriate to assume that a Type II shear wall is a rigid body and use dead load away from the ends of the wall to reduce the overturning forces at the wall ends. FEMA 451 (FEMA 2006) entitled "NEHRP Recommended Provisions: Design Examples" Section 10.1.4.10.2 states: "… calculations involving seismic overturning and counter-balancing moments are assumed not to be applicable for perforated shear walls, as they are not expected to act as rigid bodies resisting global overturning."

Adequate load paths to transfer shear from diaphragms to collectors and ultimately into shear walls must also be provided. For seismic design in accordance with AISI S400, the required strength of collectors and connections is based on the expected strength of the shear wall but need not exceed the seismic load effects determined from the applicable load combinations including overstrength. The available strength of the collectors and connections must be greater than or equal to the required strength.

Adequate connectors to transfer shear forces into lower level diaphragms or foundations must also be provided. For seismic design, these connectors are a critical connection that is not part of the designated energy-dissipating mechanism. Accordingly, the required strength of the connectors is based on the expected strength of the shear wall but need not exceed the seismic load effect determined from the applicable load combinations including overstrength.

RP3-1.7.3.5   Deflection

Consideration of horizontal deflection of the top of shear walls is important whether the design is governed by wind or seismic forces. Excessive deflection can lead to damage such as cracking in finish materials (e.g., stucco, gypsum board, windows, etc.). It can also result in member or assembly failure or collapse.

Currently, there is no code drift limit for walls resisting in-plane wind loads. However, ASCE 7-16, non-mandatory Appendix C, Section C2.2, states "Lateral deflection or drift of structures and deformation of horizontal diaphragms and bracing systems caused by wind effects shall not impair the serviceability of the structure." ICC-ES acceptance criteria AC322 (ICC 2016) has adopted an in-plane drift limit for wind of H/180 where H equals the height of the tested shear wall assembly.

For seismic design ASCE 7-16, Table 12.12-1 provides allowable story drift limits based on structure type and Risk Category. The drift limits vary from a maximum of $0.025h_{sx}$ for non-masonry structures four stories or less in Risk Category I or II to a minimum of $0.010h_{sx}$ for other non-masonry structures in Risk Category IV, where h_{sx} is defined as the story height below level x. For example, a three-story CFS structure using shear walls sheathed with steel sheet sheathing or wood structural panels in Risk Category I or II with a story height of 10 feet has an allowable story drift of $0.025(10 \text{ ft})(12 \text{ ft/in}) = 3.0$ inches.

Seismic design story drift (Δ) is determined as the difference of the deflections at the centers of mass at the top and bottom of the story under consideration where the deflection at level x, δ_x, is calculated as the anticipated inelastic drift per ASCE 7-16, Section 12.8.6 based on LRFD level seismic forces.

The deflection equation estimates the top of the wall horizontal deflection of a Type I shear wall without openings on a rigid base. It does not consider other components that may contribute to deflection. Examples of items that may result in additional deflections include raised floors, wood sills or beams beneath the shear wall (see AISI S240 Commentary Section B5.2.5 and AISI S400 Commentary Section E1.4.1.4-1).

Multi-story shear walls should also consider the effect of the deformations of shear walls above and below to determine the total deformation. For example, the upper shear wall of a two-story stacked shear wall assembly will experience additional deflection due to axial shortening of the compression chords and lengthening of the tension chords as well as hold-down deformation of the lower level shear wall.

The deflection of perforated shear walls, in accordance with AISI S240 and AISI S400, must be determined by principles of mechanics considering the deformation of the sheathing and its attachment, chord studs and hold-downs. While AISI S240 and S400 do not provide specific recommendations on the application of the principles of mechanics to perforated shear walls, the American Wood Council's *Special Design Provisions for Wind & Seismic*, 2015 edition (AWC SDPWS) (ANSI/AWC 2015) recommends that deflection of perforated shear walls be determined using the provisions for non-perforated shear walls by taking the unit shear, *v*, as the shear force in the perforated wall divided by the shear capacity adjustment factor and the sum of the perforated shear wall segment lengths including adjustment for segments with aspect ratios greater than 2:1. This method could be useful in estimating the deflection of perforated CFS shear walls as well.

RP3-1.7.4   Special Seismic Requirements

For seismic design of light-frame bearing wall systems using ASCE 7-16, Table 12.2-1, the Response Modification Coefficient, *R*, is 6.5 for light-frame (cold-formed steel) walls sheathed with either wood structural panels rated for shear resistance or steel sheets. In Seismic Design Category D, E or F, the height of these structures is limited to 65 feet. No height limitation is imposed on structures in Seismic Design Category B or C. The relatively high *R* factor assigned to these shear wall systems implies that ductility, as opposed to strength alone, is how these structures survive large earthquakes. Accordingly, the codes and standards provide special design and detailing requirements to ensure ductile behavior of the lateral force-resisting system (LFRS). AISI S400 was developed, in part, to provide a straightforward, consistent approach to applying these requirements.

RP3-1.7.4.1   Design for Seismic Design Categories A through C

In Seismic Design Category A, or in Seismic Design Categories B or C when the response modification factor R is taken equal to 3, as a "Steel Systems Not Specifically Detailed for Seismic Resistance, excluding Cantilever Column Systems" (Line H in ASCE 7-16 Table 12.2-1), the special seismic requirements of AISI S400 do not apply. For these cases, the LFRS for both wind and seismic forces can be designed in accordance with AISI S240. The designer still must multiply the tabulated nominal shear values by the appropriate resistance factor, ϕ, or divide by the appropriate safety factor, Ω, to obtain the available strength of the shear wall for LRFD or ASD, respectively.

RP3-1.7.5   Shear Wall System Performance and Mechanisms

Light-frame cold-formed shear walls have been used as lateral force-resisting elements for many years. There has been a considerable amount of testing performed on these systems, including monotonic, cyclic, and shake table testing, in addition to nonlinear time history analyses. Typically, the available strengths of shear wall assemblies used to resist wind loads are determined through monotonic tests in accordance with ASTM E564, *Standard Practice for Static Load Test for Shear Resistance of Framed Walls for Buildings* (ASTM 2006). Another monotonic test standard that is used to determine sheathing strength only is ASTM E72, *Standard Test Methods of Conducting Strength Tests of Panels for Building Construction* (ASTM 2015).

The LFRS encompasses all of the parts of the seismic load path including diaphragms, chords, collectors and the SFRS. The designated energy-dissipating mechanism, sometimes called the "fuse", is the specific part of the SFRS that will dissipate seismic energy. AISI S400 defines the designated energy dissipating mechanism for each SFRS. For steel sheet and wood structural panel sheathed shear walls, the designated energy-dissipating mechanism is the structural member-to-sheathing connection and the sheathing itself.

AISI S400, Sections E1.4.1.2 (wood structural panel shear walls) and E2.4.1.2 (steel sheet sheathed shear walls) specify that the required strength of collectors, chord studs, other vertical boundary elements, hold-downs and anchorage connected thereto, and all other components and connections of the shear wall that are not part of the designated energy-dissipating mechanism, be determined from the expected strength of the shear wall, but need not exceed the seismic load effect determined from the applicable load combinations including overstrength. The available strength of each of these components must be greater than or equal to the required strength. In the U.S. and Mexico, foundations are not required to be designed for the seismic load effect including overstrength.

RP3-1.7.6   Shear Wall System Additional Resources

AISI S240, Section D3.1.1 provides Quality Control and Quality Assurance provisions for lateral force-resisting systems, including shear walls.

Determination of the wind or seismic force transmitted to the shear wall assembly and its components and determination of the shear wall assembly's available strength are illustrated in AISI D113-19 (AISI 2019) for five different shear wall and design load conditions. Detailed shear wall component design is performed for several examples.

RP3-1.7.7   References for Section RP3-1.7

ASCE, 2016. Minimum Design Loads and Associated Criteria for Buildings and Other Structures 2016 edition, (ASCE/SEI 7-16). ASCE, Reston, Virginia.

AISI (2009), North American Specification for Cold-Formed Steel Framing – Lateral Design with Supplement 1, 2009 Edition (AISI S213-07w/S1-09).

AISI (2012), North American Specification for the Design of Cold-Formed Steel Structural Members, 2012 Edition (AISI S100-12).

AISI (2015), North American Standard for Cold-Formed Steel Structural Framing, 2015 Edition (AISI S240-15).

AISI (2016), North American Standard for Seismic Design of Cold-Formed Steel Structural Systems with Supplement 1, 2016 Edition (AISI S400-15/S1-16).

AISI (2016), Cold-Formed Steel Design Guide, 2016 Edition (AISI D110-16).

AISI (2019), Cold-Formed Steel Shear Wall Design Guide, 2019 Edition (AISI D113-19).

ANSI/AWC (2015), Special Design Provisions for Wind and Seismic (SDPWS-2015).

ASTM (2006), Standard Practice for Static Load Test for Shear Resistance of Framed Walls for Buildings (ASTM E564-06(2018)).

ASTM (2015), Standard Test Methods of Conducting Strength Tests of Panels for Building Construction (ASTM E72-15).

FEMA (2006), NEHRP Recommended Provisions: Design Examples (FEMA 451).

ICC (2012), 2012 International Building Code.

ICC (2015), 2015 International Building Code.

ICC (2018), 2018 International Building Code.

ICC (2016), AC322, Prefabricated, Cold-formed Steel, Lateral-force-resisting Vertical Assemblies.

Yu, C. (2007), Steel Sheet Sheathing Options for Cold-Formed Framed Shear Wall Assemblies Providing Shear Resistance.

RP3-1.8   Design of Wood Shear Walls – Cobeen/Line

RP3-1.8.1   Introduction

The majority of wood light-frame structures with engineered seismic force-resisting systems are braced with wood-frame shear walls with wood structural panel sheathing (plywood or OSB). This section provides a general introduction to this shear wall type. The shear wall system and construction are introduced, and an overview is provided of: design concepts, methods, and details; system seismic performance; intended energy-dissipating mechanisms; and approaches to analytical modeling.

RP3-1.8.2   Shear Wall System Description and Construction

The primary elements of wood-frame shear walls include minimum 2x nominal studs at 16 or 24 inches on center, wood structural panel sheathing, and nails attaching the sheathing to the framing (Figure 1.8-1). For purposes of design, the sheathing is considered to act exclusively in shear. Also part of the shear wall system are the shear load path (Figure 1.8-2) and the overturning load path (Figure 1.8-3). The shear load path includes transfer of load into the top of and out of the bottom of each shear wall at each story level. The overturning load path uses a tension and compression couple to resolve overturning moment (Figure 1.8-3), with the compression carried in wood framing members that are often posts or groups of studs. Tension

is carried in either steel rods continuous over the multi-story wall height, or wood framing (posts or studs) acting in tension with through-floor tension connections. Most of the devices used for tension load path connections are proprietary. Figures 1.8-1 and 1.8-3 illustrate the later method, using posts or studs and through-floor connections. Shear and overturning load paths are required to have continuity over the multi-story height of the shear wall structure.

RP3-1.8.3   Shear Wall System Design

Design of wood light-frame shear walls is primarily governed by the Special Design Provisions for Wind and Seismic (SDPWS) (AWC, 2015), with some details of design also relying upon the National Design Specification for Wood Construction (NDS) (AWC, 2018). These wood design standards are used in combination with the requirements of ASCE/SEI 7 (ASCE, 2016). In general, each shear wall is designed for in-plane shear, a shear load path, and an overturning load path, as previously introduced. Also included in the design process are drift checks, as required by ASCE/SEI 7.

Details of shear wall design differ somewhat among three types of shear walls addressed in SDPWS: individual full height wall segments (segmented shear walls), perforated shear walls, and shear walls designed for force transfer (continuity) around openings (Figure 1.8-4). Segmented shear walls can be visualized as a series of isolated walls, each extending one story in height and cantilevered up from their base. Each shear wall is sheathed for the full story clear height, and the sheathed dimensions of the wall must meet minimum aspect ratio requirements (Figure 1.8-5). All other sheathed portions of a wall line including full height sheathed wall areas not meeting aspect ratio requirements and sheathed wall areas above and below openings are ignored for the purposes of determining the design strength and stiffness. Lateral forces are distributed to the cantilevered shear walls in a line based on the relative stiffnesses of the cantilevered wall elements; the stiffness is determined using a SDPWS equation for shear wall deflection or simplified distribution assumptions provided in SDPWS. Shear load paths are provided for load into and out of each cantilevered wall element at each story level. Similarly, overturning load paths are provided by tension and compression chord elements at each end of each cantilevered shear wall segment and a continuous load path to the foundation.

Shear walls designed for force transfer (continuity) around the openings use rational methods to incorporate door and window openings within the shear wall. This design method makes use of the sheathed areas above and below openings in a manner similar to coupling beams, linking the individual full-height walls together to mobilize overturning of the wall as a whole. This method of design develops high unit shear stresses in the wall areas above and below the openings and in wall piers next to window openings. SDPWS requires that a rational analysis be provided to determine these shears. Detailing commensurate with the rational analysis must be provided. Several methods of rational analysis for this wall type are published (SEAOC, 2016) (Diekmann, 1998). Lateral forces are distributed to the force-transfer shear walls in a line based on the relative stiffness of the walls. The reference capacity and in-plane shear stiffness of the wall is based on the requirements for individual full-height shear walls with adjustments to account for the details of the force-transfer design.

Perforated shear wall design also incorporates door and window openings within the shear wall, but rather than using special detailing as used in the force transfer walls, take advantage of the inherent continuity and coupling effect provided by typical shear wall detailing. The capacity and stiffness reduction factor, C0, applicable to design of this wall type, has been derived through wall testing. This factor is a function of the portion of the wall length having full height sheathing, and the height of openings relative to the wall clear height. Lateral forces are distributed to perforated shear walls in a line based on the relative stiffness of the perforated shear walls. The reference capacity and stiffness of the perforated shear wall is based on requirements for individual full-height shear walls, reduced by the application of the C_0 factor to account for the presence of openings. SDPWS provides a series of specific design limitations and detailing requirements for this wall type in order to align the design requirements with the underlying testing. The

continuity and capacity of this wall type is thought to be provided by a combination of fully and partially restrained cantilevered walls, partially fixed coupling beams, and tension and compression struts above and below windows.

An important aspect of the design of wood-frame shear wall systems, deserving of emphasis, is that analytical modeling for seismic design almost always incorporates significant simplifications. First and most important is that only the strength and stiffness provided by the wood structural panel shear wall system is included; not included are the very significant strength and stiffness effects of the finish materials (stucco, plaster, gypsum wallboard, etc.) that are installed both on the shear walls and on other interior and exterior walls not designated as shear walls. Another simplification is the neglecting in the design model of strength and stiffness that is provided by wood structural panel sheathing above and below openings or not meeting aspect ratios. These design simplifications comes about because the design standards either prohibit consideration of the contributions to strength and stiffness, or greatly penalize inclusion through increased seismic demands. This simplified design approach is believed to provide a structure that will meet the collapse prevention seismic performance targeted by ASCE/SEI 7 and building code seismic design provisions. On the other hand, the simplified model that is used in design is known to provide poor estimates of the actual seismic performance of the structure, because the model does not properly reflect the strength and stiffness of the constructed building.

Recent projects conducting testing and numerical modeling of wood light structures have moved towards inclusion of finish materials in order to be able to investigate structure performance. The inclusion of finish materials considerably increases the complexity of modeling because of the wide range of materials that are used in construction, and the wide variability of strength and stiffness properties within any one material type. One outcome of recent numerical studies with finish materials included is an observed increase in the tendency for drifts in multistory light-frame buildings to be concentrated in the lowest story which has the highest seismic demands.

Design and detailing of the shear and overturning load paths and their fasteners and connections is performed using simple free-body diagrams. Design of the load path is performed at either an ASD or LRFD force level, and does not include consideration of overstrength factors except in cases where this is triggered by the irregularity provisions of ASCE/SEI 7. Because this approach is taken, it has not been necessary to separately define ordinary, intermediate, and special shear wall systems for wood-frame shear walls. The standard detailing used across all seismic design categories is understood to provide the equivalent of special detailing due to inherent ductility.

ASCE/SEI 7 requires that the design story drift, Δ, be less than a specified allowable story drift. The design story drift is determined using shear wall deflection equations provided in SDPWS and a deflection amplification factor given in ASCE/SEI 7. This is compared to the allowable story drift defined by ASCE 7. In multi-story wood light frame buildings, this drift limit can in some cases force the use of stronger and stiffer walls than would be required by the load requirements alone. A number of other drift-related provisions in ASCE/SEI 7 might be applicable to design of wood light-frame structures.

RP3-1.8.4   Shear Wall System Performance and Mechanisms

Laboratory shake table testing and observed building performance to date indicate that the primary seismic response of light-frame wood structural panel shear wall buildings is the in-plane racking displacement of the wall elements while the deformation demand on floor and roof diaphragms remains small. The few recorded instances of damage to diaphragms in light-frame buildings have involved irregularly shaped diaphragms with re-entrant corners (CUREE, 2001a; Christovasilis et al., 2007). Consequently, the walls are understood to be the structural elements that determine the seismic response characteristics of light-

frame shear wall buildings. Note that wood-frame diaphragms can have a significant influence on the seismic behavior of concrete and masonry shear wall buildings, which are beyond the scope of this section.

Testing of wood light-frame shear walls has demonstrated that the load-deflection performance under both cyclic and monotonic loading is primarily influenced by yield behavior in bending of the nails attaching the sheathing to the framing (sheathing-to-framing nails), combined with associated wood bearing deformations under the nail shank and head. This is the typical and preferred mechanism for energy dissipation and ductility in wood structural panel shear walls. At higher levels of displacement, the primary failure mechanisms also involve the sheathing-to-framing nailing, with nail withdrawal from the framing, nail tear out at the side of the sheathing panel, and nail head pull through being commonly seen.

In general, tests have shown that shear and overturning load paths designed in accordance with SDPWS are able to support the development of the sheathing-to-framing nailing as the weak link. Some exceptions to this behavior have been seen in the laboratory and following earthquakes. When other weak links have been observed, design provisions have generally been revised to delay the formation of or avoid these weak links. Included are splitting of foundation sill plates when loaded in cross-grain tension (caused by uplift of the sheathing during typical wall racking behavior); steel plate washers are required on anchor bolts to help delay this behavior. Tie-down brackets bolted to tie-down posts have been seen to result in splitting failure of the posts along the bolt line; there has since been a move away from use of tie-down brackets that bolt to tie-down posts. Splitting of studs in shear walls with closely spaced nailing has been seen; requirements for 3x framing at abutting panel edges and staggering of sheathing nails into two rows have been required to delay this behavior.

RP3-1.8.5 Shear Wall System Analytical Modeling

In order to evaluate the distribution of design forces and drifts, a building analytical model in accordance with ASCE/SEI 7 Section 12.7.3, is needed. Generally, the analysis uses the equivalent lateral force procedure (ASCE/SEI 7, Section 12.8). The primary analysis model includes only those elements designated as structural shear walls, and considers only the strength and stiffness effects of the wood structural panel sheathing. Analysis is often performed using spreadsheet tools developed within individual design offices, but some software is commercially available.

Vertical distribution of forces is required to be in accordance with ASCE/SEI 7, which dictates a triangular (first mode) distribution for short period buildings under the equivalent lateral force procedure. Horizontal distribution of forces is required to be in accordance with one of three scenarios identified in ASCE/SEI 7: diaphragms that are clearly very flexible relative to the vertical elements, diaphragms that are clearly very rigid relative to the vertical elements, and everything else. For "everything else," it is required that a semi-rigid diaphragm model be used for distribution of horizontal seismic forces. ASCE/SEI 7 also includes an exception permitting light frame structures with diaphragms of wood structural panel or untopped steel decking to be categorized as flexible.

Other buildings braced by wood light-frame shear walls fall into the "everything else" category. For these other buildings, one approach to meeting the semi-rigid diaphragm requirement is evaluating force distribution using both rigid and flexible diaphragm models and designing each shear wall and diaphragm for the worst-case force. For this approach, the flexible diaphragm model should be analyzed first, followed by an iterative rigid diaphragm distribution analysis.

Where non-uniform distribution of finish materials might trigger significant torsional behavior in the structure, additional analytical studies including the effects of finish materials are not explicitly required, but should be considered.

RP3-1.8.6 Shear Wall System Additional Resources

Additional resources for those interested in design of wood light-frame shear walls include:

2015 NEHRP Recommended Seismic Provisions: Design Examples (FEMA P-1051) (FEMA, 2016).

FEMA P-1052 2015 NEHRP Provisions: Training and Instructional Materials (FEMA P-1052) (FEMA, 2016).

NEHRP Provisions, 2009 Edition: "Resource Paper 13: Light-Frame Wall Systems with Wood Structural Panel Sheathing," (FEMA, 2009).

SDPWS Commentary (AWC, 2015).

Figure 1.8-1 Segmented shear wall with studs, sheathing, and posts and tie-down connectors at each end (Figure credit: FEMA P-1052)
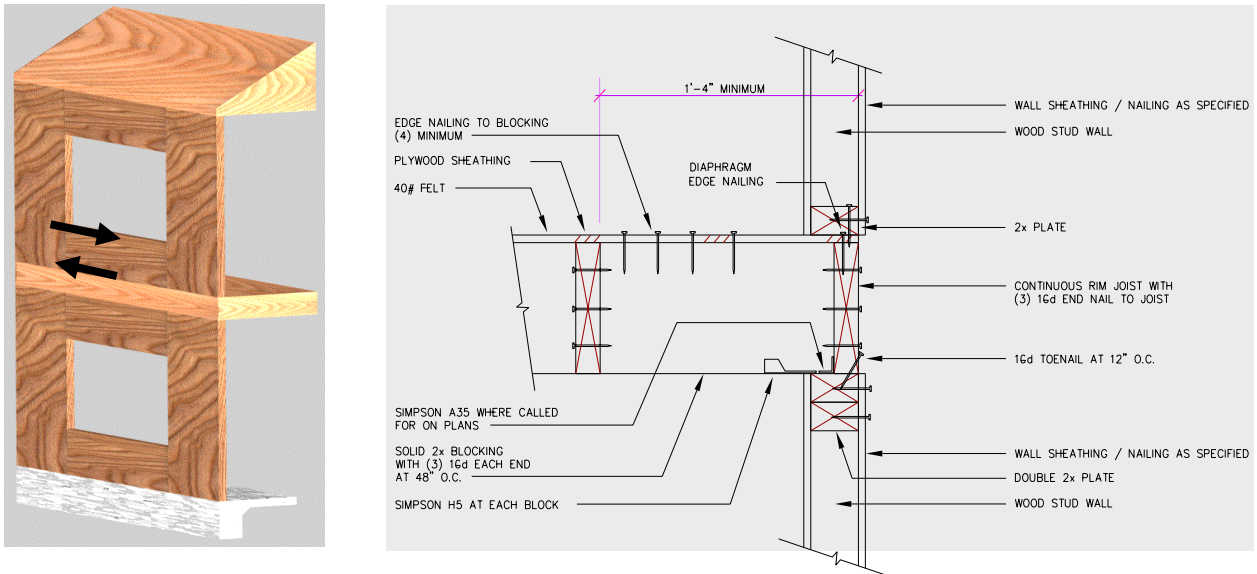
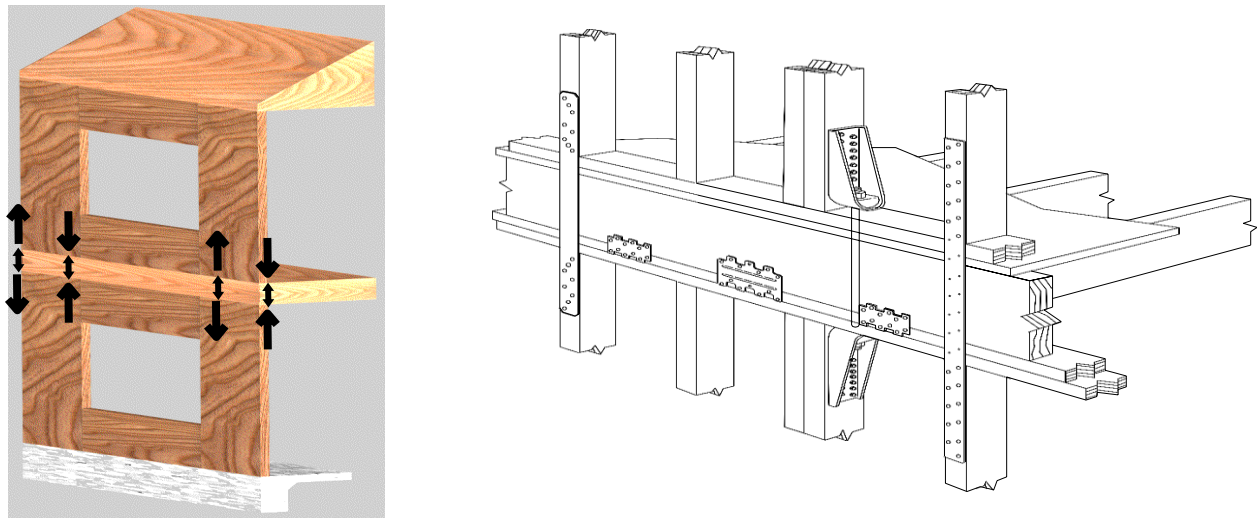**Figure 1.8-2 Shear load path for shear walls (Figure credit: FEMA P-1052).**

Figure 1.8-3 Overturning load path for shear walls (Figure credit: FEMA P-1052)
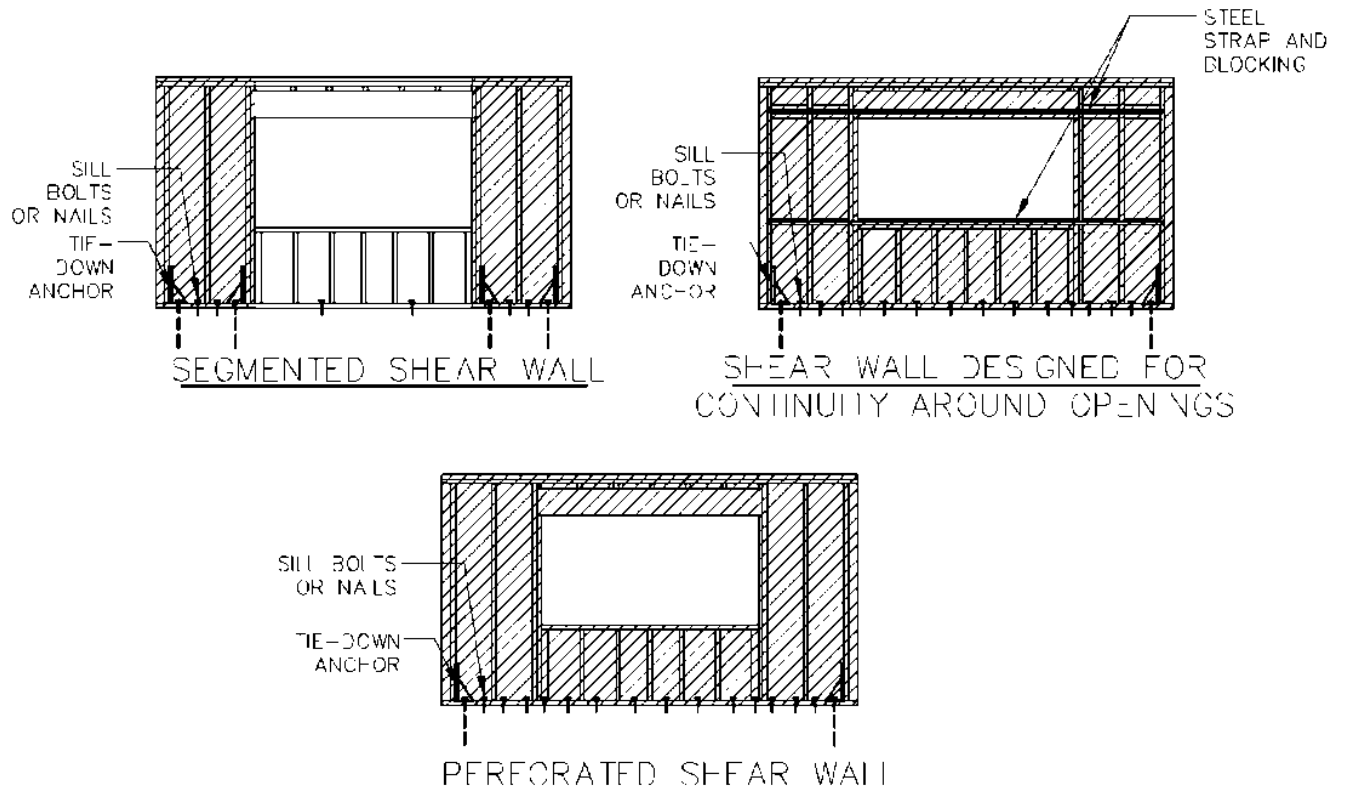
Figure 1.8-4 Three types of wood light-frame shear walls (Figure Credit: K. Cobeen).
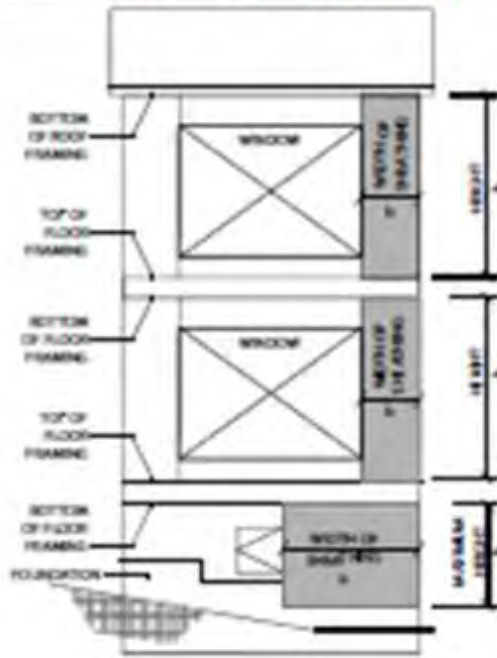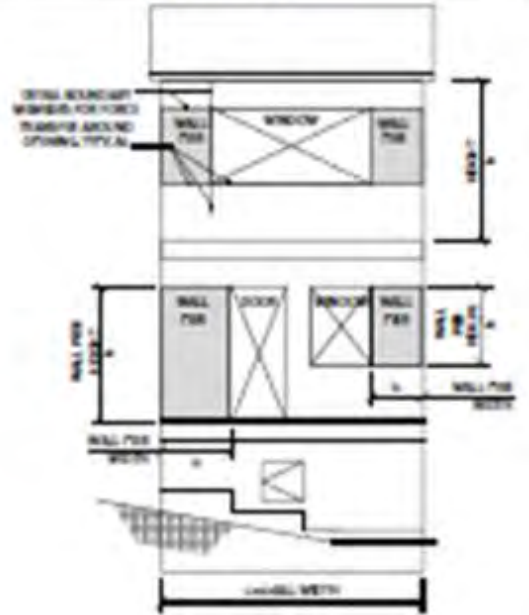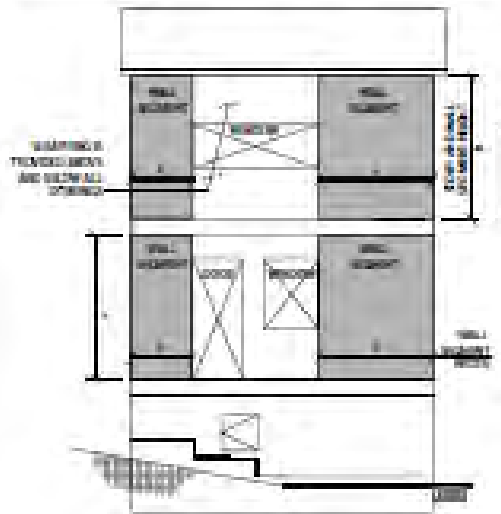
Figure 1.8-5 Aspect ratio requirements for the three types of wood light-frame shear walls (Figure Credit: SDPWS).

RP3-1.8.7 References for RP3-1.8

ANSI/AWC (2018), National Design Specification for Wood Construction (NDS-2015), American Wood council, Washington, D.C.

ANSI/AWC (2015). Special Design Provisions for Wind and Seismic (SDPWS), 2015 edition, American Wood council, Washington, D.C.

ASCE, 2016. Minimum Design Loads and Associated Criteria for Buildings and Other Structures 2016 edition, (ASCE/SEI 7-16). ASCE, Reston, Virginia.

Christovasilis, I.P.,Filiatrault, A.and Wanitkorkul, A., (2007). Seismic Testing of a Full-Scale Two-Story Light-FrameWood Building: NEESWood Benchmark Test, NEESWood Report NW-01, November.

Consortium of Universities for Research in Earthquake Engineering. 2001a. Woodframe Project Case Studies, CUREE W-04. CUREE, Richmond, California.

Diekmann, 1998. Diekmann, Edward, F. "Diaphragms and shear Walls," Wood Construction and Engineering Handbook, 3rd. Ed., K.F. Faherty and T.G. Williamson, eds., McGraw-Hill, New York, NY.

FEMA, 2009. NEHRP Recommended Seismic Provisions, 2009 Edition (FEMA P-750), Federal Emergency Management Agency, Washington, DC.

FEMA, 2016. 2015 NEHRP Provisions: Training and Instructional Materials (FEMA P-1052). Federal Emergency Management Agency, Washington, DC.

RP3-2   COUPLED SHEAR WALLS

RP3-2.0   Introduction

This chapter explains the concept of coupled shear walls and how they differ from isolated shear walls. It is pointed out that part of the overturning moment is resisted by the couple due to the compression and tension forces induced in the walls by the coupling beams. This chapter also draws a distinction between coupled shear wall systems in general and ductile coupled reinforced shear walls as defined in ACI 318-19. Further, the different types of coupling beams that are used to connect shear walls are listed. Three types of coupling beams are described in detail.

Some shear wall systems can incorporate coupling beams, which work in shear and bending to convert a portion of the overturning moment into a vertical-force couple between two proximate walls (Figure 2.0-1). Coupling beams are typically repeated at every story between two walls, such that the beams essentially work in parallel to transfer overturning forces between the walls, to the extent that walls rotate as rigid bodies at the base. The deformation of the coupling beam is related to lateral drift and to vertical deformations of the wall boundaries (one in tension and the other in compression); deformations may be small at lower levels, limiting the participation of those beams. The coupling beam flexural reinforcement must be fully developed at the wall faces and the coupling beam shear reinforcement must also be fully anchored for the coupling beams to be fully effective.

The coupling beam vertical component (shear) gets transferred to the wall or wall pier as axial force.

A subset of coupled wall systems have been defined as ductile coupled shear walls, discussed in this Chapter and Chapter 3.

The high compression due to coupling may control design. The coupling ratio or degree of coupling, defined as the ratio of the overturning moment resisted by the tension-compression couple to the total overturning moment, has been used as an index of how coupled a system is. This can range from high coupling where combined walls act like a single wall, to low coupling. Degree of coupling loses meaning when inelastic deformations develop in the coupling beams. Degree of coupling can vary significantly over the course of nonlinear response history analysis (NLRHA). In Figure 2.0-2, the step-by-step degree of coupling during NLRHA is shown for a variety of coupling beam depths in systems subject to large displacements. In the elastic range one might compare degree of coupling, but in the inelastic range the degree of energy dissipation is the correct indicator of coupled wall response.
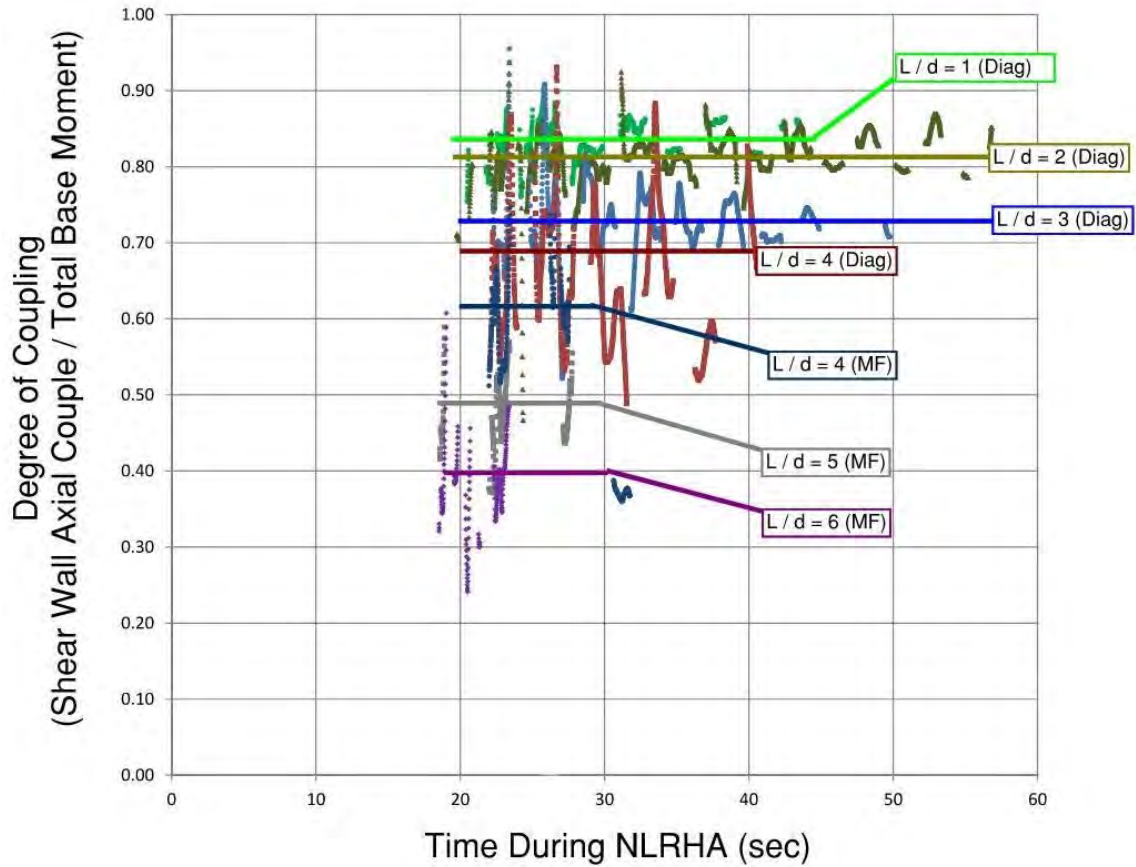
Figure 2.0-1 NLRHA Varying degrees of coupling at large displacements during nonlinear response history analysis [Courtesy: Magnusson Klemencic Associates]
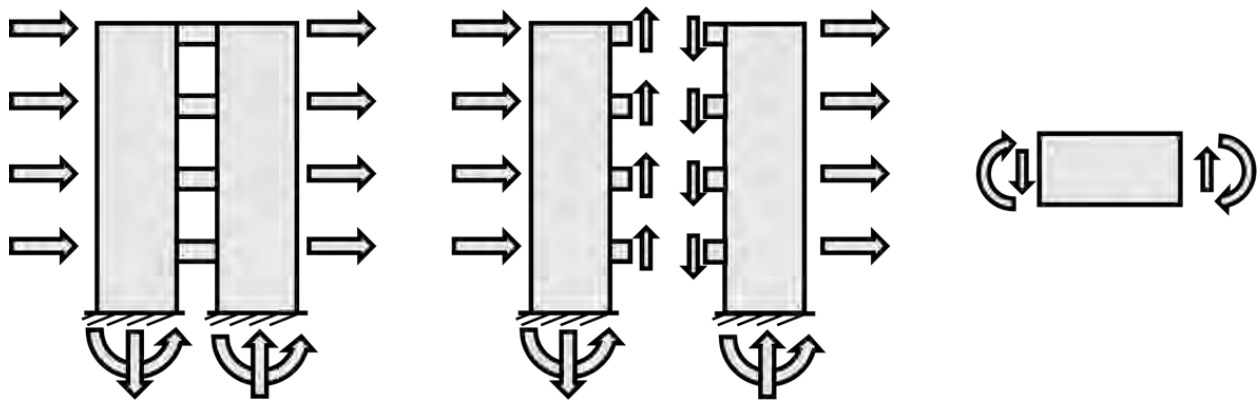

Figure 2.0-2 (a) Overall free-body diagram of coupled shear wall system, (b) Free-body diagrams of individual coupled walls, (c) Free-body diagram of an individual coupling beam

RP3-2.1　Types of Coupling Beams

Wood light frame shear walls do not formally recognize the term coupled shear walls, but do include two shear wall design methods by which partial or full coupling of walls in recognized to occur. These are the perforated shear wall design method and design for continuity around openings, respectively. Both methods include dimensional limits on the coupled wall piers and extensive design requirements. Neither method imposes dimensional limits on the coupling beams. See Chapter RP3-6 of this Resource Paper.

Masonry coupling beams are considered not to be viable. See Chapter RP3-4 of this Resource Paper.

All the different types of coupling beams discussed below are used between concrete cast-in-place concrete shear walls. Precast shear walls and their coupling are discussed in Section RP3-1.3.2 of this Resource Paper. Steel coupling beams are used between steel plate shear walls. Encased steel composite coupling beams are used between composite steel plate shear walls.

In a recently published Structure magazine paper, Liao and Pimentel (2019) have stated: "As one of the most critical members in RC buildings, coupling beams should exhibit excellent energy dissipation capacity with only modest stiffness and strength degradation under cyclic loading. Good ductile hysteretic performance is usually achieved by providing sophisticated detailing, which induces construction difficulties. By varying rebar layout schemes and exploring different materials, various types of coupling beams are considered in searching for a balance between ductile hysteretic performance and construction practicality."

According to Liao and Piementel, there are five commonly-used types of coupling beams that are currently adopted by building codes and the design industry:

- Conventionally reinforced concrete coupling beams
- Diagonally reinforced concrete coupling beams
- Steel coupling beams
- Encased steel composite coupling beams (Figure 2.1-1)
- Embedded steel plate composite coupling beams (Figure 2.1-2)

Two other types of concrete coupling beams need to be added to the list:

- Unbonded post-tensioned precast concrete coupling beams
- Steel-fiber-reinforced concrete coupling beams

Conventionally and diagonally reinforced concrete coupling beams are discussed in detail in Section RP3-2.1.1 below.

Steel coupling beams and encased steel composite coupling beams are used as viable alternatives to avoid the construction difficulties inherent in diagonally-reinforced concrete coupling beams. The steel members for the two coupling beam types are implicitly wide-flange steel members, although steel tubes were also used in early research (Figure 2.1-1). Extensive experiments indicate that both steel coupling beams and encased steel composite coupling beams can provide excellent ductility and energy dissipation capacities, which are comparable to those of diagonally-reinforced concrete coupling beams. These coupling beams are discussed in more detail in Section RP3-2.1.2 of this Resource Paper.
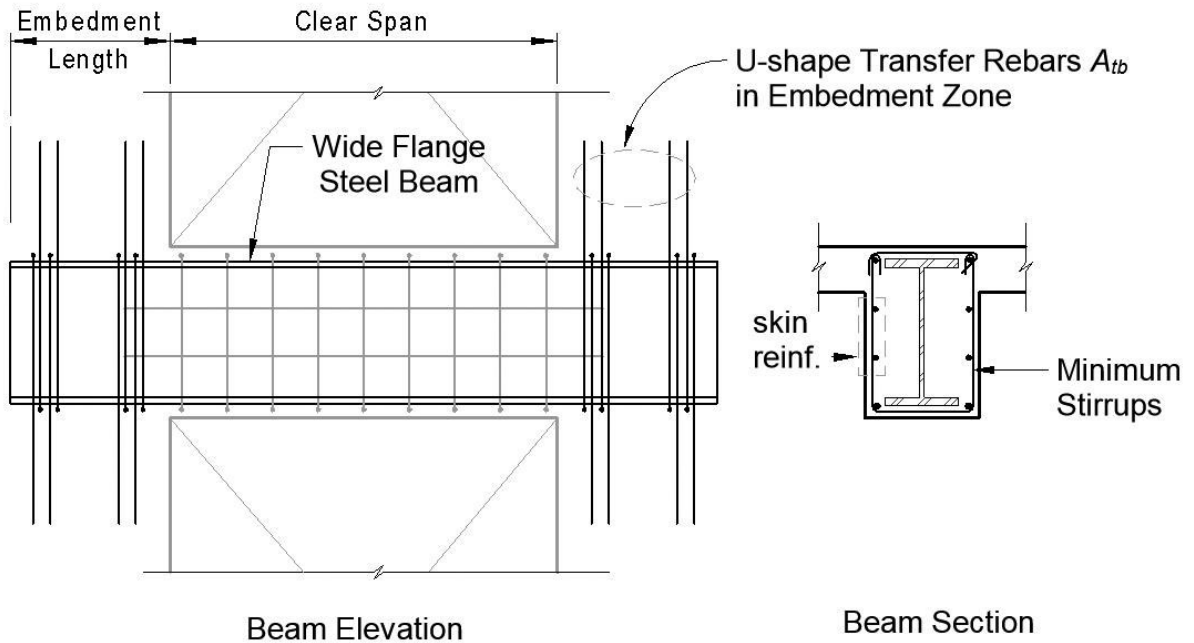
Figure 2.1-1 Encased steel composite coupling beams (Source: Liao and Pimentel 2019)

To alleviate the conflict between steel members and shear wall reinforcement, designers can consider the use of **embedded steel plate composite coupling beams**. As shown in Figure 2.1-2, headed studs are welded to both vertical faces of the steel plate in a typical embedded steel plate composite coupling beam and pose much less disturbance to shear wall vertical reinforcement, although special detailing is still needed for the horizontal/confinement rebars. The headed studs are necessary to provide appropriate anchorage and transfer forces between the concrete portion and the steel plate. Research indicates that the presence of the steel plates can effectively hinder the development of diagonal cracks and prevent brittle failures of concrete coupling beams, and the embedded steel plate composite coupling beam exhibits much better ductile performance and deformability than comparable conventional RC coupling beams. Similar to the encased steel composite coupling beam, proper embedment design of the steel plate is critical to ensure good ductile performance of this type of coupling beam.
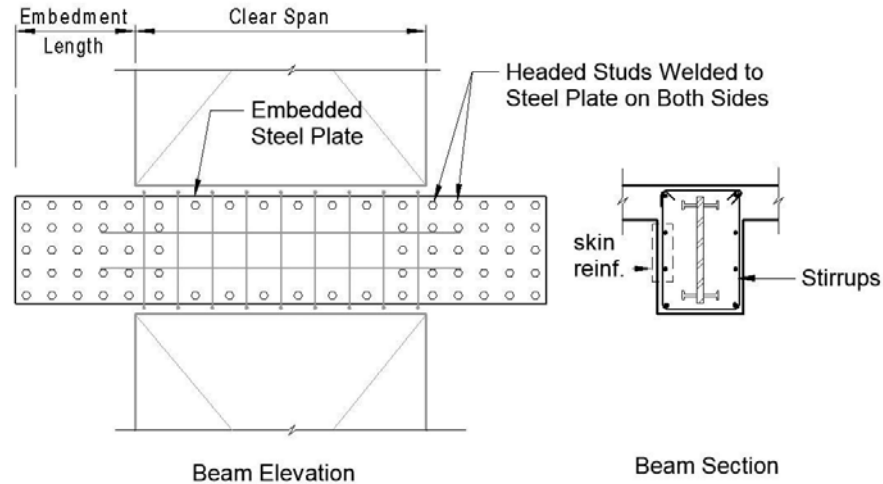
Figure 2.1-2 Embedded steel plate composite coupling beams (Source: Liao and Pimentel 2019)

Unbonded post-tensioned coupling beams offer many advantages including reduced damage to the overall structure, significant self-centering capability, and simpler design and construction for the beams and the wall piers. Different from conventional systems that use monolithic cast-in-place reinforced concrete coupling beams or embedded steel coupling beams, the nonlinear behavior of post-tensioned precast concrete coupling beams is governed by the opening of gaps at the beam ends. Steel top and seat angles are used at the beam-to -wall connections to yield and dissipate energy in the event of a large earthquake. Analytical results show that the coupling beams have stable behavior through large rotations, significant self-centering capability due to the post-tensioning force, and significant energy dissipation due to the yielding of the top and seat angles provided at the beam-to -wall connections. Different from conventional systems with monolithic cast-in -place reinforced concrete coupling beams, the lateral resistance of unbonded post-tensioned precast concrete coupling beams develops through the formation of a diagonal compression strut along the span, upon the opening of gaps at the beam-to -wall interfaces. As a result of these gaps, the tensile stresses in the beam and the wall piers remain relatively small even under large nonlinear displacements, thus, significantly reducing the amount of bonded mild steel reinforcement needed inside the beam.

Steel-fiber-reinforced concrete coupling beams are discussed in detail in Section RP3-2.1.3.
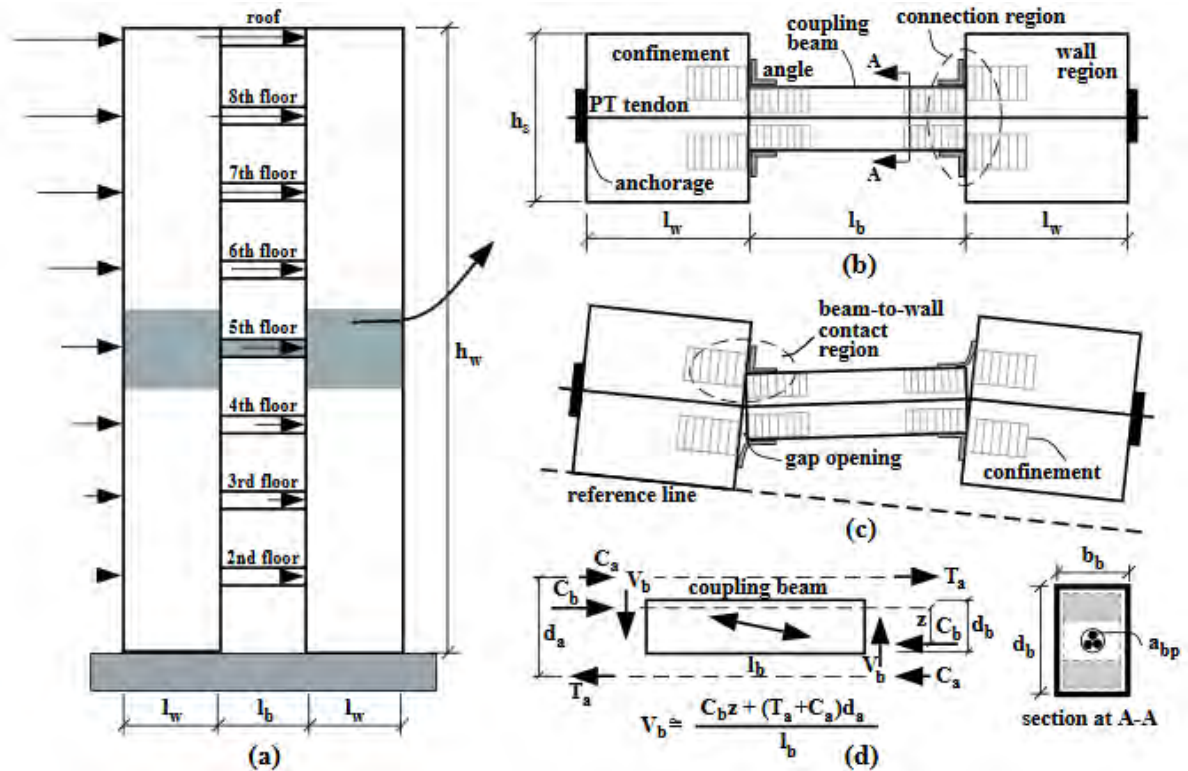
Figure 2.1-3 Coupled wall system – (a) multi-story wall; (b) subassembly; (c) deformed shape; (d) coupling forces

RP3-2.1.1   Cast-in-place concrete coupling beams

ACI 318, for many editions now, has specific detailing rules for coupling beams linking special   (specially detailed) shear walls that are permitted to part of the seismic force-resisting systems of buildings assigned to SDC D, E, or F.

ACI 318-19 (ACI 2019) requires that coupling beams with clear span to total depth ratio $l_n/h \geq 4$ be designed and detailed as beams of special moment frames in compliance with Section 18.6, with the wall boundary considered to be a column.

Coupling beams with $l_n/h < 2$ and $V_u > 4\sqrt{f'_c}A_{cw}$, are required to be reinforced with two intersecting groups of diagonally placed bars symmetrical about midspan.

Coupling beams that do not fall in either of the above groups can be diagonally reinforced as indicated above or can be deigned and detailed like beams of special moment frames in accordance with Sections 18.6.3 through 18.6.5, with the wall boundary considered to be a column.

Through ACI 318-05, the two groups of diagonal bars had to be individually confined basically like reinforcing bars in a special moment frame column (Figure 2.1-4). From 318-08 onwards, a second option is also available. Instead of confining the two groups diagonal bars individually, the entire coupling beam can be confined as shown in Figure 2.1-5. When the first option (confinement of individual diagonals) is chosen, the requirements illustrated in Figure 2.1-6 must be followed.

(a)

Confinement of
Diagonal Bars
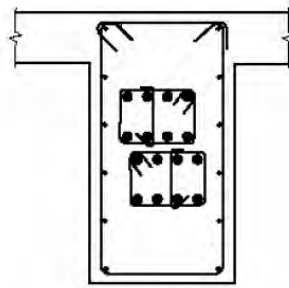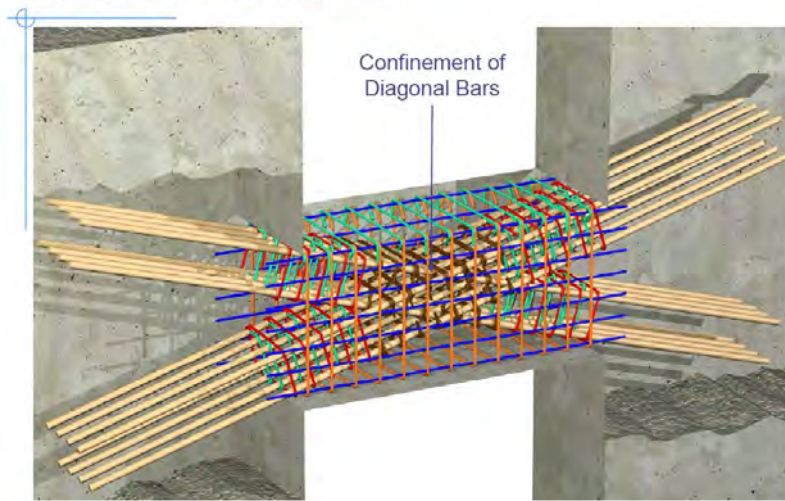
(b)

**Figure 2.1-4 Diagonally reinforced coupling beam, with diagonals confined individually
(Source: http://nees.seas.ucla.edu/pankow)**

(a)   (b)
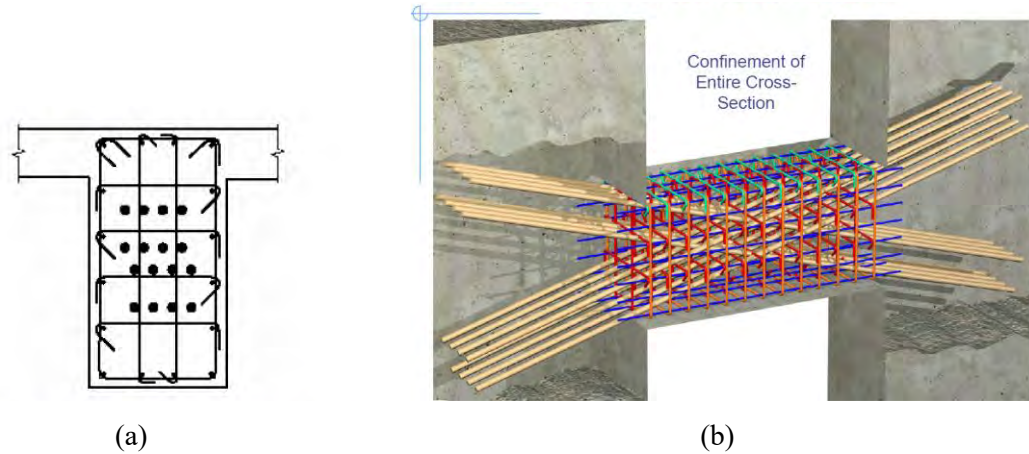
Figure 2.1-5 Diagonally reinforced coupling beam, with entire coupling beam confined (Source: http://nees.seas.ucla.edu/pankow)
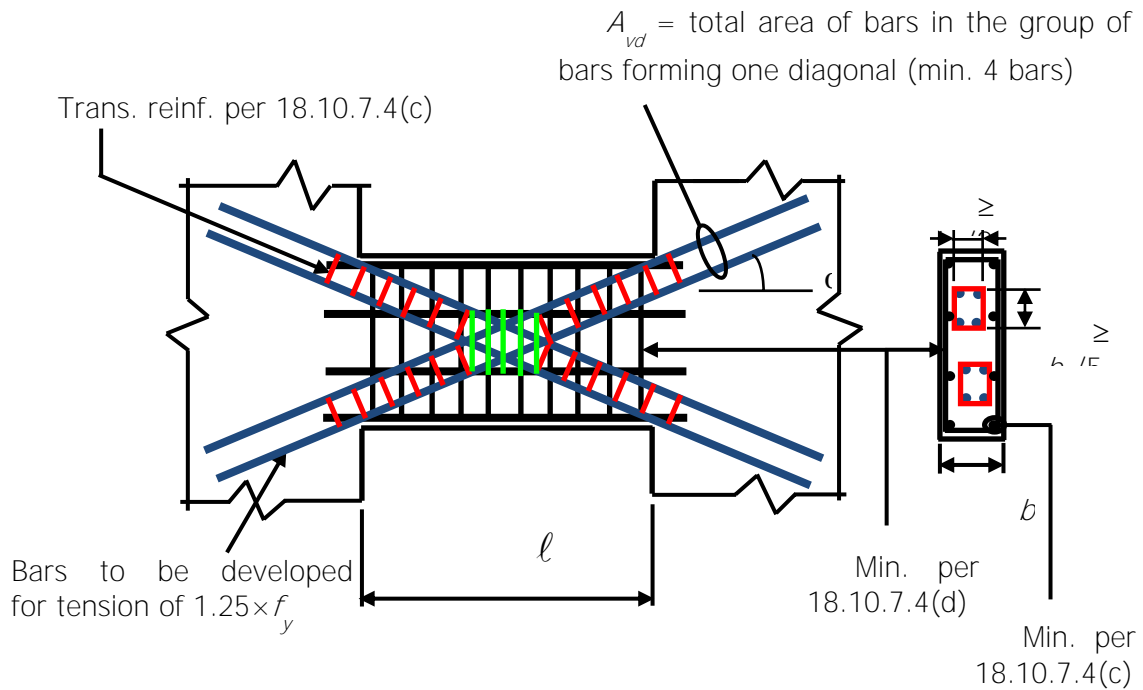
Figure 2.1-6 Detailing requirements for individually confined groups of diagonal bars in a coupling beam (ACI 318-19 Section 18.10.7.4) [Figure Credit: S. K. Ghosh Associates LLC]

ACI 318-19 detailing requirements for coupling beams linking special shear walls are illustrated in Figure 2.1-7, adapted from NIST Tech Brief (Moehle et al. 2012). Note that the use of strut and tie models for beams of very low span-to-depth ratios is optional, not mandatory. Please note also that, according to ACI 318-19 Section 21.2.4.3, ϕ for diagonally reinforced coupling beams is 0.85.
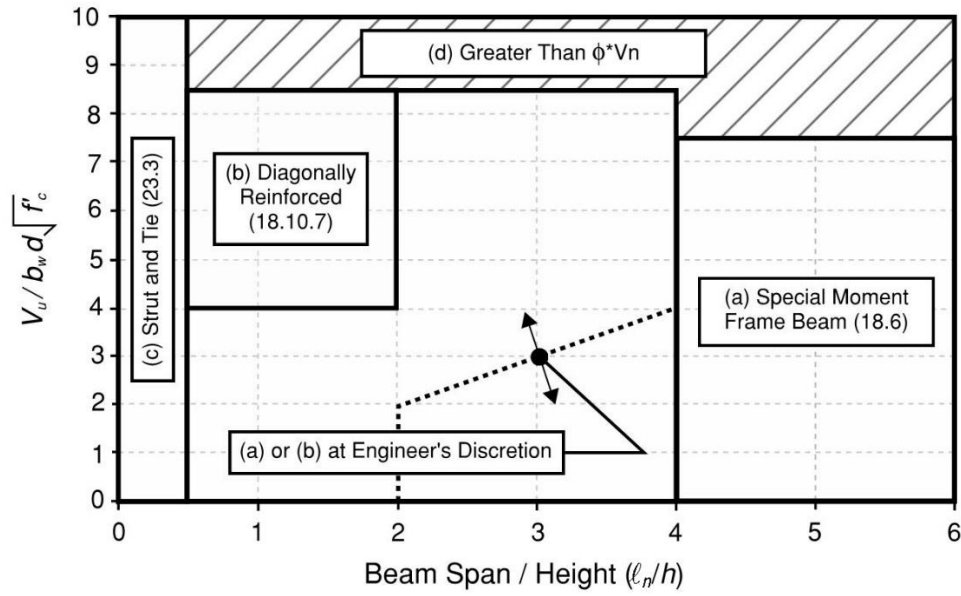
Figure 2.1-7 Summary of ACI 318-19 detailing requirements for reinforced concrete coupling beams (Source: Moehle et al. 2012)

A diagonally reinforced coupling beam complying with ACI 318 detailing requirements is shown in Figure 2.1-8.

Figure 2.1-8 A diagonally reinforced coupling beam
(Source: http://nees.seas.ucla.edu/pankow)

RP3-2.1.2   Concrete encased steel composite coupling beams

The use of steel coupling beams within a concrete shear wall lateral system has gained momentum in recent years as a viable alternative to concrete coupling beams. Research by Motter et al. (2014) has demonstrated

that appropriately proportioned beams and properly detailed embedment regions result in wall coupling that provides high strength and large ductility.

The design philosophy for steel coupling beams originated from embedded steel bracket connections first published in the 1971 PCI Design Handbook (PCI 1971). Known as corbels per current terminology, these cantilever elements generally carry high shears and low moments, and transfer forces to a concrete support via opposing vertical compression forces (Figure 2.1-9).
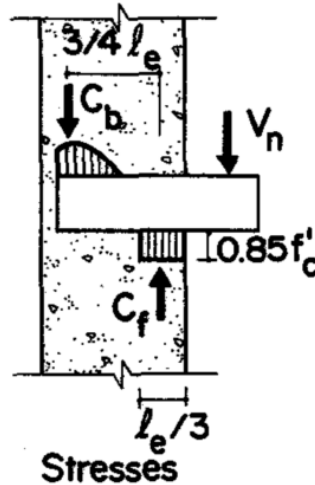
Figure 2.1-9 Steel bracket to supporting concrete element connection

In the 1980's, research by Marcakis and Mitchell (1980) as well as Mattock and Gafar (1982) sought to establish a rational analytical model for the design of these elements based on physical experimental results. The effects of beam-to-wall width ratio, wall vertical reinforcement ratio, wall vertical strain, and vertically welded flange reinforcement were all studied. The resulting design equations, focusing primarily on the length of the embedment region, have remained largely unchanged by subsequent research results.

Work by Harries, K.A., Gong, B., and Shahrooz, B.M. (2000) in the 1990's extended these concepts from brackets to coupling beams. The behavior and transfer of forces from a steel bracket to a concrete support are effectively the same as for a coupling beam considered on one side of its center inflection point. Tests were conducted with concrete-encased steel wide-flange sections subject to multi-cycle plastic deformations (Figure 2.1-10).
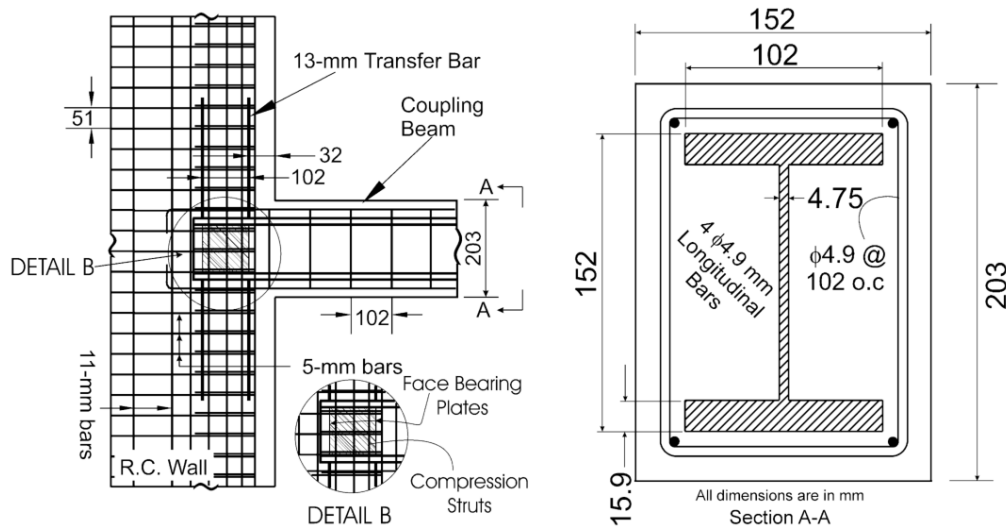
Figure 2.1-10 Tests of concrete-encased steel wide-flange sections

These tests validated the ability to achieve stable hysteretic behavior, determined the effective point of fixity, studied the effect of wall confinement, and generally quantified the contribution of the encasement to beam strength and stiffness. Their findings largely serve as the basis for the subsequent AISC Seismic Provisions (AISC 2016) for composite steel coupling beams.

Current AISC 341-10 (AISC 2010) provisions also include design requirements for bare steel coupling beams used in Composite special Shear Walls (C-SSW). Examples of bare steel coupling beams are unknown. Such an application would require the beam to be fireproofed and architecturally enclosed anyway. The form closure where the bare beam enters the concrete or composite shear wall also presents a challenge. A bare steel coupling beam will have notably reduced stiffness as compared to a composite steel coupling beam. For slender coupled shear wall systems, coupling beam stiffness contributes significantly to overall system stiffness. Lastly, bare steel coupling beams were not included in Motter's testing of large-scale high-ductility elements. Although coupling beam ductility is not expected to be compromised by the absence of concrete encasement (given proper lateral bracing), the full hysteretic behavior of such beams, including embedment region effects, is not currently known. This presents additional uncertainty in non-linear modeling.

While steel coupling beams have been included in a material reference standard since the early 2000's, they have not been regularly used in design. Concerns regarding constructability, particularly in challenging detailing requirements and overlap between the concrete and steel trades, have limited the use of steel coupling beams.

In the early 2010's, a testing program was conducted by Motter et al. (2013) to address these existing obstacles to widespread use. Vertical flange bars were eliminated, wall boundary confinement was preserved by means of through-rods and face plates, and beam sections were twice as deep as those tested previously (approximating two-thirds scale).
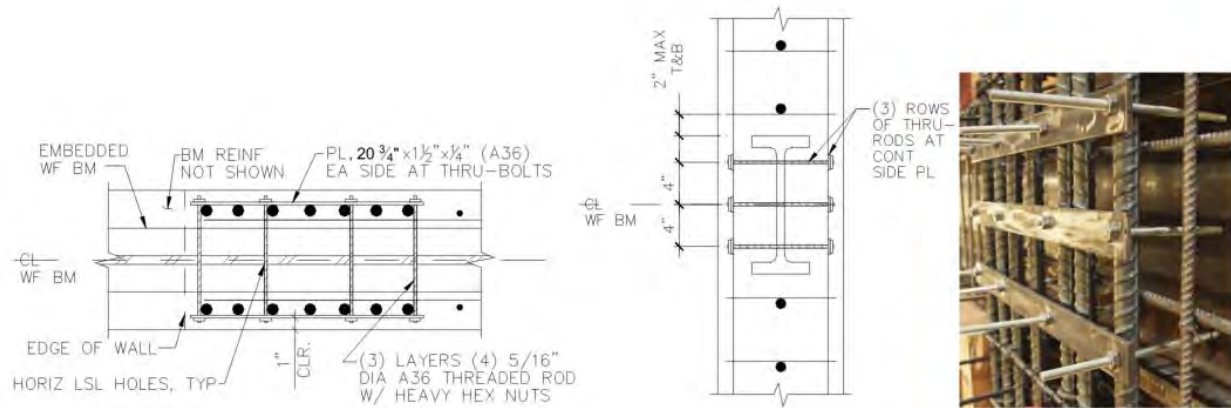
Figure 2.1-11 Large-scale tests of concrete-encased steel wide-flange sections

Primary variables studied were 1) embedment length of the beam into the wall support and 2) wall confinement density above and below the embedment region. The experimental results and related findings establish requirements for embedment and confinement necessary to achieve "special" behavior equivalent to that of special concrete coupling beams. Somewhat pinched hysteretic behavior and lower ductility capacity were found for tests not satisfying these requirements; the details used in these tests were deemed appropriate for use in an "ordinary" lateral system. Backbone modeling parameters, for use in non-linear evaluations, were also published in this study (Figure 2.1-12).

. While the recommendations of Motter et al. (2017) are not adopted by the concrete reference standard, ACI 318, Performance Based Seismic Design methodologies are commonly used to design and detail steel coupling beams.

RP3-2.1.3 Design of Steel Fiber-Reinforced Concrete Coupling Beams

RP3-2.1.3.1 Background, behavior, and research

Reinforcement congestion has long been the bane of concrete construction in high seismic regions. Some of the most difficult and congested reinforcement is found in shear wall coupling beams. Traditionally, diagonal bars are used to reinforce these coupling beams, combined with tightly spaced stirrups and ties (Figure 2.1-13). This creates significant congestion and conflict between the diagonal bars and adjacent shear wall boundary element reinforcement.
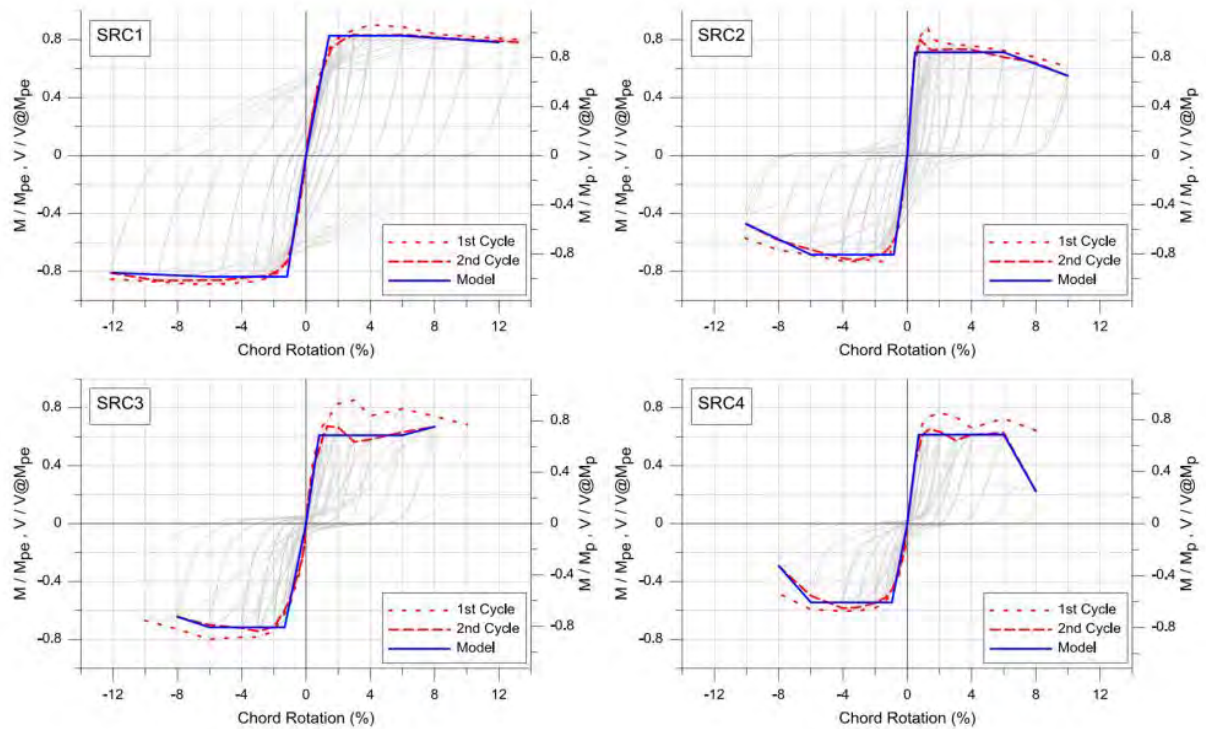
Figure 2.1-12 Backbone modeling and load-displacement response of concrete-encased steel coupling beams (Motter et al. 2013)
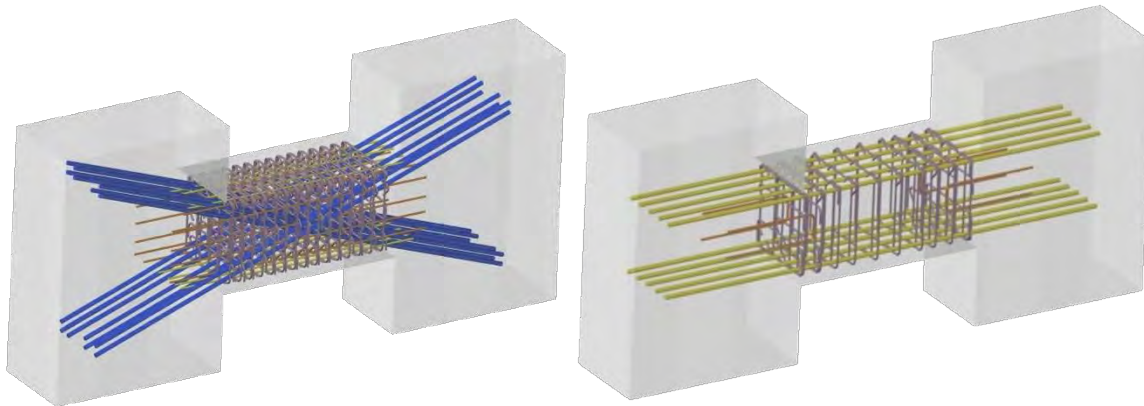
Figure 2.1-13 Diagonally reinforced and steel-fiber-reinforced coupling beams with similar capacity [Figure Credit: CKC Structural Engineers]

While steel fibers are commonly used in tunnel linings, industrial floors, and other applications where high toughness is required, their use in building structures has thus far been limited. After more than a decade of research and development, SFRC (steel-fiber-reinforced concrete) for use in shear wall coupling beams is now available. It involves mixing high-strength steel fibers into the concrete used to construct coupling beams (Figure 2.1-14). SFRC can be used for designs in regions of high seismicity, providing

improved strength and added ductility. Further, this innovation saves significant labor and material, because steel fibers replace the tedious process of placing and tying much of the rebar in what are typically very heavily congested zones. Discussions with general contractors have indicated that the removal of the diagonal bars can save up to a full day per floor in the construction schedule. The added cost of the steel fibers in the concrete and the crane time needed to bucket the SFRC were overcome by the savings in reinforcement quantity and placing labor as determined by the contractor's pricing studies.
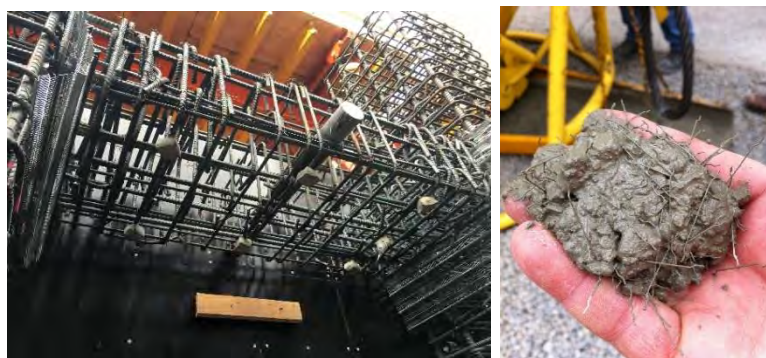
Figure 2.1-14 SFRC Coupling Beam [Figure Credit: CKC Structural Engineers]

The added steel fibers benefit the design of coupling beams in a number of ways. Typically, in regions of high seismicity, the concrete is assumed to have no contribution to the shear strength of the coupling beam. However, testing has shown that the addition of the steel fibers can contribute up 60% of the total shear strength of the beam, as well as up to 15% of the flexural strength of the coupling beam. Essentially, coupling beam strengths can be maintained, or even enhanced, by adding steel fibers and reducing the quantity of traditional reinforcement.

The value of the fibers extends beyond strength considerations and they can increase the durability and ductility of the coupling beam (Figure 2.1-15). At higher levels of rotation, the SFRC beams tend to develop many small cracks that are distributed over larger areas of the concrete. In a side-by-side test (Figure 2.1-16), a coupling beam without added steel fibers was shown to exhibit high levels of localized damage and concrete spalling, while a similarly reinforced SFRC beam at the same rotation held together better as a single unit and had less damage distributed over larger areas of the beam. This can be partly attributed to the ability of the steel fibers to increase the tensile strength of the concrete, raising the force threshold at which spalling occurs.

The study of SFRC coupling beams started at the University of Michigan with financial support from the National Science Foundation. Further research was funded by the National Science Foundation Network for Earthquake Engineering Simulation (NEES), and Bekaert, a Belgium-based global supplier of steel fibers, as well as the Charles Pankow Foundation.
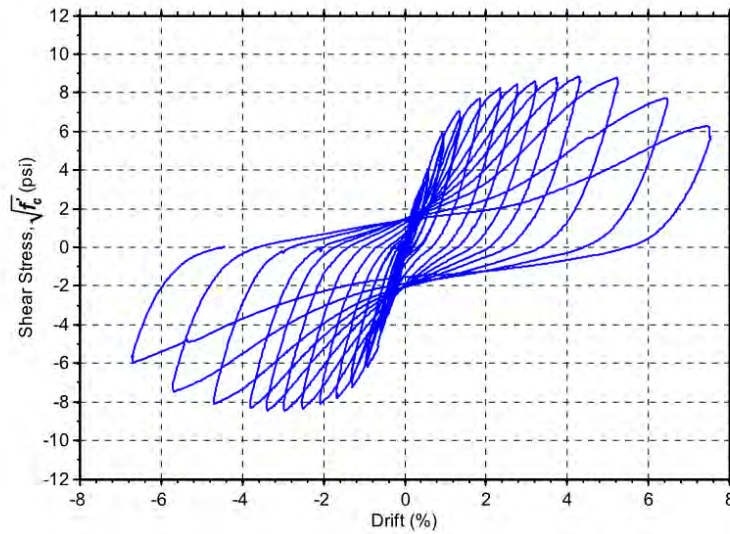
Figure 2.1-15 Example SFRC coupling beam hysteresis loops [Figure Credit: Setkit, 2012]

Conventional RC
Coupling Beam

SFRC Coupling
Beam

Figure 2.1-16 Comparative Testing [Figure Credit: Lequesne, 2011]

RP3-2.1.3.2   Design Philosophy

Similarly to conventionally reinforced coupling beams designed per ACI 318-19, SFRC coupling beams follow capacity design principles. Tensile yielding of the longitudinal reinforcement at or near the ends of the beam is the primary mechanism by which seismic energy is dissipated. For adequate spread of plasticity,

dowel reinforcement, typically U-shaped, is provided at each end of the coupling beam. The dowel reinforcement has been proven effective with embedded lengths on the order of 6 to 9 dowel reinforcement bar diameters from the face of the joint into the coupling beam (Perez-Irizarry and Para-Montesinos 2016). Flexural strength is evaluated at two critical sections: at the extreme end of the beam, where the longitudinal reinforcement and dowel reinforcement contribute to flexural strength; and at the termination of the dowel reinforcement, where flexural strength is determined assuming tensile contribution from both the longitudinal reinforcement and the SFRC itself. Beam is designed to resist the shear associated with the probable flexural strength of the beam. Both transverse reinforcement and contribution of the SFRC are considered for determination of the beam shear strength. Full volumetric confinement per ACI 318-19 is provided at each end of the beam, where flexural yielding is likely to occur. Laboratory testing has been performed with beam span-to-depth ratios from 2.0 to 3.3. SFRC coupling beams are ideally used where relatively high shear stress demands exist at these aspect ratios (see shaded region in Figure 2.1-17).
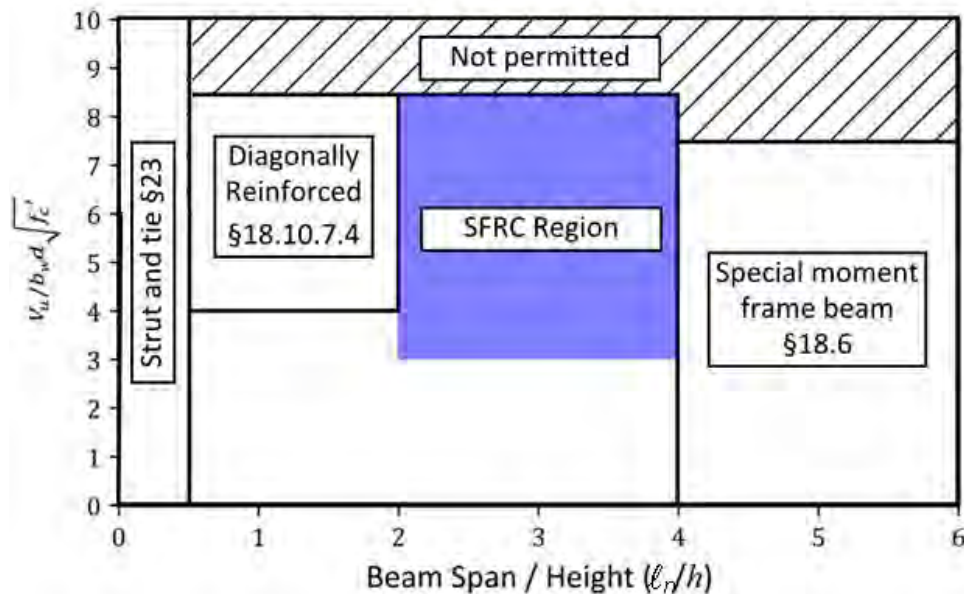
Figure 2.1-17 Coupling beam design space with SFRC region (Adapted from Moehle et al. 2012)

RP3-2.1.3.3   Design procedure recommendation

A proposed design procedure as developed from the initial research at the University of Michigan and early project implementation of SFRC coupling beams is as follows:

- Calculate the required flexural strength of the SFRC coupling beam at the face of wall, with no assumed SFRC contribution to flexural strength.
- Design the dowel reinforcement to resist approximately 20% to 30% of the total flexural demand at the face of the coupling beam.
- Design the longitudinal reinforcement to resist the remaining flexural demand at the face of the coupling beam.
- Determine the shear associated with the probable flexural strength at the ends of the dowel reinforcement and the shear corresponding to the probable flexural strength at the beam ends. The use of dowel reinforcement embedded 6 to 9 bar diameters into the coupling beam has proven to be effective in contributing to flexural strength at the beam-to-wall interface and in attaining the

desired spread of inelasticity, when the ratio of aforementioned shears associated with the two probable flexural strengths is less than 1.1.

- Determine the amount of transverse shear reinforcement required near beam mid-span. The design shear for this determination should envelope the analytical shear demand, - the shear associated with the probable flexural strength at the beam ends, and the shear associated with the probable flexural strength at the termination of the dowel reinforcement. A contribution of up to $4A_{cv}\sqrt{f'_c}$ can be provided by the SFRC when a steel fiber volume fraction of 1.5% is used (smaller shear contributions are associated with SFRC when the 1.5% volume fraction is reduced, see Perez-Irizarry and Parra-Montesinos, 2016). This contribution of the SFRC to the shear strength of the coupling beam should be limited such that the SFRC contributes no more than 60% of the total shear strength. Thus, no less than 40% of the shear strength of the coupling beam must come from the contribution of transverse reinforcement.

- Provide transverse confinement reinforcement, similar to what is required per ACI 318-19 at potential plastic hinge regions of columns of Special Moment Frames, over a length of half the beam depth from the wall face at each end of the coupling beam. The amount of transverse reinforcement provided for confinement at the beam ends should not be less than the transverse reinforcement required for contribution to shear strength.

- Check that adequate shear friction strength is provided at the wall-beam interface for force transfer. Contributions to the shear friction capacity from the longitudinal reinforcement, dowel reinforcement, and adequately developed skin reinforcement (if present) may be assumed.

RP3-2.2   References

ACI Committee 318 (2019). *Building Code Requirements for Structural Concrete (ACI 318-19)* and *Commentary (ACI 318R-19)*. American Concrete Institute, Farmington Hills, MI.

ASCE Committee 7 (2017). *Minimum design loads and associated criteria for buildings and other structures, ASCE/SEI 7-16.* American Society of Civil Engineers, Reston, VA.

ASCE Committee 41 (2014). *ASCE Standard, ASCE/SEI 41-13: Seismic evaluation and retrofit of existing buildings*. American Society of Civil Engineers, Reston, VA.

Harries, K.A., Gong, B., and Shahrooz, B.M. (2000), "Behavior and Design of Reinforced Concrete, Steel, and Steel-Concrete Coupling Beams," *Earthquake Spectra*, November 2000, Vol. 16, No. 4, pp. 775-799.

Moehle, J., Ghodsi, T., Hooper, J., Fields, D., and Gedhada, R. (2011, Revised 2012)). *Seismic Design of Cast-in-Place Concrete Special Structural Walls and Coupling Beams: A Guide for Practicing Engineers*, NEHRP Seismic Design Technical Brief 6, NIST GCR 11-917-11REV-1. National Institute of Standards and Technology, Gaithersburg, MD.

Motter, C.J., Fields, D.C., Hooper, J.D., Klemencic, R., and Wallace, J.W. (2013), "Large-Scale Testing of Steel Reinforced Concrete (SRC) Coupling Beams Embedded into Reinforced Concrete Structural walls," *UCLA SGEL Research Report*, University of California, Los Angeles.

Motter, C.J., Fields, D.C., Hooper, J.D., Klemencic, R., and Wallace, J.W. (2017), "Steel-Reinforced Concrete Coupling Beams II: Modeling," *Journal of Structural Engineering*, ASCE, Vol.143 (3).

Paulay, T. and Priestley, M. J. N. (1992). *Seismic Design of Reinforced Concrete and Masonry Buildings.* John Wiley & Sons, Inc., New York, NY.

Liao, S., and Pimentel, B. (1919). "Coupling Beam Types," *Structure*, January, pp. 8-12.

Parra-Montesinos, G. J., Wight, J.K., Kopczynski, C., Lequesne, R., Setkit, M., Conforti, A., and Ferzli, J. (2014). "High-Performance Fiber Reinforced Concrete Coupling Beams: From Research to Practice," *Proceedings*, Tenth U.S. National Conference on Earthquake Engineering, Anchorage, AK.

Lequesne, R. D., Parra-Montesinos, G. J. and Wight, J. K. (2009), "Test of a Coupled Wall with High Performance Fiber Reinforced Concrete Coupling Beams," Thomas T. C. Hsu Symposium: Shear and Torsion of Concrete Structures, SP-265, American Concrete Institute, Farmington Hills, MI.

Perez-Irizarry, A. and Parra-Montesinos, G. J. (2016). *Evaluation of Seismic Behavior of Coupling Beams with Various Types of Steel Fiber Reinforced Concrete*. The University of Wisconsin, Madison, WI

Lequesne, R. D. (2011). *Behavior and Design of High-Performance Fiber-Reinforced Concrete Coupling Beams and Coupled-Wall Systems*. The University of Michigan, Ann Arbor, MI.

Marcakis K. and Mitchell D. (1980), "Precast concrete connections with embedded steel members," *Prestressed Concrete Institute Journal*, 25 (4), 88-116

Mattock A. H. and Gaafar G. H. (1982), "Strength of embedded steel sections as brackets," *ACI Journal*, 79 (2).

Setkit, M. (2012). *Seismic Behavior of Slender Coupling Beams Constructed with High-Performance Fiber-Reinforced Concrete*. The University of Michigan, Ann Arbor, MI.

Weldon, B. and Kurama, Y. (2012). "Analytical Modeling and Design Validation of Posttensioned Precast Concrete Coupling Beams for Seismic Regions," *J. of Structural Engineering*, Vol. 138, No. 2, February, pp. 224-234.

Weldon, B. and Kurama, Y. (2010). "Experimental Evaluation of Post-Tensioned Precast Concrete Coupling Beams," *J. of Structural Engineering*, Vol. 136, No. 9, September, pp. 1066-1077.

Weldon, B. and Kurama, Y. (2007). "Nonlinear Behavior of Precast Concrete Coupling Beams," J. of Structural Engineering, Vol. 133, No. 11, November, pp. 1571-1581

RP3-3   CONCRETE SHEAR WALLS

RP3-3.0   Introduction

The purpose of this chapter is to present a systematic treatment of one of the most common types of seismic force-resisting elements: concrete shear walls. This summary is intended to provide information that is not commonly available. Different wall configurations are discussed. The influence of core wall configuration on the seismic performance of buildings is explained. A discussion of wall buildings with irregularities is included. The definition of ductile coupled reinforced concrete shear walls is introduced. The distribution of lateral deformations along the heights of multi-story core wall buildings is described; it is pointed out that there is typically very little yielding of the longitudinal reinforcement anywhere along the height of a structurally regular multi-story building. Various aspects of the shear design of reinforced concrete shear walls are discussed in depth. A very important ACI 318-19 change amplifying the design shear force for special reinforced concrete shear walls is described, and background given. Several important changes made in ACI 318-19 concerning the detailing requirements of slender special reinforced concrete shear walls are enumerated. Finally, through work done by IT-4, separate line items featuring ductile coupled reinforced concrete shear walls are expected to be introduced in Table 12.2-1 of ASCE 7-22. The FEMA P695 study that supplied the justification for this important change is briefly described in this chapter.

RP3-3.1   Wall Configurations

Concrete shear wall configurations are numerous and are dependent on the building functional requirements, lateral demands and architectural constraints (Figure 3.1-1). These walls will be subject to axial, lateral and torsional forces depending on their geometric configuration, orientation, and location within the building plan. This section describes common concrete wall shapes and provides general guidelines concerning favorable wall layouts in buildings.

(a) Rectangular shape   (b) "Bar bell" shape

(c) Flanged walls in common T, L, C and I shapes

(d) Possible configuration of a core-wall
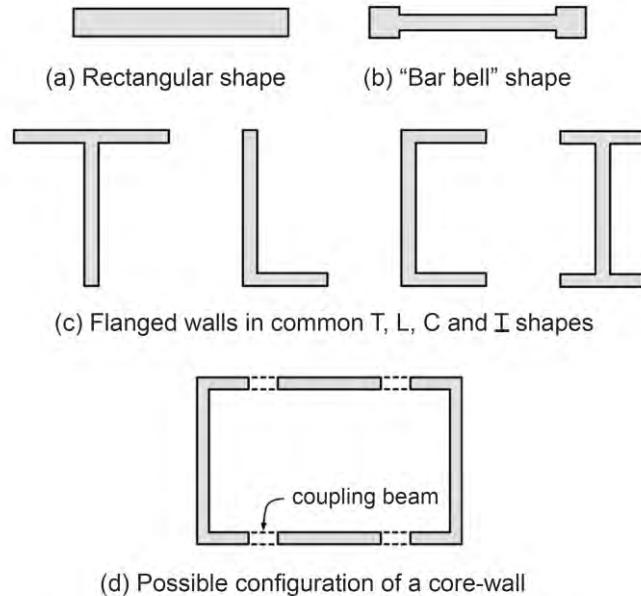
Figure 3.1-1 Wall Cross Sections [Figure Credit: NIST Tech Brief 6]

Planar walls with rectangular cross sections are commonly used in buildings due to the ease of design and construction as well as the ability to integrate the wall within the architectural layout. Planar walls have reduced lateral stability about the week axis of the wall and rely on additional perpendicular walls to resist out of plane forces. Figure 3.1-2 illustrates stable and unstable planar wall systems. Planar wall application

is common in buildings of moderate height, where building drift is limited and added lateral stiffness is not required.
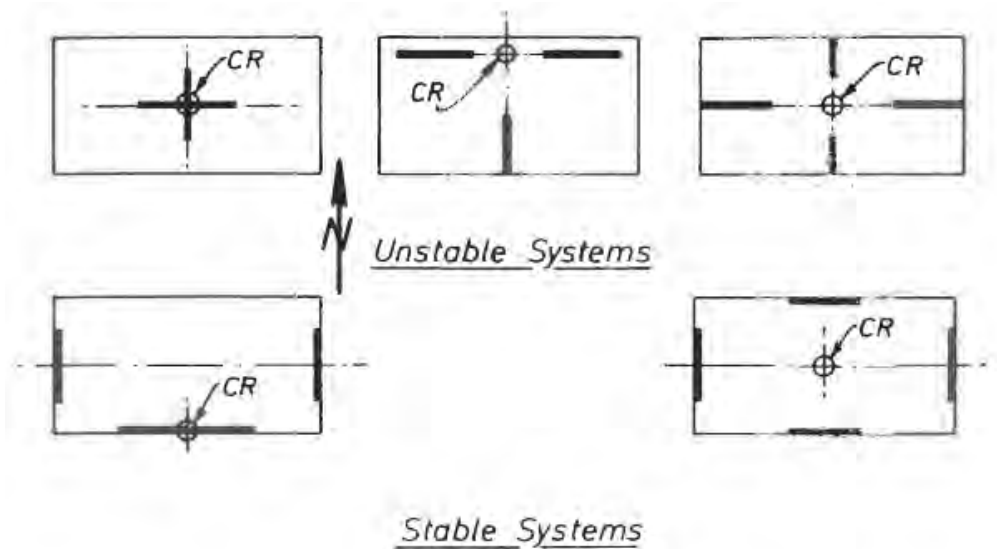
Figure 3.1-2 Torsional Stability of Planar Wall Systems [Figure Credit: Paulay and Priestley]

Shear walls can be conFigured in numerous ways (Figure 3.1-1). Rectangular walls are common, but very thin walls can have performance problems and should be avoided. Barbell walls have boundary columns that contain longitudinal reinforcement for moment resistance, improve wall stability, and provide an element to anchor beams framing into the wall. The boundary columns, however, might be architecturally undesirable and might increase forming costs. Intersecting wall segments can be combined to create flanged walls, including T, L, C, U, H, and I configurations. Core walls enclose elevators, stairways, and similar vertical spaces, with coupling beams often connecting wall components over doorways.

Research results suggest the best earthquake performance is achieved when a symmetric configuration, in which lateral loading activates similarly sized and similarly reinforced compression and tension regions, is employed (Birely 2012). Examples of symmetric wall configurations include symmetrically reinforced rectangular (i.e. planar), barbell, H-shaped and I-shaped walls as well as coupled C-shaped walls, as shown in Figure 3.1-1.

In contrast to symmetric walls, asymmetric walls exhibit poorer seismic performance. Consider the T-shaped wall in Figure 3.1-1. When the flange is in tension, the base of the web is in compression. Clearly, the tension capacity of the flange greatly exceeds the compressive capacity, and this results in the wall experiencing large compressive demands, which ultimately results in the wall experiencing a relatively non-ductile compression-controlled failure.

This phenomenon and the potential for asymmetric walls to exhibit poor seismic performance have been demonstrated by research and recent earthquake damage in the Chilean Earthquake of 2010. Figure 3.1-3 shows fragility curves dependent on cross-sectional shape from a test database with over 50 ductile walls. The symmetric flanged (e.g., I-shaped cross section) walls have significantly more drift capacity than asymmetric flanged walls (e.g., T-shaped cross section). A review of buildings exposed to the 2010 Chilean earthquake concluded that wall configuration contributed to localization and accumulation of damage;

although for Chilean buildings wall configurations were typically complex and damage was typically associated with floor-to-floor changes in wall configuration rather than asymmetry.
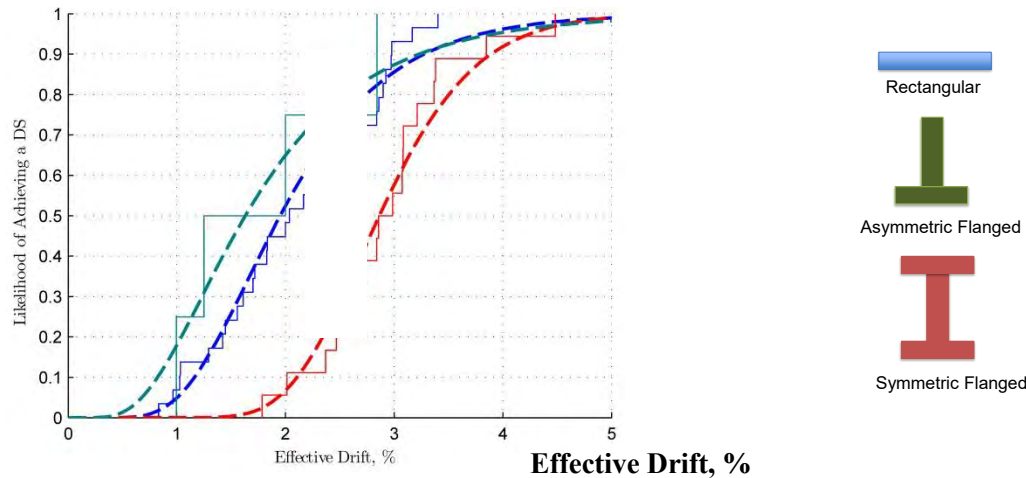
Figure 3.1-3 Probabilistic drift capacity models for rectangular and asymmetric and symmetric flanged walls.

RP3-3.2   Core wall configuration and seismic performance

Concrete walls are commonly applied in buildings as coupled walls that form a core wall system. These core wall systems are the predominant seismic force-resisting system for tall concrete buildings in high seismic regions along the west coast. Core wall systems consist of a combination of wall piers that are solid or connected with coupling beams with various span to depth ratios. Figure 3.2-1 illustrates an example core wall system for a 40-story tower with basement levels.
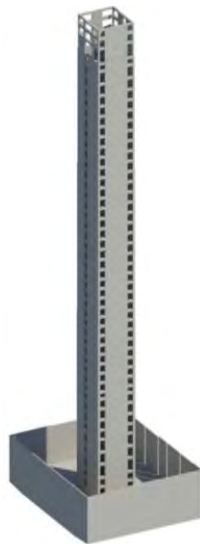
Figure 3.2-1 Example Core Wall System in 40-Story Tower [Figure Credit: CKC Structural Engineers]

The lateral response of the coupled wall system is mainly impacted by two factors: the ground motions and the geometry of the seismic force-resisting system, where the structural engineer can have the most influence on the overall behavior of the building. A seismic force-resisting system with low energy dissipation leads to higher shear, flexural, and diaphragm demands. The seismic energy generated by ground motions is dissipated in the core walls through two mechanisms; elastic deformation and plastic hinging. Relying primarily on elastic deformations to resist lateral loads leads to much larger force demands on the entire seismic force-resisting system. Seismic energy is more efficiently dissipated via flexural yielding and the formation of plastic hinges, typically at or near the base of the shear wall core. This response allows the vertical reinforcement to yield and undergo inelastic deformations. This is a well-established method and the current building code has specific requirements for reinforcement detailing at the potential hinge regions.

Rather than only considering plastic hinging of the shear walls near the base of the structure, a proven and efficient way to dissipate seismic energy is to introduce a series of coupling beams throughout the shear wall core. These structural fuses are detailed to accommodate large inelastic deformations while maintaining adequate strength. The internal forces generated in the system, such as core wall moment and shear, can be significantly reduced while increasing the system ductility. The introduction of coupling beams increases the redundancy of plastic hinging mechanisms in a core wall system. This redundancy can improve the building response during a seismic event and mitigate the damage to the vertical elements of the seismic force-resisting system such as the shear wall piers.

Note: S/D is coupling beam span to depth ratio
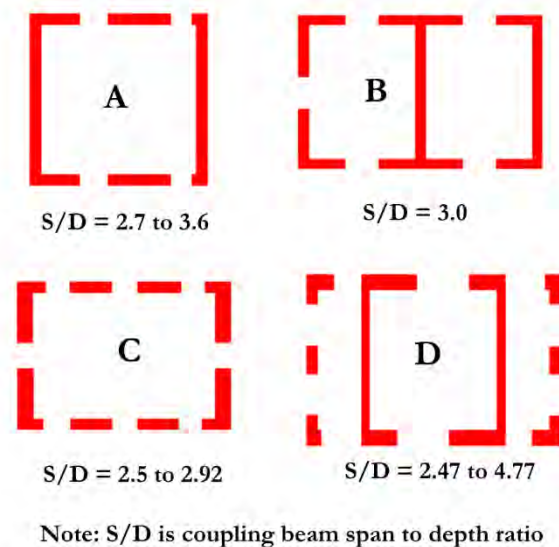
Figure 3.2-2 Couple Core Wall Configurations [Figure Credit: CKC Structural Engineers]

To better understand the impact of coupling beams in wall configurations, a series of sensitivity studies was conducted to evaluate core shear and inter-story drift with and without additional openings and coupling beams being introduced into solid shear walls. It was observed that the shear demands in the system could be significantly reduced, both in the shear walls and at the transfer diaphragms, without excessive impact on the seismic drift of the building by the addition of coupling beams at targeted locations. Figure 3.2-2 illustrates a variety of core wall layouts subjected to high seismic ground motions representative of the West Coast of the United States. These four core wall configurations utilized a special reinforced concrete shear wall seismic force-resisting system and were 400 ft (122 m) to 500 ft (152 m) tall. Nonlinear models were generated using PERFORM-3D software and each model was subjected to at least seven pairs of scaled, maximum considered earthquake (MCE) ground motions. As indicated in Figure

3.2-2, coupling beams with span to depth ratios varying between 2.5 and 4.77 were located at every floor level. The coupling beams were designed and detailed using a combination of diagonal and horizontal reinforcement.

Core wall A represents the seismic force-resisting system of a 42-story tower with 5 levels below grade. A nonlinear model was used to verify the acceptability of the special reinforced concrete shear wall seismic force-resisting system. The core wall is comprised of four coupling beams with diagonal reinforcement per ACI 318 in one direction, and solid concrete piers in the orthogonal direction. The span to depth ratios of the coupling beams are all in the range of 2.7 to 3.6. This core configuration illustrates the effect that coupled shear walls can have on energy dissipation. While the overall shape of the shear wall core is relatively square, the shear response of the building varied significantly. In the solid wall direction, the peak core shear forces were approximately 12,000 kips (53,378 KN) near the base. In the coupled wall direction, the peak core shear forces were approximately 4,500 kips (20,000 KN) near the base (Figure 3.2-3). The difference in core shear between the two orthogonal directions can be directly attributed to the geometries of the coupled and solid wall layout.
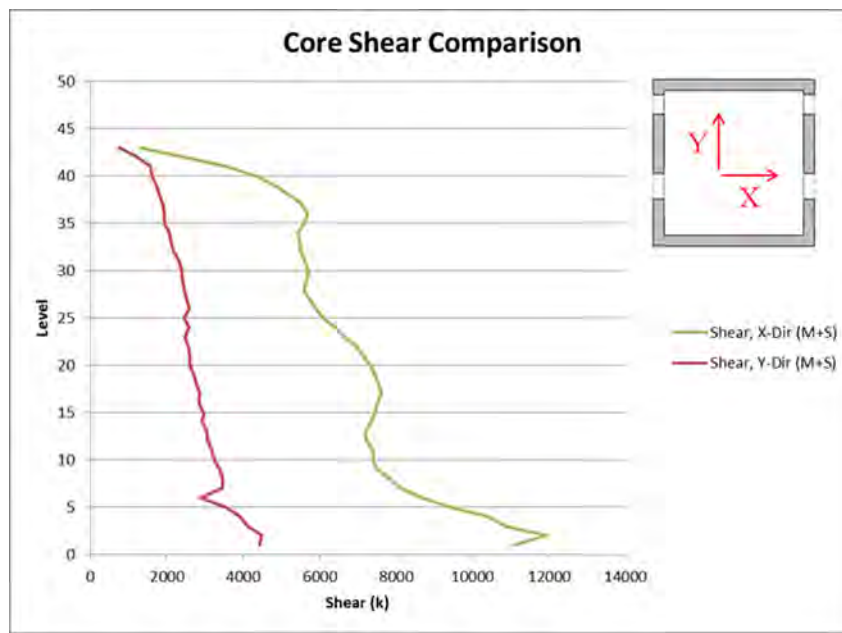
Figure 3.2-3 Core Wall A Shear Results [Figure Credit: CKC Structural Engineers]

The effect of the coupling beams on the shear core demand is exemplified in the Core Wall B configuration study. Core Wall B is two-celled and represents a 31-story tower that is 450 ft (137 m) tall. All coupling beams have a span-to-depth ratio of 3.0. A parametric study was completed where the number of coupling beams was varied in the short direction of the core and compared to solid wall piers. The results were quite dramatic.

With only one coupled wall and two solid walls, the peak core shear forces were approximately 22,000 kips (97,860 KN) at the base. When all three walls in the same direction where coupled with steel fiber-reinforced coupling beams, the peak core shear forces reduced to 12,500 kips (55,602 KN). This corresponds to a 45% drop in shear demand at the base of the core wall system, by simply introducing coupling beams.

Core Wall D configuration shown in Figure 3.2-2 had a similar response to Core Wall A configuration. Even though coupling beams were introduced in the direction where solid walls are shown, the shear

resistance in the solid wall direction was provided mostly by the solid walls. Limited contribution to the lateral force resistance was made by the coupled walls parallel to the solid walls.

Core Wall C in Figure 3.2-2 is the perfect example of increasing ductility in core wall systems by introducing coupling beams. Coupling beams were introduced on all sides of the core that helped mitigate shear demands. While some of these openings were required by the architectural layout, several openings were added to introduce distributed ductility and additional energy dissipation through coupling beams in the seismic force-resisting system.

The results of these studies clearly indicate that coupled wall systems are sensitive to the location and combination of wall piers and coupling beams. To develop a ductile response, it is recommended to provide coupling beams on all walls. It is also recommended to place coupling beams in a symmetric configuration away from intersecting wall piers.

RP3-3.3   Classification of RC shear walls

This section discusses classification of shear walls based on detailing (ordinary, intermediate, or special), based on coupling between walls (coupled versus uncoupled), and based on mode of seismic response, which is to a large degree dependent on the wall aspect (h_w/ℓ_w) ratio.

RP3-3.3.1   Ordinary, Intermediate, and Special Walls

Shear walls are classified as ordinary, intermediate, or special depending upon how they are detailed. A specially detailed shear wall has high inelastic deformation capacity, while an ordinary shear wall has relatively low inelastic deformation capacity. The inelastic deformation capacity of an intermediate wall is between those of an ordinary and a special shear wall. An ordinary shear wall can be cast-in-place or precast. A special shear wall can also be cast-in-place or precast. However, an intermediate shear wall can only be precast; ACI 318 does not recognize intermediate cast-in-place shear walls.

Ordinary shear walls are designed and detailed in compliance with ACI 318 (ACI, 2019) Chapter 11. Intermediate (precast) shear walls are detailed in accordance with ACI 318 Section 18.5. Special cast-in-place shear walls are detailed in accordance with ACI 318 Section 18.10. A special precast shear wall must comply with the requirements for a special cast-in-place shear wall (ACI 318 Sec. 18.10) and also the requirements for an intermediate precast shear walls (ACI 318 Sec. 18.5).

In buildings assigned to Seismic Design Category B, ordinary, intermediate, and special shear walls are allowed to be used as part of the seismic force-resisting system. In a buildings assigned to SDC C, ordinary shear walls are not allowed to be part of the seismic force-resisting system; the shear walls must have intermediate or special detailing. In a building assigned to SDC D, E or F, only special shear walls are allowed to be part of the seismic force-resisting system.

RP3-3.3.2   Coupled vs. Uncoupled Shear Walls

Functional and often structural requirements make the use of shear walls desirable in many buildings. More often than not, such walls are pierced by numerous openings for windows, doors, and other purposes. Two or more walls separated by vertical rows of openings, with beams at every floor level between the vertically arranged openings, are referred to as coupled shear walls. When a coupled shear wall system is subject to lateral loads due to wind or earthquake forces, shear forces generated at the ends of the coupling beams accumulate into a tensile force in one of the coupled wall piers and into a compression forces in the other wall pier. The couple due to these tension and compression forces resists a part of the overturning moment at the base of the wall system, with the remainder of the overturning moment being resisted by the wall piers themselves (Figure 3.3-1). The ratio of the overturning moment resisted by the tension-compression couple to the total overturning moment at the base of the coupled wall system is often referred to as the

degree of coupling. The shorter and deeper the coupling beams, the higher the degree of coupling. When the degree of coupling is very low, the two wall piers tend to behave like isolated walls, and when the degree of coupling is very high, the entire coupled wall system tends to behave like a shear wall with openings. It should be noted, however, that as and when inelastic displacements develop in the coupling beams, the degree of coupling tends to lose its significance.
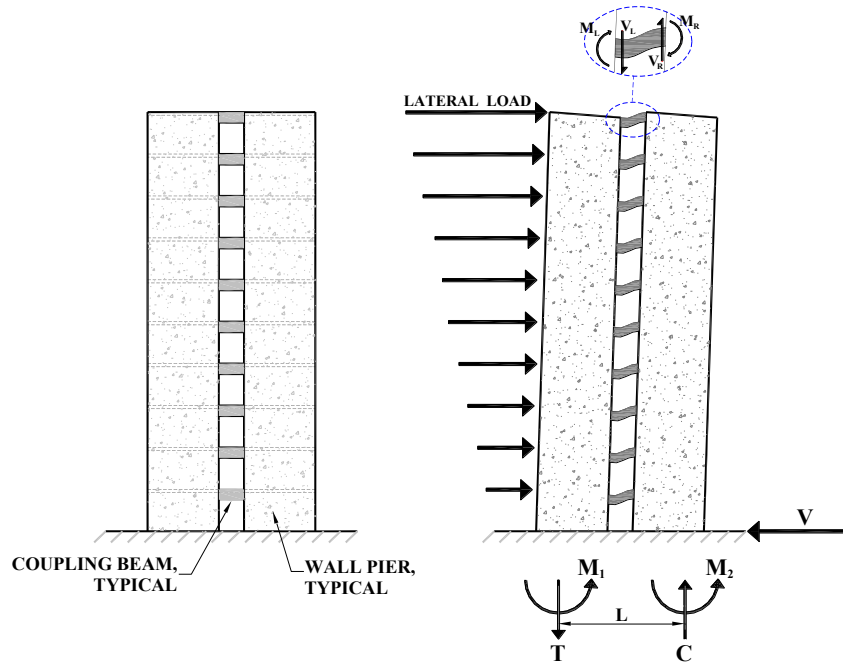
Figure 3.3-1 Coupled shear walls (from Fortney, not published)

RP3-3.3.3   Slender Versus Squat Shear Walls

Expected behavior of walls depends partly on wall aspect ratio. Slender walls ($h_w/\ell_w \geq 2.0$) tend to behave much like flexural cantilevers. The preferred inelastic behavior mode of slender walls is ductile flexural yielding, without shear failure. In contrast, walls with very low aspect ratios ($h_w/\ell_w \leq 0.5$) tend to resist lateral forces through a diagonal strut mechanism in which concrete and distributed horizontal and vertical reinforcement resist shear. Wall behavior transitions between these extremes for intermediate aspect ratios. Shear yielding of slender walls generally is considered unacceptable because it reduces inelastic deformation capacity below expected values. Shear yielding of very squat walls is often accepted because such walls tend to have high inherent strength and low ductility demands.

The slender walls, with their seismic response dominated by flexure, have sometimes been referred to as flexural walls, but this terminology has not caught on. The flexure-dominated slender walls, the shear-dominated squat walls, and all the walls in between are referred to as shear walls. The following text, reproduced from NIST Tech Brief 6 (NIST, 2011) succinctly describes the flexure-dominated behavior of slender walls, the shear dominated behavior of squat walls, and the corresponding design considerations.

RP3-3.3.3.1   Slender Walls

For slender walls, the design should aim to achieve ductile flexural yielding at the base of the wall. For slender coupled walls, the target mechanism should include ductile yielding of coupling beams over the

height of the wall plus ductile flexural yielding at the base of the walls. Wall shear failure and failure of diaphragms and foundations generally should be avoided.

Where the design intent is to have a single critical section for flexure and axial force, the designer should provide a distribution of strength over wall height that inhibits yielding at other critical sections. One approach is to design the selected critical section to have strength in flexure and axial force closely matching the required strength, with some overstrength provided at other locations.

In some cases, alternative mechanisms have to be accepted. In very tall buildings, higher-mode response may cause some wall flexural yielding in intermediate stories in addition to the primary yielding mechanism. In highly irregular walls, including walls with irregular openings, it can be difficult to precisely identify and control the yielding mechanism. Some conservatism in the design of these systems can help achieve the desired performance.

RP3-3.3.3.2   Squat Walls

Squat walls tend to have high inherent flexural strength and thus are prone to inelastic response in shear rather than flexural yielding. Unlike in slender walls, such behavior can provide sufficient post-yield stiffness and deformation capacity.

Squat walls are prone to two types of shear failure. "Shear yielding" within the wall web involves development of inclined cracks (Figure 3.3-2). Horizontal force equilibrium of segment cde requires distributed horizontal reinforcement resisting force F_h. Moment equilibrium of segment cde about e, or segment ab about b, requires distributed vertical reinforcement providing force F_v. Thus, ACI 318 requires both vertical and horizontal reinforcement to resist shear in squat walls. "Shear sliding" tends to occur at construction joints, including the wall-foundation interface. Axial force N_u and distributed vertical reinforcement A_{vf} (including added dowels) provide a clamping force across the interface that resists sliding. Reinforcement A_{vf} is most effective if distributed. Thus, it may be preferred to distribute the flexural reinforcement uniformly without concentrated boundary elements. Reinforcement A_{vf} is more effective in resisting sliding if oriented at an angle of ±45°, although this creates a constructability challenge. When concrete is placed against previously hardened concrete at this interface, ACI 318 requires the surface be clean and free of laitance.
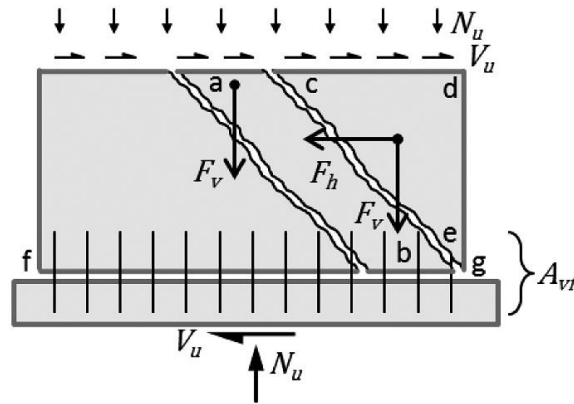
Figure 3.3-2 Shear yielding and shear sliding in a squat wall. [Figure credit: NIST Tech Brief 6]

RP3-3.4   Non-prestressed

This section addresses modeling and performance assessment for flexure-controlled reinforced concrete walls; walls that are controlled by shear capacity and exhibit a shear failure are not covered. In most cases, squat walls are more likely to be shear controlled.

In current seismic code-compliant design, more slender walls are sized and detailed to ensure flexural loading. Typically, flexure-controlled walls have shear demands that do not exceed shear strength calculated by the current version of ACI 318 and are slender with effective height-to-length ratio that exceeds 1.5-2.0 (ACI uses 2.0; research shows 1.5 is appropriate). In addition, walls designed by prior to current codes also exhibit flexural behavior. This chapter provides an overview of the behavior, performance and modeling of flexural walls.

Under lateral loading, flexure-controlled walls develop a flexural yield mechanism at the critical section(s), with loss of lateral load carrying capacity caused by buckling and subsequent tensile rupture of longitudinal reinforcement, simultaneous concrete crushing and buckling of compression reinforcement or, for walls with high shear demands and large cross-sectional aspect ratios (ratio of wall length to thickness), simultaneous crushing of concrete at the both ends of the compression region.

Wall cross section is largely a function of architectural layout. Mid to high-rise buildings typically have a central elevator core; these buildings have a core wall as indicated in Figure 3.4-1. Typically, the core walls are C or L in shape and coupled with coupling beams; the openings for the elevator are formed with the wall edges and coupling beams (Figure 3.4-1a). In lower rise buildings or other buildings without a central elevator core, it is more common to have walls distributed throughout the floor plate; the location and shape of the walls is typically constrained by the architectural layout. In many cases, asymmetric wall shapes are used (the most common asymmetric section is in the shape of an "L") as well as planar walls (Figure 3.4-1b).

| (a) Core Wall | (b) Distributed Planar and Flanged Walls |
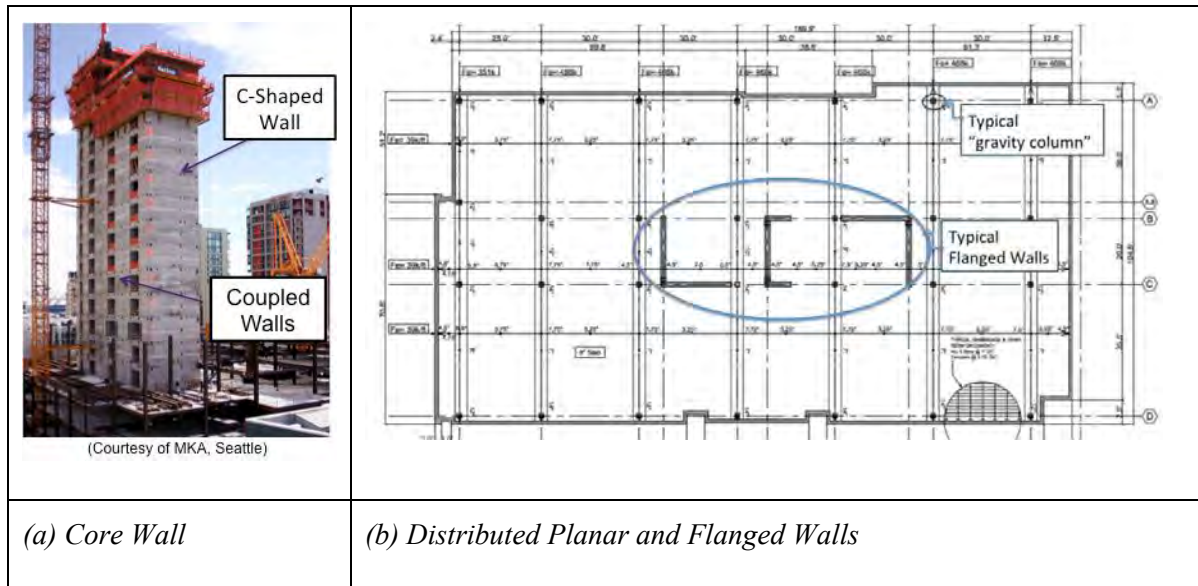
Figure 3.4-1 Core vs. Distributed Planar Walls

In the case of isolated walls, wall demands include shear, bending moment and axial force; these are idealized in Figure 3.4-2. In current design, wall section geometry, in particular wall thickness, is determined to meet shear strength and stiffness requirements. Thin walls may be susceptible to large shear or premature compression failure (Wallace 2015). Design of flexural concrete walls includes: (1) determination of reinforcement required for flexural demand; typically this reinforcement is concentrated at the ends of the walls in regions referred to as boundary elements, (2) detailing of the confinement reinforcement and (3) design of the horizontal reinforcement to meet the amplified shear demand resulting from seismic excitation. Note that the unamplified seismic demand is calculated using equivalent lateral forces (ELF), as shown in Figure 3.4-2a, or modal response spectrum analysis (MRSA); additional information on determining seismic demand may be found in ASCE 7-16 (ASCE 2016).

Figure 3.4-2 shows typical vertical and confining reinforcement layouts for ductile [this term is thrown in all of a sudden] walls. In buildings assigned to high seismic design categories, large volumes of confining reinforcement are required in "boundary element" regions of shear walls that are expected to experience high compression demands under earthquake loading (Figure 3.4-2c). For planar walls and some flanged walls, an efficient design for strength results from placement of a large volume of longitudinal reinforcement in the boundary elements of the wall (Figs. 3.4-2b, c and d). For nonplanar walls that resist loading in orthogonal directions, longitudinal reinforcement may be uniformly distributed; walls with uniformly distributed reinforcement typically require heavily confined boundary elements but may require confinement of the entire cross section. The ACI Code allows longitudinal reinforcement to be spliced at the base of the wall where the maximum flexural demand typically occurs; since splicing reinforcement at this location facilitates construction, splices are common at the base of the wall.

In contrast to the boundary elements, the interior of the wall web or flange, as indicated in Figure 3.4-2b, is lightly reinforced, with reinforcement ratios equal to or just larger than 0.25% being common.

This interior section of the wall is expected to sustain large shear strains through diagonal cracking and straining of the interior steel (Figure 3.4-2a). In flanged walls it is not uncommon for wall webs to sustain significant spalling and crushing of the concrete; however, most walls are not confined in this region.

RP3-3.4.1 Behavior of flexural concrete walls under lateral and gravity loading

This section focuses on reinforced concrete walls with height-to-length ratios exceeding 1.5, which sustain shear demands less than the shear strength given by ACI 318 (2014), and therefore exhibit flexure-controlled response. Table 3.4.1 describes response of various flexural walls.

(a) EFL Demands on Individual Wall or Pier	(b) Flanged Wall
(c) Planar Wall	(d) Wall Reinforcement
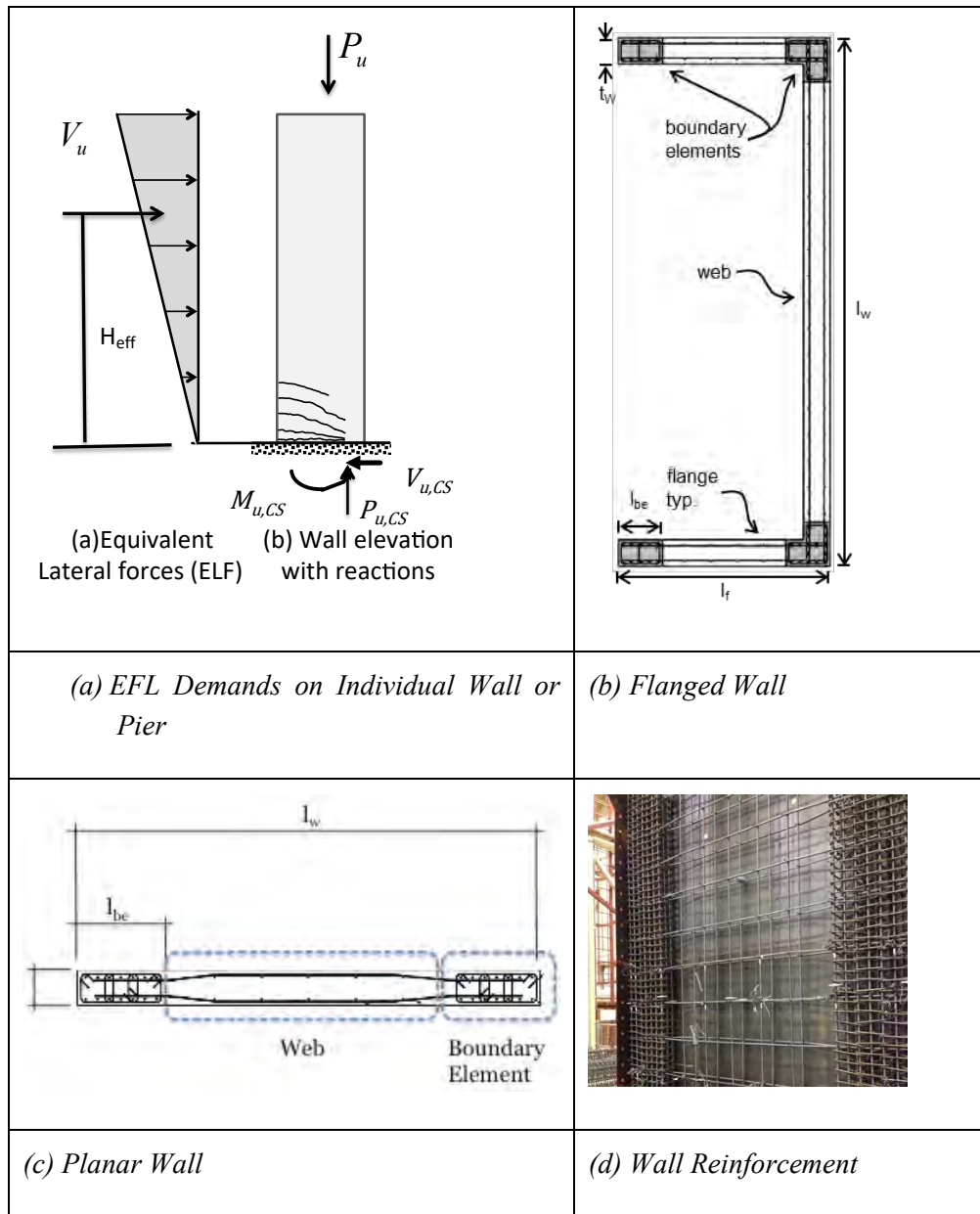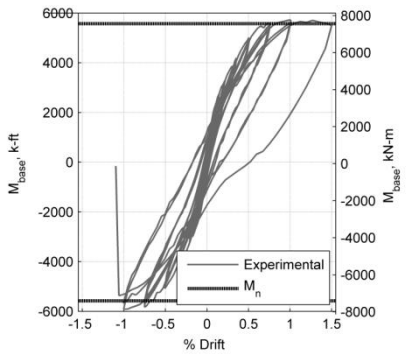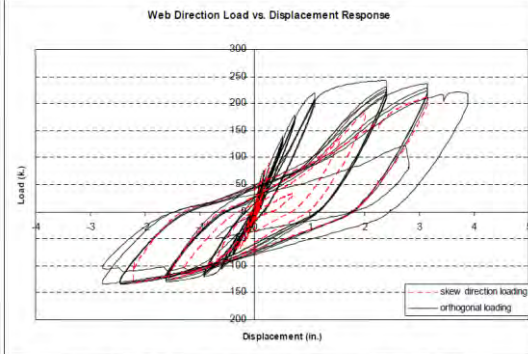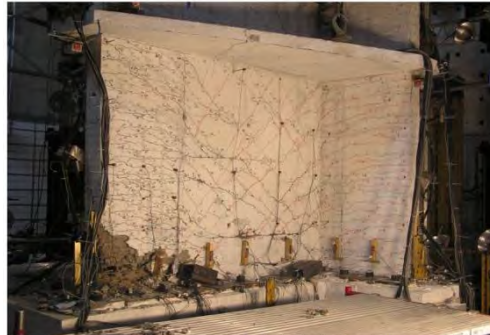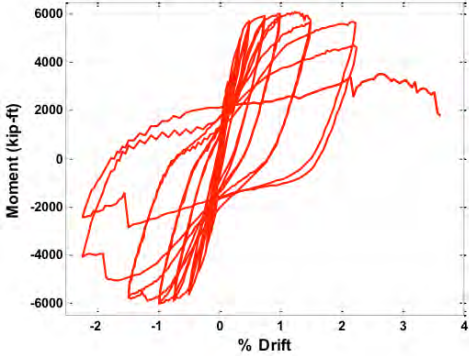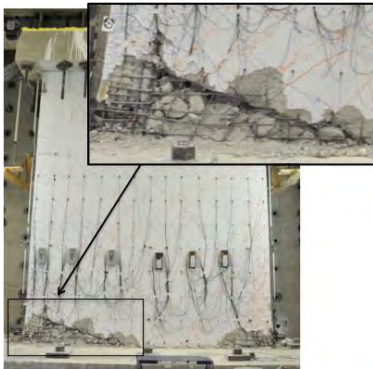
Figure 3.4-2 Demands on and Reinforcement Configuration of Wall Cross Sections

Table 3.4.4.1 Response of and Damage to Flexural Walls

Planar Wall (Lowes et al.2012)		
Asymmetric Flanged Wall (Breuggen 2009)	Figure 6.18. Web direction load versus displacement response of NTW2	Figure 6.7. First story web of NTW2 after web failure.
Symmetric Flanged Wall (Mock 2014)		

Coupled Wall (Lehman et al. 2013)
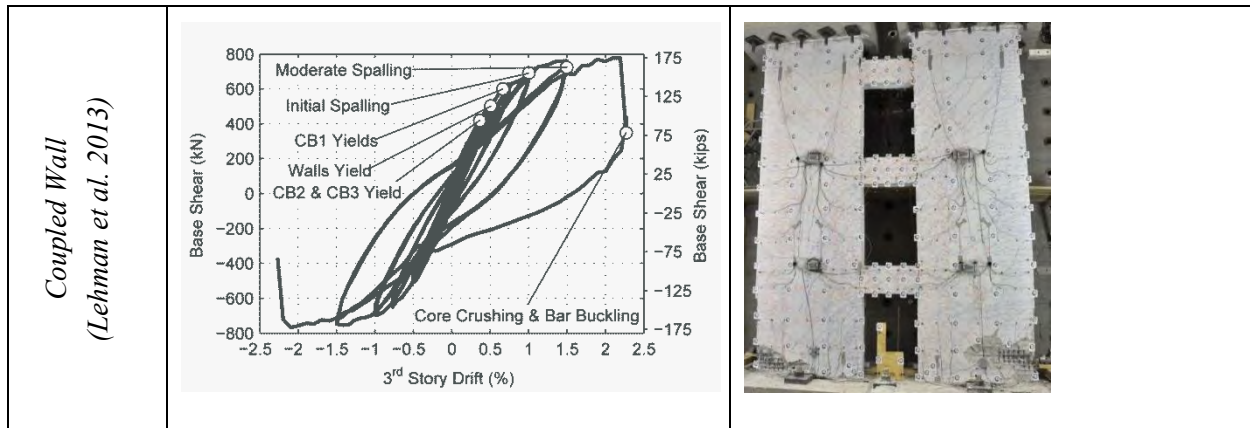
Table 3.4.1 shows measured load versus drift response histories for the four types of concrete walls: i) planar, ii) asymmetric flanged, iii) symmetric flanged, and iv) coupled. The measured response indicates the following characteristics: i) a flexural strength that is accurately estimated using standard methods (e.g. plane-section analysis), ii) minimal hardening under increasing drift demand (i.e. final strength is approximately the nominal moment strength M_n computed using expected strengths), iii) minimal strength deterioration under multiple cycles to the same drift demand, and iv) relatively rapid strength loss with increasing drift demand after development of a failure mode.

As shown in the images in Table 3.4.1, wall failure mechanisms (Birely 2012, Whitman 2015) results from either: i) simultaneous concrete crushing and buckling of longitudinal reinforcement in the extreme compression region of the wall (compression-buckling, CB, failure) ii) rupture of previously buckled longitudinal reinforcement (buckling-rupture, BR, failure), or iii) concrete crushing across a large portion of the compression-region due to the combined compression demands resulting from ***flexural*** and shear loading. As shown in Table 3.4.1, failure typically results in severe damage to the web and boundary element concrete, which can result in failure of the wall.

Structural concrete walls are one of the most common seismic force-resisting systems. Yet recent earthquakes and experimental testing have demonstrated that walls and wall buildings are vulnerable to damage.

RP3-3.4.2   Design of reinforced concrete walls for flexure-dominated response

The design of slender concrete walls is governed by the current versions of the *International Building Code* (ICC 2018), ACI 318 (2014) and ASCE/SEI 7[i]. In some jurisdictions, additional requirements apply for the design of shear walls in tall buildings; these additional requirements typically include peer review. Research conducted to date suggests that slender walls of varying height that are designed to meet code requirements may not achieve the intended earthquake performance. Specifically, performance objectives related to damage resistance and drift capacity might not be realized. Walls designed to meet code requirements may exhibit i) shear failure prior to flexural yielding, ii) flexural yielding at multiple locations over the height of the wall, iii) premature compression damage and failure, and iv) undesirable collapse probabilities for design and maximum considered earthquake demand levels.

The design recommendations presented here are based on the results of experimental testing and

numerical simulation and are intended to result in walls that achieve ductile response, including a tension-controlled flexural response mechanism, flexural yielding confined to locations identified by the engineer, and the desired low collapse probabilities for design and maximum considered earthquake demand levels.

The general design process is as follows:

1. Provide the layout of walls throughout the building floor plan.
2. Determine wall cross-sectional configurations.
3. Estimate lateral forces for use in design of the system. Note that these forces depend on the ASCE 7 response modification factor (*R*), which may depend on the wall design and expected response.
4. Estimate wall thickness based on shear demand, using lower-bound estimate of shear strength.
5. Using initial estimates of wall layout, configuration, and size (thickness), conduct demand analysis. Typically, the initial (and perhaps final) demand analysis will be an elastic modal response spectrum analysis. This type of analysis uses elastic elements for the wall (either line elements or shell elements, depending on the type of software) and requires an effective stiffness for those elements.
6. Design flexural reinforcement.
7. Repeat demand analyses as required. In some cases, nonlinear analyses are conducted to provide a more accurate estimate of the time-dependent and maximum deformations as well as demands resulting from ductile yielding of wall components.
8. Size and detail web reinforcement to meet shear demands resulting from a capacity-design approach. If resizing of wall is required, steps 5-8 must be repeated.
9. Size and detail confining reinforcement to meet codified procedures in current version of ACI 318.
10. If required, conduct performance-based design using linear or nonlinear analysis results.

Additional information on wall design can be found in the following resource documents: TBI (2018) and Lowes et al. (2014) [Pankow document].

RP3-3.5   Wall Buildings with Irregularities

Irregularities in concrete shear wall buildings can have a significant effect on performance. The following discusses commonly occurring vertical and horizontal irregularities, and effects observed in earthquake performance, laboratory testing and numerical modeling studies.

RP3-3.5.1   Earthquake Response of Concrete Walls with Vertical Irregularities

The impact of vertical irregularities caused by openings in a wall or walled building was studied three ways: (1) investigating damage patterns in buildings damaged in recent earthquakes, (2) conducting finite element analyses of individual walls to investigate the stress distribution and damage pattern and (3) conducting nonlinear response history analyses (NLRHA) of walled buildings to determine the impact of discontinuities on collapse probabilities. A summary of the findings for each study is presented below. The findings indicated that:

- Discontinuities in the lower stories are most impactful. In particular, removing part of the compression region present in the upper stories will increase damage and reduce the drift capacity of the wall.

- Walls with openings present modeling and detailing challenges. It is important to increase the confining reinforcement and horizontal reinforcement around the openings. However, it is not necessary nor desirable to increase the vertical (longitudinal) reinforcement around openings because it will increase the flexural strength and therefore increase the shear demand. The combination of shear and compression stress can result in premature strength loss, especially if the compression region is reduced because of the opening.

- In the studied buildings, openings increased the collapse probability by about 25%. Note that in most cases, collapse of the building results from loss of the gravity system and therefore a reduction in deformation capacity does not translate to an equivalent increase in the probability of collapse.

RP3-3.5.1.1 Damage in Earthquakes

Damage to walled buildings during recent earthquakes demonstrates the potential for vertical irregularities to impact earthquake performance as well as suggests vertical irregularities that are highly correlated with damage and particularly detrimental to building performance. For example, evaluation of buildings damaged during the 2010 Maule, Chile Earthquake identified a number of building system design and configuration issues that could be expected to result in poor earthquake performance. Many of the walled buildings damaged during the Maule earthquake were observed to have significant vertical discontinuities in walls that were primary elements of the seismic force-resisting system. Figures 3.5-1 and Figure 3.5**Error! Reference source not found.**-2 show vertical discontinuities due to a significant wall length reduction from an upper to a lower story.

Figure 3.5-1 Coupled walls in upper stories do not continue to lower story (Plaza del Rio Building, Concepcion, Chile)

Figure 3.5-2 A change in the wall section from the upper to lower story (circled) results in a loss of wall area and localization of flexural yielding (Plaza del Rio Building, Concepcion, Chile)

A vertical discontinuity arises also when coupled walls terminate in a solid wall panel either below or above the coupled region, or both, as shown in Figs. 3.5-3a and 3.5-3b. The solid panel constitutes a discontinuity region that can be subjected to large shear stresses when the coupled walls are loaded laterally. Figure 3.5-3b shows a typical damage pattern observed following the Maule earthquake. Figure 3.5-4 shows similar damage patterns in a wall system with a similar discontinuity observed following the Loma Prieta earthquake.
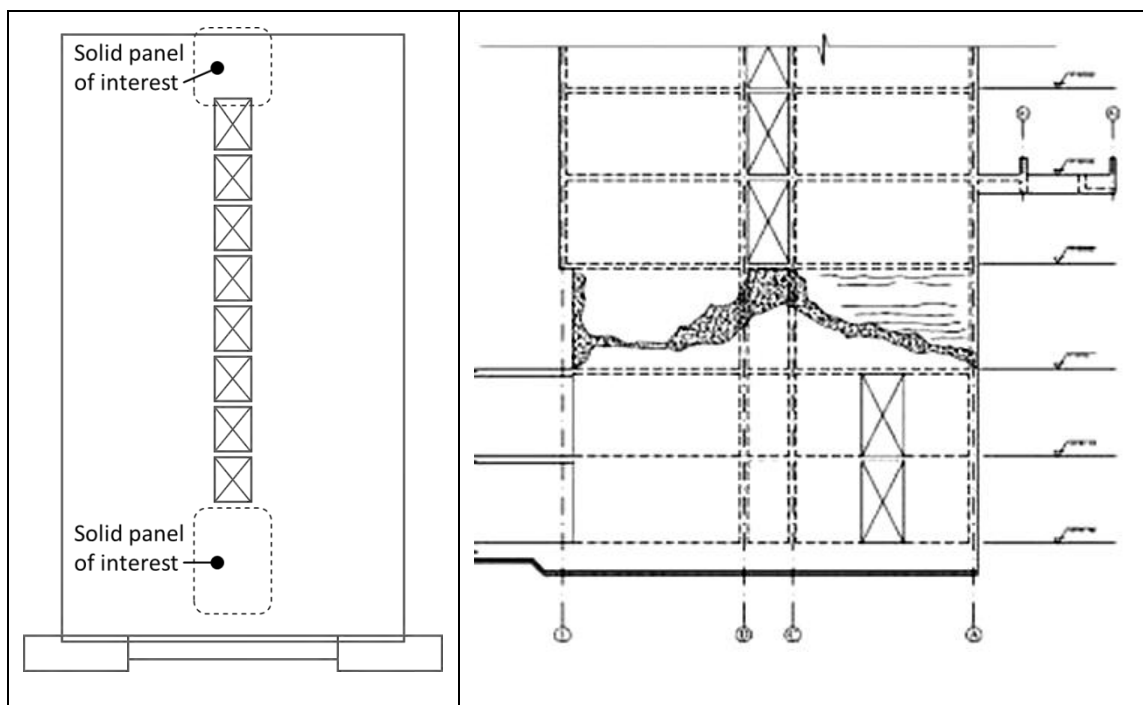
Figure 3.5-3 (a) Coupled wall with stack of openings terminating in a solid wall and (b) Damage map along a grid line of the Alto Rio Building in Concepción, Chile following the 2010 earthquake.
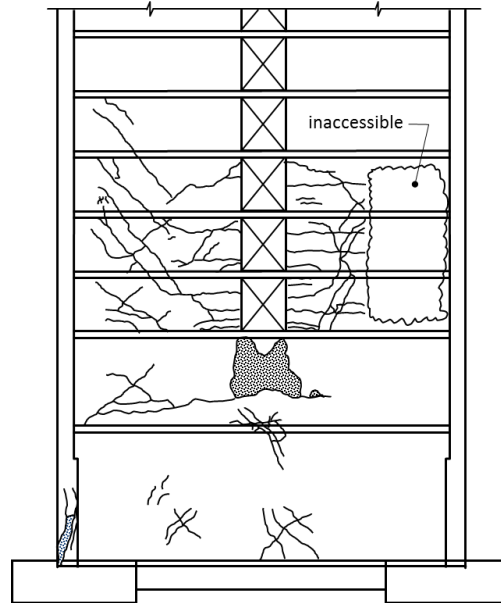
Figure 3.5-4 Damage to building sustained during the 1989 Loma Prieta earthquake (image from Moehle 2012)

The 2016 M 6.7 Meinong Earthquake in Southern Taiwan resulted in severe damage to reinforced concrete buildings. The majority of the damaged buildings utilized moment-resisting frames as the primary seismic force-resisting system. However, a couple of high-rise buildings with reinforced concrete walls and frames were damaged. Figure 3.5-5 shows an example of a reinforced concrete wall with openings. As shown in the Figure, the primary damage was to a "column" at the exterior of the wall. It is likely that the large axial force on the column resulted in the compression damage.
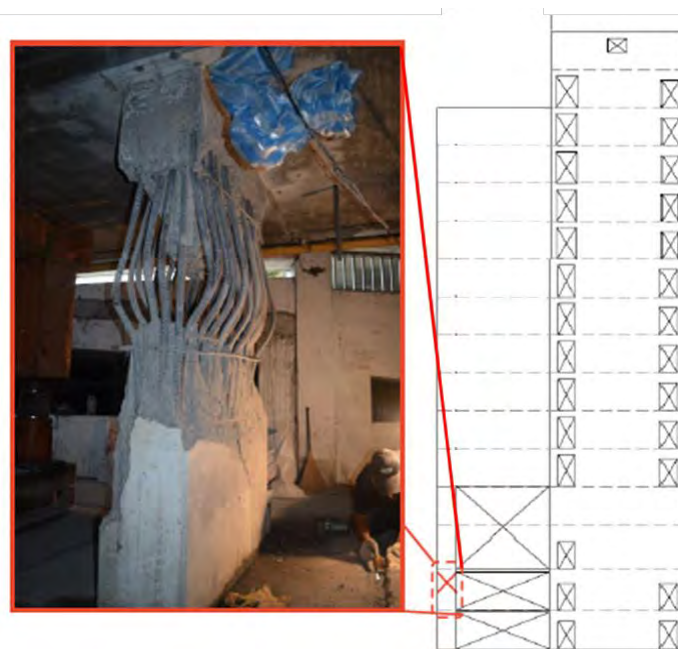
Figure 3.5-5 Damage to "Column" at Wall Discontinuity in 20-Story High-Rise Building (2016 Meinong Earthquake)

Based on review of earthquake damage following the 2010 Maule earthquake, and supported by damage data presented above, primary findings with respect to the impact of wall configuration on earthquake performance are as follows:

- Damaged walls often did not have a clearly defined location where a plastic hinge could form.

- Lateral load can be transferred through severe vertical discontinuities in a wall. However, this requires adequate detailing around the discontinuity in the individual wall and/or adequate detailing and strength for the components (beams or slab) that contribute to the load transfer.

- Damage consistent with wall coupling, such as crushing of wall concrete due to high compressive loads and cracking and crushing of concrete in coupling beams and slabs, was observed; however, the extent of coupling requires further evaluation.

- Buildings that were essentially undamaged typically had a thick, well-reinforced mat foundation and a continuous core.

Investigation of Impact of Vertical Discontinuities Using Nonlinear Continuum Analysis

Nonlinear continuum-type analysis was used to investigate the impact on wall performance of the horizontal location of an opening introduced in the bottom story of a midrise wall. Continuum analyses use solid elements and 3D constitutive models for the concrete. Reinforcement can be modeled as smeared or discrete bars or a combination of the two. To capture bar buckling, a discrete bar modelling approach is preferred using beam-column elements. To simulate the response at the bar-concrete interface, elements

capable of simulating movement at the interface (e.g., surface or discrete spring elements) are used with calibrated bond-slip constitutive models. This modeling approach is computationally intensive and therefore rarely used to model a full building. Instead it is used to understand response and validate simpler modeling approaches including multilayer shell element and line element models. Four opening locations were considered: no opening and openings at the center of the wall, on the right side of the wall and on the left side of the wall. A monotonically increasing lateral load was applied pushing the wall to the right such that an opening on the right side interrupted the compression region.

An 8-story wall (30 ft long by 2 ft thick by 106 ft tall) with uniformly distributed vertical and horizontal reinforcement was used in the study. Figure 3.5-6 shows this reference wall configuration with openings (7.5 ft long by 10 ft tall) introduced and supplemental horizontal reinforcement added above the opening to prevent damage directly above the opening. Figure 3.5-7 shows base shear, normalized by $\sqrt{f_c'}A_g$ with $f_c' = 6500$ psi and A_g equal to the area of the reference wall ($A_g = 60$ ft^2), versus drift at the point of the applied load. Figure 3.5-8 shows concrete minimum principal stress at onset of strength loss for the different wall configurations. These data show also a very different stress field for the wall with the opening on the right; this is consistent with the reduced strength and deformation capacity of this wall.

The data in Figs. 3.5-7 and 3.5-8 show that:

Introducing an opening at the middle of the wall has minimal impact on the stiffness, strength and deformation capacity of the wall,

Introducing an opening in the tension region of the wall (left side) reduces stiffness and strength slightly, as it reduces the volume of longitudinal reinforcement activated to resist lateral loading, and increases deformation capacity, as it reduces compression demands and thereby delays onset of compression failure, which triggers overall strength loss.

Introducing an opening in the compression region of the wall (right side) significantly reduces strength and deformation capacity, as it reduces capacity of the flexural compression region resulting in early onset of compression failure, and thus early onset of overall strength loss.
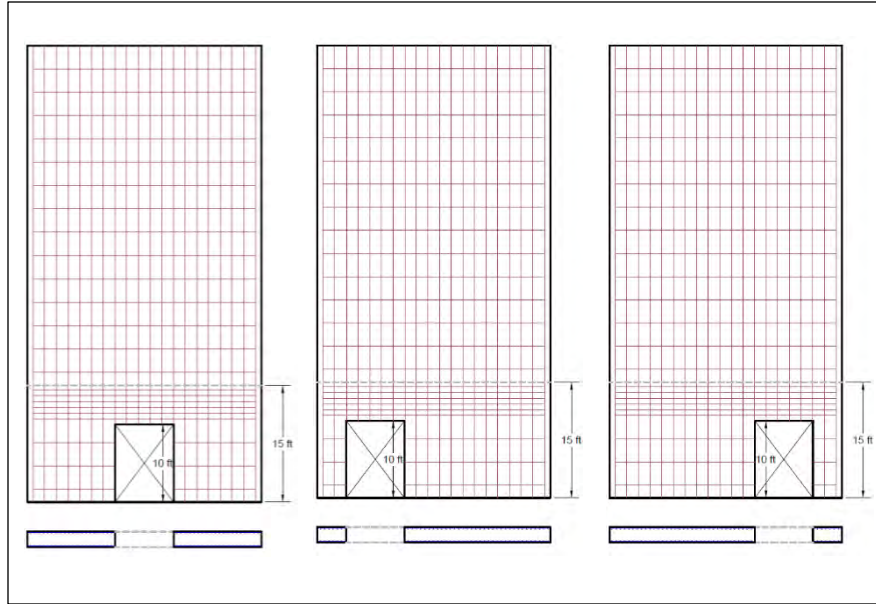
Figure 3.5-6 Wall configurations and designs used for ATENA analyses to investigate the impact of opening location
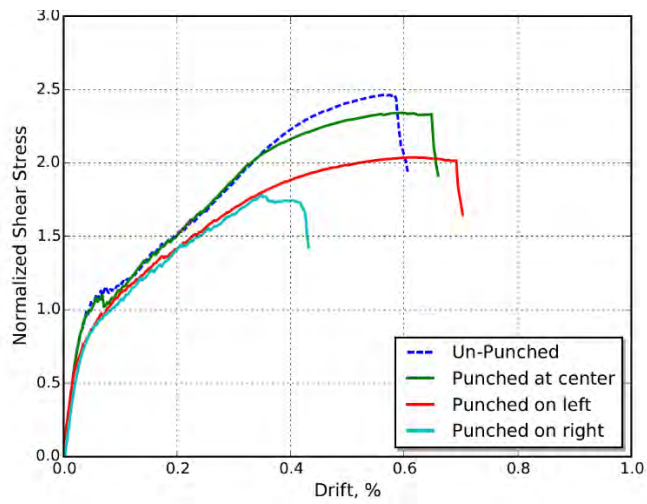
Figure 3.5-7 Normalized base shear stress $\left(V_{base}/\left(A_{cv}\sqrt{f'_c}\right)\ in\ psi\right)$ **versus drift at the effective height.**

| Opening in Center | Opening in Tension Region | Opening in Compression Region |

Figure 3.5-8 Minimum Principal Stress at Compression Failure for Walls with and without Openings
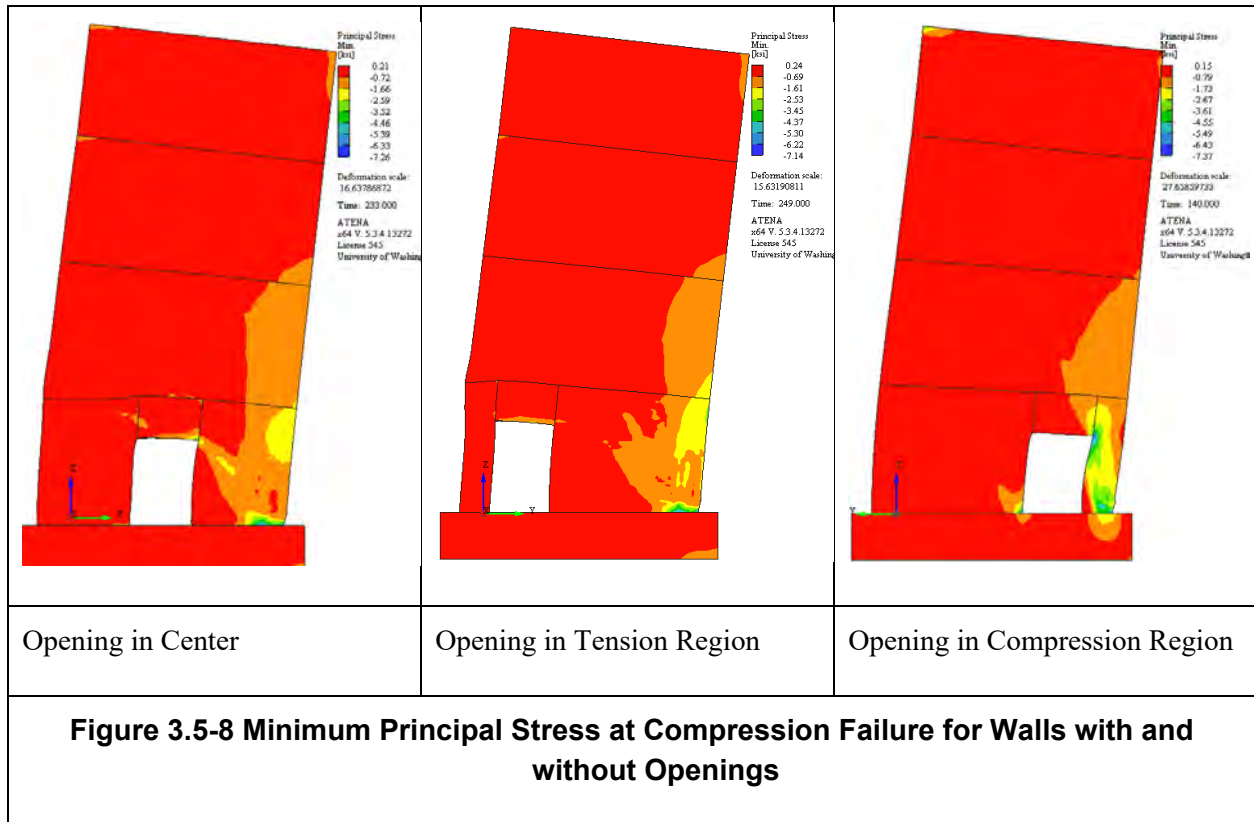
Collapse Assessment using NLRHA of Walled Buildings

This section summarizes the analytical studies of reinforced concrete (RC) wall buildings that were designed per ASCE/SEI 7-16, *Minimum Design Loads and Associated Criteria for Buildings and Other Structures* (ASCE, 2017a). For walls with discontinuities, ACI 318 requires an adequate load path around the discontinuity (ACI, 2014) and placement of reinforcing steel to resist loads and ensure capacity through multiple load cycles.

To investigate the impact of vertical irregularities on the earthquake performance of mid-rise reinforced concrete wall buildings, a series of reinforced concrete wall buildings were designed without openings and then with openings located at the 1st, 1st and 2nd, and an upper story. Design of the baseline 8-story reinforced concrete wall building resulted in walls 30 ft long by 2 ft thick, with 6 ft long boundary elements having 2.5% longitudinal reinforcement, and longitudinal and horizontal reinforcement of 0.25% in the web region. Opening length was determined to achieve a stiffness for the stories with the openings that was either 50% or 75% of the corresponding stiffness in the baseline building. Wall demands were determined using the ASCE/SEI 7-16 ELF procedure (ASCE, 2017a). Figure 3.5-9 shows elevation views for the 8-story reinforced concrete wall buildings with an opening of (i) 2.5 ft to create a story stiffness equal to 75% of the stiffness of the baseline building and (ii) an opening of 7.5 ft to create a story stiffness equal to 50% of the story stiffness of the baseline building.

(a)   (b)   (c)   (d)
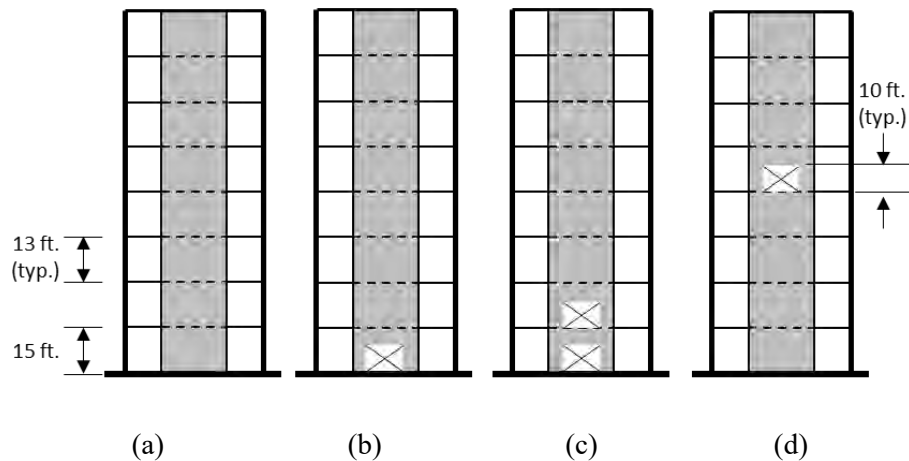
Figure 3.5-9 Idealized building elevations (a) without openings; (b) with openings in 1st story; (c) with openings in 1st and 2nd stories; and (d) with openings in upper stories.

The FEMA P695 methodology was used to assess the collapse risk posed by the 8- and 12-story reinforced concrete wall building designs. Nonlinear dynamic analyses were conducted using the OpenSees analysis platform. For each building archetype, collapse risk was computed using the suite of nonlinear analysis results, for two different definitions of collapse: (1) collapse due to failure of the gravity system at a maximum story drift of 5%; and (2) collapse due to a sidesway mechanism characterized by a maximum story drift in excess of 10%. Results show that collapse risks for reinforced concrete wall structures, with and without introduction of openings in lower stories, is relatively low (less than 4%). For 8- and 12-story reinforced concrete wall buildings designed for the D_{max} spectrum and considering collapse associated with failure of the gravity system at a maximum interstory drift of 5%, the collapse probability of the solid wall system is low (0.5% to 1.2%). The introduction of a vertical stiffness irregularity increases collapse risk and reduces the collapse margin ratio by less than 25%. Additional information about this study can be found in the ATC 123 report (project is ongoing at the time of publication).

RP3-3.5.2   Horizontal Irregularities [Coupled walls and coupling beams]

Coupled core wall systems have several configurations as described in Section RP3-3.2. Core wall location on plan is critical to minimizing torsional eccentricities. Figs 3.5-10 (a) and (b) illustrate a concentric and an eccentric core, respectively, relative to the floor plan.

(a)   (b)
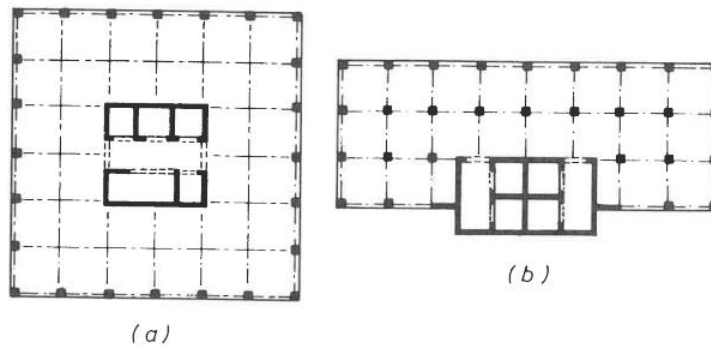
Figure 3.5-10 Core Wall systems plan location [Figure Credit: Paulay and Priestley]

Figure 3.5-10 (b) creates significant torsional imbalance that will lead to unfavorable core wall performance and should be avoided if possible. In addition to the unbalanced loading due to the horizontal offset of the core to one side of the plan, diaphragm load transfer to core wall elements located outside the floor footprint or not connected to the diaphragm will be challenging. In addition to the core wall location, the horizontal regularity and symmetric placement of wall piers and coupling beams is critical to the overall performance and ductility of the coupled core wall system. For instance, Figure 3.5-10 (a) shows a concentric core wall, however, the addition of the baffle walls within the core develops horizontal irregularities and leads to unfavorable response. It is preferable in this case to eliminate the interior walls or transform them to non-structural walls that do not participate in the seismic force-resisting system. If additional stiffness is required to reduce building drift, it might be prudent to increase the thickness of the outside symmetrically placed wall piers instead of adding baffle walls that may cause horizontal irregularity.

The importance of horizontally regular core wall configuration to core performance is discussed in Section RP3-3.2. Figure 3.2-2 illustrates four core wall configurations with different horizontal wall pier and coupling beam placement. Core wall configuration C is perfectly symmetric in both directions. This horizontal regularity in addition to concentrically locating the core wall to the floor plan would produce the most favorable seismic response of all four core wall configurations shown.

RP3-3.6   Coupled Walls and Coupling Beams

The prevalent seismic force-resisting system used for modern high-rise concrete buildings in high seismic regions is the reinforced concrete core wall system. Current design practice uses the provisions of ACI 318 for special structural walls (Chapter 18) and the seismic design coefficients from ASCE 7 (R = 5 or 6, for example). The special reinforced concrete shear wall has historically included all shear wall variations. Differentiation in behavior is not recognized between slender and squat walls, flanged versus blade (rectangular) walls, and coupled versus cantilever walls. As of the 2019 edition of ACI 318, a new system definition has been created to recognize the Ductile Coupled Structural Wall (DCSW).

The performance objective of the ductile coupled shear wall system is for the majority of energy dissipation to occur in the coupling beams. This is analogous to strong column weak beam behavior in moment frames. Studies were conducted (see Appendix A) to identify system characteristics that lead to coupling beam energy dissipation of no less than 80% of total system energy dissipation under MCE ground motions. In these studies, non-linear response history analyses were conducted using spectrally matched ground motion records on a variety of coupled shear wall archetypes. Archetypes ranged from 5 to 50 stories in height, and considered a range of longitudinal reinforcement ratios in the coupling beams as well as the shear walls. Results of these analyses are presented in Figure 3.6-1. The x-axis represents the aspect ratio (clear span to total depth) of the coupling beams, with D designating a diagonal reinforcement design and M designating a moment frame beam design. The y-axis is the percentage of total system energy dissipation that occurs in the coupling beams alone. The resulting trend shows an energy "dome" with coupling beams dissipating the majority of system energy between aspect ratios of 2 and 5.
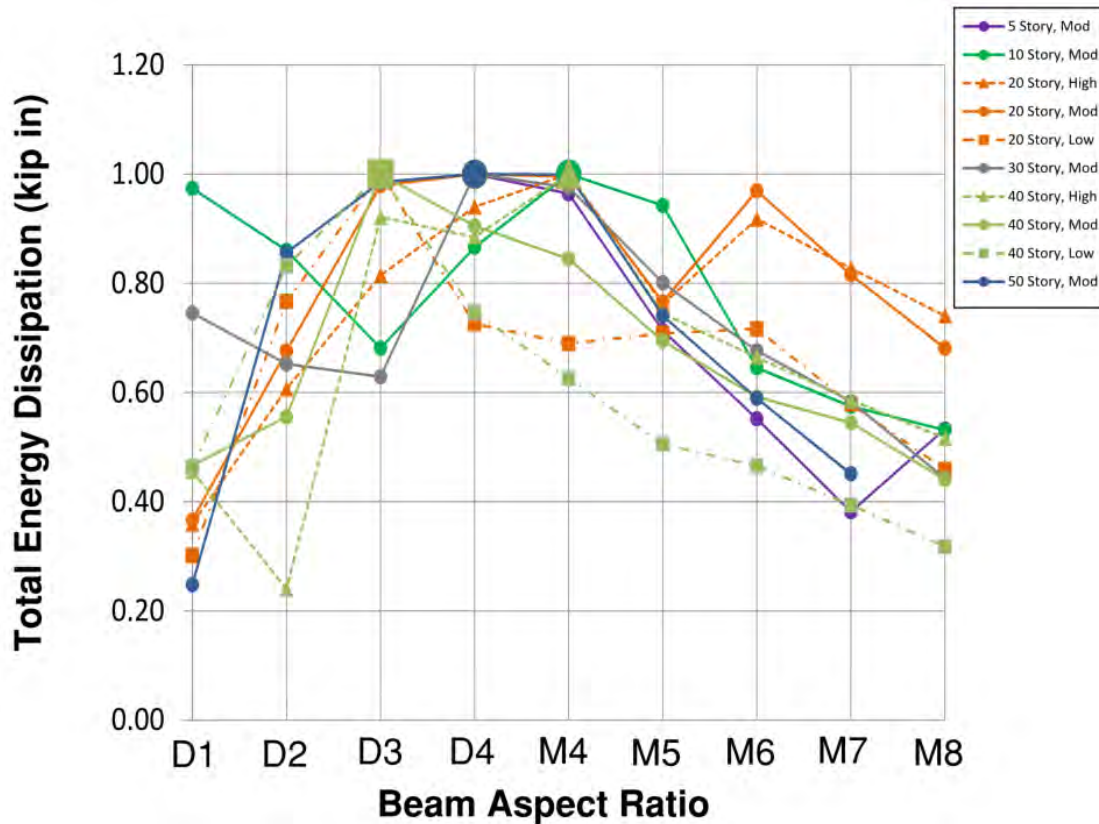
Figure 3.6-1 Energy dissipation in coupling beams.

The primary characteristics of such a system are geometry based. Squat walls were found to be too stiff to allow sufficient story drift for coupling beams to become inelastic. For this reason, shear walls in the DCSW system need to have total height to length aspect ratio of no less than 2.0. Squat coupling beams were found to over-couple the seismic force-resisting system, and lead to significant energy dissipation in the shear walls. As such, coupling beams in DCSW systems need to have length to total depth aspect ratio of no less than 2.0 in all cases. Very slender coupling beams, designated as having aspect ratio greater than 5.0, are too weak to contribute sufficient hysteretic energy dissipation, and are allowed in no more than 10% of the levels of the building. Lastly, coupling beams conforming to these geometric constraints are required to be present at all levels and are required to develop $1.25f_y$ at each end in order to dissipate the intended amount of energy. This last requirement is intended to preclude the use of fixed-pinned coupling beams that have been utilized where insufficient length exists to develop the coupling beam reinforcement into the adjacent shear wall.

The requirements of the Ductile Coupled Structural Wall system are in addition to those required for Special Structural Walls and Coupling Beams. The final language of the DCSW definition in ACI 318-19 reflects the input of ACI 318 Subcommittee H as well as BSSC Issue Team 4.

RP3-3.7   Deformation and Force Demands in Slender Shear Wall Buildings

Analysis of buildings in high seismic regions is presumed and allowed to be conducted with an elastic

procedure per ASCE 7-10 Table 12.6-1. Elastic analysis procedures (and associated seismic design coefficients) have been calibrated primarily for the determination of story shear and roof displacement. However, non-linear response history analysis (NLRHA) provides a much more comprehensive and accurate view of the deformation demands at the element level.

See Appendix B for global and element deformation demands as determined by NLRHA for a 40-story concrete tower analyzed in a high seismic region.

RP3-3.8   Shear Design of Shear Walls

RP3-3.8.1   ACI determination of required shear strength

ACI 318 requires beam and column sections of special moment frames to be designed for the largest shear V_e that can develop at such a beam or column section (ACI 318-19 Sections 18.6.5.1 and 18.7.6.1.1, respectively). In no case can V_e be smaller than the factored shear obtained at that section from an analysis of the structure comprising the beams and the columns under code-prescribed seismic forces.

A special shear wall section, however, is designed for the factored shear V_u obtained at the section from analysis of the structure that includes the shear wall under code-prescribed seismic forces. No attempt is made to determine the largest shear that can develop at the shear wall section. This has now changed in ACI 318-19, as indicated in Section RP3-3.8.4 of this Resource Paper.

RP3-3.8.2   Φ-factor used in shear design of shear walls

To compensate in part for the lack of realism in determining required shear strength, the strength reduction factor φ for shear must be 0.60, rather than 0.75, for a shear wall (or any structural member) designed to resist earthquake effects if its nominal shear strength is less than the shear corresponding to the development of the nominal flexural strength of the member. This is typically applicable to low-rise shear walls.

As a rule of thumb, walls with h_w/ℓ_w ratios smaller than or equal to one will fail in shear before they have a chance to fail in flexure. Walls with h_w/ℓ_w ratios of two or more, on the other hand, will have flexural failure preceding shear failure, as long as they are designed in compliance with ACI 318 requirements. Walls with h_w/ℓ_w ratios larger than one and smaller than two may have flexural failure preceding shear failure or shear failure preceding flexural failure, depending upon a number of factors. Thus, there is no reason to use a φ of 0.6 in the shear design of shear walls wait h_w/ℓ_w of two or more. To be overly conservative, one could take the threshold as 2.5, rather than 2.0. In any case, it is not productive to design a shear wall with a h_w/ℓ_w ratio of 5, for instance, using a φ of 0.6. That way, money would be wasted providing unnecessary shear reinforcement, without adding to safety in any way.

ACI 318-19 requires cross-sections of a special shear wall to be designed for the V_u obtained from analysis of the structure under code-prescribed seismic forces amplified by an overstrength factor Ω [Ω_v in ACI 318-19) and a dynamic amplification factor ω_v, as indicated in Section RP3-3.8.4 of this Resource Paper. The requirement to use $\phi = 0.6$ in the shear design of shear-governed shear walls remains.

RP3-3.8.3   Flexural overstrength – Lowes

For flexure-controlled walls, flexural overstrength reduces collapse risk and may improve performance; however, also for flexure-controlled walls exhibiting nonlinear response, shear demand is determined in part by flexural strength. Thus, flexural overstrength contributes to increased shear demand and is considered in defining shear demand used in design [ACI 318-19]. The question arises what is the flexural overstrength of concrete walls? Flexural overstrength refers to $M_{pr} > M_n > M_u/\phi$ where M_n is the nominal

flexure strength per ACI 318-19 computed using specified material strengths, M_{pr} is the probable flexural strength computed using expected material strengths including a reinforcing steel strength of at least $1.25f_y$, M_u is the moment demand computed using demands defined in ASCE 7-16, and ϕ the strength reduction factor per ACI 318-19. Specifically, flexural overstrength, Ω, is defined as follows:

$$\Omega = M_{pr}/M_u = M_{pr}/(\phi M_n) \tag{1}$$

Here it should be noted that flexural overstrength results from $1/\phi > 1$ and $M_{pr}/M_n > 1$ due to strain hardening of reinforcing steel, as suggested by Eq. 1, as well as additional longitudinal reinforcement required to meet construction constraints or other design requirements.

Multiple studies have investigated flexural overstrength with the objective of determining typical overstrength values for inclusion in design requirements to account for shear amplification. These studies have typically employed idealized building designs that likely employ a minimum volume of "additional longitudinal reinforcement required to meet construction or other design requirements". An example of one such study is Pugh et al. (2015, which shows that for idealized planar and coupled wall building designs ranging in height from 6 to 20 stories $\Omega = 1.4$ to 1.6, with $\Omega = 1.5$ recommended for use in design.

Multiple design codes, standards and guides around the world specify flexural overstrength to be used in design. Examples include the following:

CSA A23.3 (2014) specifies $\Omega = 1.25/\phi$ not less than 1.3

Eurocode 8 specifies $\Omega = 1.5$ for moderate-ductility walls, where amplification of shear demand in walls is not affected by dynamic amplification.

RP3-3.8.4   Dynamic amplification

Multiple studies have investigated and multiple design codes, standards and guides around the world specify dynamic amplification of shear demand in concrete walls. Typically, dynamic shear amplification is characterized by the following equation:

$$V_u' = \omega_v \, \Omega V_u \tag{2}$$

where V_u' is the maximum shear demand experienced by a concrete wall that exhibits nonlinear response under design-level earthquake loading, ω_v is the dynamic amplification factor, Ω is the flexural overstrength factor discussed in the preceding section, and V_u is the design base shear demand as specified by ASCE 7.

Research by Pugh et al. (2017) showed, using nonlinear dynamic analysis of idealized walled buildings ranging in height from 6 to 24 stories, that the dynamic amplification factor, ω_v, can range from 1.1 to 2.5. Multiple design codes, design recommendations and researchers around the world provide guidance on calculation of dynamic amplification of wall shear demand. The simplest approaches quantify dynamic amplification on the basis of building height. For example the New Zealand design code (NZ3101) employs equations proposed by Paulay and Priestly (1992):

$$\omega_v = 0.9 + n/10 \text{ for } n \leq 6 \tag{3a}$$

$$\omega_v = 1.3 + n/30 \leq 1.8 \text{ for } n > 6 \tag{3b}$$

where n is the number of stories, and SEAOC (2008) recommends

$$\omega_v = 1.2 + n/50 > 1.5 \tag{4}$$

again, with n equal to the number of stories. More sophisticated approaches define dynamic amplification as a function of parameters that better characterize the dynamic response of the walled building. For example, Priestley et al. (2007) recommended:

$$\omega_v = 1 + \mu/\Omega \, C_{(2,T)} \tag{5a}$$

$$C_{(2,T)} = 0.067 + 0.4(T_i - 0.05) \le 1.15 \tag{5b}$$

where μ is the ductility demand and T_i is the fundamental period of the wall building using elastic material properties. Eibl and Keintzel (1988) defined

$$V_u' = \sqrt{V_{max,1}^2 + V_2^2 + V_3^2 + \cdots + V_n^2} \tag{6}$$

where $V_{(max,1)}^2$ is the maximum base shear for Mode 1 response, which is determined by ΩM_n, and V_2 through V_n are the unreduced shear demands associated with response Modes 2 through n. Pugh et al. (2017) modified the relationship proposed by Eibl and Keintzel to better represent data for walled buildings ranging in height from 6 to 24 stories:

$$\omega_v V_u = \sqrt{\left(\frac{V_1}{R}\right)^2 + V_2^2 + V_3^2 + \cdots + V_n^2} \quad for \quad V_1 = max(V_2, V_3, \ldots V_n) \tag{7a}$$

$$\omega_v V_u = \sqrt{V_1^2 + \left(\frac{V_2}{R}\right)^2 + V_3^2 + \cdots + V_n^2} \quad for \quad V_2 = max(V_1, V_3, \ldots V_n) \tag{7b}$$

where V_i is the unreduced shear demand for response Mode i and R is the ASCE 7 response modification coefficient.

Pugh et al. (2017) showed that dynamic amplification of shear demand in walled buildings, as observed from nonlinear analyses data, is best represented by equations 7a and 7b. Pugh et al. showed also that dynamic amplification equations included in the New Zealand design code (Eq 3a and 3b) as well as those recommended by SEAOC (Eq. 4), both of which define dynamic amplification on the basis of building height, provide fairly consistent, modest underprediction of dynamic amplification (ratio of predicted to observed ranges from 0.75 to 0.9 for buildings designed using current ASCE 7 response modification coefficients).

RP3-3.8.5   Dynamic Amplification in ACI 318-19

As indicated in Section RP3-3.8.2 of this Resource Paper, ACI 318-19 requires cross-sections of a special shear wall to be designed for an amplified shear V_u' (V_e in ACI 318-19) equal to the V_u obtained from analysis of the structure under code-prescribed seismic forces, amplified by an overstrength factor Ω [Ω_v in ACI 318-19) and a dynamic amplification factor ω_v

$$V_u' = \omega_v \, \Omega \, V_u \tag{2}$$
$$\le 3V_u$$

Per ACI 318-19 Section 18.10.3.1.2, $\Omega = M_{pr}/M_u$ for the load combination producing the largest value of $\Omega \geq 1.5$, as long as h_w/ℓ_w (h_{wcs}/ℓ_w in ACI 318-19) > 1.5. $\Omega = 1$ for $h_w/\ell_w \leq 1.5$.

For $h_w/\square_w < 2.0$, $\omega_v = 1.0$. *For all other walls,* ACI 318-19 requires dynamic application defined by Eq. 3:

$$\omega_v = 0.9 + \frac{n}{10} \; for \; n \leq 6 \tag{3a}$$

$$\omega_v = 1.3 + \frac{n}{30} \leq 1.8 \; for \; n > 6 \tag{3b}$$

where n (n_s in ACI 318-19) is the number of stories.

RP3-3.8.6 Shear strength of concrete under high rate of loading, and effects of flanges

Only limited material has been found supporting the notion of a shear strength increase in shear walls due to high rate of loading. A paper from Kajima Corporation, Japan, (Mizuno et al., 1994) reported on experimental as well as analytical studies on the effects of loading rate on the shear strength-deformation relationships of RC shear walls. They concluded as follows. (1) For the inelastic behavior of reinforced concrete shear walls under rapidly induced lateral loads such as severe earthquake load and impact load, the shear strength of shear walls increases significantly due to increases in concrete and reinforcement strength. The shear strain at the maximum load increases as the loading rate increases, as well. (2) Taking into account the dynamic properties of concrete and reinforcement as a function of strain rate, the inelastic behavior of shear walls such as load-deformation relationships and the shear strength under high speed loading are well simulated by finite element analyses.

RP3-3.8.7 Effect of compressive stress on shear strength

Only limited material has been found supporting the concept of a shear strength increase in shear walls due to increased compressive loading. In a study (Yuen and Kuang, 2014) devoted primarily to the effect of axial compression on the ductility of reinforced concrete shear walls, the authors found that the shear strength of shear walls increased significantly under higher axial compression.

RP3-3.8.8 Shear migration to compression pier and shear-compression interaction in a coupled shear wall system

To meet architectural constraints, including elevator, stair and doorway openings, common configurations include walls coupled together with heavily reinforced, low-aspect-ratio coupling beams. Coupled walls are typically used in mid to high-rise construction, where the walls are coupled together with beams. Under lateral loading, the coupling beams are subjected to double curvature and are intended to yield. The resulting shear demands in the beams are transferred to the wall piers as axial tension and compression loads. The coupling of these axial forces provide resisting base moment which is additive with the moments at the base of each pier, resulting in a large flexural resistance and high axial forces.

Previous experimental tests of coupled walls were reviewed to establish understanding of coupled wall performance as well as to identify previously studied parameters, geometries and design characteristics. Taken as a whole, the prior tests demonstrated that:

1. A coupled wall with diagonally reinforced coupling beams exhibits significantly greater drift capacity than a nominally identical coupled wall with conventionally (i.e. horizontally) reinforced coupling beams (Santhakumar 1974).

2. During cycles to large drift demands, the compression wall pier carries most of the base shear, which can determine the performance of a coupled wall system (Santhakumar 1974, Shiu et al. 1981, Ozselcuk 1989, Lequesne 2009, Lehman et al. 2013).

3. Drift capacity of coupled walls for which the coupling beams are well-detailed and a significant (more than 30%) portion of the base moment results from coupling of axial forces in the wall piers is determined by failure of the compression wall pier (Santhakumar 1974, Shiu et al. 1981, Ozselcuk 1989).

4. Wall pier stiffness is significantly affected by axial demand (Ozselcuk 1989).

These results are demonstrated considering testing on a large-scale coupled wall specimen (Lehma et al. 2013). The full-scale wall had 365.8 cm (12.0 ft.) story heights, a 914.4 cm (30.0 ft.) total wall length, 45.7 cm (18.0 in.) thick walls and coupling beams, 365.8 cm (12.0 ft.) long wall piers, and 182.9 cm (6.0 ft.) long by 91.4 cm (3.0 ft.) deep coupling beams with an aspect ratio (i.e. the span-to-depth ratio) of 2.0. The geometry of Specimen was one-third of the full-scale dimensions described above, resulting in a total wall length of 304.8 cm (10.0 ft) (two 121.9 cm (4.0 ft) piers and 61.0 cm (2.0 ft) long coupling beams) and thickness of 15.2 cm (6.0 in.). Coupling beam heights were 30.5 cm (1.0 ft) resulting in a coupling beam aspect ratio of 2.0. Each floor was 121.9 cm (4.0 ft.) high. The constructed specimen was the bottom three stories of a ten-story wall; loads developed in the upper stories of the wall system were applied to the specimen using the load and boundary condition boxes (LBCBs) available at the UIUC NEES facility. The ten-story wall dimensions were used for design. The coupled wall reinforcement was designed following appropriate design documents and a target degree of coupling of less than 55%, as recommended by Harries (2001).

The measured base shear verses third floor drift response of CW1 and the final damage state of the compression pier are shown in Figure 3.8-1. At a third floor drift of 2.27%, the base shear decreased suddenly from the peak by 55%. Upon reverse loading at a maximum negative drift of -2.25%, the base shear dropped to 52% of the maximum peak base shear, resulting from compression failure of the compression pier.
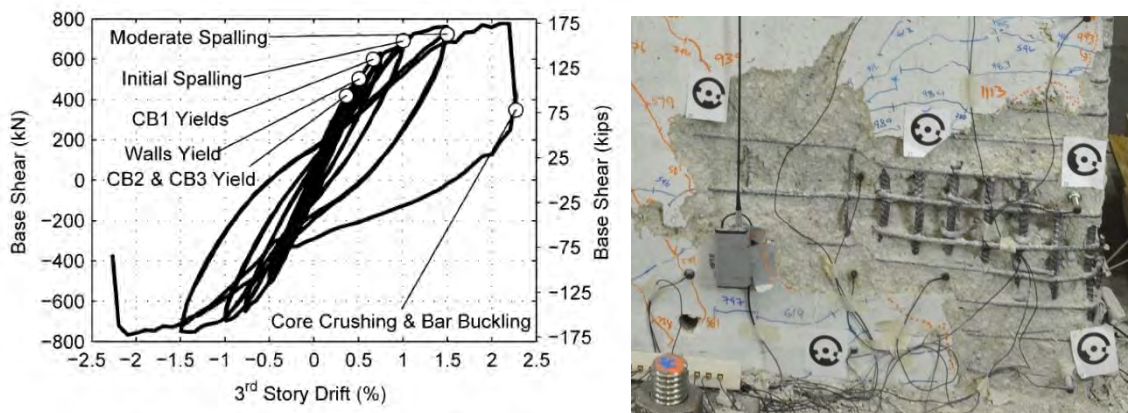
Figure 3.8-1 Response of and Damage Sustained by Coupled Wall with Ductile Detailing

The wall carried a maximum base shear of 778.4 kN (175 kips), which corresponds to an average shear stress demand of $0.33\sqrt{f_c}$ MPa ($4.0\sqrt{f_c}$ psi) averaged over both wall piers. However, considering the shear demand in the compression pier, the average shear stress was $0.9\sqrt{f_c}$ MPa ($10.8\sqrt{f_c}$ psi), or an approximate increase of 3. The maximum axial stress in the compression pier increased from 0.1 to approximately $0.4A_g f'_c$ (Figure 3.8-2). This increase in axial stress increases the moment capacity of the pier, and therefore the shear demand.
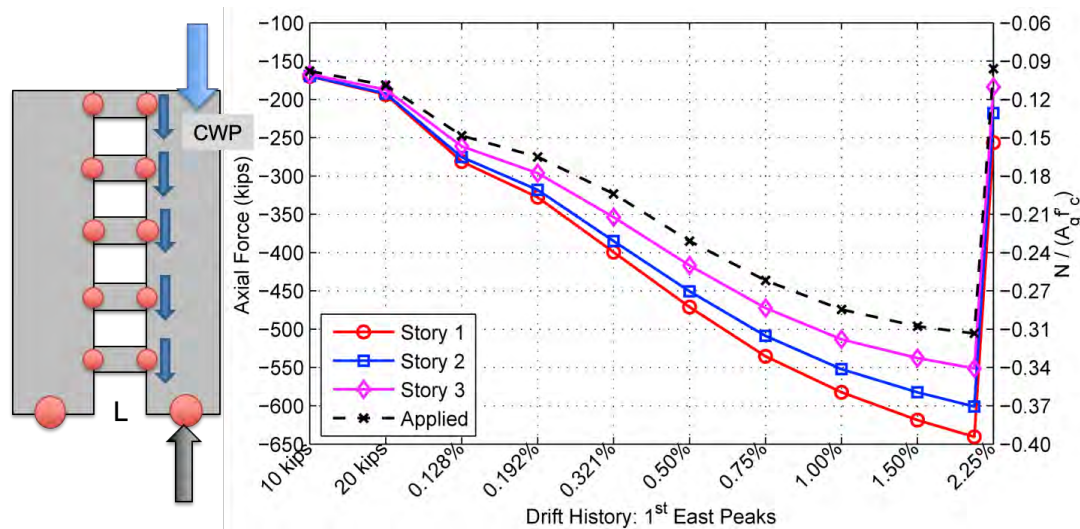
Figure 3.8-2 Normalized Axial Stress Demands in Compression Pier

The results indicate very large compressive stresses in the boundary region; most importantly the stresses exceed the compressive strength of the concrete for the area corresponding to cover spalling, which may have contributed directly to the observed failure mode. The computed ratios were 90% and 10% of the total base shear in the compression and tensions wall piers, respectively. This is consistent with the results of previous research (Santhakumar 1974, Shiu et al. 1981) which demonstrated that shear carried by the compression wall pier was substantially larger than that carried by the tension pier. In cases that use an area within the compression pier, the local shear stress demands are very high. It is likely that the high shear stress demands interacting with the high compressive stresses contributed to the observed failure. The principal stresses in the wall piers resulted from the interaction of the vertical compressive and shear stresses; thus compression-shear interaction is important. The large local stresses resulted in an explosive, sudden failure of the compression wall pier; thus, these local stresses must be limited to prevent this failure mode.

RP3-3.9   Ductile Coupled Shear Walls FEMA P-695 Study

As noted in Section RP3-3.6 of this Resource Paper, a Ductile Coupled Structural Wall system of reinforced concrete has now been defined in ACI 318-19. IT-4 developed a proposal, now approved, to add three line items to ASCE 7-16 Table 12.2-1, Design Coefficients and Factors for Seismic Force-Resisting Systems, featuring the ductile coupled structural or shear wall system of reinforced concrete. The line items will be under: A. Bearing Wall Systems, B. Building Frame Systems, D. Dual Systems with Special Moment

Frames. Based on a FEMA P-695 study, $R = 8$, $C_d = 8$, and $\Omega_o = 2.5$ have been proposed in all the line items. The height limits are the same as for corresponding uncoupled isolated wall systems. A minimum height limit of 60 ft has been imposed on seismic force-resisting systems featuring the ductile coupled walls. Several changes made in ACI 318-19 for the design and detailing of special structural walls were implemented in the design of the prototypes for the FEMA P-695 study.

The proposed response modification factors for seismic force-resisting systems featuring the ductile coupled shear walls of reinforced concrete were validated using the FEMA P695 methodology. A series of forty-one coupled wall archetype buildings were designed for Seismic Design Category D (D_{max} as defined in FEMA P695) in conformance with the most recent provisions of ASCE 7-16 and ACI 318-19. The archetypes considered addressed a range of variables expected to influence the collapse margin ratio, with the primary variables being building height (i.e., 6, 8, 12, 18, 24, and 30 stories), wall cross section (i.e., planar and flanged walls), coupling beam aspect ratio (ℓ_n/h) ranging from 2.0 to 5.0, and coupling beam reinforcement arrangement (diagonally and conventionally reinforced). The range of variables was chosen considering those used to define a ductile coupled structural wall system in ACI 318-19. The archetypes were optimally designed to have the minimum wall area (length and thickness), which is governed by shear amplification and the requirement that the nominal shear stress in walls sharing a common shear force not exceed a value of $8\sqrt{f'_c}A_{cv}$. Typical floor plans and a wall elevation view are presented in Figure 3.9-1.
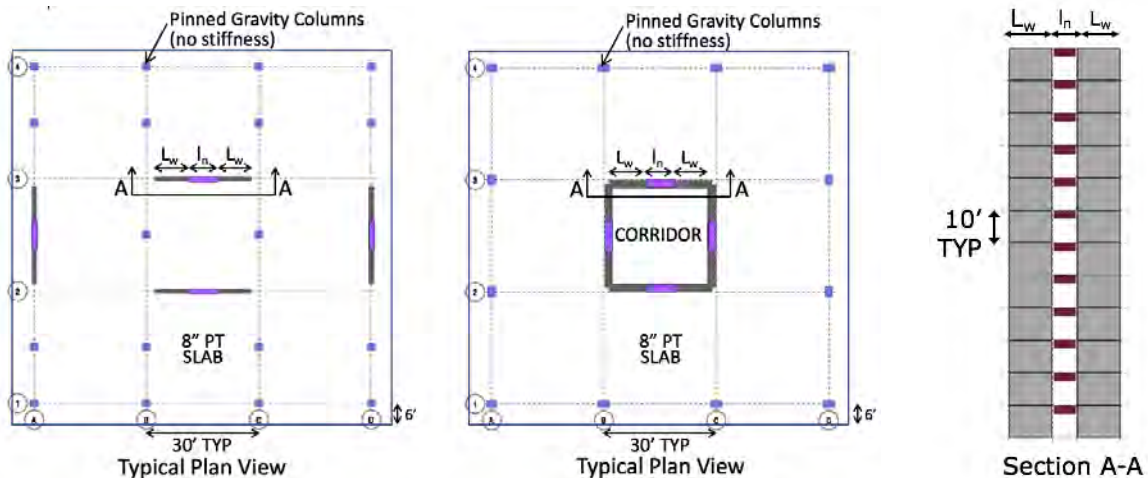
(a) <u>Planar Walls (6, 8, 12 Story)</u> (b) <u>Flanged Walls (18, 24, 30 Story)</u> (c) <u>Elevation View</u>

Figure 3.9-1 Archetype floor plans and typical wall elevation view

Important design considerations adopted in the FEMA P695 study included four ACI 318-19 changes. The wall piers were designed per ACI 318-19 Section 18.10.3 considering wall shear force amplification as described in Section RP3-3.8.4 of this Resource Paper, in an effort to reduce the likelihood of shear failure preceding flexural failure. Moreover, the wall drift capacity was checked per ACI 318-19 Section 18.10.6.2, to verify that wall piers have sufficient drift capacity to resist Design Earthquake (DE) demands with a low (roughly 10%) probability of strength loss. Other implemented ACI 318-19 changes include ACI 318-19 Section 18.10.6.4, which requires improved wall boundary and wall web detailing (i.e, overlapping hoops if the boundary zone aspect ratio exceeds 2:1, crossties with 135-135 hooks on both ends, and 135-135 crossties on web vertical bars) as well as ACI 318-19 Section 18.10.2, which requires

minimum wall boundary longitudinal reinforcement in order to limit the potential of brittle tension failures in walls that are lightly reinforced.

Following the design, two-dimensional nonlinear models were created for each archetype with the OpenSees computational platform in which fiber elements with uniaxial material relations and linear shear springs were used to model the wall piers, while beam-column elements and nonlinear shear springs were used to model the coupling beams. Seismic weights were assigned at the element nodes at each story level, while gravity loads tributary to the wall were assigned at the same nodes. P-delta effects were considered by using a column with zero lateral stiffness. The modeling approaches used for the structural elements have been validated with experimental data from isolated wall tests, isolated coupling beam tests, and from a 12-story coupled wall test performed at the Building Research Institute facility in Japan.

To assess collapse, three primary failure modes were considered to capture lateral strength loss and failure, i.e., 1) flexural failure (crushing of concrete, buckling of reinforcing bar, tensile fracture of longitudinal reinforcement) was assessed using a statistical drift capacity model developed based on an extensive database of wall tests, 2) shear failure (diagonal tension/compression) assessment was based on the relationship between wall shear force and tensile strain of wall longitudinal reinforcement, following Los Angeles Tall Buildings Seismic Design Council or LATBSDC (2017) recommendations, and 3) axial failure was estimated using a shear friction model. For the study, collapse was defined as being associated with either flexure or shear, meaning that the axial failure model did not govern because the lateral drift values at axial failure generally exceeded 5%; the axial failure model also has not been verified (although collapse of buildings with reinforced concrete walls has rarely been reported following strong earthquakes). Because amplified wall shear demands were used in design, shear failures were mostly suppressed, and flexure-related collapse was typically defined by the drift capacity model for most archetypes. Overall, the criteria used for collapse assessment in the study were conservative, since the failure models predict the onset of strength loss (a 20% drop in lateral strength) and not necessarily collapse. The approach is conservative because loss of axial load carrying capacity typically does not occur until lateral strength drops to near zero. In some studies, axial failure has been assumed to occur at a specified roof drift ratio, which has been typically defined as 4 to 5% (NIST GCR-10-917-8), whereas, in this study, the conservative approach used resulted in drift ratios at failure that were typically about 3%.

Nonlinear static pushover (NSP) analyses and incremental dynamic analyses (IDA) using the 44 far-field ground motion records defined in Appendix A.9 of FEMA P695 were conducted for each Archetype. The pushover analyses were used to obtain an estimate of the system overstrength factor (Ω_o) and system ductility (μ_T), whereas IDA results were used to determine the median collapse intensity and collapse margin ratio for each Archetype. Uncertainties associated with ground motion records (β_{RTR}=0.4), code design requirements (β_{DR}=0.2), available test data (β_{TD}=0.2), and computational modeling approaches (β_{MDL}=0.2) were estimated to determine a total system uncertainty value of about 0.525 per FEMA P695 Table 7.2a. Based on this total system uncertainty value of 0.525, the acceptable adjusted collapse margin ratios as specified in FEMA P695 Table 7-3 were determined as 1.56 for each archetype and 1.96 for the mean of each performance group.

As a result of the FEMA P695 study, a system overstrength factor of Ω_o = 2.5 was proposed based on nonlinear static pushover analysis results indicating that mean overstrength values of the performance groups ranged from 1.3 and 2.2. The proposed response modification factor R = 8 was validated based on incremental dynamic analysis results indicating that mean Adjusted Collapse Margin Ratio values of the performance groups ranged from 2.1 to 2.9, corresponding to collapse probabilities of less than 10%, based

on using a conservative definition of collapse as noted in the prior paragraph. A deflection amplification factor of $C_d = 8$ was proposed based on damping considerations and the assessment of median roof drift responses from design earthquake level shaking compared to design roof drifts. A minimum height limit of 60 ft is recommended for ductile coupled wall systems, with the proposed seismic response parameters to be adopted in ASCE 7, because coupled walls are generally not efficient seismic force-resisting systems for shorter buildings. Overall, the results of this study suggest that an overstrength factor of $\Omega_o = 2.5$, a response modification factor $R = 8$, and a deflection amplification factor of $C_d = 8$ were appropriate seismic design parameters for RC Ductile Coupled Wall systems that are designed per ASCE 7-16 and ACI 318-19 provisions.

A report summarizing the FEMA P-695 study on Reinforced Concrete Ductile Coupled Walls is available (Tauberg et al, 2019).

RP3-3.10   References

ACI Committee 318. (2019). *Building Code Requirements for Structural Concrete* (ACI 318-19) *and Commentary* (ACI 318R-19), American Concrete Institute, Committee 318, Farmington Hills, MI, 2019.

Birely, A.C. (2012), *Seismic Performance of Slender Reinforced Concrete Structural Walls*, Ph.D. Thesis, University of Washington, WA.

CSA Group (2014). *Design of Concrete Structures*, CSA A23.3-14, Canadian Standards Association, Toronto, Ontario, Canada.

Eibl, J. and E. Keintzel (1990). "Seismic design shear forces in RC cantilever shear wall structures," *European Earthquake Engineering*, Vol. 3, pp. 7–16.

Harries, K. A. (2001). "Ductility and deformability of coupling beams in reinforced concrete coupled wall." *Earthquake Spectra*, EERI, 17(3):457-478.

Kircher, C. A., Deierlein, G. D., Hooper, J. D., Krawinkler, H., Mahin, S. A., Shing, B., Wallace, J. W.(2010). *Evaluation of the FEMA P-695 Methodology for Quantification of Building Seismic Performance Factors*, Report NIST GCR-10-917-8, 268 pp.

Lehman, D. E., Lowes, L. N., Turgeon, J., Birely, A., Kuchma, D. A., Marley, K. P., and Hart, C. (2013) "Seismic Behavior of Modern Coupled Walls", *ASCE Journal of Structural Engineering*, 139, SPECIAL ISSUE: NEES 2: Advances in Earthquake Engineering, 1371–1381, July.

Lequesne, R. D., Wight, J. K., and Parra-Montesinos, G. J. (2010). "Seismic detailing and behavior of coupled-wall systems with high-performance fiber-reinforced concrete." *Proceedings of the 9th U.S. National and 10th Canadian Conference on Earthquake Engineering*, Toronto, Ontario, Canada.

Lowes, L. N., Lehman, D. E., Kuchma, D. A., Behroozi, A, Mock, A. (2014). "Large Scale Testing of C-Shaped Reinforced Concrete Walls," A Report to the Charles Pankow Foundation on Grant , 78p.

Marley, K. P. (2011). *Evaluation of Concrete Compressive Models Applied to Large-Scale Structural Walls*." Ph.D. Thesis, University of Illinois at Urbana-Champaign, Champaign, IL.

Massone, L. M., Bonelli, P., Lagos, R., Lüders, C., Moehle, J. P., and Wallace, J. W. (2012). "Seismic Design and Construction Practices for RC Structural Wall Buildings," *Earthquake Spectra* , Vol. 28, No. S1, pp. S245-S256.

Mizuno, J., Matsuo, I., Suzuki, A., Morikawa, H., Ishida, M., Koiso, T., Kasai, Y., Nakamura, N., and Ohno, T. (1999). "Effects of Loading Rate on Reinforced Concrete Shear Walls, Part 3, High Speed Loading Tests of Reinforced Concrete Shearwalls and FE Simulation Analyses," *Transactions on the Built Environment*, Vol. 38, WIT Press, Southampton, UK.

Moehle, J. P., Ghodsi, T., Hooper, J. D., Fields, D. C., and Gedhada, R. (2011). *Seismic design of cast-in-place concrete special structural walls and coupling beams: A guide for practicing engineers*," NEHRP Seismic Design Technical Brief No. 6, National Institute of Standards and Technology, Gaithersburg, MD.

Standards New Zealand (2006). *Concrete Structures Standard, Part 1: The Design of Concrete Structures: Part 2: Commentary on the Design of Concrete Structures*, NZS 3103, Wellington, New Zealand.

Ozselcuk, A. R. (1989). *Experimental and Analytical Studies of Coupled Wall Structures*. Ph.D. Thesis, University of California, Berkeley, CA.

Pacific Earthquake Engineering Research Center (PEER) (2017). Tall Building Initiative (TBI) *Guidelines for Performance-Based Seismic*, PEER Report 2017/06, University of California, Berkeley.

Paulay, T. and Priestley, M. (1992), *Seismic Design of Reinforced Concrete and Masonry Buildings*, Willey Interscience, Ed. United States of America: ISBN 0-471-54915-0, 1992.

Pugh, J. (2012). *Numerical Simulation of Walls and Seismic Design Recommendations for Walled Buildings*," Ph.D. Thesis. University of Washington, Seattle, WA.

Pugh, J.S., Lowes, L.N., Lehman, D.E. (2017) "Accurate Methods for Elastic Seismic Demand Analysis of Reinforced Concrete Walled Buildings" *Journal of Structural Engineering*, ASCE, 143(8).

Santhakumar, A. R. (1974). *The Ductility of Coupled Shear Walls*." Ph.D. Thesis, University of Canterbury, Christchurch, New Zealand.

Structural Engineers Association of California (2008). "Reinforced concrete structures," Tech. Rep. Article 9.01.010, Sacramento, CA.

Shiu, K. N., Aristizabal-Ochoa, J. D., Barney, G. B., Fiorato, A. E., and Corley, W. G. (1981). *Earthquake resistant structural walls – coupled wall tests*. Report to National Science Foundation, Construction Technology Laboratories, A Division of Portland Cement Association, Stokie, IL.

Tauberg, N., Kolozvari, K, Wallace, J.W. (2019). *Ductile Reinforced Concrete Coupled Walls: FEMA P695 Study*, Final Report, July, 145 pp.

Turgeon, J. A. (2011). *The Seismic Performance of Coupled Reinforced Concrete Walls*. Master's Thesis, University of Washington, Seattle, WA.

Yuen, Y.P. and Kuang, J.S., "Axial Compression Effect on Ductility Design of Reinforced Concrete Structural Walls," *Proceedings,* Second European Conference on Earthquake Engineering and Seismology, Istanbul, 2014.

RP3-4   MASONRY SHEAR WALLS – BENNETT

RP3-4.0   Introduction

Two masonry-related topics are discussed in this chapter. The first is partially grouted masonry shear walls which are primarily used in buildings assigned to moderate seismic design categories. The shear strength of these walls is discussed with background and it is recommended that attention should be focused on measures to improve the ductility of these shear walls. The second topic is coupled reinforced masonry shear walls. It is pointed out that masonry shear walls more often than not are inherently coupled by the floor slabs, although such coupling is not intended. This coupling may enhance the flexural strength of the shear wall core; since normally the shear strength of the core will not be increased, this may result in non-ductile shear failure.

RP3-4.1   Partially grouted shear walls

Partially grouted masonry shear walls are masonry shear walls in which only the vertical cells and horizontal courses that contain reinforcement are grouted. An elevation and cross-section view of a partially grouted masonry shear wall is shown in Figure 4.1-1. The advantage of a partially grouted shear wall is the cost savings on grout and a partially grouted shear wall typically has only 50-60% of the mass of a fully grouted shear wall. In higher seismic areas, the vertical and horizontal reinforcement will become closer spaced, which often leads to fully grouting the wall.
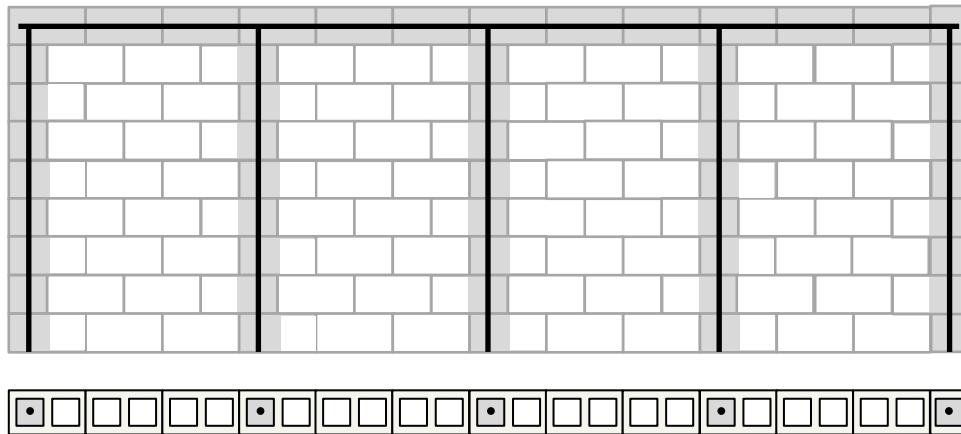
Figure 4.1-1 Partially grouted masonry shear wall

Several concerns have been raised with respect to partially grouted masonry shear walls. These relate to the appropriateness of the design equations for the shear strength of the wall, and the seismic behavior of partially grouted shear walls. This paper addresses both issues.

RP3-4.1.1   Brief History of Shear Strength Provisions in TMS 402

In 2002 strength design provisions were added to the TMS 402 code. Most of the provisions were based on research conducted as part of the Technical Coordinating Committee for Masonry Research (TCCMaR) program. This research program resulted in 63 research reports from 1985-1992. The shear strength provisions for masonry shear walls were very different from the existing allowable stress design provisions. The shear strength provisions were based on Shing et al. (1990a, 1990b).

One notable difference between strength design and allowable stress design was that allowable stress design did not permit the strength from the masonry and the strength from shear reinforcement to be added;

either the masonry had to be designed to carry all the shear or the reinforcement had to be designed to carry all of the shear. The strength provisions allowed the shear strength of the masonry and the shear strength of the reinforcement to be added.

In the 2011 edition of the TMS 402 standard, there was a major change to allowable stress design. All of the allowable stresses were recalibrated as a result of the removal of the one-third stress increase provision. As part of the recalibration effort, the shear strength provisions were reexamined. Based on work by Davis et al. (2010), the TMS 402 strength design provisions were chosen to also be used for allowable stress design, with the nominal strength equations converted to allowable stress equations by dividing by the area and using a factor of safety of approximately two (Bennett et al., 2011). Davis et al. (2010) had examined 56 tests of masonry walls failing in-plane shear. The average ratio of the test strength to the calculated strength was 1.17 with a standard deviation of 0.17, and a coefficient of variation of 0.15. The standard deviation of 0.17 was the lowest of any of the eight shear strength methods examined, with the next lowest standard deviation being 0.22. Although the test data encompassed both concrete masonry walls and clay masonry walls, all of the walls were fully grouted; no partially grouted walls were included in the database.

Several Masonry Standards Joint Committee (MSJC) members had raised concerns about the shear strength provisions being unconservative for partially grouted shear walls. During the Fall 2011 meetings, Bennett proposed a reduction factor of 0.75 for the shear strength of partially grouted shear walls. The basis of the 0.75 reduction factor was comparing the work of Davis et al. (2010) to that of Minaie et al. (2010). Minaie et al. (2010) compared the experimental strength of 64 partially grouted shear wall tests to seven different shear strength methods. For the TMS 402 Code equation, the ratio of the test strength to the calculated strength was 0.90 with a standard deviation of 0.26. The standard deviation of 0.26 was the second lowest, with Anderson and Priestley (1992) having a standard deviation of 0.21. All of the other methods had a standard deviation of greater than 0.4. Thus, the TMS 402 equation had a reasonable random error (standard deviation), but was overestimating the strength systematically. By comparing the average ratio of experimental to predicted strength of fully grouted walls to partially grouted walls, a value of $0.90/1.17 = 0.77$ was obtained. This was rounded down to 0.75 to account for the higher variability with partially grouted walls. The effect of the modification on the scatter was to lower the standard deviation, but to keep the coefficient of variation the same. This proposal was adopted in the 2013 TMS 402 standard, which introduced a partially grouted shear wall factor of 0.75 for partially grouted shear walls, and 1.0 otherwise.

Perhaps the most comprehensive analysis of shear wall experimental data was conducted by Dillon (2015). Dillon conducted a meta-analysis and included 172 tests of fully grouted shear walls and 181 tests of partially grouted shear walls. For fully grouted walls, Dillon (2015) found a mean ratio of experimental strength to predicted strength of 0.97 with a standard deviation of 0.23 (coefficient of variation of 0.23). For partially grouted walls, the mean ratio was 0.73 with a standard deviation of 0.22 (coefficient of variation of 0.30). Dillon (2016) recommends one of two methods to improve the TMS 402 shear equations. One method is to decrease the partially grouted shear wall factor from 0.75 to 0.70. The second method is to keep the partially grouted shear wall factor as 0.75, but reduce the strength-reduction factor for partially grouted walls from 0.80 (for all shear) to 0.75. The advantage of the second method is that the partially grouted shear wall factor accounts for differences between the mean shear strengths of fully grouted and partially grouted walls, while the different strength-reduction factor accounts for different variability for the two wall types.

Dillon (2015) analyzed the performance of 14 shear strength models, including a proposed new model, in terms of the root-mean-square-error, r^2, and the residuals of a plot of the predicted strength vs. the experimental strength. The current TMS 402 model out-performed all models except for Dillon's proposed model. The current TMS 402 model had $r^2 = 0.94$ for fully grouted walls and $r^2 = 0.90$ for partially

grouted walls. Dillon's proposed model had $r^2 = 0.96$ for fully grouted walls and $r^2 = 0.94$ for partially grouted walls.

RP3-4.1.2 Summary and Code Recommendations: Shear Strength of Partially Grouted Shear Walls

Since introducing the partially grouted shear wall factor of 0.75 in the 2013 TMS 402 code there has been scrutiny and criticism. The partially grouted shear wall factor was developed in a short period of time and was meant to be a stop-gap measure. Although the current design equation is based on fully grouted walls with a simple empirical adjustment for partial grout, and does not capture the actual behavior of the partially grouted wall, the equations still work well. The TMS 402 method still has one of the lowest variabilities in predicting experimental strength, is simple, and is easy to use in design. Therefore no major modifications are suggested for predicting the shear strength of partially grouted walls. One minor adjustment is to consider a slightly lower strength-reduction factor (0.75 vs. 0.80) for partially grouted shear walls to account for the higher variability when compared to fully grouted shear walls.

RP3-4.1.3 Seismic Behavior

There has been much less research related to the behavior of partially grouted masonry walls under seismic loading than for fully grouted walls. As the seismic loading, and hence the reinforcement, increases, it is often more economical to fully grout the wall. However, partially grouted masonry shear walls are used in some locations that are in Seismic Design Category D and above, and masonry construction in Seismic Design Category C and below is almost entirely partially grouted construction. A review of some of the recent work related to seismic behavior is given in the following.

Minaie et al. (2010) examined the displacement ductility of partially grouted shear walls with shear dominated behavior. They defined displacement ductility as the ratio of the displacement at failure to the displacement at yield using an elasto-plastic response with equal energy compared to the backbone curve. The average displacement ductility for 10 walls that they examined was 3.7 with a standard deviation of 2.0. Three of the walls did not conform to the TMS 402 requirements for special reinforced shear walls. If those walls are taken out of the data set, the average displacement ductility falls slightly to 3.5 with a standard deviation of 2.3. They comment that these displacement ductilities may be unconservative for R=5. However, they also point out the R=5 is not intended to represent the response of special reinforced shear walls that fail in shear. There are capacity design provisions within TMS 402 that require the design shear strength to exceed the shear corresponding to the development of 1.25 times the nominal flexural strength, except that the nominal shear strength need not exceed 2.5 times required shear strength.

Kasparik et al. (2014) performed shake table tests on five different one-third scale partially grouted piers with reinforcement ratios of 0.0007, 0.010, and 0.012. All of the piers were flexurally controlled. The piers were meant to be representative of construction in low to moderate seismic regions and did not meet the requirements for special shear walls. Due to shake table limitations, none of the walls reached their ultimate load. The average displacement ductility was 3.0 with a standard deviation of 0.57. The authors state that these can be considered lower bound displacement ductilities, since the ultimate load was not reached.

Bolhassani et al. (2016b; 2016c) tested three partially grouted walls. The walls were detailed according to the ordinary reinforced masonry wall requirements of TMS 402, and hence would only be allowed in Seismic Design Category C and below. The first wall, labeled SR, had single cell vertical reinforcement and a single course bond beam. The second wall, labeled DR, had double cells for all reinforcement and a two course bond beam. The reinforcement ratio for the SR and DR wall were approximately the same; smaller bars were used in the DR wall. The purpose of the double reinforcement was to increase the strength of the connection between the bond beam and the vertical grouted cell so the connection would be able to carry more moment, and the grouted elements behave similarly to reinforced concrete elements. The third wall, labeled DR-JR, had double cell vertical reinforcement, a single course bond beam, and W1.7 (9 gauge) joint reinforcement every course. It was hypothesized that the bed joint reinforcement in the hollow cells allows for better stress transfer between the grouted elements and more ductile behavior. The wall specimens are shown in Figure 4.1-2, which is a reproduction of Figure 1 in Bolhassani et al. (2016b).

The ultimate strengths of the three walls were similar, being 81 kips for SR, 85 kips for DR, and 86 kips for DR-JR. The displacement ductilities were quite different. Bolhassani et al. (2016c) report significantly different displacement ductilities than Bolhassani et al. (2016b). Values reported in the paper are from Bolhassani et al. (2016b), as that paper provides a more comprehensive analysis and better background. Wall SR had a displacement ductility of 3.1, wall DR had a displacement ductility of 5.0, and wall DR-JR had a displacement ductility of 28.0.

Bolhassani et al. (2016b) also performed a FEMA P695 type analysis on the three walls to determine if

Figure 4.1-2 Wall configurations: (a) single reinforcement (SR); (b) double reinforcement (DR); (c) DR with joint reinforcement (DR-JR) [reproduction of Figure 1 from Bolhassani et al., 2016b]

an *R*=2 was acceptable. A summary of the results is shown in Table 4.1.1, which is a reproduction of Table 5 in Bolhassani et al. (2016b). The SR wall failed, but was close, having an adjusted collapse margin ratio (ACMR) of 88% of that required. The other two walls easily passed, with wall DR having an ACMR 1.84 times that required and wall DR-JR having an ACRM 2.02 times that required. The authors caution that the FEMA P695 methodology needs to be performed for different building categories (i.e., different stories and dimensions) in order to make overall decisions about the behavior of a partially grouted masonry shear wall systems. The work does suggest that small detailing changes could greatly improve the seismic behavior of partially grouted masonry shear walls.

Table 4.1.1 Summary of Incremental Dynamic Analyses, Collapse Margins, and Comparison to Acceptance Criteria [Table reproduced from Bolhassani et al., 2016b]
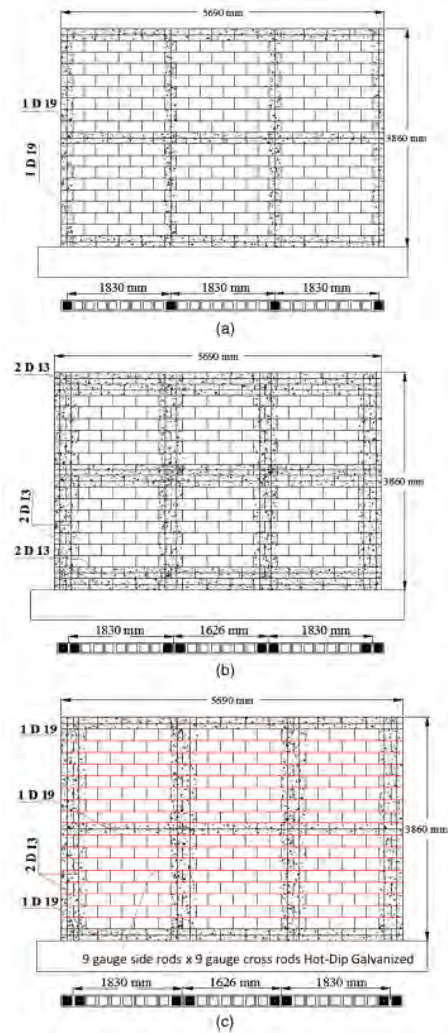
Archetype Identifier	$S_{MT}(T)$ (g)	$S_{CT}(T)$ (g)	CMR	SSF	ACMR	Accept ACMR	Pass/Fail
SR	0.75	1	1.33	1.08	1.43	1.62	Fail
DR	0.75	2	2.67	1.12	2.99	1.62	Pass
DR-JR	0.75	2.2	2.93	1.12	3.28	1.62	Pass

Johnson and Schultz (2019) tested two walls that were similar to Bolhassani et al (2016b). The walls tested by Johnson and Schultz (2019) had a central opening and flanges on the end of the walls. One wall was traditional reinforcing with vertical reinforcement in single grouted cells and single course bond beams. The second specimen had double reinforced grouted cells for vertical reinforcement. W2.8 (three-sixteenth inch) joint reinforcement was used in every other course above and below the opening, and in every course in the piers beside the opening. The capacities were similar, with the second specimen being 10% stronger than the first specimen. However, the displacement ductility was 8.6 for the second specimen, as opposed to 3.6 for the first specimen.

The above research shows that there are potentially promising details that could significantly enhance the seismic performance of partially grouted masonry shear walls. However, due to the limited testing, it is impossible to isolate the effects of the double vertical reinforcement vs. the joint reinforcement.

Koutras, A., and Shing, P.B. (2017) tested a one-story partially grouted masonry building on a shake table. The building was symmetric and had a window and door opening in each of the two walls that were in the direction of shaking. The building was designed as an ordinary reinforced masonry shear wall (R=2). Vertical reinforcement was approximately #4 @ 72 inches and horizontal reinforcement was approximately #4 @ 48 inches. The horizontal reinforcement was a result of required prescriptive stopping at 24 inches beyond the opening as allowed by TMS 402. The design base shear was 102 kips, which was determined using the largest permissible S_{DS} in Seismic Design Category C. An elastic analysis was used to determine the forces in the piers.

The initial failure was sliding at the base (TMS 402 did add shear friction design provisions in the 2016 edition). Concrete stoppers were then cast to prevent the sliding. The final failure was a brittle shear failure in the piers between the openings. The maximum load was a base shear of 277 kips, or 2.7 times the design base shear, and occurred at about 0.5% drift. The capacity was close to the capacity obtained if the calculated shear strength of all the piers was simply added, which was 310 kips. A finite element analysis was conducted. The authors concluded: "The analysis shown (sic) that the code formula for the shear strength is sufficiently accurate for the structure tested. However, the base-shear capacity of the structure cannot be calculated as a simple sum of the shear strengths of the contributing piers because of the disparity in the stiffness and the brittle behavior of the piers."

RP3-4.1.4   Summary and Code Recommendations: Seismic Behavior of Partially Grouted Shear Walls

The amount of research and data on seismic behavior of partially grouted shear walls is limited. Based on the work that is available, partially grouted walls seem to perform reasonably well. There may be some minor changes in prescriptive requirements to enhance the ductility of partially grouted shear walls that could be relatively easily implemented.

One detail that is not currently required in TMS 402 prescriptive requirements is to anchor the end

vertical bars (jamb steel) into the top bond beam with a 90° hook. This seems to improve the behavior, and has been shown by others to improve the wall behavior (e.g. Baenziger and Porter, 2011). Two possible methods to construct the detail are to have a 90° hook on the end of the bond beam reinforcement, or to have a short 90° bar that is lap spliced with the vertical reinforcement and also the bond beam reinforcement.

The double vertical bars proposed by Bolhassani need further investigation. Having two cells reinforced and grouted at the ends of shear walls may not be a significant issue. If all vertical bars are required to have double cells, designers may place bars at much wider spacings (e.g. if the design requires #5@48 inch, and double cells are required, the designer may choose to place 2-#5, one in each of the double cells, at 96 inch). This could potentially negate any benefits of double cells. Further study and testing are required before any recommendation can be made.

There seems to be significant benefit to joint reinforcement in terms of ductility. This makes sense as smaller distributed reinforcement generally performs better than larger concentrated reinforcement. Currently, TMS 402 requires three-sixteenth inch joint reinforcement if the joint reinforcement is to be used for shear reinforcement in strength design. No such restriction exists in allowable stress design. 9-gage joint reinforcement is the most common and can be used for prescriptive seismic reinforcement. Also, joint reinforcement is not currently allowed for Special Reinforced Masonry Walls, as there is a requirement that the horizontal reinforcement must be "embedded in grout". The TMS 402 committee is working on resolving these conflicts.

Most masonry walls in low to moderate seismic zones are built with 9-gage joint reinforcement at 16 inches. Intermediate bond beams are rarely used. It is unfortunate that the testing of Bolhassani did not include this configuration. Additional research to quantify the positive effects of joint reinforcement on ductility is needed.

RP3-4.1.5   Conclusions

Recently, there has been a lot of concern over partially grouted shear walls, both in terms of their shear strength and seismic behavior. Most of these concerns seem to be overstated. Major revisions to the TMS 402 partially grouted shear wall provisions are not needed. Some minor modifications may be in order as part of the normal code improvement process.

The code needs to be written so that all walls have an adequate safety level. However, several things need to be kept in mind. One is that most masonry walls are overdesigned for shear. Out-of-plane loads usually control, and generally there is much more shear wall than needed. Deflection limits can also control the design, rather than shear resistance. In fact, masonry shear walls in big box type structures may have 5-10 times the shear capacity that is needed. The code committee should also consider if all the prescriptive reinforcement needed for special walls is needed if the wall is only stressed to 10% of their shear capacity.

A second thing to keep in mind is that there are many things to consider when designing a masonry shear wall, and often something besides the shear strength controls the shear reinforcement. This could be spacing limits, prescriptive reinforcement, shear capacity design, or a variety of other things. Huston (2011) has shown that there are five things that need to be considered for ordinary reinforced shear walls, and ten things that need to be considered for special reinforced shear walls. Often it is something else besides the shear strength that controls the required horizontal reinforcement.

There likely has been sufficient research on the shear strength of partially grouted masonry shear walls. We know all the flaws of current TMS 402 shear provisions, but yet the TMS 402 equations continue to be one of the best methods, and the current equations are easy to use in design. Most proposed modifications would require iteration as parameters that are not known in design are used in the equations.

Future research should focus primarily on ductility, and simple means to increase ductility of partially grouted masonry shear walls. Specific recommendations are:

1. Examine the effects of double vertical grouted cells. This includes just having double grouted end

cells, wider spacing if double grouted cells are used, and long walls where there would be multiple control joints.

2. Examine the effects of joint reinforcement. This includes the size of the joint reinforcement (W1.7 vs. W2.8) and the spacing of joint reinforcement (every course vs. every other course). Although joint reinforcement may not contribute significantly to the strength of the wall, it could contribute significantly to the ductility of the wall.

3. Examine the effects of openings. Some preliminary unpublished research has shown that continuous bond beams above and below openings enhances the behavior, rather than terminating the bond beam 24 inches beyond the opening, as is permitted in TMS 402.

4. Examine whole building behavior. Preliminary research has shown that whole building behavior is quite different that the individual shear wall behavior. Although partially grouted shear walls have not always performed the best when tested individually, there is some indication that a whole building acting as a system may have good performance. Studies need to be conducted that examine entire building behavior.

RP3-4.2   Coupled masonry shear walls

Coupled masonry shear walls are rare. Most masonry buildings are single story. For multi-story masonry buildings, it is difficult to construct coupling beams since shear capacity design provisions generally create unrealistic levels of reinforcement. TMS 402 doesn't have explicit provisions for the design of masonry coupling beams, and the modular nature of masonry makes reinforcement patterns of diagonal bars, such as are sometimes used in concrete coupling beams, difficult to place.

ASCE 7-16 Chapter 14 does have additional provisions for masonry coupling beams. The coupling beam between shear walls is required to be designed to reach the moment or shear nominal strength before either shear wall reaches its moment or shear nominal strength. The design shear strength, ϕV_n, of coupling beams is required to satisfy the following criterion:

$$\phi V_n \geq \frac{1.25(M_1 + M_2)}{L_c} + 1.4V_g$$

where M_1 and M_2 = nominal moment strength at the ends of the beam, L_c = length of the beam between the shear walls; and V_g = unfactored shear force caused by gravity loads. The calculation of the nominal flexural moment is required to include the reinforcement in reinforced concrete roof and floor systems. The width of the reinforced concrete used for calculations of reinforcement is specified as six times the floor or roof slab thickness.

In spite of coupling beams being rare in masonry, there is coupling between masonry shear walls that occurs in multi-story masonry/reinforced concrete slab buildings. This coupling and the effects of this coupling, are examined.

RP3-4.2.1   Shake Table Tests

Stavridis et al. (2016) report on the shake table test of a three-story masonry building that had hollow-core plank aligned in the direction of shaking with a 3 inch concrete topping. There were two flanged shear walls connected by a lintel. The lintel had control joints on both sides and the bars were debonded past the control joints in an attempt to isolate the lintel and not have coupling. The configuration of the test structure is shown in Figure 4.2-1, which is a reproduction of Figure 1 in Stavridis et al. (2016).
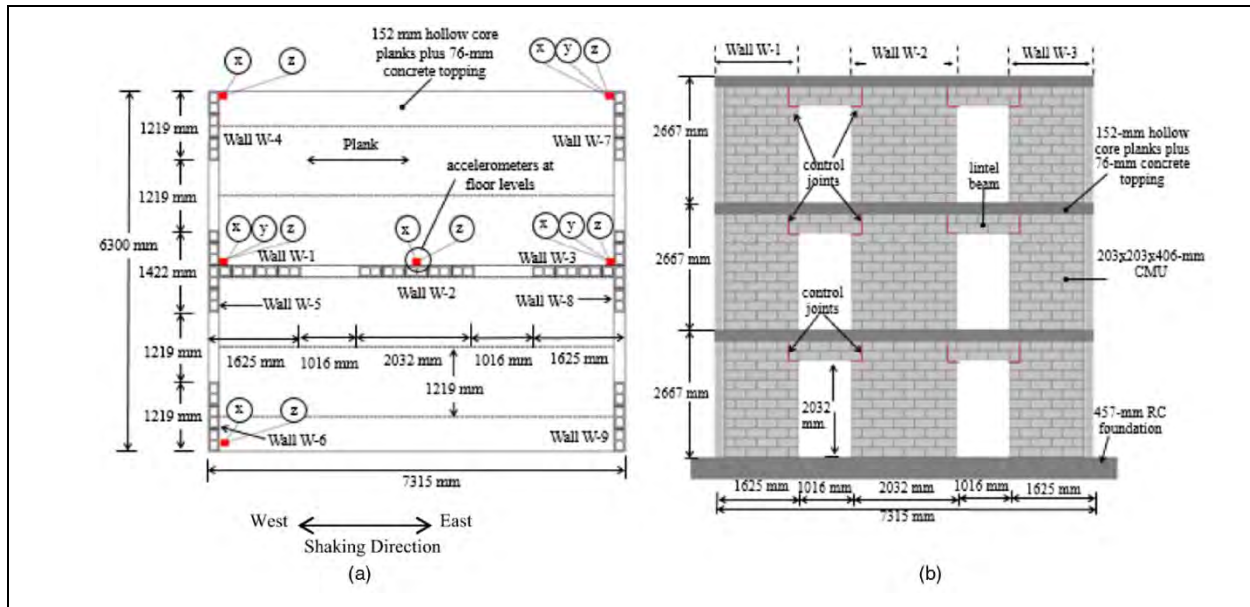
Figure 4.2-1 Configuration of shake table test structure (Reproduction of Figure 1 from Stavridis et al., 2016)

The ratio of the base-shear capacity developed by the structure to the seismic weight considered in the design was 1.35, while the design base-shear coefficient (CS) was only 0.2, or an overstrength of 6.75. The authors attribute the significant over-strength to the coupling action of the horizontal diaphragms and the lintels. Even though there were control joints and the horizontal reinforcing bars in the lintels were debonded, the lintels were still able to cause a diagonal strut action and some coupling.

The hysteretic behavior and calculated base-shear capacities are shown in Figure 4.2-2, which is a reproduction of Figure 14(b) of Stavridis et al. (2016). The experimental capacity far exceeds the flexural capacity calculated for cantilever walls, and the resistance developed in the negative direction exceeds that calculated with the fixed-fixed end conditions (rigid coupling element assumption) by 26%. The overstrength can be partly attributed to the coupling action, and partly attributed to the out-of-plane walls. The out-of-plane walls exerted a restraining effect on the rocking of the in-plane walls. The strain-gauge data indicate that the vertical reinforcement in the out-of-plane walls yielded very early and developed high tensile strains throughout the tests. The tension in the out-of-plane walls exerted an axial compression on the in-plane walls through the stiff horizontal diaphragm. The additional axial compression increased the flexural resistance of the in-plane walls.

A coupled wall system will have additional axial forces introduced in the wall elements. However, the authors ignored the influence of the axial forces on the moment capacity of the walls because the axial compression introduced in one of the two outer walls will approximately offset the effect of the axial tension introduced in the other.

Mavros et al (2016) observed similar behavior in the shake table test of a two-story reinforced masonry structure. The axial compression exerted by the out-of-plane walls through the horizontal diaphragms and lintels could increase the base shear capacity of the structure by about 50%.
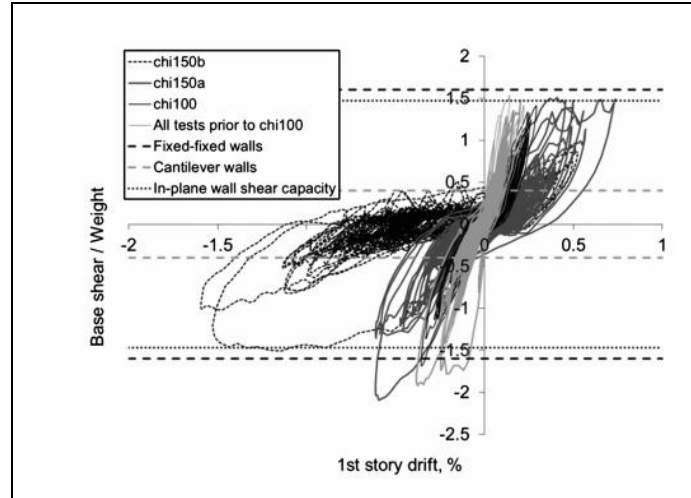
Figure 4.2-2 Hysteretic behavior and strength of masonry shear walls (Reproduction of Figure 14 (b) in Stavridis et al, 2016)

RP3-4.2.2   Slab-coupled Masonry Shear Walls: Component Behavior

Siyan et al. (2016a) tested six different one-third scale masonry walls: one rectangular, one flanged, two slab-coupled walls, and two rectangular walls representing the individual components of the slab-coupled wall systems. The wall systems are shown in Figure 4.2-3, which is a reproduction of Figure 1 of Siyan et al. (2016a). Theoretical degree of coupling was 51 and 37% for Walls W3 and W4.
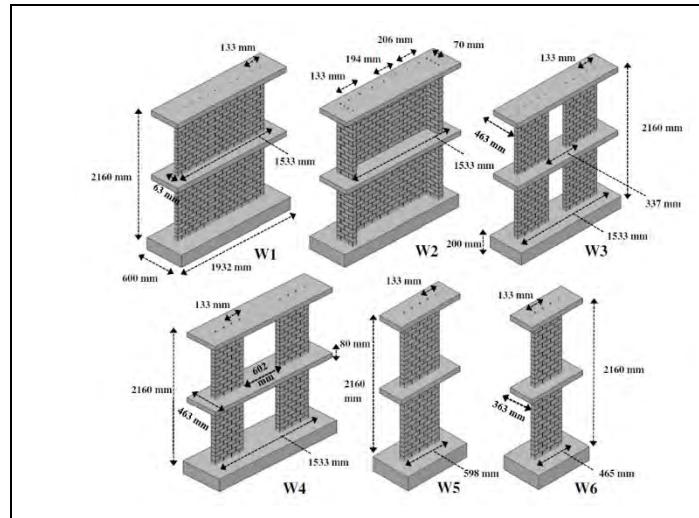
Figure 4.2-3 Wall system component tests (Reproduction of Figure 1 in Siyan et al, 2016a)

The backbone curves for the coupled walls vs. twice the individual segments, or the sum of the two individual walls in the coupled walls, are shown in Figure 4.2-4, which is a reproduction of Figure 8(c) in Siyan et al. (2016a). The slab coupling effects increased the yield strength by approximately 60% and the ultimate strength approximately 45%, while approximately doubling the stiffness. Thus, even though no special reinforcement detailing of the slabs was adopted, the slabs provided significant wall coupling that altered the strength and stiffness. This in turn indicates that ignoring slab-coupling in the design of masonry shear walls may lead to inaccurate estimation of the design lateral shear capacity, stiffness, and period. A study of seismic design parameters (Siyan et al., 2016b) indicated that in general slab-coupled walls demonstrated a better performance in terms of ultimate drifts capacities reached, period elongation and

equivalent viscous damping when compared with the rectangular and the flanged walls.

Figure 4.2-4 Backbone curves for coupled and non-coupled walls (Reproduction of Figure 8(c) in Siyan et al, 2016a)

RP3-4.2.3   Slab-coupled Masonry Shear Walls: Building Behavior

Ashour et al. (2016a) describe a three-phase testing program: phase 1 was individual components as described above, phase 2 was a one-third scale two-story building with coupling prevented by having hinges in the slabs, and phase 3 was the same two-story building but with coupling. A layout of the first floor is shown in Figure 4.2-5, which is a reproduction of Figure 3(c) in Ashour et al. (2016a). Shaking was in the north-south direction.

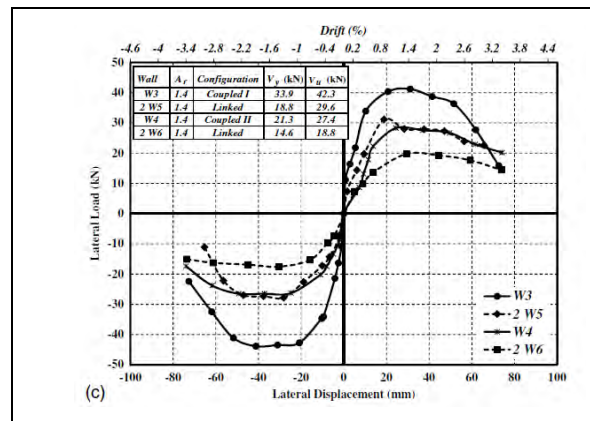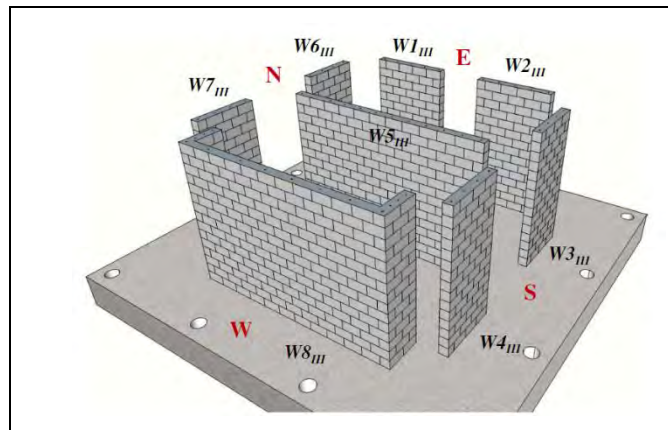**Figure 4.2-5 First floor of masonry shear wall building (Reproduction of Figure 3(c) in Ashour et al., 2016a)**

   Building II (uncoupled walls) reached its ultimate strength of 236 kN in the south direction and −245 kN in the north direction at 0.9% drift, whereas Building III (coupled walls) reached its ultimate strength of 384 kN in the south direction and −372 kN in the north direction at the same drift level. The capacity of Building III was on average 50% higher than Building II. Following the 0.9% drift level, both buildings exhibited strength and stiffness degradation where the toes of the in-plane wall started to crush and almost all the outer bars yielded. At 1.45% drift, Building III lost 20% of its capacity while Building II lost only 5% of its capacity. The capacity of Building II was reasonably well predicted by simply adding the capacities of the individual shear walls. Hysteresis curves for the uncoupled and coupled shear wall buildings are shown in Figure 4.2-6, which is a reproduction of Figure 12 in Ashour et al. (2016). A comparison of the load-deflection behavior of the two buildings and the individual shear wall segments is shown in Figure 4.2-7, which is a reproduction of Figure 3 in Ashour and El-Dakhakhni (2016b).
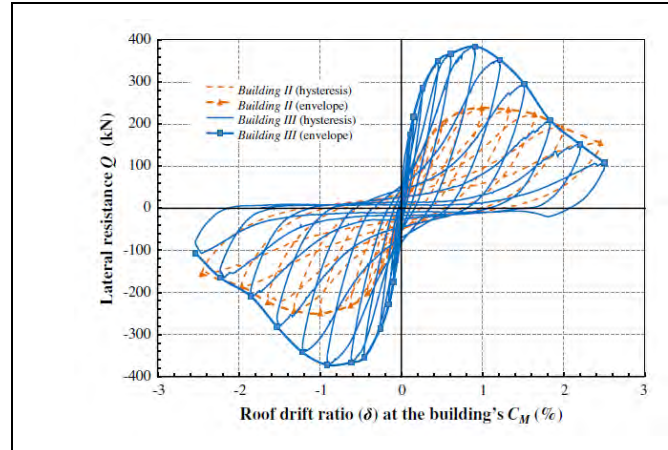
Figure 4.2-6 Hysteresis curves for coupled and non-coupled walls (Reproduction of Figure 12 in Ashour et al., 2016a)
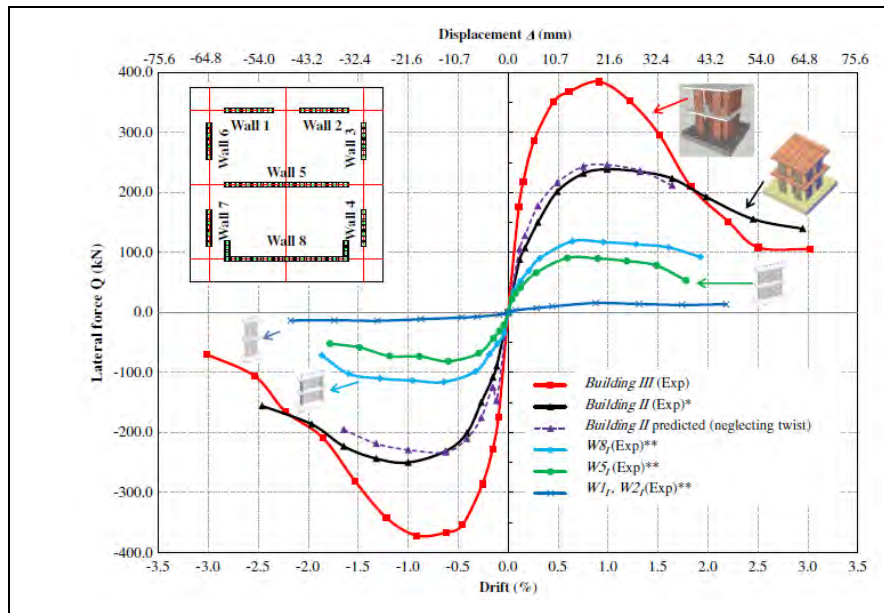
Figuer 4.2-7 Load-deflection curves for buildings and individual shear wall segments (Reproduction of Figure 3 in Ashour and El-Dakhakhni, 2016b).

Ashour and El-Dakhakhni (2016b) developed a simplified analysis technique for coupled walls that seemed to work quite well. The model was based on assuming full coupling until ultimate, but no coupling after ultimate to develop the descending portion of the load-displacement curve. Empirical parameters of 0.6 and 0.2 were used to relate the stiffness at ultimate and the stiffness on the descending branch at 80% of ultimate to the stiffness at yield. The authors admit the model would be affected by the degree of coupling, but it does provide a start to a modeling approach that could be used in routine design.

The response analysis of Building III, compared with that of Building II, showed that the orthogonal shear walls acted as tension ties, which introduced a coupling moment to the shear walls aligned along the loading direction through the diaphragm's out-of-plane stiffness. As a result, the wall boundary conditions introduced double curvature, and the system stiffness, and flexural and shear strength increased. The tension force in the walls aligned orthogonal to the loading direction was in equilibrium with the compression axial forces that acted on the walls aligned along the loading direction, which in turn resulted in increasing the

flexural and shear capacities of the latter walls. However, this resulted in reducing the differences between the system's flexural and shear capacities. The impact of this reduction was also observed in the reported combined shear and flexural damage as Building III approached its ultimate strength. As such, despite the enhancement to the building strength, the influence of the diaphragm's out-of-plane stiffness, and subsequently the wall-diaphragm coupling, has the potential to result in unexpected brittle failure modes.

If a masonry shear wall building with significant floor diaphragm stiffness and strength are designed as individual cantilevers, the building's stiffness will be underestimated, and subsequently its natural period will be overestimated. This may result in designing the building to resist significantly less seismic shear force than what it would actually experience within a coupled wall system, although for moderate height buildings (several stories) this may not be an issue. Ashour and El-Dakhakhni (2016b) state that it might be argued that the diaphragm coupling influence is an analysis issue, and does not need to be explicitly addressed in seismic design codes. However, they believe that the significance of the diaphragm influences on the system-level response should at least be highlighted in current force-based design codes and must be accounted for in the development of future displacement- and performance-based seismic design provisions.

RP3-4.2.4   Summary

Designing a true coupled masonry shear wall building is difficult. The high shear forces in the coupling beam and the lack of the ability to easily incorporate diagonal bars often make for coupling beams that cannot be constructed. It thus is not recommended that coupled masonry systems be pursued. However, coupling can occur due to slab stiffness and diagonal strut action even in lintels designed with control joints and debonded steel. This will in general increase the stiffness and strength of the system. However, an issue with coupled walls is that if not accounted for, the failure could shift to a brittle shear failure.

RP3-4.2.5   Code Recommendations

Two code recommendations are made.

The coupling provisions of Chapter 14 of ASCE 7 should be moved to TMS 402. Although coupling beams in masonry buildings are rare, these are appropriate provisions for when there are coupling beams. However, a careful definition of a coupling beam would be needed so this provision would only apply where appropriate. For example, all beams over openings are not coupling beams. Rather it is just a shear wall with openings.

Commentary should be added to the TMS 402 provisions to alert the designer to the difficulty of designing coupling beams in masonry, but that coupling can occur even when not designed for. Ashour and El-Dakhakhni (2016b) can be referenced as providing a simplified means for analyzing slab-coupled buildings. The designer should also be cautioned that coupling can increase the flexural capacity, but will not proportionately increase the shear capacity. Hence, it is possible that unintended/unaccounted for coupling can change the failure mode of a masonry building from a ductile flexural failure to a brittle shear failure.

RP3-4.3   References

Anderson, D. L., and Priestley, M. J. N. (1992). "In-Plane Shear Strength of Masonry Walls," *Proceedings*, 6th Canadian Masonry Symposium, Saskatchewan, Canada, 223–234.

Ashour, A., El-Dakhakhni, W. and Shedid, M. (2016a). "Experimental Evaluation of the System-Level Seismic Performance and Robustness of an Asymmetrical Reinforced Concrete Block Building." *J. Structural Engineering*, ASCE, 142(10).

Ashour, A. and El-Dakhakhni, W. (2016b). "Influence of Floor Diaphragm–Wall Coupling on the System-

Level Seismic Performance of an Asymmetrical Reinforced Concrete Block Building." *J. Structural Engineering*, ASCE, 142(10).

Baenziger, G. P., Porter, M. L. (2011). "Joint Reinforcement for Masonry Shear Walls,", 11th North American Masonry Conference, Minneapolis, MN, The Masonry Society, Paper No. 51.

Bennett, R.M., Huston, E.T., McLean, D.I., and Throop, D.B. (2011). "Allowable Stress Recalibration in the 2011 TMS 402 Code." 11th North American Masonry Conference, Minneapolis, MN, The Masonry Society, Paper 33.

Bolhassani, M., Hamid, A., Johnson, C.A. and Schultz, A.E. (2016a). "Shear Strength Expression for Partially Grouted Masonry Walls," *Engineering Structures*, 127, 475–494.

Bolhassani, M., Hamid, A.A., Johnson, C., Moon, F.L. and Schultz, A.E. (2016b). "New Design Detail to Enhance the Seismic Performance of Ordinary Reinforced Partially Grouted Masonry Structures," *J. Structural Engineering*, ASCE, 142(12).

Bolhassani, M., Hamid, A.A. and Moon, F.L. (2016c). "Enhancement of Lateral In-Plane Capacity of Partially Grouted Concrete Masonry Shear Walls," *Engineering Structures*, 108, 59–76.

Davis, C.L., McLean, D.I., and Ingham, J.M. (2010). "Evaluation of Design Provisions for In-Plane Shear in Masonry Walls," *TMS Journal*, The Masonry Society, 28(2), 41-59.

Dillon, P. (2015). Shear Strength Prediction Methods for Grouted Masonry Shear Walls. PhD Dissertation, Brigham Young University, Provo, UT.

Elmapruk, J.H. (2010). Shear Strength of Partially Grouted Squat Masonry Shear Walls. Master of Science Thesis, Washington State University, Pullman, WA.

Huston, E. (2011). "Harmonization of Shear Design Between ASD and SD - What Really Controls the Horizontal Reinforcement in a Reinforced Masonry Shear Wall?" 11th North American Masonry Conference, Minneapolis, MN, The Masonry Society.

Johnson, C.A., and Schultz, A. (2019). "Seismic Resistance Mechanisms in Partially Grouted Shear Walls with New Design Details," *Proceedings*, 13th North American Masonry Conference, Salt Lake City, UT, pp. 1274-1286,

Kasparik, T., Tait, M.J. and El-Dakhakhni, W.W. (2014). "Seismic Performance Assessment of Partially Grouted, Nominally Reinforced Concrete-Masonry Structural Walls Using Shake Table Testing," *J. Performance of Constructed Facilities*, ASCE, 28(2), 216-227.

Koutras, A., and Shing, P.B. (2017). "Shake-Table Testing and Performance Assessment of a Partially Grouted Reinforced Masonry Building," *Experimental Vibration Analysis of Civil Engineering Structures*, Springer International Publishing AG, 2018.

Mavros, M., Ahmadi, F., Shing, P.B., Klingner, R.E., McLean, D., and Stavridis, A. (2016). "Shake-Table Tests of a Full-Scale Two-Story Shear-Dominated Reinforced Masonry Wall Structure," *J. Structural Engineering*, ASCE, 142(10).

Minaie, M., Mota, M., Moon, F.L., and Hamid, A.A. (2010). "In-Plane Behavior of Partially Grouted Reinforced Concrete Masonry Shear Walls," *J. Structural Engineering*, ASCE, 136(9), 1089-1097.

Nolph, S.M. (2010). In-Plane Shear Performance of Partially Grouted Masonry Shear Walls. Master of Science Thesis, Washington State University, Pullman, WA.

Nolph, S.M., and ElGawady, M.A. (2012). "Static Cyclic Response of Partially Grouted Masonry Shear Walls." *J. Structural Engineering*, ASCE 138(7), 864-879.

Shing, P.B., Schuller, M.P., Hoskere, V.S., and Carter, E. (1990a). "Flexural and Shear Response of Reinforced Masonry Walls," *Structural Journal*, American Concrete Institute, 87(6), 646-656.

Shing, P.B., Schuller, M.P., and Hoskere, V.S. (1990b). "In-Plane Resistance of Reinforced Masonry Shear Walls," *J. Structural Engineering*, American Society of Civil Engineers, 116(3), 619-640.

Siyam, M.A., El-Dakhakhni, W., Shedid, M.T and Robert G. Drysdale, R.G. (2016a). "Seismic Response Evaluation of Ductile Reinforced Concrete Block Structural Walls. I: Experimental Results and Force-Based Design Parameters." *J. Performance of Constructed Facilities*, ASCE, 30(4).

Siyam, M.A., El-Dakhakhni, W., Banting, B.R. and Drysdale, R.G. (2016). "Seismic Response Evaluation of Ductile Reinforced Concrete Block Structural Walls. II: Displacement and Performance–Based Design Parameters." *J. Performance of Constructed Facilities*, ASCE, 30(4).

Stavridis, A., Ahmadi, F., Mavros, M., Shing, P.B., Klingner, R.E., and McLean, D. (2016). "Shake-Table Tests of a Full-Scale Three-Story Reinforced Masonry Shear Wall Structure." *J. Structural Engineering*, ASCE, 142(10).

RP3-5   STEEL PLATE SHEAR WALLS

RP3-5.0   Introduction

This chapter briefly discusses Special Steel Plate Shear Walls and Special Coupled Steel Plate Shear Walls. An extensive list of references is provided.

RP3-5.1   Special Steel Plate Shear Walls

As described in the Commentary to AISC 341-16, *Seismic Provisions for Structural Steel Buildings* (AISC 2016), a special plate shear wall (SPSW) comprises a boundary frame with slender unstiffened steel web plates. The boundary frame that consists of horizontal boundary elements (HBEs) and vertical boundary elements (VBEs) is capacity designed so that the web plates yield and develop large ductility during an earthquake. HBEs are connected to VBEs with moment-resisting connections that are capable of developing the plastic moment capacity of the HBE. Extensive experimental and numerical research has demonstrated the robust ductile behavior of the SPSW system (e.g., Thorburn et al., 1983; Timler and Kulak, 1983; Tromposch and Kulak, 1987; Roberts and Sabouri-Ghomi, 1992; Caccese et al., 1993; Driver et al., 1997; Elgaaly, 1998; Rezai, 1999; Lubell et al., 2000; Grondin and Behbahannidard, 2001; Berman and Bruneau, 2003a; Zhao and Astaneh-Asl, 2004; Berman and Bruneau, 2005b; Sabouri-Ghomi et al., 2005; Deng et al., 2008; Lee and Tsai, 2008; Qu et al., 2008; Choi and Park, 2009; Qu and Bruneau, 2009; Vian et al., 2009a; Sabouri-Ghomi and Roberts, 1992; Elgaaly et al., 1993; Elgaaly and Liu, 1997; Driver et al., 1997; Dastfan and Driver, 2008; Bhowmick et al., 2009; Purba and Bruneau, 2009; Shishkin et al., 2009; Vian et al., 2009b; Qu and Bruneau, 2011; Purba and Bruneau, 2014a).

RP3-5.2   Special Coupled Steel Plate Shear Walls

The coupled SPSW system is an extension of the standard SPSW system that links a pair of SPSWs with coupling beams at the floor levels. Coupled SPSWs offer potential for greater economy, efficiency and architectural flexibility while offering comparable or enhanced performance compared to standard SPSWs. Studies of coupled SPSWs are more limited than those considering standard SPSWs, but several large-scale testing programs have demonstrated the robust cyclic behavior than can be realized with the coupled SPSW configuration (Zhao and Astaneh-Asl, 2004; Li et al., 2012; Borello and Fahnestock, 2017). Similar to eccentrically braced frame (EBF) links, coupling beams joining SPSWs can be designed to yield and dissipate energy in flexure or shear (Borello and Fahnestock, 2012 and 2013). The degree-of-coupling (DC) concept that is commonly used in coupled concrete walls is also adopted for coupled SPSW. Design studies indicate that economical designs fall in the range of DC = 0.4 to 0.6, and DC = 0.5 is recommended as a good target for preliminary design (Borello and Fahnestock, 2012). Simple analytical expressions based on plastic analysis allow a designer to determine DC without needing to use detailed nonlinear analysis. Coupled SPSW designs in the optimal range of DC also demonstrate good performance when evaluated using nonlinear response history analysis (Borello and Fahnestock, 2013; Wang et al., 2017). Coupled SPSWs designed using system parameters and typical procedures used for standard SPSWs exhibit acceptable seismic response (Borello and Fahnestock, 2013; Wang et al., 2017).

RP3-5.3   References

Zhao, Q., and Astaneh-Asl, A. (2004). "Cyclic behavior of traditional and innovative composite shear walls." J. Struct. Eng., 130(2), 271–284.

Li, C.-H., Tsai, K.-C., Chang, J.-T., Lin, C.-H., Chen, J.-C., Lin, T.-H., and Chen, P.-C. (2012). "Cyclic test of a coupled steel plate shear wall substructure." Earthquake Eng. Struct. Dynam., 41(9), 1277–1299.

Borello, D. J., and Fahnestock, L. A. (2012). "Behavior and mechanisms of steel plate shear walls with coupling. " J. Constr. Steel Res., 74, 8–16.

Borello D.J., and Fahnestock L.A. (2013) Seismic design and analysis of steel plate shear walls with coupling. Journal of Structural Engineering 139: 1263–1273.

Borello D.J., and Fahnestock, L.A. (2017) Large-scale cyclic testing of steel plate shear walls with coupling. Journal of Structural Engineering 2017, 143 (10): 040171333.

Wang, M., Borello, D.J and Fahnestock, L.A. (2017) Boundary frame contribution in coupled and uncoupled steel plate shear walls. Earthquake Engineering and Structural Dynamics, 46: 2355-2380.

AISC (2016). " AISC-341 Seismic Provisions for Structural Steel Buildings." American Institute of Steel Construction, Chicago, Illinois.

AISC (2018). "Rainier Square Tower Uses Revolutionary Composite Steel Frame", Modern Steel Construction news, retrieved 1/18/2018 from https://www.aisc.org/modernsteel/news/2018/january/rainier-square-tower-uses-revolutionary-composite-steel-frame/#.WmDKQzdG2Uk

Alzeni, Y., and Bruneau, M. (2014). "Cyclic Inelastic Behavior of Concrete Filled Sandwich Panel Walls Subjected to In-Plane Flexure." Technical Report MCEER-14-0009, Multidisciplinary Center for Earthquake Engineering Research. State University of New York at Buffalo, Buffalo, NY.

Alzeni, Y., and Bruneau, M. (2017). "In-plane Cyclic Testing of Concrete Filled Sandwich Steel Panel Walls with and Without Boundary Elements." Journal of Structural Engineering, Under Review

Booth, P. N., Varma, A. H., Sener, K. C., and Malushte, S. R. (2015). "Flexural behavior and design of steel-plate composite (SC) walls for accident thermal loading." Nuclear Engineering and Design, 295, 817-828.

Bowerman, H., Gough, M., and King, C. (1999). "Bi-Steel design and construction guide." British Steel Ltd, Scunthorpe (London).

Epackachi, S., Nguyen, N.H.,Whittaker, A.S.,and Varma, A.H.(2014)."In-plane seismic behavior of rectangular steel-plate composite wall piers" Journal of Structural Engineering, 04014176(9), 1-9.

Epackachi, S., Whittaker, A. S., Varma, A. H., and Kurt, E. G. (2015). "Finite element modeling of steel-plate concrete composite wall piers." Engineering Structures, 100, 369-384.

Eom, T.-S., Park, H.-G., Lee, C.-H., Kim, J.-H., and Chang, I.-H. (2009). "Behavior of double skin composite wall subjected to in-plane cyclic loading." Journal of structural engineering, 135(10), 1239-1249.

Kurt, E. G., Varma, A. H., Booth, P., and Whittaker, A. S. (2016). "In-Plane Behavior and Design of

Rectangular SC Wall Piers without Boundary Elements." Journal of Structural Engineering, 04016026.

Oduyemi, T., and Wright, H. (1989). "An experimental investigation into the behaviour of double-skin sandwich beams." Journal of Constructional Steel Research, 14(3), 197-220.

Polat, E., and Bruneau, M. (2017). " Modeling Cyclic Inelastic In-Plane Flexural Behavior of Concrete Filled Sandwich Steel Panel Walls." Engineering Structures, Vol.148, pp.63-80,

Ramesh, S. (2013). "Behavior and design of earthquake-resistant dual-plate composite shear wall systems." Purdue University.

Sener, K., and Varma, A.H. (2014). "Steel-Plate Composite SC Walls: Experimental Database and Design for Out-of-Plane Shear." Journal of Constructional Steel Research, Elsevier Science, Vol. 100, pp. 197-210.

Sener, K., Varma, A.H., and Ayhan, D. (2015). "Steel-Plate Composite SC Walls: Experimental Database and Design for Out-of-Plane Flexure." Journal of Constructional Steel Research, Vol. 108, May, pp. 46-59, Elsevier Science.

Seo, J., Varma, A. H., Sener, K., and Ayhan, D. (2016). "Steel-plate composite (SC) walls: In-plane shear behavior, database, and design." Journal of Constructional Steel Research, 119, 202-215.

Varma, A. H., Malushte, S. R., Sener, K. C., and Lai, Z. (2014). "Steel-plate composite (SC) walls for safety related nuclear facilities: Design for in-plane forces and out-of-plane moments." Nuclear Engineering and Design, 269, 240-249.

Wright, H., et al. (1991a). "The design of double skin composite elements." Journal of Constructional Steel Research 19(2): 111-132.

Wright, H., Oduyemi, T., and Evans, H. (1991b). "The experimental behaviour of double skin composite elements." Journal of Constructional Steel Research, 19(2), 97-110.

Xie, M., and Chapman, J. (2006). "Developments in sandwich construction." Journal of Constructional Steel Research, 62(11), 1123-1133.

Zhang, K., Varma, A. H., Malushte, S. R., and Gallocher, S. (2014). "Effect of shear connectors on local buckling and composite action in steel concrete composite walls." Nuclear Engineering and Design, 269, 231-239.

RP3-6   WOOD LIGHT-FRAME SHEAR WALLS

RP3-6.0   Introduction

This chapter introduces a series of technical topics of current interest to designers of wood shear walls. These topics are driven by the trend towards four- and five-story wood structures, particularly urban infill: this includes anchorage of hold-downs to podium slabs, and the amplification of design forces for these anchors. Discuss current trends in Canadian practice for deflection computations, and compare with U.S. practice. Finally, a discussion of applying capacity-based concepts to detailing of load paths in wood shear wall elements.

RP3-6.1   Methods of Calculating Shear Wall Deflections - US versus Canadian Provisions

A methodology for calculating deflection of shear walls sheathed with wood structural panels has been provided in US codes since 1970 (ICBO, various), and in the Special Design Provision for Wind and Seismic (SDPWS) (AWC, various) since its first edition dated 2005. While there have been some modest changes to the presentation of the deflection equation, the basis and intent of the equation has remained the same over time. Starting with the 2008 edition of SDPWS, the deflection equation was expanded to other sheathing materials for which the standard provides capacity information.

The US deflection equation provides an estimate of the deflection of a shear wall under either ASD or LRFD design forces. This deflection is most representative of the deflection expected from an individual single-story shear wall element without finish materials. This is typically evaluated using hand calculations or spreadsheet-based tools, and the shear wall deflection is evaluated individually at each story level, without consideration of interaction between levels. Recent comparisons to results of nonlinear response history analyses or NLRHA (ATC, 2017) indicate that this method tends to notably overestimate seismic story drifts.

The calculated deflection is used within SDPWS to assign a relative stiffness to shear walls, so that wind and seismic forces can be distributed to wall lines and to shear wall elements within a wall line. It also may be used to calculate a building period for purposes of seismic design. In addition, there are a number of ASCE 7 provisions that relate to deflection or drift. Included are overall limits on permitted story drifts at the center of mass, requirements to demonstrate that gravity systems are capable of withstanding the estimated drift of the lateral force-resisting system, requirements for building separations, etc.

Recent discussion and development of deflection equations in US codes has focused on identifying the many contributors to deformation at the tension and compression boundary members of the shear wall. This includes identification of a number of locations of deformation in compression perpendicular to grain within the boundary member load path. Discussion of this in ongoing within the AWC standards committee.

A recent development in Canadian wood design standards has started with a similar derivation of drift on a story by story basis, but has added to it a rigid-body rotation at the base of each shear wall, starting at the second story and proceeding upwards. This rigid-body rotation is derived from the deflection of the shear wall below, and is cumulative at each upper story. This method is being called a "rational method" by the Canadian standards.

At this time the Canadian approach does not appear to be needed or of benefit for US designers. The method results in building periods that are many times larger than those available from US research (CUREE, 2004) and analytical studies (ATC, 2017). Use of the Canadian approach could result in significantly underestimating design forces. Use of the approach would also lead to significant penalties for the various ASCE 7 limits, thereby reducing the scope of buildings that can be of wood light-frame construction. The Canadian method has a lesser impact on longer walls and a greater impact on narrow walls. It is thought to result in narrow walls carrying less load, thereby requiring that more capacity be provided to resist a given level of base shear.

At this time the Canadian approach does not appear to be needed or appropriate for users of US design standards. The method results in building periods that are many times larger than those available from US research (Camelo et. Al., 2002) (CUREE, 2004) and analytical studies (ATC, 2017). There does not currently appear to be any available testing data validating the deflection or drifts estimated by the Canadian method.

Mixing of the Canadian method with US design standards could result in significant underestimating of seismic design forces. Use of the approach could also lead to significant penalties in order to conform to ASCE 7 drift-related requirements. For example it could:

- Significantly increase the story drift estimated to be experienced by the gravity system, requiring that the design engineer demonstrate acceptability of the gravity system at larger seismic drift levels,
- Significantly increase seismic separations between adjacent buildings, increasing the size of required seismic joint cover devices beyond those currently available,
- Reduce the number of stories permitted in buildings as lower stories exceed permitted drift levels.

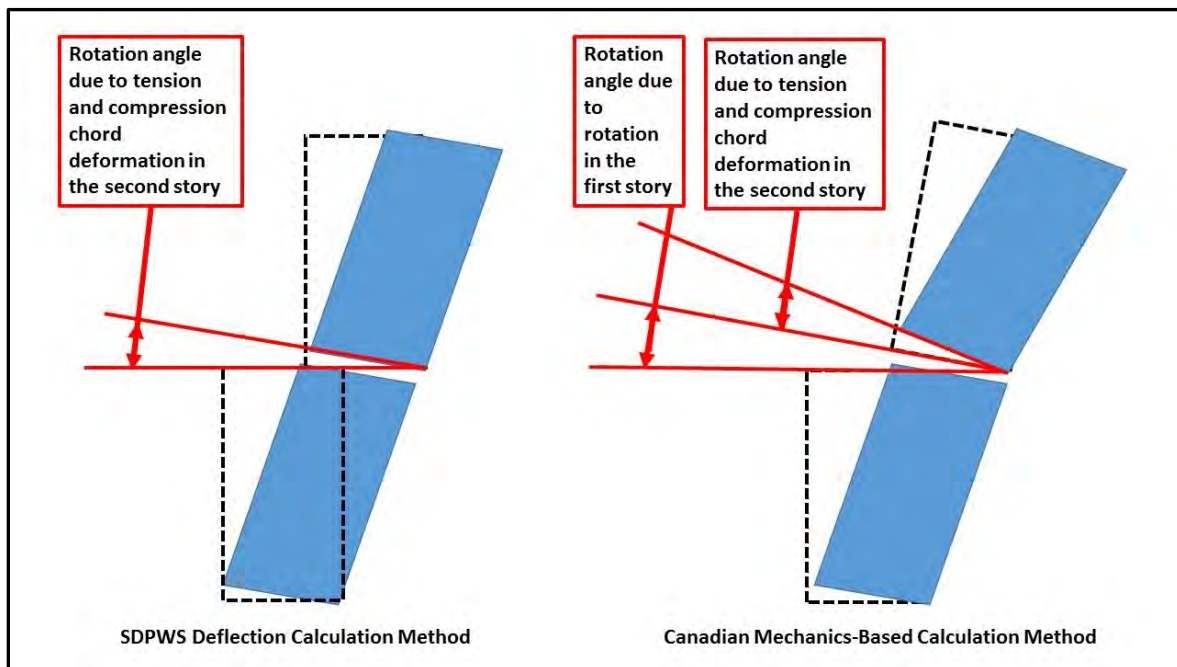There is currently no plan for incorporation of the Canadian method into US design standards.

Figure 6.1-1 Conceptual illustration of SDPWS and Canadian "Mechanics-Based" approaches for calculation of shear wall deflections.

RP3-6.2 FEMA P-1100 Incorporation of Capacity Based Load Path Connections into Seismic Retrofit Design

Recently published FEMA P-1100 (*Vulnerability-Based Seismic Assessment and Retrofit of One- and Two-Family Dwellings*, FEMA, 2018) provides minimum criteria for vulnerability-based assessment and retrofit of one- and two-family detached wood light-frame dwellings. The specific seismic vulnerabilities addressed by this prestandard include crawlspace dwelling anchorage to foundation and cripple wall bracing, living-space-over-garage dwelling ground story bracing, and hillside dwelling anchorage to the uphill foundation.

FEMA P-1100 has incorporated in its retrofit design procedures the use of an overstrength factor for design of the load path into and out of the retrofit elements (i.e., connections). This is intended to help ensure that the peak capacity of the retrofit elements can be developed without the load path acting as a weak link. Use of an overstrength factor for load path connections is an additional step beyond current design practice for new light-frame structures. The choice to use this approach was driven by two concepts. First, the determination of seismic retrofit design R-factors was based on FEMA P-695 methods using state of the art numerical study tools to estimate probability of collapse. In order to be consistent with the analytical predictions of collapse, it was necessary that the peak capacity of the retrofit and the story shear could be developed eliminating the load path as a weak link; if not, the probabilities of collapse would be under-predicted. Second, it was recognized that while retrofit design focused on additional capacity provided by new bracing walls, some bracing capacity would be provided by existing finish materials, and this bracing capacity might also contribute load to the new load path connections. The extent and capacity of contributing finish materials was recognized to be variable in the existing building stock.

An overstrength factor, Ω_0, of 1.5 is specified by FEMA P-1100 for use with ASCE/SEI 7 ASD or LRFD load combinations. The derivation of the factor, however, is different than would be commonly used for ASCE 7 seismic design parameters. The overstrength factor has been back-calculated from numerical study estimations of peak story shears, and comparison of those to peak capacities of the cripple walls, anchor bolts, and shear clips available from testing. The low value of 1.5 is influenced by the significant overstrength seen in available tests of the anchor bolts, shear clips, etc. Further information will be available in FEMA P-1100 Volume III.

It does not at this time appear that a similar change in practice is needed for seismic design of all wood light-frame structures. It is recommended, however, that thought be given to the balance of peak anticipated demands and available capacity of load path connections in the development of bracing systems and design methodologies.

Figure 6.2-1 Egmented shear wall with studs, sheathing, and posts and tie-down connectors at each end.
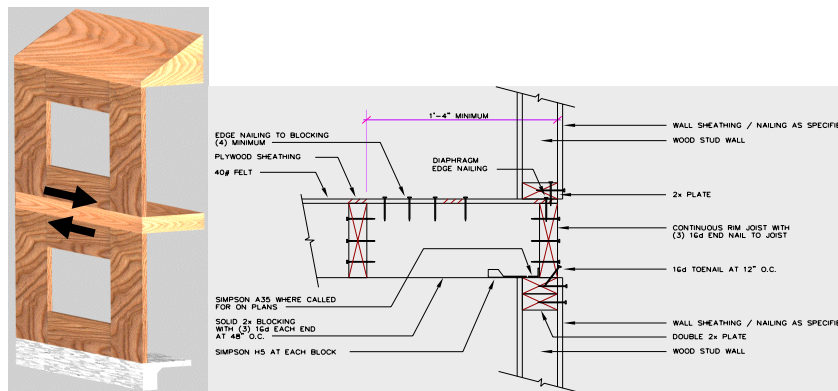

Figure 6-3 Shear load path for shear walls

RP3-6.3   References

ATC (2017). Developing Solution to the Short-Period Building Performance paradox: Study for Wood Light-Frame Buildings, Workshop Review Draft, Applied Technology Council, Redwood City, CA.

AWC (various). Special Design Provisions for Wind and Seismic, American Wood Council, Washington, DC.

RP3-APPENDIX A

Ductile Coupled Wall Definition Study

The following pages summarize the findings from additional studies as directed by ACI 318-H, compiled on September 6, 2016.

Page 2: Plan and elevation of building prototypes considered. Variants include (6) building heights, (8) coupling beam aspect ratios, (3) shear wall reinf levels, (3) coupling beam reinf levels = 432 cases considered.

Page 3: Spectra of ground motions used in this study overlain with first mode period of each moderate beam-moderate wall model. Other models not shown for clarity

Page 4: Summary of coupling beam reinforcement considered.

Page 5: Summary of shear wall vertical reinforcement considered.

Page 6: Summary of shear wall gravity loads considered.

Page 7: Comparison of fundamental periods (ETABS vs Perform).
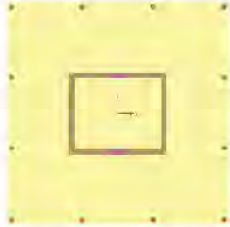
Page 8: Summary of peak story drifts from NLRHA.

Page 9: Sample results for hysteretic energy absorbed shown separately for coupling beams and shear walls.

Page 10: Total hysteretic energy absorbed for subset of models.

Page 11: Normalized total hysteretic energy absorbed for all results on page 10.

Shear Wall Layout

Representative Case

Dynamic Equivalent
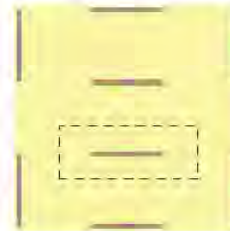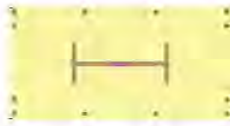
Core Schemes:
- 44'-0" x 36'-8" dimensions
- 24" thick shear walls
- Maintaining core size for all 3 cases
- 8' long link beams

- Bldg Ht = # stories x 11' (e.g. 40 stories ==> 440')
- Floor Plate: 100' x 100'
- Massing: 18pcf density
- Perform Model:
  - Stiffness of 1/2 Core (I-Shape)
  - Trib mass for 1/2 Bldg
  - Trib gravity loading to I-shape and remainder for
    of gravity load for 1/2 building to p-delta columns
  - Equivalent dynamic properties as full building

Blade Wall Schemes:
- 32' overall wall length
- 24" thick shear walls
- 8' long coupling beam length
- Maintaining blade wall length for all 3 cases.

- Bldg Ht = # stories x 11' (e.g. 20 stories ==> 220')
- Floor Plate: 100' x 100'
- Massing: 18pcf density
- Perform Model:
  - Stiffness of Single Blade Wall
  - Trib mass for 1/4 Bldg
  - Trib gravity loading to blade wall indicated with
    remainder of gravity load for 1/4 building applied
    to p-delta columns
  - Equivalent dynamic properties as full building
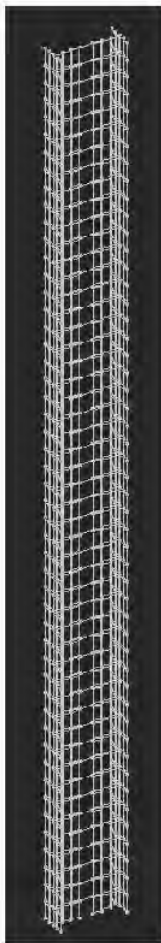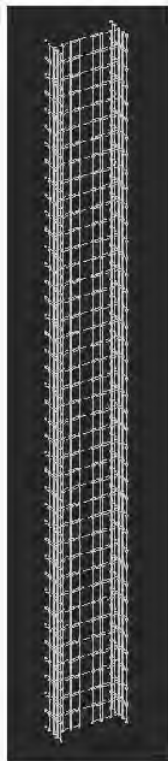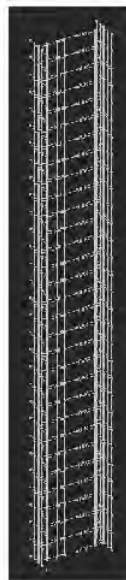
50 Story   40 Story   30 Story   20 Story   10 Story   5 Story

2

First Mode Excitation of Models Considered

Perform "MM" ("Moderate" Beam Steel, "Moderate" Wall Steel) Model
T1 Periods Overlaid on Target MCER Spectrum

Coupling Beam Designs

Shear Wall Vertical Reinforcing

50 Story Tower Reinforcement Profile

40 Story Tower Reinforcement Profile

30 Story Tower Reinforcement Profile

20 Story Tower Reinforcement Profile

10 Story Tower Reinforcement Profile

5 Story Tower Reinforcement Profile

5

Applied Gravity Loads

Total:
4 x 157.8 = 631.2
4 x 43.3 = 173.2
4 x 79.5 = 318.0
4 x 26.8 = 107.2
4 x 28.5 = 114.0
4 x 38.5 = 154.0
4 x 31.0 = 124.0
4 x 89.6 = 358.4
1980 kips / flr

Check: 100' x 100' x 11' Ht x 18 pcf = 1980 kips

Individual Blade:
157.8 x 2 + 43.3 x 2 = 402.2 / flr

Add'l P-delta (if used):
(1980 kip / 4) - 402.2 = 92.8 kips / flr

Check: 4 x (402.2 + 92.8) = 1980 kips

P-Delta

Mass:
(1980 kips / 4) / 386.1 = 1.2821
[Floor Point Mass]

Mass

Gravity Load

89.6 kips
31.0 kips
38.5 kips
28.5 kips

43.3 kips   157.8 kips
157.8 kips   43.3 kips

26.8 kips   79.5 kips
79.5 kips   26.8 kips

2-D Perform Model
(32' total length)
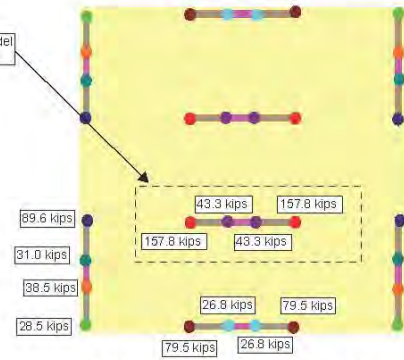
Gravity Load Applied to Blade Wall

Total:
4 x 122.4 = 488.8
4 x 21.6 = 86.4
2 x 53.0 = 106.0
4 x 70.9 = 283.6
4 x 58.6 = 234.4
4 x 91.6 = 366.4
4 x 103.3 = 413.2
1980 kips

Check: 100' x 100' x 11' Ht x 18 pcf = 1980 kips

Core Alone: 4x122.4 + 4x21.6 + 2x53
+ 4x70.9 = 965.6 kips

I Shape Alone:
2 x 122.4 = 244.8
4 x 24.05 = 96.2
2 x 70.9 = 141.8
482.8 kips

Check: 965.6 x 0.5 = 482.8 kips

Gravity Load

Add'l P-delta (if used):
(1980 kip / 2) - 482.8 = 507.2 kips / flr

Check: 2 x (482.8 + 507.2) = 1980 kips

P-Delta

Mass:
(1980 kips / 2) / 386.1 = 2.5641
[Floor Point Mass]

Mass

53.0 kips
21.6 kips
91.6 kips
122.4 kips   70.9 kips
58.6 kips
103.3 kips
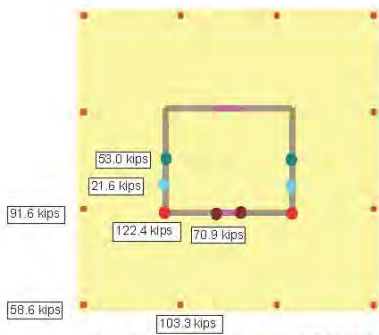
Gravity Load: Rxns from ETABS Model

21.6/2 + 53.0/4 = 24.05
122.4 kips
70.9 kips

Equivalent Pseudo 2-D Model

6

Period Comparison

ETABS Periods
(DBE Periods)

Perform
(MCE T1 Periods)

7

Peak Story Drift Summary

Stories	Beam Steel	Wall Steel	D1	D2	D3	D4	M4	M5	M6	M7	M8
			D 1	D 2	D 3	D 4	M 4	M 5	M 6	M 7	M 8
50	High	Low	---	---	---						
50	Mod	Low	---	---	---						
50	Low	Low	---	---	---						
50	High	Mod	---	---	---						
50	Mod	Mod	0.021	0.021	0.017						
50	Low	Mod	---	---	---						
50	High	High	0.019	0.021	0.017						
50	Mod	High	---	---	---						
50	Low	High	---	---	---						
40	High	Low	---	---	---	---					
40	Mod	Low	0.019	0.020	0.017	0.017					
40	Low	Low	---	---	---	---					
40	High	Mod	0.020	0.017	0.017	0.016					
40	Mod	Mod	0.020	0.017	0.016	0.018					
40	Low	Mod	0.020	0.015	0.017						
40	High	High	---	---	0.015						
40	Mod	High	0.020	0.017	0.014	0.018					
40	Low	High	---	---	---	---					
30	High	Low	---	---	---	---					
30	Mod	Low	---	---	---	---					
30	Low	Low	---	---	---	---					
30	High	Mod	---	---	---	---					
30	Mod	Mod	0.014	0.013	0.013	0.015					
30	Low	Mod	---	---	---	---					
30	High	High	---	---	---	---					
30	Mod	High	---	---	---	---					
30	Low	High	---	---	---	---					
20	High	Low	---	---	---	---	---	---			
20	Mod	Low	0.017	0.017	0.015	0.013	0.016	0.018			
20	Low	Low	---	---	---	---	---	---			
20	High	Mod	0.015	0.018	0.019	0.019	0.017	0.018			
20	Mod	Mod	0.015	0.018	0.018	0.017	0.017	0.019			
20	Low	Mod	0.015	0.017	0.016	0.018	0.018				
20	High	High	---	---	---	---	---				
20	Mod	High	0.015	0.015	0.015	0.017	0.018	0.020			
20	Low	High	---	---	---	---	---				
10	High	Low	---	---	---	---	---				
10	Mod	Low	---	---	---	---	---				
10	Low	Low	---	---	---	---	---				
10	High	Mod	---	---	---	---	---				
10	Mod	Mod	0.010	0.011	0.009	0.013	0.017				
10	Low	Mod	---	---	---	---	---				
10	High	High	---	---	---	---					
10	Mod	High	---	---	---	---					
10	Low	High	---	---	---	---					
5	High	Low	---	---	---	---	---	---	---	---	
5	Mod	Low	---	---	---	---	---	---	---	---	
5	Low	Low	---	---	---	---	---	---	---	---	
5	High	Mod	---	---	---	---	---	---	---	---	
5	Mod	Mod	0.002	0.002	0.003	0.008	0.009	0.010	0.010	0.010	0.016
5	Low	Mod	---	---	---	---	---	---	---	---	
5	High	High	---	---	---	---	---	---	---	---	
5	Mod	High	---	---	---	---	---	---	---	---	
5	Low	High	---	---	---	---	---	---	---	---	

Drifts Exceed 2%

8

Inelastic Energy Dissipation
(Varied Beam Reinforcement)

Absolute

Normalized

9

Absolute Inelastic Energy Dissipation vs Beam Aspect Ratio
(Moderate Wall Steel Case)
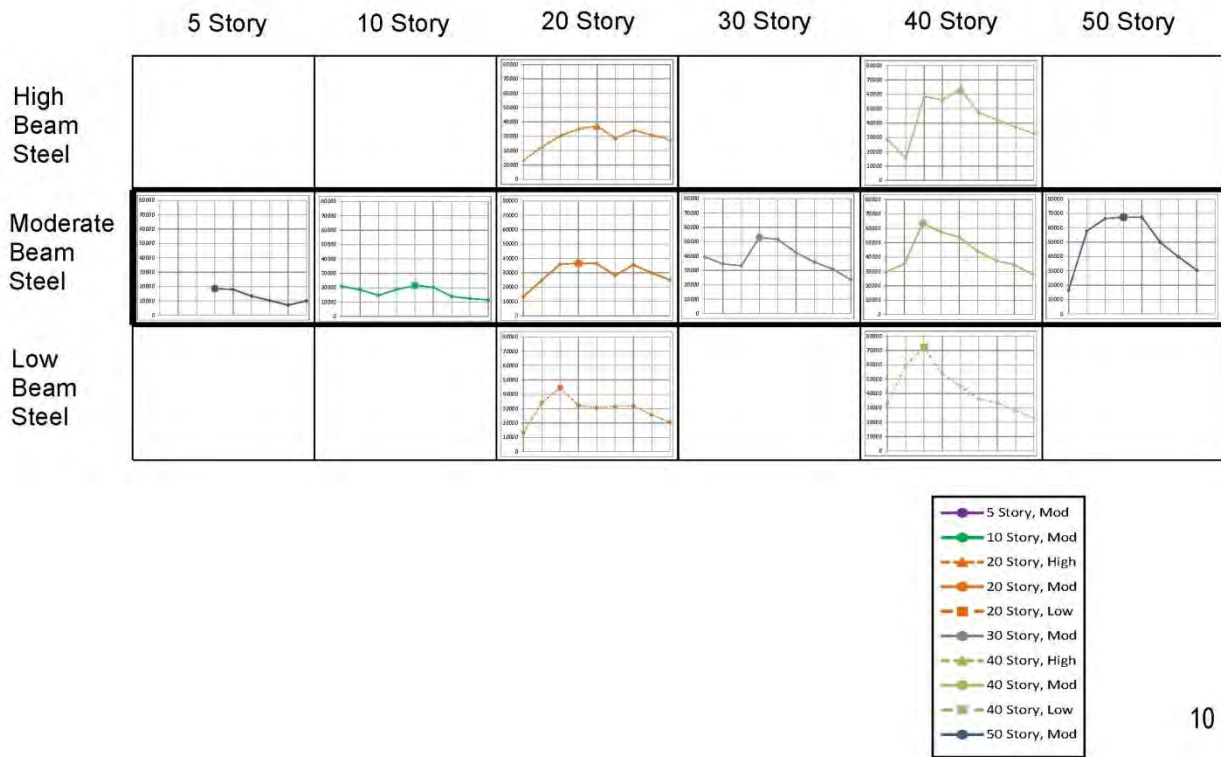
Normalized Inelastic Energy Dissipation
(All cases w/ moderate wall reinf)

11
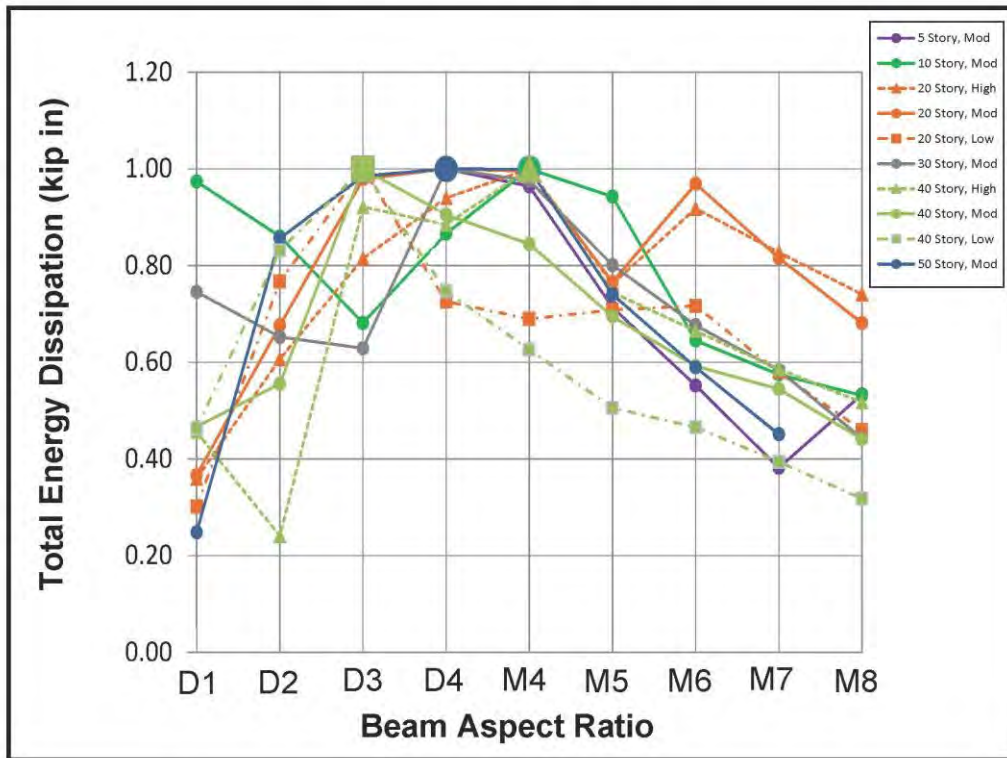
RP3-APPENDIX B
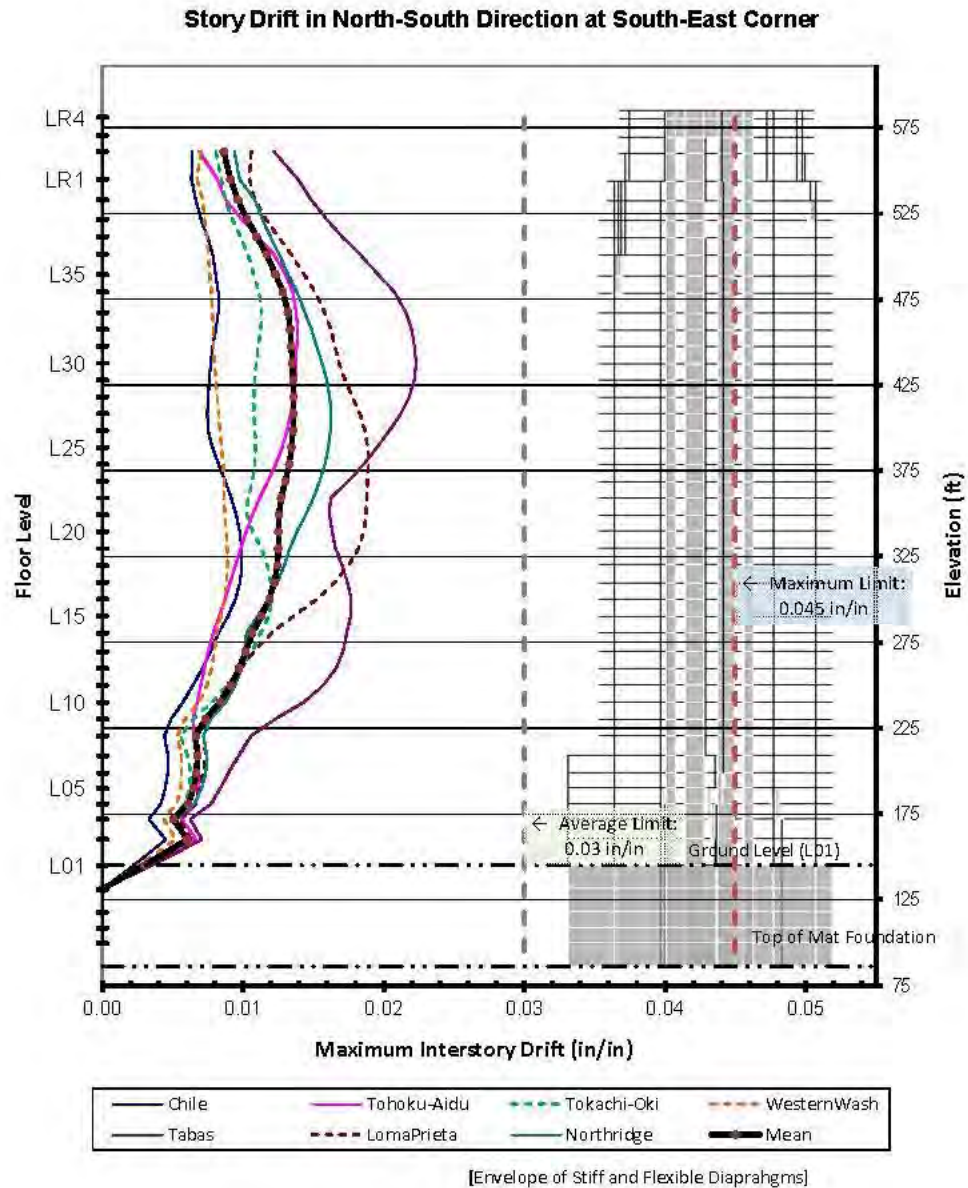
Figure 3.3-3 Building Drift at Defined Corner Points in Plan (1/8)
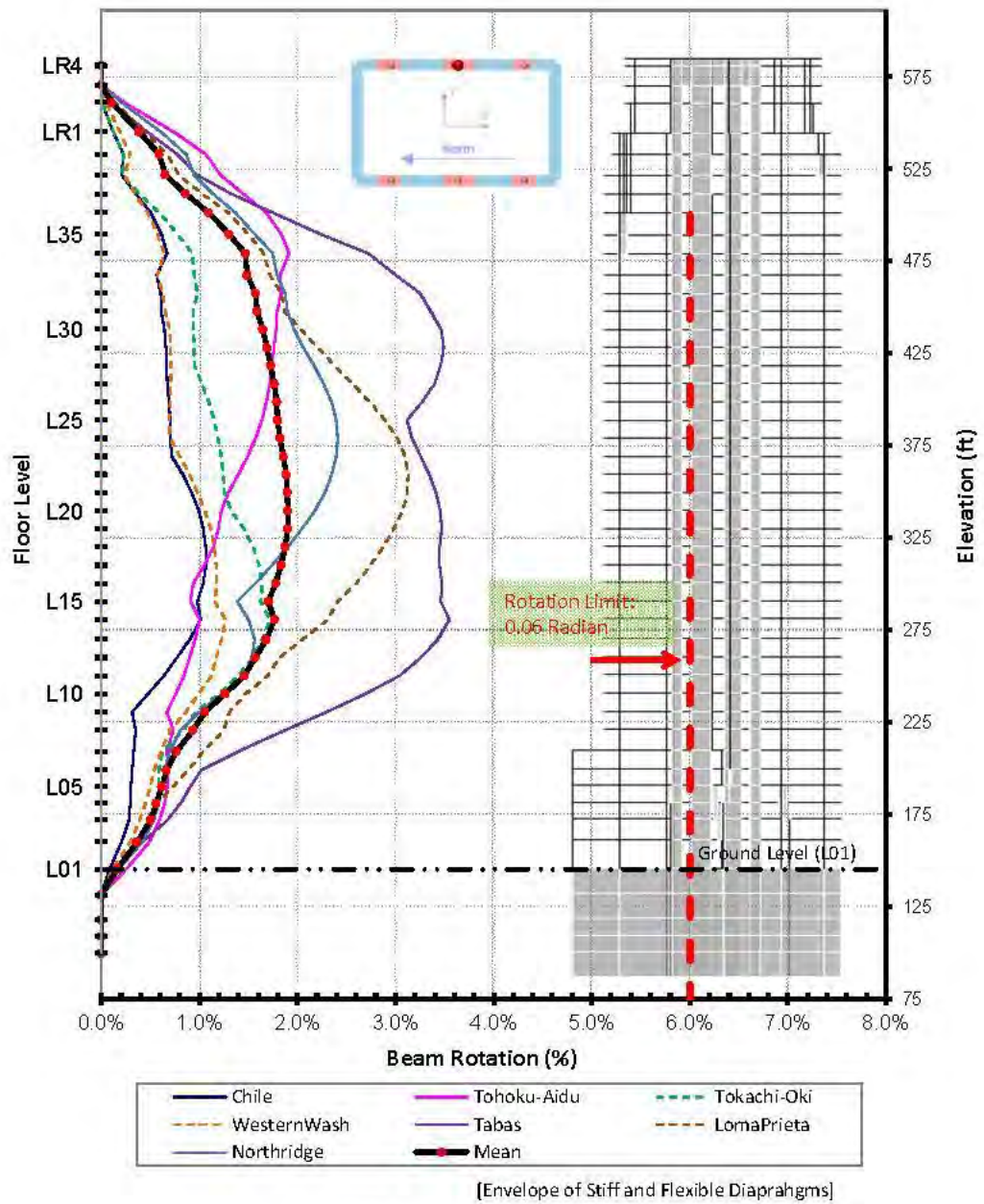
Figure 3.3-7 Link Beam Chord Rotations (2/6)
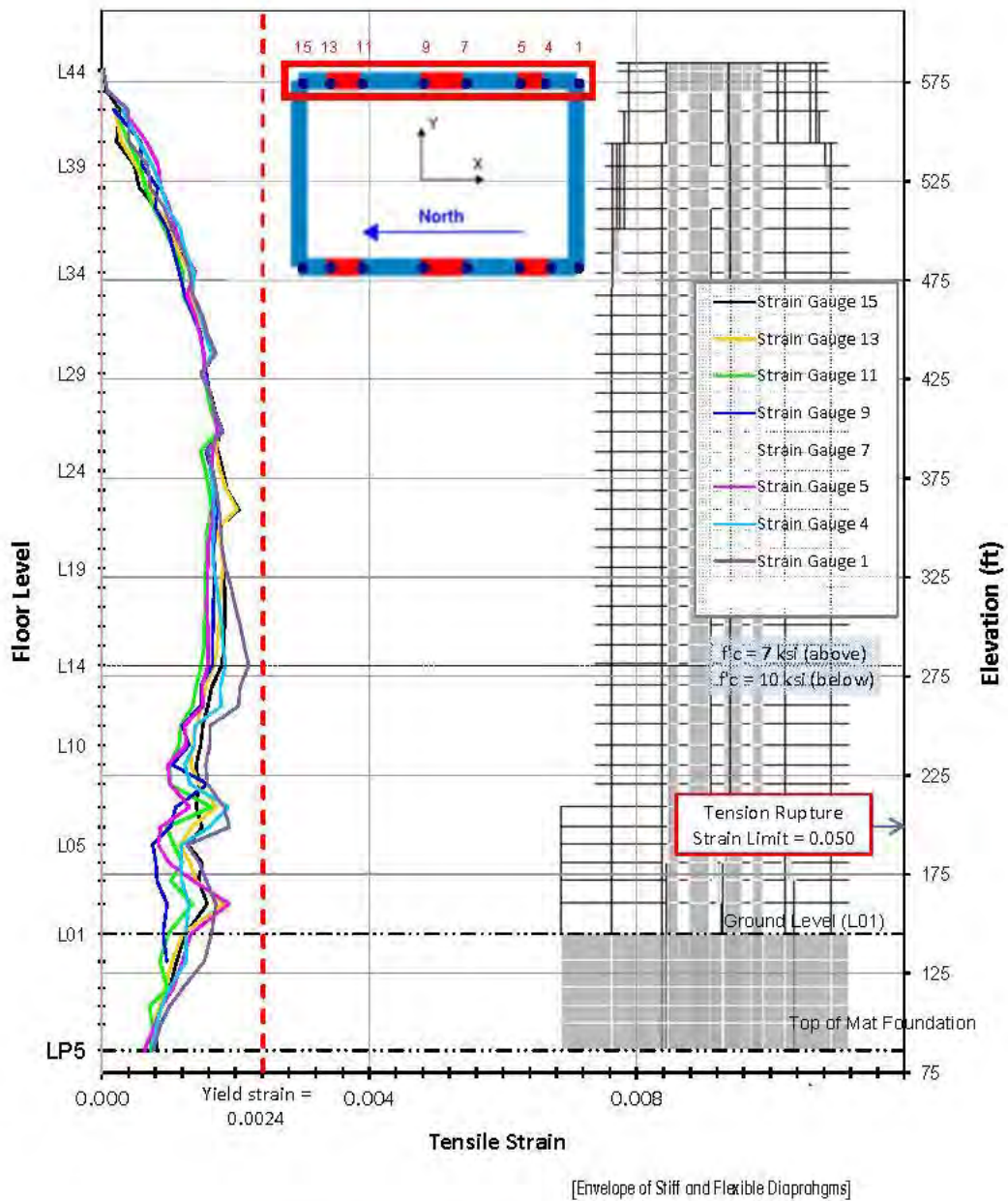
Figure 3.3-8 Wall Strain by Wall: Average of 7 Records (2/4)

Structural Calculations   NLRHA Analysis and Verification

2nd and Pine, Seattle, WA   Page 101 of 202

Figure 3.3-10 Slab-Beam Outrigger End Hinge Rotation (1/22)
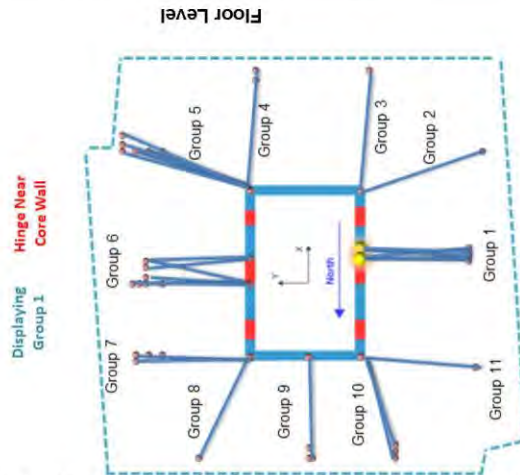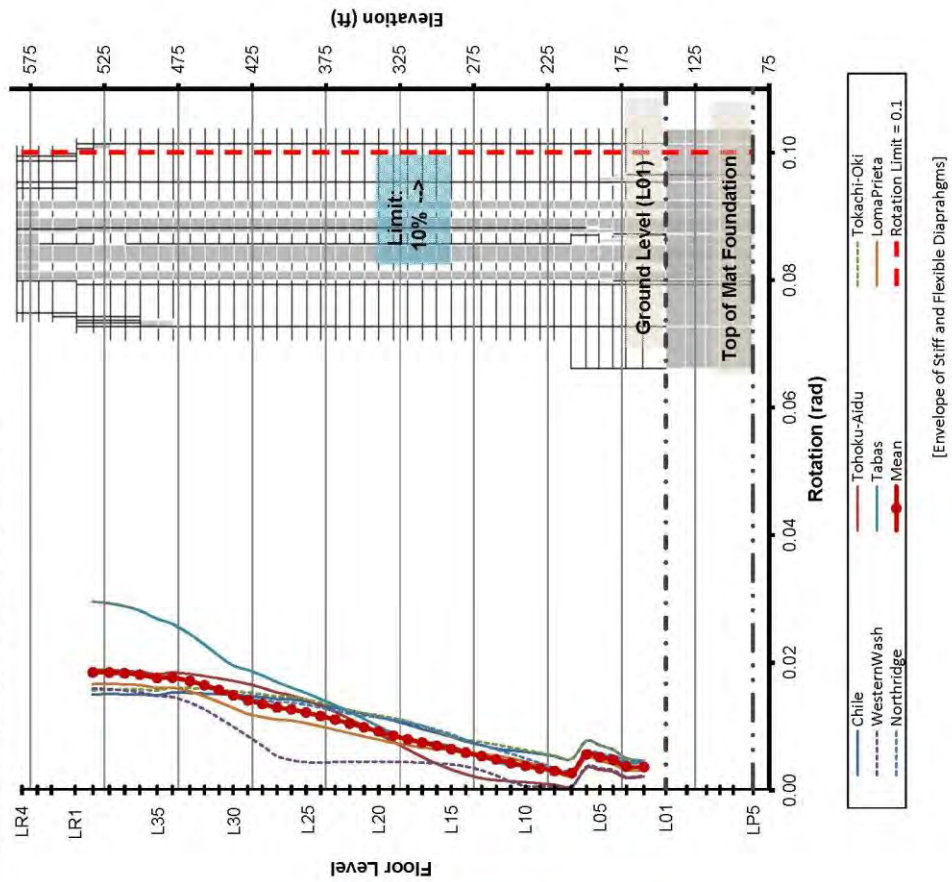
Structural Calculations

NLRHA Analysis and Verification

2nd and Pine, Seattle, WA

Page 107 of 202

RESOURCE PAPER 4 SEISMIC LATERAL EARTH PRESSURES

RP4-1   INTRODUCTION AND CONTEXT

Paragraph 1 of Section 11.8.3 in the 2009 *Provisions* requires that seismic lateral pressures on basement walls and retaining walls be determined for Seismic Design Category D, E, and F structures but does not specify the methods for calculating these pressures. NEHRP Part 3 Resource Paper 12 (BSSC, 2009) summarizes classical methods for analysis of seismic earth pressures, based primarily on the concept of a pseudo-static acceleration applied to a mass of the retained soil assumed to be at a failure state. Recent research has shown that the underlying concepts behind these classical methods have fundamental flaws, which is confirmed by a significant and growing body of experimental studies showing that classical methods tend to overestimate earth pressures.

This NEHRP Part 3 Resource Paper presents an alternative method that better accounts for the physical mechanisms that produce seismic earth pressures. The proposed method is applicable to free-standing retaining walls or restrained walls such as basement walls integrally connected to the lateral force resisting system of a structure. The procedures given here pertain to the seismic increment of earth pressure, not to the pre-seismic (static) pressure. The seismic increment of earth pressure is additive to static pressures.

RP4-2   CAUSES OF SEISMIC EARTH PRESSURES

Classical earth pressure theory shows that the direction and amount of relative displacement between the wall and the retained soil has a profound effect on static lateral earth pressures. The difference between active pressure, where the wall moves away from the retained soil by an amount that induces soil failure, and passive pressure, where the wall moves toward the retained soil and induces failure, typically spans more than an order-of-magnitude. Seismic earth pressures can be understood in the same context, but with the additional complexity that both the wall and the free-field soil are displacing as a result of earthquake shaking. At any point in time when the wall displaces away from the backfill, earth pressures drop from the static condition (if not already in a minimum active state). Conversely, and more importantly for engineering application, at any point in time when the wall displaces towards the backfill, earth pressures will rise relative to the static condition. Since earthquake loading is transient, both rises and drops in earth pressure are to be expected at different times over the duration of shaking; engineering procedures focus on the maximum values for practical application.

Mechanisms that can produce relative wall-soil displacements during earthquakes include: (1) different levels of transient displacement of a foundation system relative to the free-field (neglecting relative displacements caused by inertia of structures connected to the foundation); (2) free-field permanent ground displacements arising from soil strength loss (e.g., liquefaction, cyclic softening, etc.); and (3) force demands applied to a wall/foundation system from attached vibrating structures, which in turn produce relative foundation/free-field displacements independent from those in (1). Mechanism (1) is a kinematic soil-structure interaction problem having some similarity to the analysis of foundation input motions as described in Chapter 19 of the 2015 *Provisions*. Mechanism (2) is a ground failure problem, and is not discussed further here (further information provided in Resource Paper 12). Mechanism (3) is an inertial soil-structure interaction problem that requires analysis of the response of a structure connected to a suitable foundation system using either direct or substructure methods of analysis. Such procedures are provided in NIST (2012) and Chapter 19 of the 2015 *Provisions*.

The following sections describe the conceptual flaws in classical methods for analysis of seismic earth pressure that are based on acceleration of a soil wedge, present alternative procedures that account for kinematic and inertial sources of seismic earth pressure, and describe validation of alternate procedures for analysis of seismic earth pressures.

RP4-3   CONCEPTUAL FLAW IN CLASSICAL METHODS

As described in Resource Paper 12, classical methods of analysis for seismic earth pressures on retaining walls use a pseudo-static framework in which accelerations are applied to backfill materials, the soil is assumed to be in a state of active failure, and resulting wall demands are analyzed. Figure 1 illustrates the concept for the case of an active soil wedge with horizontal acceleration of $k_h g$ and vertical acceleration $k_v g$ (where g is acceleration of gravity), which produce horizontal and vertical inertial forces in the backfill. The force polygon in Figure 1b illustrates how these inertial forces increase the wall soil interaction force by amount P_E above the static force, P_A (assuming active conditions prior to the earthquake). By solving the equilibrium problem in Figure 1b for a variety of acceleration levels, a model for the combined thrust $P_A + P_E$ can be developed.
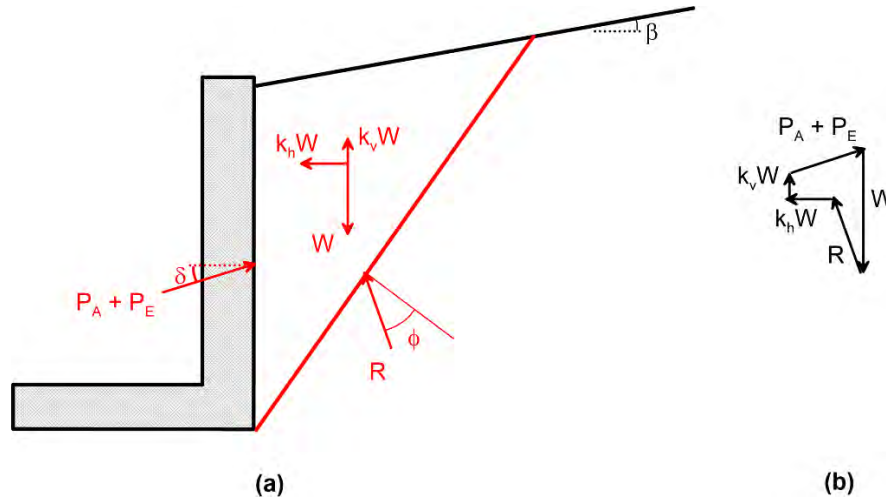
Figure 1 (a) Retaining wall with horizontal and vertical pseudo-accelerations applied to backfill wedge; (b) force polygon showing the effect of inertial forces from pseudo-acceleration on the wall-soil interaction force.

Pseudo-static methods of this type for the active case originate in the classical work by Okabe (1924) and Mononobe and Matsuo (1929) [widely known as the "Mononobe-Okabe" (M-O) method] with modest modification by Seed and Whitman (1970) and later Mylonakis et al. (2007). More accurate variants on the classical approach using non-planar failure surfaces (Chen, 1975; Chen and Liu, 1990) and accounting for the phasing of inertial demands within the wedge (Steedman and Zeng, 1990) are conceptually alike and provide similar results for the active case. Additional formulations consider the effects of cohesion on P_E (Xu et al., 2015), the seismic increment for non-yielding walls having initial at-rest earth pressures (Wood, 1973), and seismic displacements of walls as analyzed using Newmark-type procedures (Richards and Elms, 1979).

The conceptual framework behind this previous large body of work relies on an implicit assumption that seismic earth pressures are related to acceleration rather than to relative displacement between the wall and soil. This assumption is flawed, however, because there is no fundamental relationship between surface acceleration and seismic earth pressure. If both the backfill and wall are moving with comparable, in-phase displacement amplitudes, no appreciable seismic earth pressure will develop, despite the fact that the ground motion in the backfill has a finite acceleration.

Not surprisingly, when seismic earth pressures have been computed from direct analyses or measured experimentally, they seldom conform to predictions from M-O type procedures. Analytical procedures involving rigid walls retaining elastic soil resting on a rigid base produced pressures that exceed M-O predictions (e.g., Ostadan, 2005; Veletsos and Younan, 1994), while experiments involving flexible

retaining walls with a compliant base produced earth pressures that typically fall below M-O predictions (e.g., Al Atik and Sitar, 2010; Hushmand et al. 2016). These discrepancies result from the M-O methodology not representing the problem physics properly; as a result, alternatives to pseudo-acceleration based (M-O type) methods are needed.

The following sections present alternative methods for estimating seismic earth pressures. The critical conceptual distinction between the methods proposed below and M-O is that here seismic earth pressures are computed from relative foundation-ground displacements. Certain assumptions about the seismic waves exciting these structures, the soil properties, and the structural properties are made with the aim of representing commonly encountered conditions in a reasonable manner while maintaining simplicity in application. As a result of these simplifying assumptions, it could be argued that the proposed methods also do not represent the problem physics accurately (i.e., "all models are wrong…"; Box, 1976). However, our supposition is that emphasizing relative displacement as the source of seismic earth pressures leads to better outcomes than methods based on a pseudo-static acceleration (which is related to the second part of Box's quote: "… but some (models) are useful."). The degree to which this is realized can be judged through validation, as presented below. Limitations of the proposed method are provide in the *Conclusions* section.

RP4-4   ANALYSIS OF SEISMIC EARTH PRESSURES

Analysis procedures for seismic earth pressures should consider soil-structure interaction involving the wall, the supporting and retained soil, and any attached superstructures. As with other soil-structure interaction problems, both kinematic and inertial components can be significant. This section presents a unified and simple framework for computing seismic earth pressures that accounts for these effects.

RP4-4.1   Kinematic Seismic Earth Pressures

Kinematic seismic earth pressures are produced by the combined seismic excitation of shallow layers of soil at a site and a wall system embedded within those soils. Figure 2 illustrates the problem for the case of a free-standing wall.

In the kinematic problem the wall itself is assumed to have a certain flexural stiffness (but no mass) and to be connected to the soil but not to any structure. The ground motions producing the excitation occur over a wide frequency range, typically from about 0.1 to 10 Hz. If these waves can reasonably be assumed as propagating vertically near the ground surface (such that the site response is controlled by 1D ground response), they produce waves of wavelength $\lambda = V_S/f$ with a maximum amplitude at the ground surface (Figure 2a). Accordingly, at each frequency, and at a given point in time, the horizontal ground motion varies with depth. When this variation is small (i.e., for low frequencies with long wavelengths), the motion of the wall system nearly matches that of the free-field soil, relative wall-soil displacements are small (Figure 2b), and seismic earth pressures are low (Brandenberg et al. 2015). Conversely, as shown in Figure 2c, short wavelengths can produce motions that decrease significantly with depth over the height of the wall. Under such conditions, the relatively stiff wall must displace differently from the free-field soil, and the differences in displacement produce potentially large seismic earth pressures. For these short wavelength conditions, the flexibility of the wall system, the distribution of soil stiffness with depth, and the ability of the wall and soil to yield also affect seismic earth pressures.
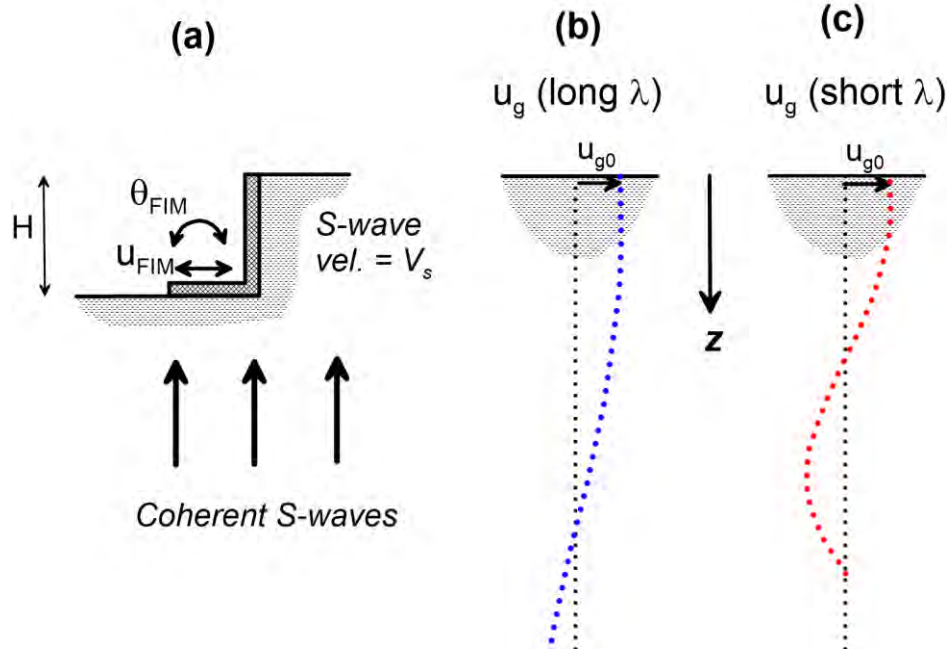
Figure 2 Schematic illustration of free-standing retaining wall subjected to seismic waves with different wavelengths. Displacement u_{FIM} applies at the foundation level of the wall, and q_{FIM} represents the rotation of a rigid wall-footing system.

The kinematic problem can be solved using direct analysis in which the ground response and SSI are solved for simultaneously in finite element or finite difference simulations. Simplified methods are useful to help conceptualize the physics of the problem and for applications where more approximate solutions suffice. Figure 3 shows conditions amenable to solution with simplified models, in which a rigid wall and foundation is excited by a single-frequency wave of angular frequency ω and surface amplitude u_{g0}. The foundation is compliant (finite stiffness) and the backfill is uniform in stiffness with depth. For the special case of rigid foundation support (K_y and $K_{xx} \to \infty$), the amplitude of seismic earth pressure resultant P_E (normalized to remove dimensions) is given by:

$$\frac{|P_E|}{k_y^i u_{g0} H} = \frac{\sin(kH)}{kH} - cos(kH) \tag{1}$$

where k is the wavenumber (ω/V_S) and H is wall height (Figure 3). The product kH is related to wavelength λ as $kH = 2\pi H/\lambda$. The normal stress on the wall is described by the product of relative wall-soil displacement and *stiffness intensity* k_y^i. The normalized height of resultant h/H, where h is measured up to result from base of foundation, is given for the same conditions as:

$$\frac{h}{H} = \frac{cos(kH) - 1 + (kH)^2 \frac{cos(kH)}{2}}{(kH)^2 cos(kH) - (kH)sin(kH)} \tag{2}$$

Eq. (2) gives h/H = five-eighths for $\lambda/H = 2\pi/(kH) > \sim 4$. Stiffness intensity is defined as translational stiffness (in conventional units of force/length) divided by area. Stiffness intensity for vertical walls supported by rigid foundations can be computed as (Kloukinas et al., 2012):

$$k_y^i = \frac{\pi}{\sqrt{(1-\nu)(2-\nu)}} \frac{G}{H} \sqrt{1 - \left(\frac{4H}{\lambda}\right)^2} \tag{3}$$

where G and ν are the shear modulus and Poisson's ratio of the backfill, respectively.
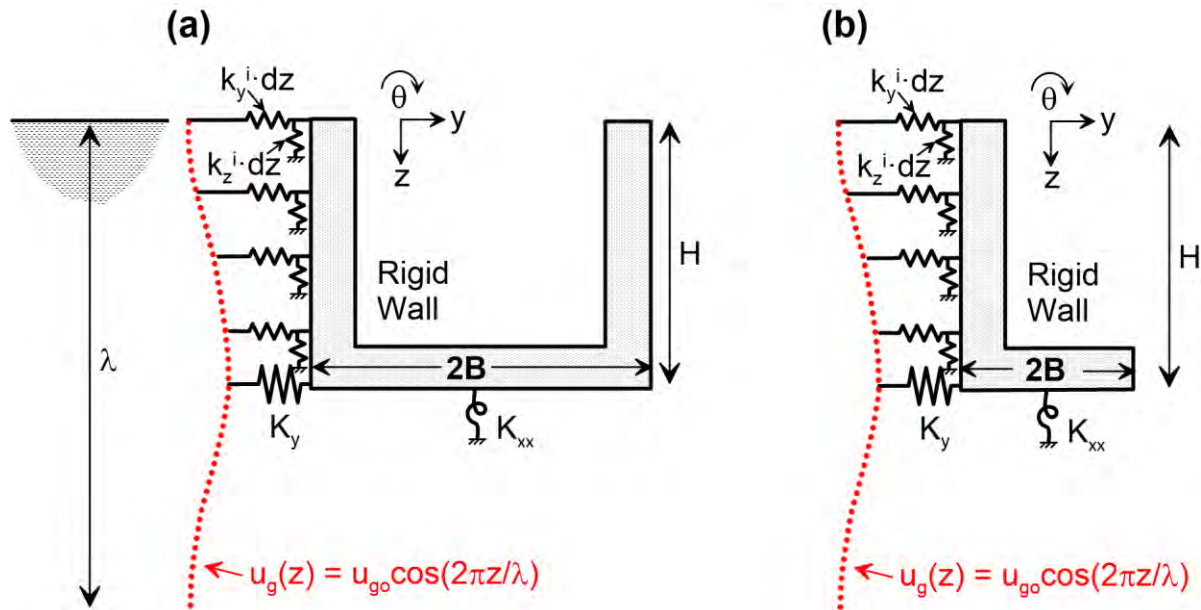
Figure 3 Rigid wall and foundation systems subjected to vertically propagating shear waves, with wall-soil interaction represented by various stiffness terms. (a) U-shaped wall (modified from Brandenberg et al. 2015) and (b) cantilever-type single wall.

For the conditions where Eqs. (1-3) apply (rigid foundation, rigid wall, and uniform backfill), Figure 4 shows the variation of the normalized force amplitude $|P_E|/(k_y^i u_{g0} H)$, and its normalized point of application h/H, with the ratio of wavelength to wall height, λ/H. The portion of this curve for $\lambda/H > \sim$ 2.7 is of special interest because it typically contains the frequency range of engineering interest. Kinematic pressures are high near the plateau at 2.7 due to large relative displacements of wall and soil. For smaller λ/H, changes in frequency strongly affect the amplitude and sign of P_E due to tensile and compressive stresses that act on different portions of the wall height; this complex behavior is simplified to a straight line as shown in Figure 4. As λ/H increases beyond 2.7, P_E decreases rapidly. In the limiting case where $\lambda/H \to \infty$, the deformed shape of the free-field soil profile becomes vertical, conforming to the shape of the rigid wall and producing zero kinematic interaction. For a given value of λ/H, the normalization of force accounts for the effects of soil stiffness and shaking amplitude on seismic earth pressures. Normalized resultant height has little variation with λ/H beyond 4.0.
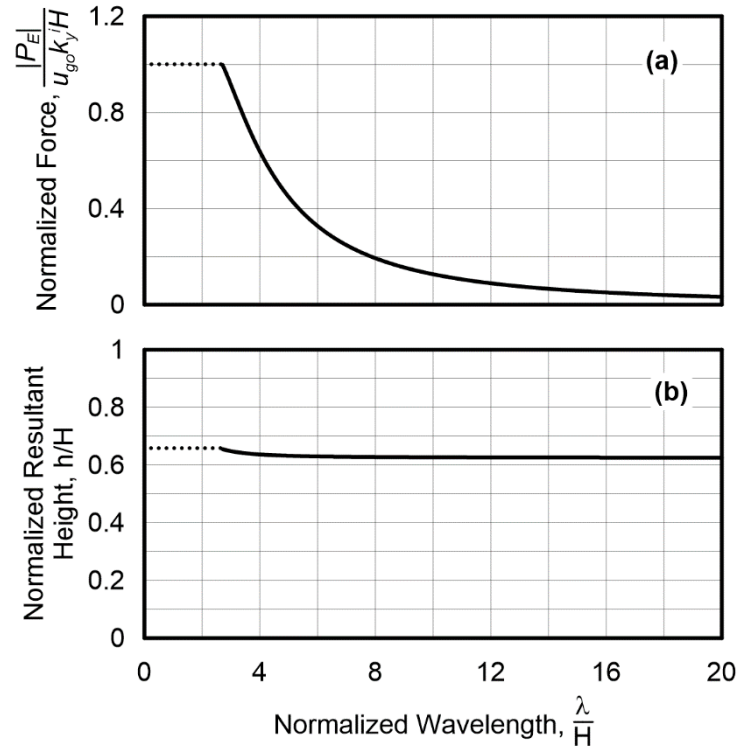
Figure 4 Variation with normalized wavelength λ/H of (a) normalized amplitude of P_E and (b) its point of application above the foundation. These results are for a rigid wall founded on rigid base and retaining uniform backfill. Dotted lines at low λ/H are approximations of exact solution.

Figure 5 shows the effects of wall flexibility, which is parameterized as (Novak, 1974):

$$\beta = \sqrt[4]{\frac{k_y^i}{4EI}} \qquad (4)$$

where E is Young's modulus of the wall material and I is the moment of inertia for the wall section (the product represents the wall flexural stiffness). β has units of 1/length, and is multiplied by H to remove dimensions. The product βH represents a ratio of backfill soil-to-wall stiffness (for a rigid wall, $\beta H \rightarrow 0$). As shown in Figure 5a, P_E decreases substantially as wall stiffness decreases (increased βH) because the wall is better able to conform with free-field ground motions when it is not rigid. Wall flexibility also affects resultant height (Figure 5b), with the resultant lowered appreciably for $\beta H > 1.5$. A condition of $\beta H < 0.5$ corresponds essentially to a rigid wall. Many practical cases fall within the range of $\beta H = 1 - 4$.
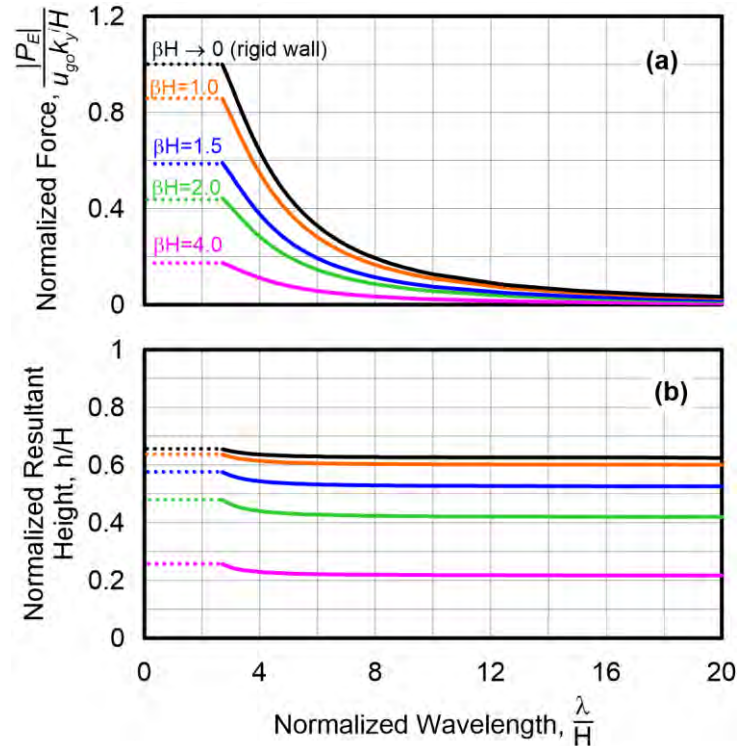
Figure 5 Effect of wall flexibility on (a) normalized wall resultant and (b) its point of application above the foundation. These results are for a rigid base and uniform backfill and were derived from finite element simulations.

Non-uniform backfill conditions have been investigated for cases in which the same time-averaged shear wave velocity within the backfill soil is used for cases having different velocity gradients (Vrettos et al 2016; Brandenberg et al. 2017). For the rigid wall case, backfill non-uniformity reduces $|P_E|$ and its resultant height, however, these effects become small for modest levels of wall flexibility. Accordingly, for simplified analysis, an equivalent uniform time-averaged velocity for the backfill is used, $V_{S,av}$.

Similarly, non-rigid (i.e., compliant) foundation conditions have been shown to strongly reduce $|P_E|$ for rigid walls (Brandenberg et al. 2015), but to have a more modest effect for flexible walls. The simplified analysis procedure is formulated considering wall flexibility effects but neglecting foundation flexibility, which introduces some conservatism. The significance of this conservatism is assessed through validation against test data (next section).

The following simplified procedure provides estimates of $|P_E|$ (resultant of seismic earth pressures) and h (point of application) in consideration of the most critical effects (ratio of wavelength to wall height and relative soil-wall stiffness):

1. Perform seismic hazard analysis (probabilistic or deterministic) to estimate PGV for the site.

2. If the estimation of PGV is based on probabilistic seismic hazard analysis, deaggregate the hazard at the return period of interest to obtain the controlling magnitude and distance. Estimate mean period, T_m, for this condition (Figure 6). If PGV is derived using deterministic methods, use the selected magnitude and distance for the estimation of mean period. Compute the corresponding angular frequency for this condition, $\omega_m = 2\pi/T_m$.

3. Develop a shear wave velocity profile for the backfill soil. Compute the average shear wave velocity, $V_{S,av}$, as the ratio of wall height, H, to shear wave travel time through the backfill.

4. Estimate the ground surface displacement as $u_{g0} = f_u PGV / \omega_m$. Adjustment factor f_u is given as a function of λ/H in Figure 7. This factor has been calibrated to match the results of single-frequency analyses to more complete Fourier series analyses.

5. Estimate k_y^i as its static counterpart (k_{y0}^i) with following approximate expression:

$$k_y^i \approx k_{y0}^i = \frac{\pi}{\sqrt{(1-\nu)(2-\nu)}} \frac{\rho V_{S,av}^2}{H} \tag{5}$$

Eq. (5) is modified from Eq. (3) by removing the frequency-dependent term (justified through validation in next section) and by taking $G = \rho V_{S,av}^2$, where ρ is backfill mass density.

6. Estimate βH from the relative soil-to-wall stiffness (Eq. 4) and wall height H. In cases where βH is unknown because wall section sizes are undetermined, an initial estimate in the range of 1-2 can be applied and will often be conservative.

7. Compute normalized force amplitude $|P_E|/(k_y^i u_{g0} H)$ and resultant height h/H. These quantities are obtained for rigid walls using Eqs. (1-2). The effects of wall flexibility can be incorporated using Figure 8 or the following expressions (which describe the change of resultant amplitude and its height with βH):

$$\frac{|P_E|}{|P_E|_{rigid\ wall}} = \xi = \begin{cases} 1 - exp\left(1 - \frac{2.9}{\beta H}\right) & \beta H < 1 \\ sin\left(-0.45 + \frac{1.43}{\beta H}\right) + cos\left(1.22 + \frac{0.34}{\beta H}\right) & \beta H > 1 \end{cases} \tag{6}$$

$$\frac{h}{H} = \begin{cases} 0.6 - exp\left(-0.12 - \frac{2.8}{\beta H}\right) & \beta H < 1 \\ sin\left(1.68 + \frac{1.5}{\beta H}\right) + cos\left(2.87 - \frac{1.92}{\beta H}\right) & \beta H > 1 \end{cases} \tag{7}$$

The relations in Eqs. (6 and 7) and Figure 8 are curve-fits to finite element simulation results (updated from Durante et al. 2018).

8. De-normalize to compute $|P_E|$. Moment can be computed as $|M| = h|P_E|$.
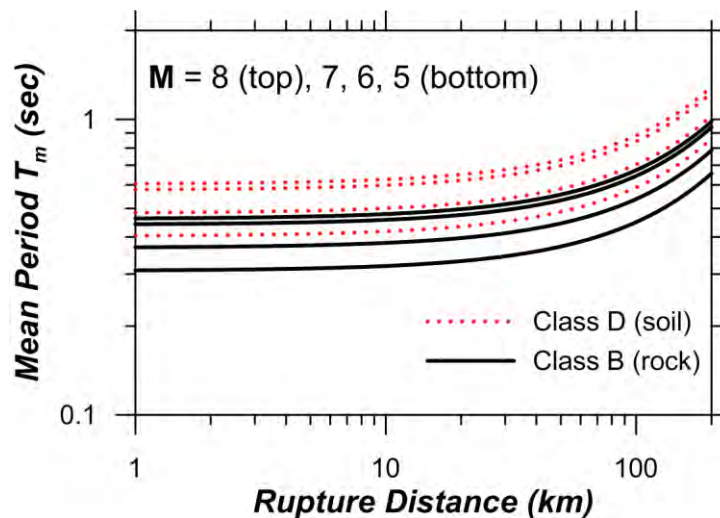
Figure 6 Variation of median values of mean period (T_m) with magnitude, distance, and site condition. Rathje et al. (2004) ground motion model.
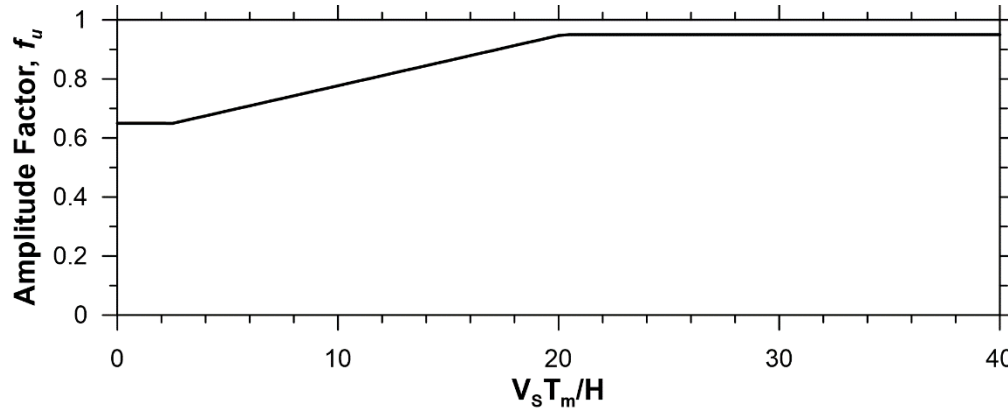
Figure 7. Ground motion amplitude adjustment factor for use with simplified method for evaluation of amplitude of seismic earth pressure resultant force, P_E.
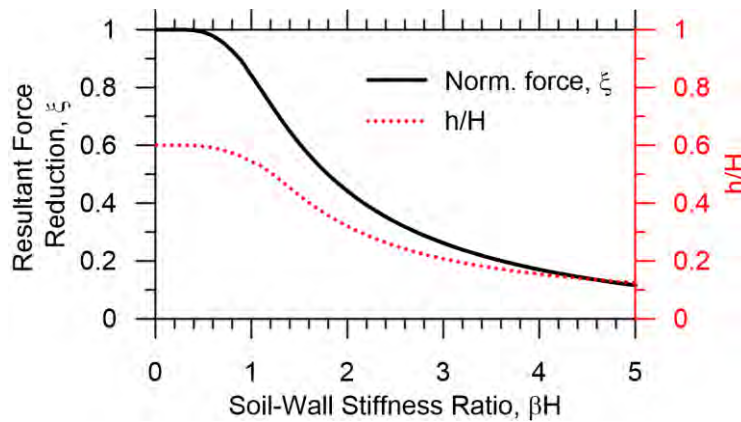
Figure 8 Effect of soil-to-wall stiffness ratio (βH) on (a) normalized resultant force and (b) normalized resultant height.

Steps 3 and 5 in the simplified procedure use small-strain shear wave velocity parameter, $V_{S,av}$. Many problems will involve shaking that produces nonlinear soil responses. The effects of nonlinearity are to reduce seismic velocities and $V_{S,av}$, producing two effects: (*i*) wavelength is reduced (since $\lambda = V_{S,av}T_m$), which reduces λ/H and hence increases normalized force; and (*ii*) k_{y0}^i is reduced per Eq. (5), which reduces P_E following de-normalization. These effects largely offset each other for most applications, hence the additional complexity that is required to consider nonlinear effects was not considered to be justified. However, for users who would like to account for nonlinearity in an approximate manner that does not require a ground response analysis, the following procedure can be applied:

a. Compute a first estimate of displacement amplitude at depth H as:

$$u_g(H) = u_{g0}cos\left(\frac{2\pi H}{T_m V_{S,av}}\right)$$ (8)

b. Compute a first estimate of average shear strain over the backfill height as:

$$\gamma_{av} = \frac{u_{g0} - u_g(H)}{H}$$ (9)

c. Compute effective shear strain as $\gamma_{eff} = \gamma_{av}(\mathbf{M} - 1)/10$ (Idriss and Sun, 1992).

d. Use an appropriate modulus reduction relationship with strain γ_{eff} to estimate the modulus reduction for the backfill, $(G/G_{max})_{av}$.

e. Compute a reduced average shear wave velocity to reflect modulus reduction effects as:

$$V_{S,av,r} = V_{S,av}\sqrt{(G/G_{max})_{av}} \qquad (10)$$

f. Use $V_{S,av,r}$ with T_m to update $u_g(H)$, γ_{av}, and γ_{eff} (Steps a-c). Use the updated γ_{eff} to re-evaluate $(G/G_{max})_{av}$ (Step d). Repeat until modulus reduction estimates do not change appreciably between iterations.

g. Using the final value of $V_{S,av,r}$ derived through the iterative process to compute wavelength and stiffness intensity.

In addition to these nonlinear effects on the soil-wall response, nonlinear site response also affects the seismic hazard at the site, as represented by intensity measure *PGV*. This source of nonlinearity is accounted for in the ground motion models used in seismic hazard analyses.

RP4-4.2   Inertial Seismic Earth Pressures

Inertial seismic earth pressures are typically most significant when structures are connected to a foundation system containing basement walls (Figure 9). Under these conditions, the base shear and moment from the vibrating structure cause the foundation to displace horizontally and rotate, producing wall reaction stresses. Analysis of this problem does not require specialized procedures – direct or substructure approaches to the SSI problem can be employed (NIST 2012; Chapter 19 of NEHRP *Provisions*). If wall-soil interaction elements are included in the SSI model, reaction stresses against walls are a natural outcome of the analysis.
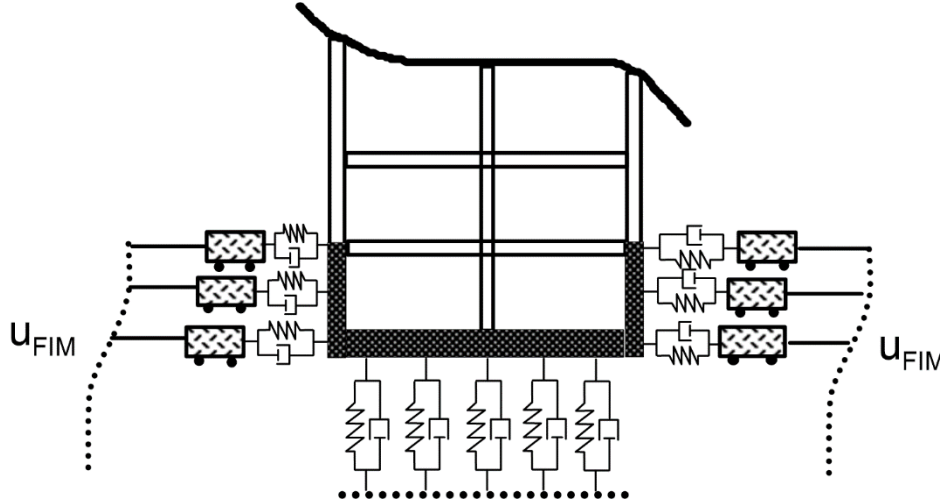
Figure 9 Structure with foundation that includes retaining walls that are connected to the lateral force resisting system and hence contribute to the transmission of base shear and moment to the soil.

An important consideration in the analysis of inertial effects on subterranean walls is the degree to which they participate in the below-ground lateral force resisting system. Figure 10 shows a building in which lateral loads are resisted by a central core of shear walls that extend directly to the foundation mat. If the foundation for the core walls is not connected to the foundations for the surrounding podium (as in Figure 10), the basement walls may see little of the inertial loading. In such cases, the loading of basement walls is likely to be controlled by kinematic mechanisms.

Peak kinematic and inertial seismic demands on basement walls are unlikely to coincide in time. When both effects are expected, load combination rules such as SRSS should be applied.
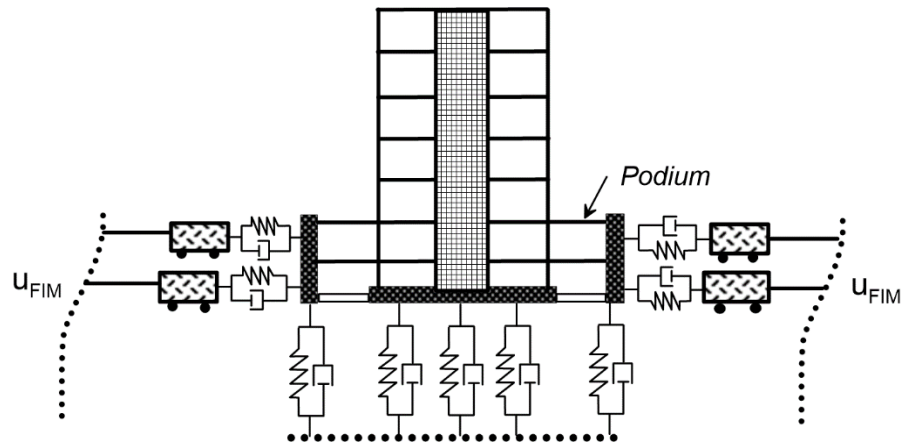
Figure 10 Structure with lateral loads resisted by central core of shear walls supported on a mat foundation that is distinct from the foundations for basement walls. In such cases, basement walls are not likely to be significantly affected by inertial interaction effects, and kinematic mechanisms are more likely dominant.

RP4-4.3   Limiting Earth Pressures Based on Soil Shear Failure

Both the proposed kinematic and inertial models represent soil-wall interaction with springs that have elastic stiffnesses. In principle, such springs have no upper limit on the forces they can develop. In reality, soil pressures are limited by the soil shear strength. As a result, it is good practice to check whether limit equilibrium state is reached under a particular loading condition.

One could utilize the M-O method to estimate the limit equilibrium upper bound pressures, as has been routine practice for many decades. However, a number of unrealistic assumptions render this procedure inaccurate, even for limit state pressures. First, M-O assumes that the peak lateral earth pressure occurs under active loading conditions (wall deflection away from backfill). In reality, peak lateral earth pressures occur when the direction of relative displacement is the opposite (i.e., when the free-field soil moves toward the wall). Second, there is no fundamental relationship between peak surface acceleration and earth pressure, as previously established in this document. Third, the M-O procedures fail to produce a physically meaningful solution when the ground shaking intensity exceeds a certain threshold value, which is often lower than design ground motions for retaining structures in seismically active regions.

Validation studies in the next section show that the proposed kinematic model is reasonably accurate even under strong shaking conditions, which suggests that a state of limiting equilibrium may not be reached for realistic conditions encountered in the field. Further, the validation study also demonstrates use of a reduced soil shear modulus to account for nonlinearity in the soil response at strain levels leading up to failure. Nevertheless, an upper bound check based on limit equilibrium principles is advisable.

RP4-5   VALIDATION

The proposed kinematic model is validated against some of the available test data and direct analysis results that are available in the literature. The validation considers two studies in which various wall specimens were tested using centrifuge modeling (Al Atik and Sitar 2009, 2010; Hushmand et al. 2016) and simulations in which a direct SSI analysis was performed (Ostadan 2005). As shown in Table 1, the selected studies encompass a range of conditions with respect to base fixity, wall flexibility, and ground motion amplitude (producing different levels of soil nonlinearity). Some recent centrifuge modeling studies have

produced additional data that has not yet been considered in the validation (e.g., Wagner and Sitar 2016).

Table 1. Summary of studies considered in validation exercise

Test Type	Pressure Measurement	Foundation Condition	βH range	Excitation	Reference
Centrifuge	Direct, bending	Flexible & fixed	1.0-3.2	Sinusoidal, broadband	Hushmand et al 2016
Centrifuge	Direct, bending	Flexible	2.0-3.2	Broadband	Al Atik & Sitar 2009, 2010
Simulation	Direct	Fixed	0	Broadband	Ostadan 2005

The centrifuge models considered by Al Atik and Sitar (2009, 2010) and a subset of those considered by Hushmand et al. (2016) have a soil layer beneath the wall foundation. Fixed base conditions were used in other Hushmand et al. (2016) specimens, and in the simulations of Ostadan (2005). While rigid wall conditions were used by Ostadan (2005), the wall specimens in the centrifuge tests have varying soil-to-wall relative stiffnesses, ranging from $\beta H = 1.0$ to 3.2.

Each of the centrifuge models consisted of a U-shaped wall that retained sand backfill. As such, the backfill stiffness is non-uniform with depth. A time-averaged shear wave velocity ($V_{S,av}$) was used in the validation analyses, which was calibrated to match observed soil column fundamental frequencies. Analyses were performed both for the case of small-strain velocities (elastic conditions) and strain-reduced average velocities (nonlinear conditions).

In both centrifuge modeling studies, lateral earth pressures were measured as a function of depth directly using different types of tactile sensors. Such sensors are known to produce noisy data and to require careful calibration (e.g., Palmer et al. 2009). As a result of these data quality concerns, Al Atik and Sitar (2009, 2010) also measured bending strains in wall specimens, which provide bending moment profiles. Such profiles can be differentiated once with respect to depth to obtain shear profiles, and a second time to estimate lateral reaction loads, which are related to earth pressures. This double-differentiation process provides an independent measure of earth pressures, but is again noisy due to sensitivity of the numerical differentiation process to small amounts of noise in the bending data. Different researchers used different methods of data interpretation; for the present application we used pressures presented by the original authors. After subtracting static earth pressure, the seismic increments of earth pressure were derived for comparison to model predictions.

Model predictions require four main inputs:

- Mean period T_m, which was obtained using standard procedures (Rathje et al. 2004) in which the centroid (on a period axis) of the measured surface motion Fourier amplitude spectrum is computed.

- Backfill surface displacement amplitude u_{g0}, which is obtained from the peak velocity and T_m as $u_{g0} = f_u PGV/\omega_m$ (f_u taken from Figure 7).

- Backfill stiffness intensity k_{y0}^i, which is obtained from Eq. (5) using $V_{S,av}$ and ν=0.3.

- Soil-to-wall flexibility ratio βH, which is obtained from Eq. (4) using wall section properties and k_{y0}^i.

Figure 11 shows aggregated data-model comparisons for the default analysis procedure in which $V_{S,av}$ is used without reduction, while Figure 12 shows similar results but with $V_{S,av}$ reduced for nonlinearity using the proposed optional procedure. In both Figures, normalized forces are shown along with force residuals computed as $ln(P_{E-meas}) - ln(P_{E-pred})$. P_{E-meas} is the resultant force from measured seismic earth pressures, while P_{E-pred} is the predicted peak force.

The results in Figure 11 (interpretation using small-strain V_S) span a range of λ/H of about 5 to 27 and demonstrate a decrease in normalized force amplitude as λ/H increases, as anticipated from the kinematic model. Some of the highest normalized forces are from Hushmand et al. (2016) Test 2, which has a fixed-base condition. All other tests have flexible-base conditions, and among those tests, some effects of soil-to-wall flexibility (βH) are apparent. In particular, Test 3A has the highest normalized forces among the flexible base tests and the stiffest walls (βH = 1.0-1.1), while Tests 1A and 4A have lower normalized forces and relatively flexible walls (βH = 1.5-3). The Ostadan (2005) simulations provide normalized forces that lie above the test data, as expected for rigid walls and fixed-base conditions, and follow the decreasing trend with λ/H. The standard deviation of the residuals for the Hushmand et al. (2016) tests is high, which is likely significantly influenced by uncertainty in the tactile pressure sensor measurements. Al Atik and Sitar (2009, 2010) utilized strain gauges to estimate lateral earth pressure resultants, which produces a less variable, albeit indirect, measure of earth pressure.

Application of the nonlinear procedure (Figure 12) lowers wavelengths and hence λ/H such that the applicable data range becomes 2.5-11. The trend of normalized forces decreasing with λ/H becomes much more apparent as the data 'climb' towards the plateau of the kinematic relationship. Despite these dramatic increases in normalized forces, de-normalized forces are not appreciably affected, due to corresponding decreases in k_{y0}^i for the nonlinear case. This is best shown by residuals, whereby the overall mean is approximately -0.2 in both cases (indicating an average over-prediction of about 20%). The standard deviation of residuals, σ_{ln} is approximately 0.3-0.4 in both cases. While there is a reduction in dispersion from including nonlinear effects, the effect is small. These findings motivated making the nonlinear steps in the procedure optional.

The average over-prediction of seismic earth pressures provided by the kinematic model likely has two principle causes:

- Omission of the frequency-dependent term in k_y^i (i.e., $\sqrt{1 - (4H/\lambda)^2}$ in Eq. 4). Had this term been included, it would reduce resultant forces.

- Neglecting the effects of base flexibility in model formulation, which if included, would reduce resultant forces.

The conservative bias is considered appropriate for a simplified procedure in NEHRP documents. More advanced procedures are encouraged for critical projects. General scatter in results, reflected by standard deviation terms, is expected because of the simplification of complex seismic waveforms using the intensity measures of PGV and T_m, the representation of soil-wall interaction with linear or equivalent-linear springs, as well as data quality issues.

Small-strain V_S

Strain-Reduced V_S
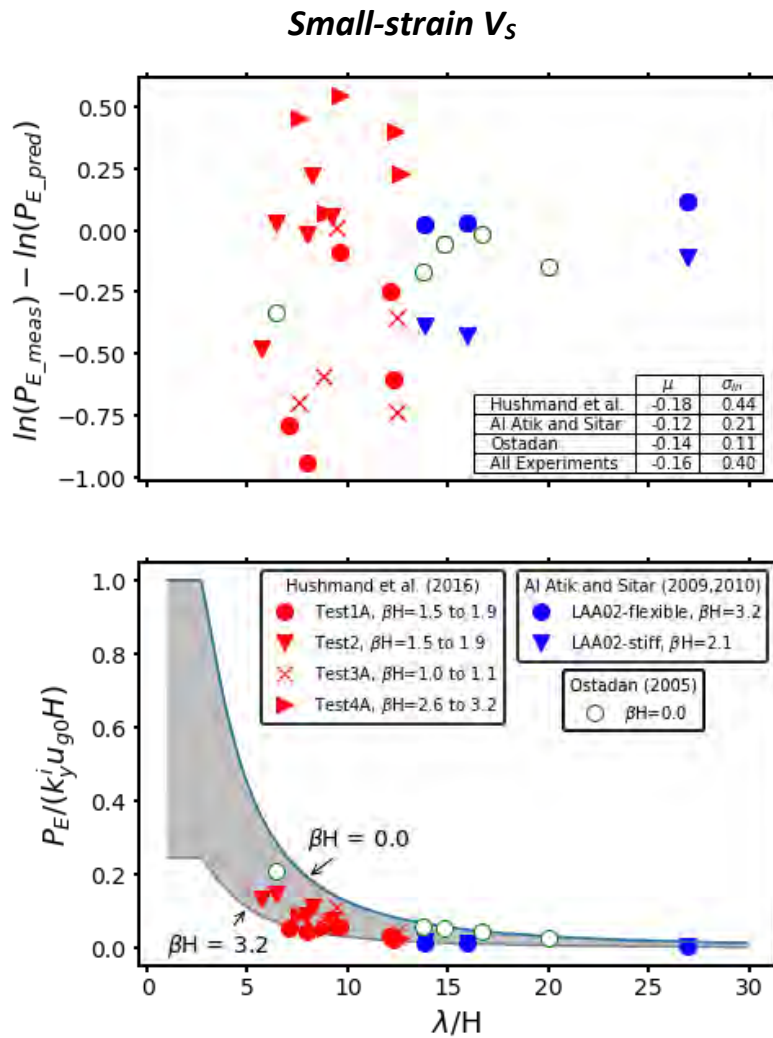
Figure 11 Data-model comparison of normalized seismic earth pressure resultant forces (bottom) and force residuals (top). Model applied using small-strain shear wave velocities
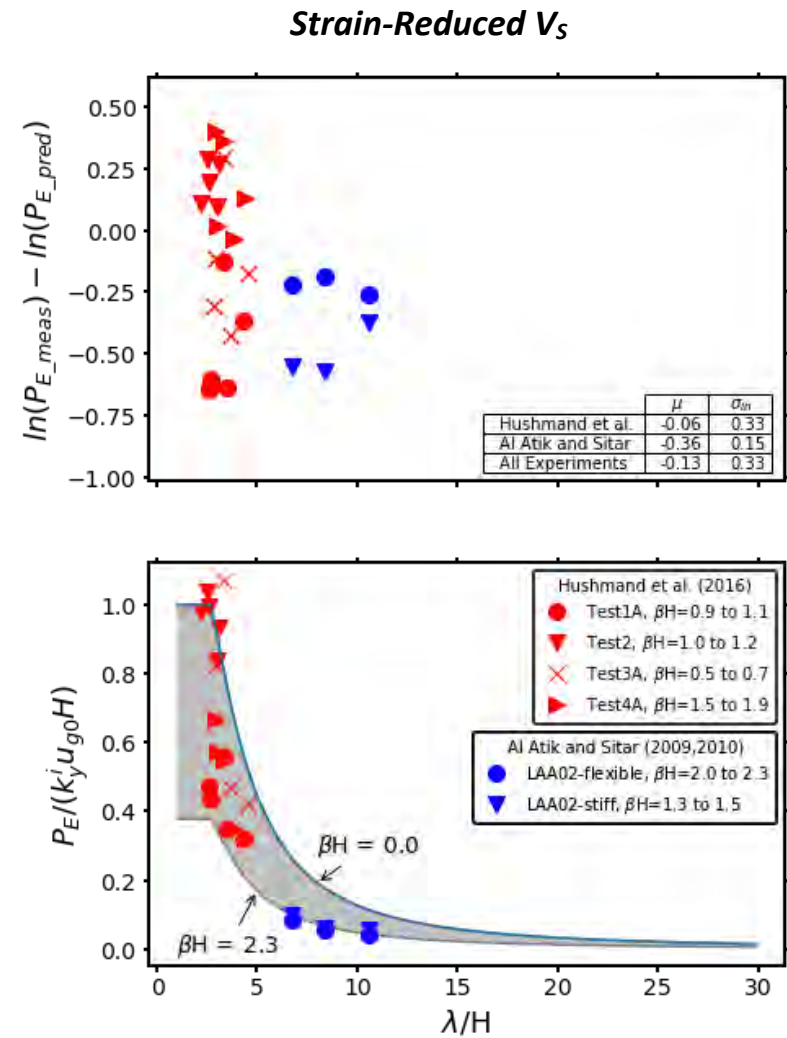
Figure 12 Data-model comparison of normalized seismic earth pressure resultant forces (bottom) and force residuals (top). Model applied using strain-reduced shear wave velocities.

For context, it is useful to compare the results in Figures 11-12 with residuals obtained using a pseudo-static approach. For this comparison, M-O analyses were performed as presented in Koseki et al. (1998). Sand friction angles of 35 degrees were used with the peak acceleration of the recorded backfill surface motion (PGA) and 65% of that value. Figure 13 shows the resulting residuals. In many cases, the peak surface acceleration is large enough that ground failure is predicted along a horizontal surface at the base of the wall. The M-O method fails to predict a physically meaningful solution for earth pressure under this condition, and residuals cannot be computed (although it can be stated that they are negative and very large in amplitude). For those cases where residuals can be computed, summary statistics (mean and standard deviation of residuals) are provided in the Figure. The results show a much stronger overprediction bias of test data for both PGA levels, especially if the large negative residuals (which are not used in the mean or standard deviation calculations) are considered. Standard deviation terms are also much larger than with the proposed method, which is expected because of the lack of consideration of the principle physical factors that produce earth pressure. In contrast, the simulation results from Ostadan are underpredicted, which is due to a combination of relatively high normalized forces (associated with the fixed base condition and rigid walls) and the relatively stiff backfill materials (producing high de-normalized resultants); these effects are not considered in the Mononobe-Okabe method.
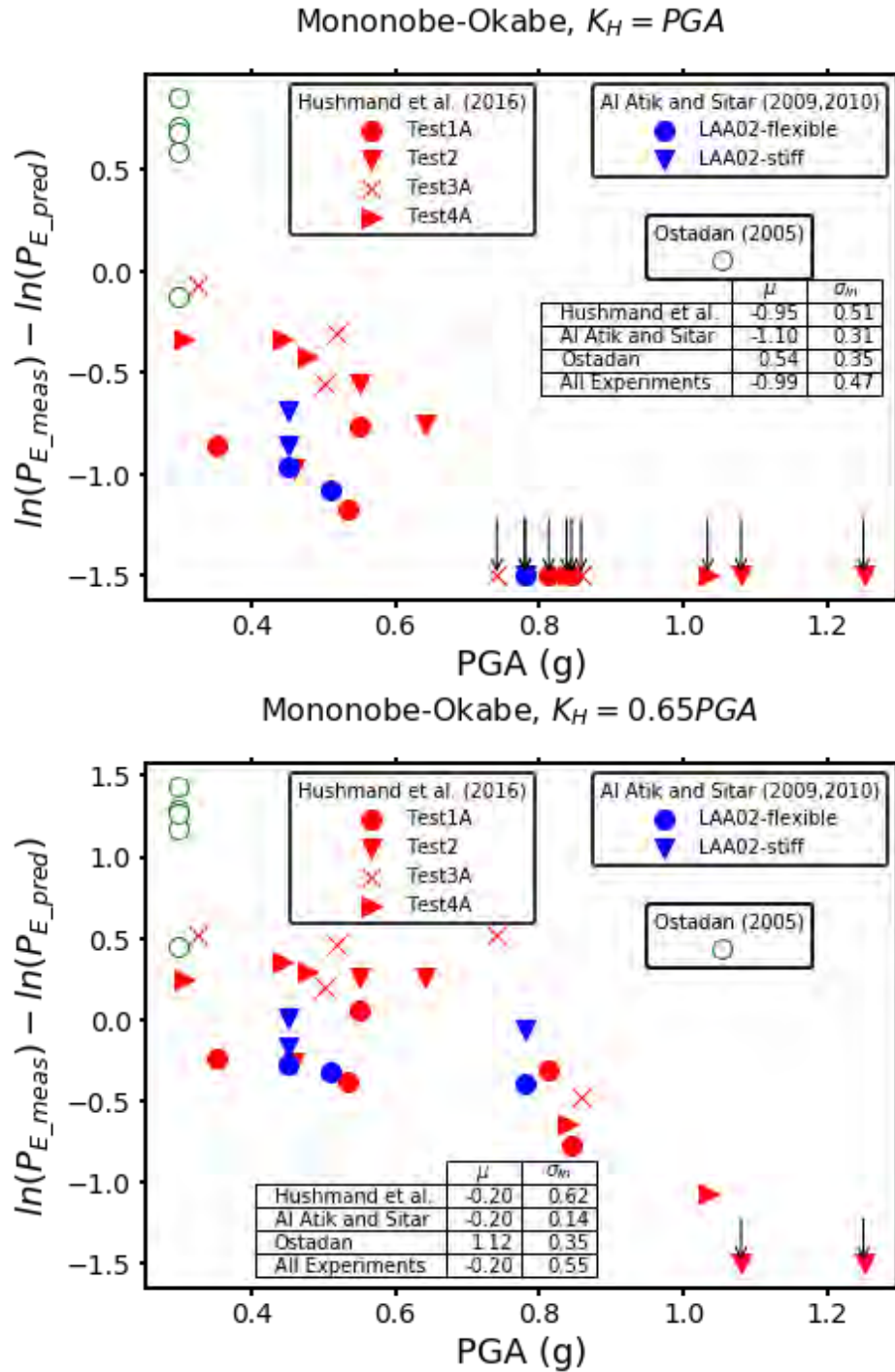
Figure 13 Residuals of predicted seismic earth pressure resultants computed using Mononobe-Okabe method as given by Koseki et al. (1998) with backfill accelerations taken using PGA and 0.65 PGA. Values marked with the arrow symbol have undefined (but very large and negative) resultant force predictions from the analysis.

RP4-6   EXAMPLE PROBLEM

To illustrate application of the proposed kinematic method, consider a free-standing wall of height $H = 9$ m retaining sand backfill soil with a relative density of about 50% (approximately 90% relative compaction from modified Proctor standard) and unit weight of 18 kN/m^3. For the purpose of defining the seismic hazard, location is taken as a site in downtown Los Angeles, CA.

The example problem follows the eight steps in the proposed method, which are described below:

Step 1 (seismic hazard): Seismic hazard analysis is performed using the UCERF3 source model-Poisson branch (Field et al. 2014) and the NGA-West2 ground motion models that have site terms for soil site conditions. We use the site location given in the heading of Figure 14, $V_{S30} = 400$ m/s, and default basin conditions. Hazard is computed using OpenSHA. The resulting mean hazard for PGV is shown in Figure 14. ASCE 7-16 uses risk-targeted maximum considered earthquake ground motions, which are defined for response spectral accelerations. Because risk-targeting procedures are not defined for the PGV intensity measure, we select the maximum considered earthquake (MCE) hazard level that preceded risk targeting, which is 2% probability of exceedance in 50 years. The resulting MCE PGV is 105 cm/s. If reduced by two-thirds for a design ground motion, the design PGV is 70 cm/s. This value is used in the example.
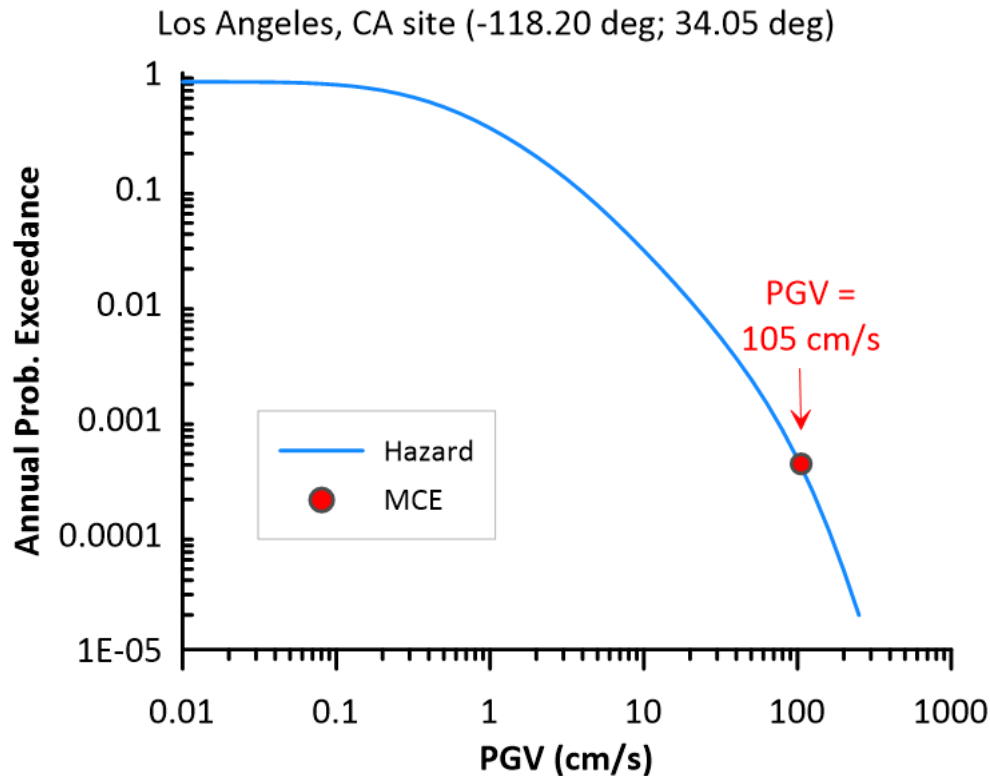
Figure 14 PGV mean hazard curve and selected MCE ground motion for hazard level of 2% probability of exceedance in 50 years

Step 2 (disaggregation and mean period): Seismic hazard is disaggregated at the MCE hazard level to identify controlling sources and the event magnitude and distance ranges that contribute most strongly to the computed ground motions. Results are shown in Figure 15, which also show epsilon (ε) levels that control hazard (i.e., the number of standard deviations above the mean). The mode of the distribution in Figure 15 is **M** 7.0 events in the 0-10 km rupture distance range, for which ε exceeds 0.5.
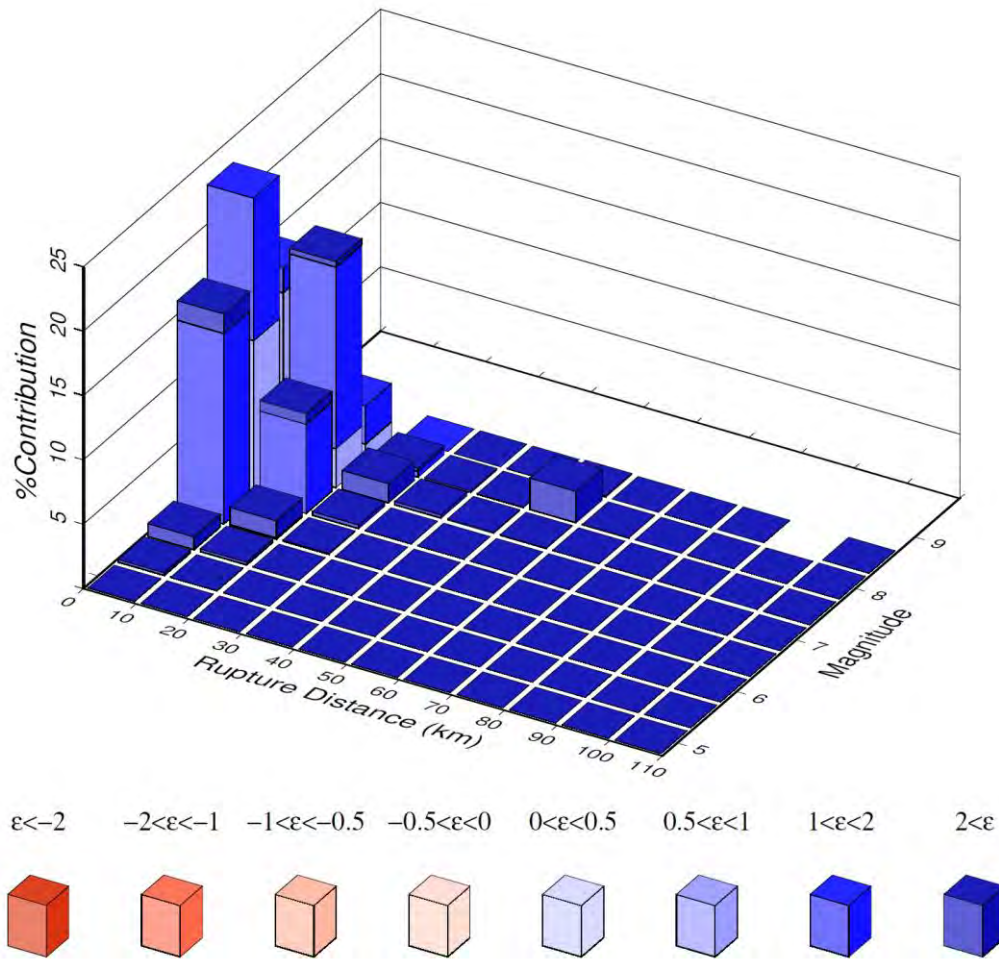
Figure 15 Disaggregation of PGV hazard at the MCE level.

Using **M** 7.0, R_{rup} = 5 km, and V_{S30} = 400 m/s, the median estimate of mean period (Figure 6; Rathje et al. 2004) is T_m = 0.49 sec, which is equivalent to angular frequency ω_m = 12.9 rad/sec.

Step 3 (V_S profile): We assume shear wave velocity has not been measured in the backfill. We use the V_S estimation procedure in Section C20.3 for sand (ASCE 7-22, proposed commentary; adapted from Brandenberg et al. 2010). We assume an equivalent overburden corrected blow count of $(N_1)_{60}$ = 15 blows/ft for sand backfill, which is roughly equivalent to 90% modified Proctor relative compaction. We convert to non-overburden corrected blow count using a total soil unit weight of 18 kN/m³. The resulting mean V_S profile, and the time-averaged velocity for a 9 m backfill height, are shown in Figure 16.
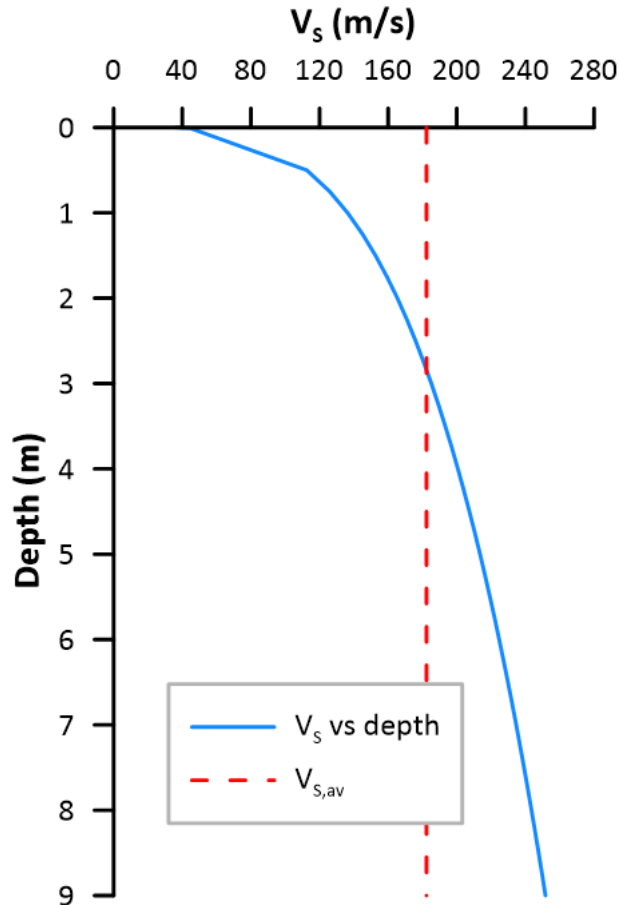
Figure 16. Shear wave velocity profile for 9 m backfill height and time-averaged value of $V_{S,av}$ = 182 m/s.

Step 4 (ground motion amplitude): Wavelength-to-height ratio is computed as $V_{S,av}T_m/H$= 9.8, from which amplitude factor f_u= 0.77 (Figure 7). Ground surface displacement amplitude is then estimated as $u_{g0} = f_u PGV/\omega_m$ = 0.042 m. The design-level PGV of 70 cm/s is used in this calculation.

Step 5 (stiffness intensity): Static stiffness intensity k_{y0}^i is computed using Eq. (5) as 2.0×10^4 kN/m²/m, using a mass density of 1830 kg/m³ and sand Poisson's ratio ν = 0.3.

Step 6 (βH): Dimensionless soil-to-wall stiffness ratio βH is taken as 1, 2, and 4 for this example calculation. For an application involving a specific wall cross section, β would be computed using Eq. (4).

Step 7 (Normalized force and resultant height): Using the wavelength-to-height ratio from Step 4 and the relative stiffness from Step 6, normalized forces and reaction heights for rigid walls (Eqs 1-2), flexibility modifiers (Eqs. 6-7), and normalized forces and reaction heights that account for wall flexibility are given in Table 2.

Table 2 Normalized forces and resultant heights for example problem with different wall flexibility effects.

	Rigid	βH=1	βH=2	βH=4
Normalized force	0.13	0.11	0.058	0.022
Wall flexibility factor, ξ	1.0	0.84	0.44	0.17
Normalized resultant height, h/H	0.625	0.54	0.32	0.15

Step 8 (De-normalize): De-normalization of wall reaction forces is applied by multiplying normalized forces by the product $u_{g0}k_{y0}^{i}H$. Results for the various cases of wall flexibility are shown in Table 3. Dimensional results are shown, as are ratios of $|P_E|$ to $0.5\gamma H^2$.

Table 3 De-normalized seismic reaction forces, and ratios of seismic to static forces, for example problem with different wall flexibility effects.

	Rigid	βH=1	βH=2	βH=4
De-normalized force, $|P_E|$ (kN/m)	965	810	430	160
$|P_E|/(0.5\gamma H^2)$	1.32	1.11	0.58	0.23

M-O pressure resultants can be compared to the results in Table 3. The MCE hazard for the example site is 0.95g, which provides a design ground motion of 0.63g. For backfill friction angles of 30 and 40 deg, respectively, M-O analyses as presented in Koseki et al. (1998) provide resultant dimensionless forces that are undetermined for a 30 deg friction angle and about 0.8 for a 36 deg friction angle.

RP4-7   CONCLUSIONS

Seismic earth pressures develop to varying degrees on retaining walls and other embedded structures depending on the amount of relative wall-soil displacement. Such relative displacements can develop as a result of kinematic or inertial soil-structure interaction mechanisms. This paper presents analysis methods that can be used to predict seismic earth pressures that are based on soil-structure interaction principles. These methods represent a substantial break from past practice in which earth pressures were derived using a pseudo-static horizontal force acting on a backfill soil wedge assumed to be at a failure state.

An engineer wishing to apply the proposed methods must first assess the degree to which external forces are likely to act on the wall. If such forces are likely, because the wall is integral to the lateral force resisting system of a structure, inertial interaction is likely to be the dominant mechanism, and such procedures should be used. If external forces are not expected, the problem can be analyzed using the kinematic method presented here. That method requires as input the results of seismic hazard analysis for peak velocity, deaggregation of the hazard, wall dimensions, and a measured or estimated shear wave velocity profile for the backfill materials.

The proposed inertial and kinematic interaction procedures have limitations. Among these are:

- The seismic excitation is simplified to a single frequency and amplitude.

- Soil layering is not considered (no strong impedance contrasts within the backfill)

- A simple planar wall is considered, without tiebacks or soil nails.

- A limit state based on soil shear failure is not explicitly included, but can be checked in an approximate manner.

Despite these limitations, the proposed method captures the principle mechanisms that produce kinematic seismic earth pressures, which are related to frequency content of input motions and the flexibility of the walls. The available experimental and simulation-based evidence demonstrate the

significance of those physical considerations, and the applicability of the proposed method for the conditions considered in the tests. Significantly, the proposed approach produces far better comparisons to observation than the M-O method.

RP4-8 REFERENCES

Al Atik, L and N Sitar, 2009. Experimental and analytical study of the seismic performance of retaining structures. *Rpt. No. PEER-2008/104*, Pacific Earthquake Engineering Research Center, UC Berkeley.

Al Atik, L and N Sitar, 2010. Seismic earth pressures on cantilever retaining structures, *J. Geotech. & Geoenv. Eng.*, 136 (10), 1324-1333.

Box, GEP, 1976, Science and statistics, *J American Statistical Association*, 71, 791–799.

Brandenberg, SJ, N Bellana, and T Shantz, 2010. Shear wave velocity as function of standard penetration test resistance and vertical effective stress at California bridge sites, *Soil Dynamics and Earthquake Engineering*, 30(10), 1026-1035.

Brandenberg SJ, G Mylonakis, JP Stewart, 2015. Kinematic framework for evaluating seismic earth pressures on retaining walls. *J. Geotech. Geoenviron. Eng.* 141(7), 04015031.

Brandenberg, SJ, G Mylonakis, JP Stewart, 2017. Approximate solution for seismic earth pressures on rigid walls retaining inhomogeneous elastic soil, *Soil Dyn. Earthquake Eng.*, 97, 468–477.

Chen, WF, 1975. *Limit analysis and soil plasticity. Developments in geotechnical engineering*. Elsevier, Amsterdam, The Netherlands.

Chen, WF and XL Liu, 1990. *Limit analysis in soil mechanics*. Elsevier, Amsterdam, The Netherlands.

Durante, MG, SJ Brandenberg, JP Stewart, G Mylonakis, 2018. Winkler stiffness intensity for flexible walls retaining inhomogeneous soil, in *Geotechnical Engineering and Soil Dynamics V: Numerical Modeling and Soil Structure Interaction*, June 10-13, 2018, Austin, TX, ASCE Geotechnical Special Publication No. 292, S.J. Brandenberg and M.T. Manzari (eds.), pp 473-482.

Field, EH, RJ Arrowsmith, GP Biasi, P Bird, TE Dawson, KR Felzer, DD Jackson, KM Johnson, TH Jordan, C Madden, AJ Michael, KR Milner, MT Page, T Parsons, PM Powers, BE Shaw, WR Thatcher, RJ Weldon II, and Y Zeng (2014). Uniform California earthquake rupture forecast, Version 3 (UCERF3)—The time-independent model, *Bull. Seism. Soc. Am.*, 104, 1122–1180.

Hushmand, A, S Dashti, C Davis, JS McCartney, B Hushmand, 2016. A centrifuge study of the influence of site response, relative stiffness, and kinematic constraints on the seismic performance of buried reservoir structures. *Soil Dyn. Earthquake Eng.* 88: 427-438.

Idriss, IM and JI Sun, 1992. SHAKE91: A computer program for conducting equivalent linear seismic response analyses of horizontally layered soil deposits, Users Guide, UC Davis.

Koseki, J, F Tatsuoka, Y Munaf, M Tateyama, and K Kojima, 1998. A modified procedure to evaluate active earth pressure at high seismic loads, *Soils and Foundations, Special Issue*, 209-216.

Mononobe, N and M Matsuo, 1929. On the determination of earth pressures during earthquakes. *Proc. World Engrg. Congress*, 9, 179–187.

Mylonakis, G, P Kloukinas, and C Papantonopoulos, 2007. An alternative to the Mononobe–Okabe equations for seismic earth pressures, *Soil Dyn. Earthquake Eng.*, 27, 957-969.

NIST, 2012. *Soil-structure interaction for building structures*, Report No. NIST GCR 12-917-21, National Institute of Standards and Technology, U.S. Department of Commerce, Washington

Novak, M, 1974. Dynamic stiffness and damping of piles, *Can. Geotech. J.*, 11, 574-598.

Okabe, S 1926. General theory of earth pressure and seismic stability of retaining wall and dam. *J. Japanese Society of Civil Engineering,* 12 (4), 34-41.

Ostadan F, 2005, Seismic soil pressure for building walls – an updated approach, *Soil Dyn. Earthquake Eng.*, 25, 785-793.

Palmer, MC, TD O'Rourke, NA Olson, and T Abdoun, 2009. Tactile pressure sensors for soil-structure interaction assessment, *J. Geotech. Geoenviron. Eng.*, 135(11), 1638-1645.

Rathje, EM, F Faraj, S Russell, and JD Bray, 2004. Empirical relationships for frequency content parameters of earthquake ground motions, *Earthquake Spectra*, 20 (1), 119-144.

Richardt, R and D Elms, 1979. Seismic behavior of gravity retaining walls, *J. Geotech. Eng. Div.*, ASCE, 105(4), 449-464.

Seed, HB and RV Whitman, 1970. Design of earth retaining structures for dynamic loads. *Proc., ASCE Specialty Conf. on Lateral Stresses in the Ground and Design of Earth Retaining Structures*, Vol. 1, pp. 103-147, Cornell Univ., Ithaca, NY.

Steedman, RS and X Zeng, 1990. The influence of phase on the calculation of pseudo-static earth pressure on a retaining wall. *Geotechnique*, 40(1), 103-112.

Veletsos AS and AH Younan, 1994. Dynamic soil pressures on rigid retaining walls. *Earthquake Eng. Struct. Dyn.*, 23 (3), 275-301.

Vrettos C, DE Beskos, T Triantafyllidis, 2016. Seismic pressures on rigid cantilever walls retaining elastic continuously non-homogeneous soil: An exact solution. *Soil Dyn. Earthquake Eng*, 82, 142-153.

Wagner, N and N Sitar, 2016. On seismic response of stiff and flexible retaining structures. *Soil Dyn. Earthquake Eng.* 91, 284-293.

Wood, JH, 1973. Earthquake induced soil pressures on structures, *Report No. EERL 73-05*, California Institute of Technology, Pasadena, CA.

Xu, SY, A Shamsabadi, E Taciroglu, 2015. Evaluation of active and passive seismic earth pressures considering internal friction and cohesion, *Soil Dyn. Earthquake Eng.*, 70, 30-47.

RESOURCE PAPER 5 SEISMIC DESIGN STORY DRIFT PROVISIONS – CURRENT QUESTIONS AND NEEDED STUDIES

RP5-1   INTRODUCTION

During the 2020 NEHRP update cycle, a series of proposals was considered by the Provisions Update Committee, intending to revise ASCE 7 (ASCE, 2017) methods for calculating design story drift. These proposals would have required that drifts calculated at strength level seismic forces be amplified by the ASCE 7 Table 12.2-1 R-factor for the applicable system, rather than the C_d factor. This concept was incorporated into a series of change proposals, each addressing a different ASCE 7 limitation related to design story drift; the provisions that would have been affected are discussed in Section RP5-3 of this paper. During discussion of these proposals the question arose as to whether or not current ASCE 7 provisions and C_d factors reasonably estimate design story drift (at design earthquake, two-thirds MCE_R). This question in turn led to an effort to collect available information from numerical studies and testing. During this process it was realized that definitively answering this question was a larger and more complicated effort than could be achieved within the NEHRP Provisions update cycle.

This resource paper has been developed by a sub-group of Issue Team 2 with the intent to document the questions that arose regarding calculation of design story drift, relevant background information, and analysis and testing information found to be available during the update cycle. In addition and most importantly, this resource paper recommends further steps needed in order to determine whether a change in calculation of design story drift is warranted. Section RP5-2 of this resource paper provides background, including a brief history of calculation of design story drift, viewpoints on this issue, and resulting questions. Section RP5-3 of this resource paper summarizes current ASCE 7 provisions addressing estimation of drift and drift limits. Section RP5-4 of this resource paper discusses the sources of information identified, initial indications from this data, and identified limitations to the data. Section RP5-5 of this resource paper contains recommended next steps. This documentation is being provided to support future studies in this area.

RP5-2   BACKGROUND

The calculation of the current ASCE 7 design story drifts was first introduced in the *Tentative Provisions for the Development of Seismic Regulations for Buildings (ATC 3-10/ NBS 510/ NSF 78-8)* (ATC, 1978). This publication introduced the C_d deflection amplification factor and provided both R and C_d factors for each listed seismic force-resisting system, very similar to the current ASCE 7. The commentary to this document, however, does not provide background on the development of listed C_d factors. The inclusion of C_d factors continued in the *NEHRP Recommended Provisions for the Development of Seismic Regulations for New Buildings* (FEMA, various) that evolved from ATC 3-06.

The same concept of amplifying the design level drift was first brought into the Uniform Building Code (UBC) (ICBO, 1997) in the 1997 Edition as part of a correlation effort between the UBC seismic provisions and the most current NEHRP Provisions. This replaced calculation of drift at ASD or strength level design forces without amplification, required in previous UBC editions. Commentary documenting inclusion of deflection amplification factors in the UBC can be found in Sections 105.9 and C105.9 of the 1999 SEAOC *Recommended Lateral Force Requirements and Commentary* (SEAOC, 1999). Similar to the 1997 UBC recognition of anticipated seismic forces using Ω_0 factors, the intent was to require explicit determination of the anticipated building drift. The story drift at design level seismic forces was calculated as the drift at design level seismic forces times 0.7R. The equation is noted in the SEAOC publication to provide "…a reasonable approximation of the maximum inelastic response displacement for regular buildings. This relation is based on the accumulated research of the past 30 years and on the intent (for the present time) to maintain parity with previous drift limitation requirements." The SEAOC publication goes on to cite studies

by Miranda and Bertero (1994) that indicate a range of inelastic drifts can be expected, varying by building type. It notes that the value 0.7R was selected as an average representation of the inelastic drift.

The International Building Code (IBC) included the C_d parameter, rather than the 0.7R factor used in the UBC. For several of the listed seismic force-resisting systems, the C_d and 0.7R values are approximately equal, while for several others C_d is close to or equal to 1.0R. Since the development of the 1997 UBC, additional testing and analytical studies have become available and have emphasized the approximate nature of this calculation method, and the many characteristics of buildings that can cause variation.

The impetus for the 2020 NEHRP update cycle proposed changes from currently tabulated C_d factors to factors equal to R is rooted in the widely recognized "equal displacement rule," (or Newmark Rule) whereby, for elastic-plastic (bi-linear or tri-linear) single degree of freedom models, the peak inelastic drift can roughly be expected to equal the computed elastic drift multiplied by the reduction factor used to compute the design forces for linear analysis (the R-factor). Studies such as FEMA 440 (FEMA, 2005) and NIST GCR 12-917-20 (NIST, 2012) have demonstrated that peak drift computed from a nonlinear analysis of a multi-degree of freedom system is not dependent on a single factor for each type of structural system. Instead it depends on the fundamental period of the structure, type of structural system, higher mode effects, the inherent damping of the seismic force resisting system and non-structural components (e.g. cladding), site conditions, the response of the foundation system including soil-structure interaction (SSI) effects, the characteristics of the ground motion (i.e. spectral intensity, duration), and in-cycle degradation of the seismic force resisting system. Taken collectively, the amplification factors derived in these studies suggest that C_d should at least equal R for long period structures and greater than R for short period structures. The results of these studies collectively suggest that the C_d factors found in ASCE 7 underestimate true peak inelastic displacements, as shown in Figure 1 (FEMA P695 Figure 1.1), and should be modified to provide a better estimate of inelastic displacements.
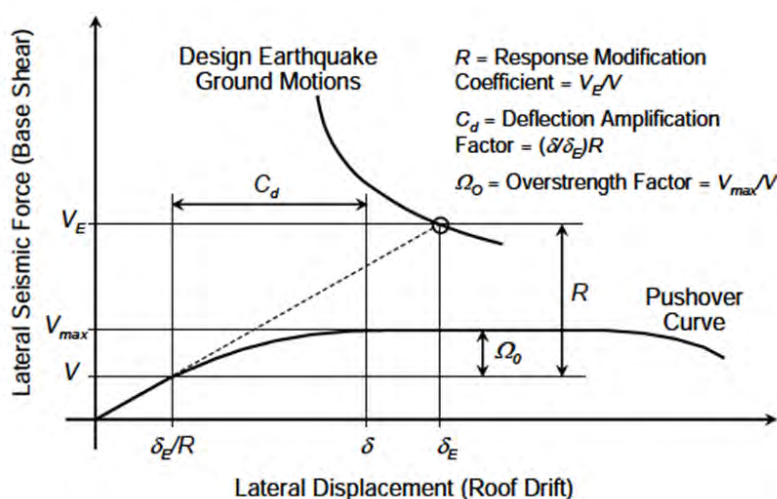
FIGURE 1 Illustration of seismic performance factors (R, Ω_0, C_d) as defined in the Commentary to the NEHRP Recommended Provisions (FEMA P695).

An alternate viewpoint looks at the methods by which design earthquake drifts are actually calculated across different materials and representative layouts of seismic force-resisting systems. This viewpoint recognizes that studies like FEMA 440 are primarily founded on analyses of single and multi-degree-of-freedom systems where the hysteretic behavior of the system is modeled to be bi or tri-linear. "Real" structural behavior, particularly with respect to when the structural system "yields", is much more complicated than these models assume. This view point also recognizes that while the Newmark Rule was

based on amplification of an elastic drift, current material design standard methods for calculating story drift at strength level seismic forces are based on elastic response for some materials (e.g. steel structures), but incorporate inelastic response for other materials (e.g. light-frame shear wall systems and concrete structures).

From the data collected, as discussed in Section RP5-4, it can be seen that modeled non-linear displacements of representative structural designs and full scale shake table tests are widely varying and not consistent with Figure 1. In this case, the question of whether ASCE 7 provisions are currently adequately estimating design story drift is best determined by comparing estimates of drift from design calculations with available predictions of drift from nonlinear response-history analysis (NLRHA) and testing.

Another related point of discussion is whether it is most appropriate to be imposing drift limitations at the design earthquake (DE, two-thirds MCE_R), or if MCE_R is the real seismic level of interest. Contributing to this question is a concern that the drift increase between DE and MCE_R might be significantly larger than the factor of 1.5 increase in force level because significant degradation can occur in some seismic force-resisting systems at MCE_R level ground motions. This has led to an interest in studying mean drift levels at MCE_R, in addition to DE, in order to better quantify their relationship.

Another point of discussion that came up during the process of collecting data is whether it might be appropriate to vary the C_d factor by story level. This was in part due to a repeated pattern of drift ratio variation over the height of a building.

RP5-3   CURRENT SEISMIC DESIGN PROVISIONS

Thirty-two ASCE 7 seismic design provisions were identified as addressing either determination of design story drift or related limitations imposed in the process of seismic design. Full details of the 32 provisions can be found in Table A-1. While the approximate nature of calculated seismic deflections and design story drifts is understood, the impact of significantly under-estimating or over-estimating of drifts can vary.

Of most significant and understandable concern is the calculation of displacement demand on bridges and other structural elements that span between structures. These elements could lose gravity support and fall if design story drifts are significantly underestimated. Section 12.12.4 of ASCE 7-16 requires that drifts be magnified by 1.5 to account for the difference between the DE and MCE_R, and requires that the drifts be further amplified by R/C_d.

Also of significant concern is the comparison of design story drifts with the ability of gravity systems to carry gravity load at those drifts; underestimation of design story drifts could lead to partial or global collapse.

The level of concern is less clear for calculation of building separations required for independent response of adjoining buildings, as pounding is not always an adverse behavior. As a result, the level of concern in exceeding the ASCE 7 Table 12.12-1 allowable story drifts is not clear. Given all of the other checks on drift that occur in ASCE 7 at this time, the purpose served by these limits is not clear.

A number of additional provisions address design of various nonstructural components in structures. With the range of drift-based requirements, and the significant concern for several of them, it may seem best to err on the conservative side and plan to overestimate design story drifts. Overestimation could have a significant affect, however, on the ability to build with the systems that currently have seismic design controlled by drift (i.e. design needs to be increased above minimum strength requirements in order to meet drift requirements), as well as broadening the groups of systems and structures that would be drift controlled. The range of permitted sizes and configurations of structures could be significantly reduced from current practice, and designers using such systems will look for confirmation that further limits are necessary. One of the systems types that is likely to be affected is light frame construction (wood or cold-

formed steel) where lower stories in multi-story buildings are often drift controlled. For this reason, adequate study of the need for revision to current design story drift requirements is suggested.

RP5-4   INITIAL DATA COLLECTION DURING THE 2020 NEHRP UPDATE CYCLE

Data sets that were identified as being available during the 2020 update cycle included the following:

- Numerical studies using NLRHA of one- to four-story wood light-frame shear wall buildings, as part of analytical studies of wood-frame structures for the ATC project titled "Solutions to the Issues of Short-Period Building Seismic Performance" (ATC-116 Project) (ATC,2017).
- NLRHA models developed by Magnusson Klemencic Associates for design of new structures:
  - Composite BRBF, 240 feet
  - Composite SMF, 240 feet
  - BRBF, 240 feet
  - Concrete Shear wall, 400 feet
- NLRHA models developed by Degenkolb Engineers for design of new buildings:
  - SMRF
  - BRBF
  - Concrete Shear Wall
- NLRHA numerical studies of steel special moment frame structures conducted by NIST as part of a study to benchmark ASCE 41 performance-based design methodologies against code provisions used for design of new buildings (NIST Technical Notes 1863-1, 1863-2, 2015):
  - SMF, ELF, 8 stories
  - SMF, RSA, 8 stories
- Testing of a cold-formed steel structure conducted by Ben Schafer et al. as part of the NEES funded CFS-NEES project titled "Advancing Cold-Formed Steel Earthquake Engineering."
  - CFS shear wall building, 2 stories
- NLRHA numerical studies of steel concentric braced frames from Hsiao, Lehman and Roeder (2013).
  - SCBF, 3 stories
  - SCBF, 9 stories
  - SCBF, 20 stories
- NLRHA numerical studies of reinforced concrete shear wall structures featuring new modeling methods to capture strength losses (Lehman, Lowes and Marifi, publication pending).
  - 6, 8 and 12 stories
- NLRHA numerical studies of ductile coupled concrete shear wall structures (Tauberg et al., 2019).
- NLRHA numerical studies of special coupled steel plate shear wall structures (Kizilarslan et al., 2018, 2019).

Information available varied in type and level of detail, and the modeling approaches and assumptions were not scrutinized. For these reasons it was decided to not draw more than very initial observations from the data group. Instead, a more detailed study is recommended. Selected portions of information collected are summarized in spread sheet form in Tables B-1 to B-4.

The initial observations indicated no clear trend from the data collected. The data from the steel moment frame and steel concentrically braced frame examples (NIST 2015a, 2015b) generally suggests that the peak inelastic displacements should be larger than computed based on elastic displacement and currently defined C_d factors. However, these results need to be viewed with the qualification that many of these models recorded very high drifts and had experienced significant damage and degradation suggesting

that they were near or beyond collapse. As a result, further review of these models is needed before conclusions are drawn from them.

Light framed structures generally demonstrated the opposite (based on data from ATC, 2017), and suggest that the peak non-linear displacements should be substantially smaller than the computed design story drift. One rationale for this observation is that these types of structures are highly non-linear at very low levels of displacement. The strength-level displacement that is computed involves factors like nail slip that are inherently non-linear at small displacements; such that calculation of an elastic stiffness is not possible. Because of this, design story drifts calculated using a secant stiffness and then amplified by C_d can significantly over estimate those seen in analytical studies. Also to be considered in wood light-frame studies is the significant difference in reported peak drifts between analytical models that include exterior and interior wall finish materials (gypsum wallboard, stucco, etc.) and those that do not.

RP5-5   RECOMMENDED FURTHER STEPS

It is recommended that a definitive set of data be collected by which the adequacy of current ASCE 7 provisions for estimation of design story drift can be judged. Once the data is collected, this can serve as a technical basis from which to evaluate whether or not there is a driving need to change to the way drifts are estimated using current code procedures. The exact basis of such decisions will need to be made by those conducting the further study and based on knowledge gained from the collected data.

NLRHA data remains the most widely available source of information, supplemented by data from a limited number of full-scale tests. For each structure for which data will be used, sufficient information is needed to review in some detail the design process and resulting estimation of drift and the NLRHA or test data in order to verify it is appropriate to include in the data set. Further, it is found that most NLRHA studies available were focused on behavior at MCE_R more than DE. As a result, it is believed that additional post-processing of data will be needed to extract DE information in addition to MCE_R. Further, the data sets available did not necessarily have individual story data. In some cases roof drifts were the only data point available. It would be of value in these cases to collect individual story drift in addition to roof drift.

The following are identified as information to be collected:

General Information

    Material

    Seismic Force Resisting System

    Number of stories

    Roof height above base

Seismic Design Information

    S_{DS}, S_{D1}

    T_a

    $C_u T_a$

    Response Modification Factor, R

    Base Shear and analysis approach (ELF, MRSA, etc.)

    Base Shear Coefficient

    Strength level calculated story drifts (per story)

    C_d

    Design Story Drift using C_d

Numerical Model Information

Model Period X and Y direction

Model Period Type (initial or effective at DE)

DE predicted mean story drifts

DE predicted mean roof drift

MCE_R predicted mean story drifts

MCE_R predicted roof drift

It is understood that fully detailed outputs of NLRHA results are not commonly retained due to the large volume of the data. For this reason it is anticipated that future data collection will entail rerunning of analyses using the already developed models and extracting of relevant data.

Data from instrumented buildings that experienced ground shaking at levels near DE or higher would also provide valuable information.

In the process of studying these changes, consideration might potentially also be given to other fundamental changes that are suggested by studies such as NIST GCR 12-917-20, including explicit analysis at the MCE_R versus the DE, period-dependent R-factors, and recalibration of the R-factors and height limits in ASCE 7 Table 12.2-1.

RP5-6   REFERENCES

ATC, 1978. *Tentative Provisions for the Development of Seismic Regulations for Buildings (ATC 3-06, NBS 510, NSF 78-8)*, Applied Technology Council, Redwood City, CA.

ASCE, 2017. *Minimum Design Loads and Associated Criteria for Buildings and Other Structures*, 2016 Edition (ASCE7-16), American Society of Civil Engineers, Reston, VA.

ATC, 2017. *Developing Solutions to the Short-Period building Performance Paradox: Study for Wood Light-Frame Buildings*, Workshop Draft - 2017, Applied Technology Council, Redwood City, CA.

FEMA, 2005. *Improvement of Nonlinear Static Seismic Analysis Procedures* (FEMA 440). Federal Emergency Management Agency, Washington, DC.

FEMA, 2009. *Quantification of Building Seismic Performance Factors* (FEMA P-695), Federal Emergency Management Agency, Washington, DC.

Hsiao, Lehman and Roeder, 2013. "Evaluation of the response modification coefficient and collapse potential of special concentrically braced frames," Earthquake Engineering and Structural Dynamics (42:1547-1564), International Association of Earthquake Engineering, X, X.

Kizilarslan, E., Seo, J., Broberg, M., Shafaei, S., Varma, A.H., Bruneau, M., (2018). ―R-Factors for Coupled Composite Plate Shear Walls—Concrete Filled (Coupled-C-PSW/CF), Interim Project Report #2, Submitted to the Charles Pankow Foundation for CPF research grant #06-16.

Kizilarslan, E., Seo, J., Broberg, M., Shafaei, S., Varma, A.H., Bruneau, M., (2019). ―Seismic Design Coefficients and Factors for Coupled Composite Plate Shear Walls—Concrete Filled (Coupled-C-PSW/CF), to be published.

NIST, 2012. *Tentative Framework for Development of Advanced Seismic Design Criteria for New Buildings* (NIST GCR 12-917-20), National Institute of Standards and Technology, Gaithersburg, MD.

NIST, 2015a. *Assessment of First Generation Performance-Based Seismic Design Methodologies for New Steel Buildings, Volume 1: Special Moment Frames* (Technical Note 1863-1), National Institute of Standards and Technology, Gaithersburg, MD.

NIST, 2015b. *Assessment of First Generation Performance-Based Seismic Design Methodologies for New Steel Buildings, Volume 1: Special Concentrically Braced Frames* (Technical Note 1863-2), National Institute of Standards and Technology, Gaithersburg, MD.

ICBO, 1997. *Uniform Building Code*, 1997 Edition, International Conference of Building Officials, Whittier, CA.

SEAOC, 1999. *Recommended Lateral Force Requirements and Commentary, 1999 Edition* (SEAOC Bluebook), Structural Engineers Association of California, Sacramento, CA.

Miranda and Bertero, 1994. "Evolution of Strength Reduction Factors for Earthquake-Resistant Design," *Earthquake Spectra, Vol 10, No.2*, Earthquake Engineering Research Institute, Oakland, Ca.

Tauberg, N.A., Kolozvari, K., and Wallace, J.W. (2019). "Ductile Reinforced Concrete Coupled Walls: P695 Study". Draft Final Report (90%), Report No. *SEERL 2019-XX*, University of California, Los Angeles, Department of Civil and Environmental Engineering, 106pp.

Table A-1 Seismic Design Story Drift Related Provisions in ASCE 7-16

Section	Topic	Provision	Comments
2.12.1	Story Drift Limit	The design story drift (Δ) as determined in Sections 12.8.6, 12.9.1, or 12.9.2 shall not exceed the allowable story drift (Δ_a) as obtained from Table 12.12-1 for any story.	If C_d were modified without modifying Table 12.12-1, drift controlled systems would be required to be designed with a higher effective base shear.
12.12.3	Structural Separation	All portions of the structure shall be designed and constructed to act as an integral unit in resisting seismic forces unless separated structurally by a distance sufficient to avoid damaging contact as set forth in this section. Separations shall allow for the maximum inelastic response displacement (δ_M). δ_M shall be determined at critical locations with consideration for translational and torsional displacements of the structure including torsional amplifications, where applicable, using the following equation: $$\delta_M = \frac{C_d \delta_{max}}{I_e} \quad (12.12\text{-}1)$$ where δ_{max} = maximum elastic displacement at the critical location. Adjacent structures on the same property shall be separated by at least δ_{MT}, determined as follows: $$\delta_{MT} = \sqrt{(\delta_{M1})^2 + (\delta_{M2})^2}$$ $$(12.12\text{-}2)$$ where δ_{M1} and δ_{M2} are the maximum inelastic response displacements of the adjacent structures at their adjacent edges. Where a structure adjoins a property line not common to a public way, the structure shall be set back from the property line by at least the displacement δ_M of that structure. EXCEPTION: Smaller separations or property line setbacks are permitted where justified by rational analysis based on inelastic response to design ground motions.	The effect of the $C_d = R$ proposal would be to increase the structural separation and require larger offsets from property lines in buildings comprised of many seismic force-resisting systems. There are inherent inconsistencies with regard to the purpose of the building code in this structural separation provision. For one, this provision provides more reliability against a building drifting beyond the property line than it does for protecting adjacent buildings from pounding by allowing the sum root square on displacements for adjacent buildings. From the perspective of safety and collapse reliability, there is no rational reason to allow the sum root square on displacement. Furthermore, this provision protects buildings from contacting one another in the design basis earthquake and not the MCE$_R$. If we are to believe that building pounding is a collapse hazard and are to believe that the intent of the code is to prevent collapse at the MCE$_R$, then the MCE$_R$ drifts should be considered explicitly. The reality is that building pounding is not necessarily a collapse hazard, and quite often is not a significant concern. It would be entirely possible to compile a list of prescriptive requirements that would exempt buildings from the offset requirements. However, given how political this issue would be, to suggest a code change proposal without research would be imprudent. This important issue warrants further study. However, in the interim, there is no rational reason why we should be providing significantly more reliability of buildings with certain systems from pounding (those with C_d/R ratios near 1), than others. Consequently, while the effect of making $C_d = R$ with respect to structural separations is

Section	Topic	Provision	Comments
			significant, it would be warranted if and where supported by collected data.
12.12.4	Members Spanning Between Structures	Gravity connections or supports for members spanning between structures or seismically separate portions of structures shall be designed for the maximum anticipated relative displacements. These displacements shall be calculated as follows: 1. Using the deflection calculated at the locations of support, per Eq. (12.8-15) multiplied by $1.5R/C_d$, 2. Considering additional deflection caused by diaphragm rotation including the torsional amplification factor calculated per Section 12.8.4.3 where either structure is torsionally irregular, 3. Considering diaphragm deformations, and 4. Assuming that the two structures are moving in opposite directions and using the absolute sum of the displacements.	This provision currently requires that C_d equal R and requires that the building drift be multiplied by the ratio of R/C_d. This provision also recognizes that the code intends to protect against collapse at the MCER by requiring the drifts be multiplied by 1.5. Consequently, this provision would be modified should Cd be set equal to R by simply not requiring drifts be multiplied by R/C_d. The implication of this provision is that members spanning between adjacent structures do not have (or are not connected in a way that possesses) any reliable inherent ductility, and recognizes the consequence of these elements failing. This provision is an important point of comparison with respect to other provisions that are affected by building drift.

Section	Topic	Provision	Comments
12.12.5	Deformation Compatibility for Seismic Design Categories D through F	For structures assigned to Seismic Design Category D, E, or F, every structural component not included in the seismic force-resisting system in the direction under consideration shall be designed to be adequate for the gravity load effects and the seismic forces resulting from displacement caused by the design story drift (Δ) as determined in accordance with Section 12.8.6 (see also Section 12.12.1). EXCEPTION: Reinforced concrete frame members not designed as part of the seismic force-resisting system shall comply with Section 18.14 of ACI 318. Where determining the moments and shears induced in components that are not included in the seismic force-resisting system in the direction under consideration, the stiffening effects of adjoining rigid structural and nonstructural elements shall be considered, and a rational value of member and restraint stiffness shall be used.	The effect of the $C_d = R$ proposal would be to increase the drift at which deformation compatibility is checked in buildings comprised of many seismic force-resisting systems. Because elements not designed as part of the seismic force-resisting system are largely designed independently of the seismic force-resisting system, there is no rational reason why, should collected data warrant assignment of $C_d = R$, these elements and connections would be designed with more reliability in buildings with systems with C_d/R ratios close to 1 than in other buildings Given that deformation compatibility is not assessed at the MCER, the implication of this provision is that components that are not part of the seismic force-resisting system possess inherent ductility. While this is certainly almost always the case, especially for elements and connections detailed to today's material standards, this is an important point of comparison with respect to other provisions that are affected by building drift.
13.1.7	Reference Documents	Where a reference document provides a basis for the earthquake-resistant design of a particular type of nonstructural component, that document is permitted to be used, subject to the approval of the Authority Having Jurisdiction and the following conditions: 1. The design earthquake forces shall not be less than those determined in accordance with Section 13.3.1. 2. Each nonstructural component's seismic interactions with all other connected components and with the supporting structure shall be accounted for in the design. The component shall accommodate drifts, deflections, and relative displacements determined in accordance with the applicable	The effect of the $C_d = R$ proposal would be to increase the drift at which interactions discussed in Item 2 are checked

Section	Topic	Provision	Comments
		seismic requirements of this standard. 3. Nonstructural component anchorage requirements shall not be less than those specified in Section 13.4	
13.1.8	Reference Documents Using Allowable Stress Design	The component shall also accommodate the relative displacements specified in Section 13.3.2.	The effect of the $C_d = R$ proposal would be to increase the seismic relative displacement in most cases, assuming the drift limits are revised to reflect the higher design drifts.
13.3.2	Seismic Relative Displacements	Procedures for determining seismic relative displacements, D_p, within and between structures. D_p is a function of either the design story drift, which is a function of C_d, or the story drift limit, which is not.	The effect of the $C_d = R$ proposal would be to increase the seismic relative displacement in most cases, assuming the drift limits are revised to reflect the higher design drifts.
13.5.2	Forces and Displacements (Architectural Components)	Architectural components that could pose a life-safety hazard shall be designed to accommodate the seismic relative displacement requirements of Section 13.3.2. Architectural components shall be designed considering vertical deflection caused by joint rotation of cantilever structural members.	The effect of the $C_d = R$ proposal would be to increase the seismic relative displacement in most cases, assuming the drift limits are revised to reflect the higher design drifts.
13.5.3	Exterior Nonstructural Wall Elements and Connections	Exterior nonstructural wall panels or elements that are attached to or enclose the structure shall be designed to accommodate the seismic relative displacements defined in Section 13.3.2 and movements caused by temperature changes. Such elements shall be supported by means of positive and direct structural supports or by mechanical connections and fasteners in accordance with the following requirements: 1. Connections and panel joints shall allow for the story drift caused by relative seismic displacements (D_{pl}) determined in Section 13.3.2, or 0.5 in. (13 mm), whichever is greater. 2. Connections accommodating story drift through sliding mechanisms or	The effect of the $C_d = R$ proposal would be to increase the seismic relative displacement in most cases, assuming the drift limits are revised to reflect the higher design drifts since designers have the option to design to the drift limits rather than the design drift.

Section	Topic	Provision	Comments
		bending of threaded steel rods shall satisfy the following: a. Threaded rods or bolts shall be fabricated of low-carbon or stainless steel. Where cold-worked carbon steel threaded rods are used, the rods as fabricated shall meet or exceed the reduction of area, elongation, and tensile strength requirements of ASTM F1554, Grade 36. Grade 55 rods shall also be permitted provided that they meet the requirements of Supplement 1; and b. Where threaded rods connecting the panel to the supports are used in connections using slotted or oversize holes, the rods shall have length to diameter ratios of 4 or less, where the length is the clear distance between the nuts or threaded plates. The slots or oversized holes shall be proportioned to accommodate the full in-plane design story drift in each direction, the nuts shall be installed finger-tight, and a positive means to prevent the nut from backing off shall be used; and c. Connections that accommodate story drift by bending of threaded rods shall satisfy Eq. (13.5-1): $$(L/d)/D_{pl} \geq 6.0 \ [1/\text{in.}]$$	
13.5.4	Glass	Glass in glazed curtain walls and storefronts shall be designed and installed to accommodate without breakage or dislodgement the relative displacement requirement of Section 13.5.9. Where glass is secured to the window system framing by means of structural sealant glazing, the requirements contained in the reference standards listed in Table 13.5-2 shall also apply.	The effect of the $C_d = R$ proposal would be to increase the seismic relative displacement in most cases, assuming the drift limits are revised to reflect the higher design drifts since designers have the option to design to the drift limits rather than the design drift.
13.5.5	Out-of-Plane Bending (Architectural Components)	Transverse or out-of-plane bending or deformation of a component or system that is subjected to forces as determined in Section 13.5.2 shall not exceed the deflection capability of the component or system.	Depending on the configuration of the component, the effect of the $C_d = R$ proposal would be to increase the seismic relative displacement, assuming the drift limits are revised to reflect the higher design drifts since designers have the option to design to the drift limits rather than the design drift.

Section	Topic	Provision	Comments
13.5.9	Glass in Glazed Curtain Walls, Glazed Storefronts, and Glazed Partitions	Glass in glazed curtain walls, glazed storefronts, and glazed partitions shall meet the relative displacement requirement of Eq. (13.5-2): $$\Delta_{fallout} \geq 1.25\ D_{pl}$$	The effect of the $C_d = R$ proposal would be to increase the seismic relative displacement in most cases, assuming the drift limits are revised to reflect the higher design drifts since designers have the option to design to the drift limits rather than the design drift.
13.5.10	Egress Stairs and Ramps	Egress stairs and ramps not part of the seismic force-resisting system of the structure to which they are attached shall be detailed to accommodate the seismic relative displacements, D_{pl}, defined in Section 13.3.2 including diaphragm deformation. The net relative displacement shall be assumed to occur in any horizontal direction. Such elements shall be supported by means of positive and direct structural supports or by mechanical connections and fasteners in accordance with the following requirements: a. Sliding connections with slotted or oversize holes, sliding bearing supports with keeper assemblies or end stops, and connections that permit movement by deformation of metal attachments, shall accommodate a displacement , but not less than 0.5 in. (13 mm), without loss of vertical support or inducement of displacement-related compression forces in the stair. b. Sliding bearing supports without keeper assemblies or end stops shall be designed to accommodate a displacement, but not less than 1.0 in. (25 mm) without loss of vertical support. Breakaway restraints are permitted if their failure does not lead to loss of vertical support. c. Metal supports shall be designed with rotation capacity to accommodate seismic relative displacements as defined in item b. The strength of such metal supports shall not be limited by bolt shear, weld fracture, or other brittle modes. d. All fasteners and attachments such as bolts, inserts, welds, dowels, and anchors shall be designed for the	This provision requires that C_d be closer to R and requires that the building drift be multiplied by 1.5 for certain types of connections. It requires ductile connections to the structure or increased bearing lengths for stairs, and increases lateral forces for stairs that are not provided with ductile or sliding connections by a factor of at least 2.5.

Section	Topic	Provision	Comments
		seismic design forces determined in accordance with Section 13.3.1 with R_p, a_p, and Ω_0 as given in Table 13.5-1. EXCEPTION: If sliding or ductile connections are not provided to accommodate seismic relative displacements, the stiffness and strength of the stair or ramp structure shall be included in the building structural model of Section 12.7.3, and the stair shall be designed with Ω_0 corresponding to the seismic force-resisting system but not less than 2-one-half.	

Section	Topic	Provision	Comments
13.6.2	Mechanical Components	HVACR ductwork shall meet the requirements of Section 13.6.6. Piping systems shall meet the requirements of Section 13.6.7. Boilers and vessels shall meet the requirements of Section 13.6.10. Elevators shall meet the requirements of Section 13.6.11. All other mechanical components shall meet the requirements of Section 13.6.13. Mechanical components with I_p greater than 1.0 shall be designed for the seismic forces and relative displacements defined in Sections 13.3.1 and 13.3.2 and shall satisfy the following additional requirements: Provision shall be made to eliminate seismic impact for components vulnerable to impact, for components constructed of nonductile materials, and in cases where material ductility will be reduced because of service conditions (e.g., low-temperature applications). The possibility of loads imposed on components by attached utility or service lines, caused by differential movement of support points on separate structures, shall be evaluated. Where piping or HVACR ductwork components are attached to structures that could displace relative to one another and for isolated structures where such components cross the isolation interface, the components shall be designed to accommodate the seismic relative displacements defined in Section 13.3.2.	The effect of the $C_d = R$ proposal would be to increase the seismic relative displacement for components with Ip greater than 1.0, assuming the drift limits are revised to reflect the higher design drifts since designers have the option to design to the drift limits rather than the design drift.
13.6.3	Electrical Components	Conduit, cable tray and raceways shall meet the requirements of Section 13.6.5. Utility and service lines shall meet the requirements of Section 13.6.9. Other electrical components shall meet the requirements of Section 13.6.13. All electrical components with I_p greater than 1.0 shall be designed for the seismic forces and relative displacements defined in Sections 13.3.1 and 13.3.2 and shall satisfy the following additional requirements ... Where conduit, cable trays, or similar electrical distribution	The effect of the $C_d = R$ proposal would be to increase the seismic relative displacement for components with I_p greater than 1.0, assuming the drift limits are revised to reflect the higher design drifts since designers have the option to design to the drift limits rather than the design drift.

Section	Topic	Provision	Comments
		components are attached to structures that could displace relative to one another and for isolated structures where such components cross the isolation interface, the components shall be designed to accommodate the seismic relative displacements defined in Section 13.3.2	
13.6.4	Component Supports	Mechanical and electrical component supports (including those with I_p=1.0) and the means by which they are attached to the component shall be designed for the forces and displacements determined in Sections 13.3.1 and 13.3.2. Such supports include structural members, braces, frames, skirts, legs, saddles, pedestals, cables, guys, stays, snubbers, tethers, and elements forged or cast as a part of the mechanical or electrical component.	The effect of the $C_d = R$ proposal would be to increase the seismic relative displacement for components, assuming the drift limits are revised to reflect the higher design drifts since designers have the option to design to the drift limits rather than the design drift.
13.6.5	Distribution Systems: Conduit, Cable Tray, and Raceways.	Cable trays and raceways shall be designed for seismic forces and seismic relative displacements as required in Section 13.3.	The effect of the $C_d = R$ proposal would be to increase the seismic relative displacement for components, assuming the drift limits are revised to reflect the higher design drifts since designers have the option to design to the drift limits rather than the design drift. There are however a number of exceptions for conduit, cable trays and raceways based on size and geometry.
13.6.6	Distribution Systems: Duct Systems	HVACR and other duct systems shall be designed for seismic forces and seismic relative displacements as required in Section 13.3.	The effect of the $C_d = R$ proposal would be to increase the seismic relative displacement for components, assuming the drift limits are revised to reflect the higher design drifts since designers have the option to design to the drift limits rather than the design drift. There are however a number of exceptions for duct systems based on size and geometry.

Section	Topic	Provision	Comments
13.6.7	Distribution Systems: Piping and Tubing Systems.	Unless otherwise noted in this section, piping and tubing systems shall be designed for the seismic forces and seismic relative displacements of Section 13.3. ASME pressure piping systems shall satisfy the requirements of Section 13.6.7.1. Fire protection sprinkler piping shall satisfy the requirements of Section 13.6.7.2. Elevator system piping shall satisfy the requirements of Section 13.6.11.	The effect of the $C_d = R$ proposal would be to increase the seismic relative displacement for components, assuming the drift limits are revised to reflect the higher design drifts since designers have the option to design to the drift limits rather than the design drift. There are however a number of exceptions for piping and tubing systems based on size, geometry, and the nature of the connections to equipment.
13.6.10	Boilers and Pressure Vessels	Boilers or pressure vessels designed and constructed in accordance with ASME BPVC shall be deemed to meet the force, displacement, and other requirements of this section. In lieu of the specific force and displacement requirements provided in ASME BPVC, the force and displacement requirements of Sections 13.3.1 and 13.3.2 shall be used. Materials that meet the toughness requirements of ASME BPVC shall be considered high-deformability materials. Other boilers and pressure vessels designated as having an $I_p = 1.5$, but not designed and constructed in accordance with the requirements of ASME BPVC, shall comply with the requirements of Section 13.6.13.	The effect of the $C_d = R$ proposal would be to increase the seismic relative displacement for components, assuming the drift limits are revised to reflect the higher design drifts since designers have the option to design to the drift limits rather than the design drift.
13.6.11	Elevator and Escalator Design Requirements	Elevators and escalators designed in accordance with the seismic requirements of ASME A17.1 shall be deemed to meet the seismic force requirements of this section, except as modified in the following text. The exceptions of Section 13.6.7.3 shall not apply to elevator piping. 13.6.11.1 Escalators, Elevators, and Hoistway Structural Systems. Escalators, elevators, and hoistway structural systems shall be designed to meet the force and displacement requirements of Sections 13.3.1 and 13.3.2. 13.6.11.2 Elevator Equipment and Controller Supports and Attachments. Elevator equipment and controller supports and attachments shall be	The effect of the $C_d = R$ proposal would be to increase the seismic relative displacement for components, assuming the drift limits are revised to reflect the higher design drifts since designers have the option to design to the drift limits rather than the design drift.

Section	Topic	Provision	Comments
		designed to meet the force and displacement requirements of Sections 13.3.1 and 13.3.2.	
13.6.12	Rooftop Solar Panels	Rooftop solar panels and their attachments shall be designed for the forces and displacements determined in Section 13.3.	Due to the nature of roof top panel installations, the change of $C_d=R$ will have little effect. In addition, most arrays are designed using an exception that permits the use of ballasted, unanchored arrays.
15.4.5	Drift Limit	The drift limit of Section 12.12.1 need not apply to nonbuilding structures if a rational analysis indicates that they can be exceeded without adversely affecting structural stability or attached or interconnected components and elements such as walkways and piping. P-delta effects shall be considered where they are critical to the function or stability of the structure. P-delta effects, when considered, shall be based on displacements determined by an elastic analysis multiplied by using the appropriate value from Tables 12.2-1, 15.4-1, or 15.4-2.	The effect of setting $C_d = R$ would be to increase the drift at which P-delta is accounted for in nonbuilding structures. This implication seems minor.
15.4.7	Drift, Deflection, and Structure Separation	Drift, deflection, and structure separation calculated using strength level seismic forces shall be determined in accordance with this standard unless specifically amended in Chapter 15.	The impact to related provisions such as separation would have a similar impact as the Structural Provisions in Chapter 12.

Section	Topic	Provision	Comments
15.5.2	Pipe Racks	In addition to the requirements of Section 15.5.1, pipe racks supported at the base of the structure shall be designed to meet the force requirements of Section 12.8 or 12.9.1. Displacements of the pipe rack and potential for interaction effects (pounding of the piping system) shall be considered using the amplified deflections obtained from the following equation: $\delta_x = C_d\,\delta_{se}\,/\,I_e$ (15.5-1) where C_d = deflection amplification factor in Table 15.4-1; δ_{se} = deflections determined using the prescribed seismic design forces of this standard; and I_e = Importance Factor determined in accordance with Section 15.4.1.1. See Section 13.6.2 for the design of piping systems and their attachments. Friction resulting from gravity loads shall not be considered to provide resistance to seismic forces.	Pipe racks are explicitly required to be designed for interaction effects. The effect of making $C_d = R$ would be to effectively increase the separation between pipe racks constructed using certain seismic systems. Most cantilevered rack systems per table 15.4-1 contain ordinary detailing whereby C_d is already equal to R. Consequently, there would be no net effect for most racks.
15.5.5	Structural Towers for Tanks and Vessels	c. Seismic displacements of the tank and vessel shall consider the deformation of the support structure where determining P-delta effects or evaluating required clearances to prevent pounding of the tank on the structure. P-delta effects shall be based on displacements determined by an elastic analysis multiplied by C_d/I_e using the appropriate C_d value from Table 15.4-2. Tanks and vessels supported by structural towers that are integral to the tank or vessel shall be designed according to Section 15.7.10.1.	These provisions clarifies that the deformation of the support structure needs to be considered when calculating the displacement of the tank/vessel. The effect of making $C_d = R$ is discussed in the P-delta provision and Tank and Vessel Provision.
15.6.2	Chimneys and Stacks	Chimneys and stacks are permitted to be either lined or unlined and shall be constructed from concrete, steel, or masonry. Steel stacks, concrete stacks, steel chimneys, concrete chimneys, and liners shall be designed to resist seismic lateral forces determined from a substantiated analysis using reference documents. Interaction of the stack or chimney with the liners shall be	Chimneys and stacks are required to be designed for structural separation. The effects of making $C_d = R$ would be to effectively increase the separation between stacks constructed using certain seismic systems.

Section	Topic	Provision	Comments
		considered. A minimum separation shall be provided between the liner and chimney equal to C_d times the calculated differential lateral drift.	
15.7.4	Flexibility of Piping Attachments	Design of piping systems connected to tanks and vessels shall consider the potential movement of the connection points during earthquakes and provide sufficient flexibility to avoid release of the product by failure of the piping system. The piping system and supports shall be designed so as not to impart significant mechanical loading on the attachment to the tank or vessel shell. Mechanical devices that add flexibility, such as bellows, expansion joints, and other flexible apparatus, are permitted to be used where they are designed for seismic displacements and defined operating pressure. Unless otherwise calculated, the minimum displacements in Table 15.7-1 shall be assumed. For attachment points located above the support or foundation elevation, the displacements in Table 15.7-1 shall be increased to account for drift of the tank or vessel relative to the base of support. The piping system and tank connection shall also be designed to tolerate C_d times the displacements given in Table 15.7-1 without rupture, although permanent deformations and inelastic behavior in the piping supports and tank shell are permitted. For attachment points located above the support or foundation elevation, the displacements in Table 15.7-1 shall be increased to account for drift of the tank or vessel. The values given in Table 15.7-1 do not include the influence of relative movements of the foundation and piping anchorage points caused by foundation movements (e.g., settlement or seismic displacements). The effects of	Seismic interaction effects are required to be considered for the attachment of piping to tanks and vessels. Because the support structures for tanks and vessels could be comprised of special type detailing where currently $C_d < R$, the effect of changing $C_d = R$ could require larger deformations to be considered when designing tanks and vessels.

Section	Topic	Provision	Comments
		the foundation movements shall be included in the piping system design, including the determination of the mechanical loading on the tank or vessel, and the total displacement capacity of the mechanical devices intended to add flexibility.	
15.7.10.3	P-Delta Effects	The lateral drift of the elevated tank shall be considered as follows: a. The design drift, as determined by an elastic analysis, shall be increased by the factor for evaluating the additional load in the support structure. b. The base of the tank shall be assumed to be fixed rotationally and laterally. c. Deflections caused by bending, axial tension, or compression shall be considered. For pedestal tanks with a height-to-diameter ratio less than 5, shear deformations of the pedestal shall be considered. d. The dead load effects of roof-mounted equipment or platforms shall be included in the analysis. e. If constructed within the plumbness tolerances specified by the reference document, initial tilt need not be considered in the P-delta analysis.	Elevated tanks and vessels are required to be designed considering P-Delta effects. Because the support structures for tanks and vessels could be comprised of special type detailing where currently $C_d < R$, the effect of changing $C_d = R$ could require larger deformations to be considered for P-Delta effects when designing tanks and vessels.

Section	Topic	Provision	Comments
16.1.2	Linear Analysis	In addition to nonlinear response history analysis, a linear analysis in accordance with one of the applicable procedures of Chapter 12 shall also be performed. The structure's design shall meet all applicable criteria of Chapter 12. Where soil–structure interaction in accordance with Chapter 19 is used in the nonlinear analysis, it shall be permitted to also use the corresponding spectral adjustment in the linear analysis.EXCEPTIONS: 1. For Risk Category I, II, and III structures, Sections 12.12.1 and 12.12.5 do not apply to the linear analysis. Where mean computed drifts from the nonlinear analyses exceed 150% of the permissible story drifts per Section 12.12.1, deformation-sensitive nonstructural components shall be designed for two-thirds of these mean drifts. 2. The overstrength factor, Ω_0, is permitted to be taken as 1.0 for the seismic load effects of Section 12.4.3. 3. The redundancy factor, ρ, is permitted to be taken as 1.0. 4. Where accidental torsion is explicitly modeled in the nonlinear analysis, it shall be permitted to take the value of A_x as unity in the Chapter 12 analysis.	The drift limits do not apply to the linear analysis that is required when using the nonlinear analysis provisions. Consequently the effect of having $C_d = R$ would have no implications on non-linear analysis in Chapter 16.
17.5.6	Drift Limits	The maximum story drift of the structure above the isolation system shall not exceed. The drift shall be calculated by Eq. (12.8-15) with C_d for the isolated structure equal to R_l as defined in Section 17.5.4.2.	For linear analysis of isolated systems, C_d is set equal to R in ASCE 7-16. Consequently the effect of having $C_d = R$ would have no implications on the design of base isolated structures in Chapter 17.
18.7.4.1	Seismic Force-Resisting System	The seismic force-resisting system shall satisfy the requirements of Section 12.2.1 using seismic base shear and design forces determined in accordance with Section 18.7.1.2 or 18.7.2.2. The design story drift, Δ_D, as determined in either Section 18.7.1.3.3 or 18.7.2.3.3 shall not exceed (R/C_d) times the allowable	Where linear procedures are used to design structures with damping systems, the deformations are computed using pseudo displacements based of the dynamics of the structure. To keep the requirements consistent with Chapter 12, Chapter 18 of ASCE 7-16 increases the drift limits of table 12.12.1 by R/C_d.

Section	Topic	Provision	Comments
		story drift, as obtained from Table 12.12-1, considering the effects of torsion as required in Section 12.12.1.	Setting $R = C_d$ would have no net effect on Chapter 18 linear design.

Table B-1 Preliminary Drift Data from Analysis and Testing

Structure Model	Structure Type	Design Estimated Roof Drift - ASCE 7-16		NLRHA Average Peak Roof Drift DE		Underestimated by ASCE 7-16?	
		Drift (in)	Drift Ratio Percent	Drift (in)	Drift Ratio Percent	Ratio Est./NLRHA	Yes/No
ATC-116 MFD3B (1)	Wood Shear Wall KC Calc	5 to 8	1.0 to 1.6	4.15	0.9	1.1 to 1.8	No
	Wood Shear Wall JH Calc	7.8	1.6	4.15	0.9	1.88	No
MKA1 NS (2)	Composite BRBF	81.10	4.1	33.7	1.7	2.41	No
MKA1 EW (2)	Composite SMF	49.40	2.5	25.7	1.3	1.92	No
MKA2 NS (2)	BRBF	37.80	1.9	19.4	1.0	1.95	No
MKA2 EW (2)	BRBF	50.50	2.5	21.8	1.1	2.32	No
MKA3 NS (2)	Concrete SW	37.80	1.1	39.8	1.2	0.95	No
MKA3 EW (2)	Concrete SW	50.50	1.5	31.0	0.9	1.63	No

(1) NLRHA numerical studies conducted as part of the "Solutions to the Issues of Short-Period Building Seismic Performance," ATC-116 Project.

(2) NLRHA models developed by Magnusson Klemencic Associates for design of new structures.

Table B-2 Preliminary Drift Data from Analysis and Testing

Structure Model	Structure Type	1.5 *DE Estimated Story Drift - ASCE 7-16		NLRHA Average Peak Story Drift MCE	Underestimated by ASCE 7-16?	
		(in)	%	(in)	Ratio Est./NLRHA	Yes/ No
Degenkolb1EW (3)	SMRF (Sideplate)	Roof	1.29%	1.37%	0.94	No
		5th	1.61%	1.60%	1.01	No
		4th	1.60%	1.57%	1.01	No
		3rd	1.52%	1.56%	0.97	No
		2nd	1.02%	1.25%	0.82	Yes
Degenkolb1NS (3)	BRBF	Roof	1.22%	1.11%	1.10	No
		5th	1.26%	1.31%	0.96	No
		4th	1.16%	1.41%	0.82	Yes
		3rd	1.11%	1.45%	0.76	Yes
		2nd	0.87%	1.10%	0.79	Yes
Degenkolb #2 (3)	Concrete Shear Wall	Roof	2.12%	2.24%	0.94	Yes
		Level 6	2.06%	2.14%	0.96	No
		Level 5	1.95%	1.99%	0.98	No
		Level 4	1.76%	1.79%	0.98	No
		Level 3	1.34%	1.48%	0.90	Yes
		Level 2	0.57%	0.92%	0.62	Yes

(3) NLRHA models developed by Degenkolb Engineers for design of new buildings.

Table B-3 Preliminary Drift Data from Analysis and Testing

Structure Model	Structure Type	Story	Design Estimated Story Drift - ASCE 7-16		NLRHA Average Peak Story Drift at DE		Underestimated by ASCE 7-16?	
			(in)	%	(in)	%	Est./NLRHA	Yes/No
NIST 1863-1 MC8 ELF Design (4)	Steel Moment Frame	8	2.25	1.3		2.3	0.56	Yes
		7	2.83	1.7		2.3	0.74	Yes
		6	2.81	1.7		2.2	0.77	Yes
		5	3.00	1.8		2.2	0.82	Yes
		4	3.06	1.8		2.3	0.78	Yes
		3	3.11	1.9		2.4	0.79	Yes
		2	2.96	1.8		2.4	0.75	Yes
		1	2.93	1.4		2.2	0.63	Yes
NIST 1863-1 MC8 RSA Design (4)	Steel Moment Frame	8	1.84	1.1		3	0.37	Yes
		7	2.38	1.4		3	0.46	Yes
		6	2.75	1.6		3	0.53	Yes
		5	2.92	1.7		4	0.42	Yes
		4	2.90	1.7		6	0.28	Yes
		3	2.99	1.8		8	0.22	Yes
		2	2.86	1.7		8	0.21	Yes
		1	2.84	1.3		8	0.16	Yes

(4) NLRHA numerical studies of steel special moment frame structures conducted by NIST as part of a study to benchmark ASCE 41 performance-based design methodologies against code provisions used for design of new buildings (NIST Technical Notes 1863-1, 1863-2, 2015)

Table B-4 Preliminary Drift Data from Analysis and Testing

Structure Model	Structure Type	Condition	Story	Design Estimated Roof Drift - ASCE 7-16		Shake Table Test Peak Story Drift		Underestimated by ASCE 7-16?	
				Drift (in)	Drift Ratio Percent	Drift (in)	Drift Ratio Percent	Ratio Est./Test	Yes/No
CFS-NEES (5)	CFS Shear Wall	DE no finishes	2		1.2		0.8	1.5	No
			1		2.4		1.2	2.0	No
		DE with finishes	2		1.2		0.25	4.8	No
			1		2.4		0.5	4.8	No
		MCE w/ finishes	2		1.2		0.7	1.7	No
			1		2.4		0.7	3.4	No

(5) Testing of a cold-formed steel structure conducted by Ben Schafer et al. as part of the NEES funded CFS-NEES project titled "Advancing Cold-Formed Steel Earthquake Engineering."

RESOURCE PAPER 6 DIAPHRAGM DESIGN FORCE REDUCTION FACTOR, R$_S$, FOR COMPOSITE CONCRETE ON METAL DECK DIAPHRAGMS

RP6-1   INTRODUCTION

The diaphragm design force reduction factor, R$_s$, is an integral part of the alternative diaphragm design procedure in ASCE 7 (2016). In the alternative diaphragm design procedure, diaphragm force demands are calculated using a series of equations intended to predict the elastic diaphragm design force which is then divided by the R$_s$ factor. The R$_s$ factor is dependent on the material and construction of the diaphragm system and accounts for the overstrength and inelastic displacement capacity (ductility) that these systems possess. Diaphragm design force reduction factors have been defined for several types of diaphragm systems using a range of approaches. This resource paper brings forward, for the benefit of the users of the NEHRP Provisions, the evidence to support the selection of an R$_s$ factor for composite concrete on metal deck diaphragms and a discussion of steel deck diaphragm research nearing completion.

Three approaches for defining the R$_s$ factor will be described: (a) the use of past test data on composite concrete on metal deck diaphragms to quantify ductility and overstrength and then apply this information to estimate R$_s$; (b) application of the identical approach employed in the development of R$_s$ for cast-in-place concrete diaphragm systems; and finally (c) validation/estimation of R$_s$ based on an extension of the FEMA P695 (FEMA 2009) methodology wherein a large suite of nonlinear computational building models are used to assess system performance. Current progress toward this computational verification will be discussed.

RP6-2   R$_S$ USING TEST DATA WITH MEASURED DUCTILITY AND OVERSTRENGTH

The commentary to ASCE 7 (ASCE 2016) Section C12.10.3.5 describes a method for calculating the diaphragm design force reduction factor, R_s, based on measured ductility and overstrength obtained from test data. That method is the same as described in ATC 19 (ATC 1995). In this method, the R_s factor is made up of two components: the first is associated with the expected overstrength of the diaphragm, R_Ω, and the second is associated with the ductility, R_μ, as provided in Eq. (1). The overstrength component (Eq. (2)) is the ratio of the measured (maximum) strength of the diaphragm, S_{max}, to the predicted (design) strength, S_d.

The ductility component, R_μ, as given in Eq. (3) is dependent on whether the structure has a medium or long period. The limits on period given in Eq. (3) come from ATC 19 (not specified in the ASCE 7 Commentary) and ATC 19 states that R_μ should be interpolated between values from Eq. (3a) and (3b) for periods between 0.5 sec and 1.0 sec. Specifying the ductility component as period dependent in this way recognizes that while long period structures generally follow an equal displacement rule (peak displacements of an inelastic system are approximately the same as an elastic system), medium period structures follow more of an equal energy rule (the inelastic system displaces more than the elastic system such that the area under their load-displacement curves is equal) (see Newmark and Hall 1982).

$$R_s = R_\Omega R_\mu \tag{1}$$

$$R_\Omega = \frac{S_{max}}{S_d} \tag{2}$$

$$R_\mu = \sqrt{2\mu_{sys} - 1} \quad \text{for 0.12 sec} < \text{T} < \text{0.5 sec} \tag{3a}$$

$$R_\mu = \mu_{sys} \quad \text{for T} > \text{1.0 sec} \tag{3b}$$

The equation for R_μ is a function of the diaphragm system ductility, μ_{sys}, not the ductility of a cantilever diaphragm test. O'Brien et al. (2017) identified that a diaphragm span has a linearly varying shear demand and as such, it is only the end regions of the span that reach their shear strength, become inelastic, and fail. Since much of the diaphragm span remains elastic, the ductility (measured as the ultimate displacement divided by the yield displacement) of the diaphragm span is smaller than the ductility of a cantilever diaphragm specimen. O'Brien et al. (2017) derived a relationship between the ductility of a cantilever diaphragm test, μ_{sub}, and the expected ductility of an entire diaphragm span, μ_{sys}, as given in Eq. (4). To use this equation, it is necessary to estimate the ratio of the length of the inelastic end region of the diaphragm span, L_p, to the total length of the diaphragm span, L. Based on a review of the literature, O'Brien et al. (2017) suggested a value of $L_p/L=0.1$.

$$\mu_{sys} = 1 + 4\left(\mu_{sub} - 1\right)\frac{L_p}{L} \tag{4}$$

This approach for calculating R_s is applied here to a set of 16 cantilever diaphragm tests on composite concrete on metal deck specimens. There are several additional assumptions made in these calculations:

1. The predicted strength of the concrete on metal deck diaphragm (S_d) is calculated using expressions currently being balloted for inclusion in the next edition of AISI S310 (see O'Brien et al. 2017 for more details). The strength prediction equation that currently exists in AISI 310-16 results in significantly smaller predicted strength and thus would result in greater overstrength ($R_\square$) and larger R_s.
2. A value of L_p/L equal to 0.1 is assumed.
3. The overstrength factor, R_Ω, is calculated as the measured shear strength divided by the predicted shear strength and does not include the resistance factor ($\square$). It is noted that the resistance factor for concrete on metal deck diaphragms (AISI S310-16) is currently 0.5; however a value of 0.8 is currently under ballot for use in future AISI S310 editions based on the available data under the limit state of diagonal tension cracking. If the resistance factor is considered in the calculation of overstrength, the resulting R_s factor would be larger.

Sixteen specimens were selected as described in Table 6-1 including 13 cantilever diaphragm tests conducted by Porter and Easterling (1988) and three specimens recently tested by Avellaneda et al. (2019). This set of tests includes 13 specimens that were reported to have experienced diagonal tension cracking and 3 specimens that experienced perimeter fastener failure. In terms of perimeter fasteners to the supports, 7 specimens used arc spot welds, 6 specimens used a combination of welds and shear studs, and 3 specimens used only shear studs.

The failure mode listed in Table 6-1 was reported by the original authors. The value of stiffness, G', was calculated as the secant stiffness through a point at 40% of the peak load, which is consistent with AISI S310. The shear strength, S_{max}, is the maximum shear load measured during the test divided by the specimen length. The shear angle at yield, γ_y, is calculated per Eq. (5). The ultimate shear angle, γ_{ult}, is obtained as the shear angle when the shear force drops below 80% of the maximum shear strength. The subassemblage ductility, μ_{sub}, is calculated according to Eq. (6).

$$\gamma_y = \frac{S_{max}}{G'} \tag{5}$$

$$\mu_{sub} = \frac{\gamma_{ult}}{\gamma_y} \tag{6}$$

Table 6-1 Calculation of Subassemblage Ductility from Test Data

Specimen	Perimeter Connection[3]	Failure Mode[4]	Measured Stiffness, G' (kip/in)	Measured Strength, S_{max} (k/ft)	Yield Shear Angle, γ_y (rad)	Ultimate Shear Angle, γ_{ult} (rad)	Specimen Ductility, μ_{sub}
12[1]	W	DT	1710	12.1	0.590	2.30	3.90
13[1]	W	DT	2020	16.8	0.693	2.23	3.22
16[1]	W	DT	920	8.0	0.726	2.39	3.29
18[1]	W	DT	1580	10.7	0.564	2.27	4.02
19[1]	W	DT	930	9.8	0.877	2.26	2.58
22[1]	W	DT	1650	10.5	0.530	2.09	3.94
24[1]	W	DT	1660	11.2	0.562	2.37	4.22
25[1]	W+SS	DT	1730	12.0	0.578	2.26	3.91
26[1]	W+SS	DT	1590	5.8	0.304	1.35	4.44
27[1]	W+SS	P	1750	6.1	0.289	1.38	4.77
28[1]	W+SS	P	1580	8.0	0.421	1.41	3.35
29[1]	W+SS	DT	1890	9.0	0.397	1.24	3.12
30[1]	W+SS	P	1540	7.7	0.416	1.37	3.29
3/6.25-4-L-NF-DT[2]	SS	DT	1615	9.3	0.478	5.67	11.87
3/7/5-4-N-NF-DT[2]	SS	DT	1798	15.3	0.709	1.66	2.34
2/4-4-L-NF-DT[2]	SS	DT	1080	8.9	0.689	5.18	7.52

[1] from Porter and Easterling (1988) [2] from Avellaneda et al. (2019)

[3] W = arc spot welds only, W+SS = welds and shear studs, SS = shear studs only

[4] DT = concrete diagonal tension cracking, P = perimeter fastener failure; as reported by the author

Table 6-2 presents the resulting values for diaphragm system ductility, the ductility and overstrength components of R_s, and the computed R_s factors. The following gives example calculations for the first row of Table 6-2 which is Specimen 12 from Porter and Easterling (1988).

1. Calculate the expected system level ductility using Eq. (4) based on the ductility of the specimen:

$$\mu_{sys} = 1 + 4(\mu_{sub} - 1)\frac{L_p}{L} = 1 + 4(3.90 - 1)0.1 = 2.16$$

2. Calculate the system overstrength, R_Ω, using Eq. (2). The predicted strength was calculated using the equations under ballot for inclusion in AISI S310 to be $S_d = 9.7$ k/ft.

$$R_\Omega = \frac{S_{max}}{S_d} = \frac{12.1\,\text{k/ft}}{9.7\,\text{k/ft}} = 1.25$$

3. The system ductility factor is calculated using either the equal energy rule (Eq. (3a)), or the equal displacement rule (Eq. (3b)):

$$R_\mu = \sqrt{2\mu_{sys} - 1} = \sqrt{2(2.16) - 1} = 1.82 \qquad \text{Medium Period}$$

$$R_\mu = \mu_{sys} = 2.16 \qquad \text{Long Period}$$

4. The R_s factor is then given by the following which was rounded down to R_s=2.0 for flexure-controlled cast-in-place concrete diaphragms:

$$R_s = R_\Omega R_\mu = (1.25)(1.82) = 2.28 \qquad \text{Medium Period}$$

$$R_s = R_\Omega R_\mu = (1.25)(2.16) = 2.70 \qquad \text{Long Period}$$

Table 6-2 Calculation of Diaphragm Design Force Reduction Factor

Specimen	Diaphragm System Ductility, μ_{sys}	Predicted Strength, S_d (k/ft)	Over-strength Factor, R_Ω	Ductility Factor Long T, R_μ	Ductility Factor Med. T, R_μ	R_s Factor for Long T	R_s Factor for Med. T
12	2.16	9.7	1.25	2.16	1.82	2.70	2.28
13	1.89	14.2	1.18	1.89	1.67	2.23	1.97
16	1.92	7.8	1.02	1.92	1.68	1.96	1.72
18	2.21	9.2	1.17	2.21	1.85	2.58	2.16
19	1.63	9.4	1.05	1.63	1.50	1.71	1.57
22	2.18	9.8	1.08	2.18	1.83	2.34	1.97
24	2.29	11.0	1.02	2.29	1.89	2.33	1.92
25	2.16	11.5	1.04	2.16	1.82	2.26	1.90
26	2.38	7.2	0.81	2.38	1.94	1.92	1.56
27	2.51	2.5	2.48	2.51	2.00	6.22	4.97
28	1.94	10.8	0.74	1.94	1.70	1.43	1.25
29	1.85	8.9	1.02	1.85	1.64	1.88	1.67
30	1.92	10.1	0.76	1.92	1.68	1.46	1.28
3/6.25-4-L-NF-DT	5.35	9.1	1.02	5.35	3.11	5.46	3.18
3/7/5-4-N-NF-DT	1.54	15.1	1.02	1.54	1.44	1.56	1.46

two-fourths- 4-L-NF-DT	3.61	5.7	1.56	3.61	2.49	5.62	3.88
Average	2.34	9.5	1.14	2.34	1.88	2.73	2.17
Standard Deviation	0.93	3.0	0.41	0.93	0.41	1.56	1.01

If the result for medium period structures is conservatively chosen over the long period value, the average result is R_s=2.17. This may be rounded down to a value of R_s=2.0.

The selected value of R_s pertains to a shear-controlled limit state. It is assumed that composite concrete on metal deck diaphragms do not readily experience a flexure-controlled failure mechanism because even if the chords are inadequate, there is often steel framing (i.e. beams) that add to the flexural strength of the diaphragm system.

RP6-3 R_S APPLYING CAST-IN-PLACE CONCRETE DIAPHRAGM APPROACH

In some ways, a concrete on metal deck diaphragm is similar to a cast-in-place concrete diaphragm, so it is instructive to examine the related R_s factors. In this section, the methodology for obtaining R_s factors for cast-in-place concrete diaphragms is summarized and then applied to concrete on metal deck diaphragms.

ASCE 7-16 Commentary Section C12.10.3.5 describes that since there were no test results for cast-in-place concrete diaphragms, the data from reinforced concrete shear walls subjected to cyclic testing was used. The procedure for calculating the R_s factor was as follows (the variable names used here match the previous section, not ASCE 7):

1. Based on data from shear wall tests, a diaphragm system ductility of μ_{sys}=3.0 was estimated.
2. The design ductility was taken as two-thirds of the estimated system ductility, so μ_{sys}=2.0.
3. The equal energy rule (Eq. (3a)) was used to get:
$$R_\mu = \sqrt{2\mu_{sys} - 1} = 1.73$$

4. It was assumed that the actual strength of the diaphragm is $S_{max} = 1.1\ S_d$, and the resistance factor is included in the calculation of overstrength such that:
$$R_\Omega = \frac{S_{max}}{\phi S_d} = \frac{1.1 S_d}{0.9 S_d} = 1.22$$

5. The R_s factor is therefore given by the following which was rounded down to R_s=2.0 for flexure-controlled cast-in-place concrete diaphragms:
$$R_s = R_\Omega R_\mu = (1.22)(1.73) = 2.11$$

For shear-controlled cast-in-place concrete diaphragms, it is assumed that the diaphragm will have an overstrength, R_Ω =1.5 and the ductility part is taken as R_μ = 1.0 in an effort to keep the diaphragm near-elastic. The result is R_s=1.5 for shear-controlled cast-in-place concrete diaphragms.

The same procedure can be applied to composite concrete on metal deck diaphragms. In this case, test data does exist to quantify the ductility and overstrength parts, so measured values will be used. Also, since composite concrete on metal deck diaphragms fail in a shear-controlled mechanism, no flexure-controlled value is calculated. The following applies the same five steps as those used for cast-in-place diaphragms:

1. Based on the test data provided in Table 6-2, the average diaphragm system ductility is found to be μ_{sys} = 2.34.
2. The design ductility is taken as two-thirds of the estimated system ductility, so μ_{sys}=1.56.

3. Eq. 3a is used to calculate the ductility component:

$$R_\mu = \sqrt{2\mu_{sys} - 1} = \sqrt{1.56 - 1} = 1.46$$

4. Based on the test data provided in Table 2, the overstrength component is calculated as:

$$R_\Omega = \frac{S_{max}}{\phi S_d} = \frac{S_{max}/S_d}{\phi} = \frac{1.14}{0.8} = 1.43$$

Note, S_d and ϕ are based on strength prediction expressions currently under ballot for AISI S310. If AISI S310-16 is employed S_d is lower and ϕ higher, resulting in a larger R_Ω.

5. The R_s factor is therefore given by the following for shear-controlled composite concrete on metal deck diaphragms:

$$R_s = R_\Omega R_\mu = (1.43)(1.46) = 2.09$$

Based on this calculation procedure, after rounding, R_s=2.0.

RP6-4   COLLAPSE SIMULATIONS AND FEMA P695

FEMA P695 is an approach for defining and validating response modification factors, R, for buildings based on computational simulations to determine probability of collapse. The objective is to limit the probability of collapse at the maximum considered earthquake to 10% on average for a group of archetype buildings or 20% for any individual archetype building. Conceptually, the FEMA P695 approach could be extended to evaluate horizontal Seismic Force Resisting Systems (SFRS) in addition to its traditional use to evaluate vertical SFRSs. To apply this methodology to validate the selection of a diaphragm design force reduction factor, R_s, entails several steps:

1. Establish a design procedure, detailing requirements, and a trial value for R_s.
2. Define a set of archetype buildings, preferably a set that creates reasonably large demand to capacity ratios in the diaphragm.
3. Develop nonlinear computational building models. Nonlinear models of the diaphragm must be consistent with the established detailing requirements and thus experimental data is typically necessary.
4. Conduct nonlinear response history building analyses with scaled ground motions.
5. Determine the ground motion scaling that causes 50% of the records to cause collapse. Define the ratio of this ground motion scaling to the MCE ground motion scaling as the collapse margin ratio.
6. Modify the collapse margin ratio based on spectral shape, record to record uncertainty, quality of design requirements, quality of test data, and quality of modeling to establish an Adjusted Collapse Margin Ratio (ACMR).
7. Determine whether the ACMR is sufficient to limit probably of collapse at MCE to 10% for the group of buildings or 20% for an individual archetype building. If so, then the established design procedure, detailing requirements and R_s value are validated. If not, something about the design procedure, detailing or R_s must be changed and the process restarted.

Beyond the obvious challenges of creating and running a large number of 3D nonlinear computational models, there are several challenges / considerations associated with applying the FEMA P695 methodology to the validation of R_s factors (See 2020 NEHRP Provisions Resource Paper X, "Next Steps Towards the Development of Diaphragm Design Force Reduction (R_s) Factors"). A few are listed here:

1. FEMA P695 was developed and has been used exclusively for evaluating vertical SFRS. Considering diaphragm inelasticity in computational models typically leads to more collapses because the larger drifts (caused by a combination of elastic and inelastic deformations in both the vertical SFRS and the diaphragm) creates larger destabilizing P-Delta forces. Although diaphragm

inelasticity can sometimes reduce the force demands in the vertical SFRS, it has been found that the effect of larger drifts and P-Delta lead to more collapses in computational models. Applying the same criteria for collapse probabilities whether diaphragm inelasticity is considered or not, may lead to inconsistent results. It may be prudent to include a factor in future versions of FEMA P695, similar to the factor in FEMA P695 that relaxes the criteria when 3D analysis is used.

2. There is an interaction between inelasticity in the vertical SFRS and the diaphragm. Inelasticity in the vertical SFRS reduces force demands in the diaphragm. To accurately capture all possible combinations of vertical SFRS and diaphragm would require many archetype buildings – many more than a typical P695 analysis because of this added variable of vertical SFRS.

A FEMA P695 type of study is currently being conducted for buildings with concrete on metal deck floor diaphragms and bare steel deck roof diaphragms. See Wei et al. (2019), and Foroughi et al. (2019) for a description of some of the initial models. The study includes eight 3D archetype buildings with vertical SFRS consisting of buckling restrained braced frames and special concentrically braced frames to evaluate the effect of a high ductility and lower ductility vertical SRFS on collapse probabilities. Four building heights are considered: 1-story, 4-story, 8-story, and 12-story buildings. A design procedure with detailing requirements has been developed with an assumed value of R_s=2.5 for the bare deck diaphragms at the roof (with special seismic detailing), and R_s=2.0 for the composite concrete on metal deck diaphragms in the floors. The computational study is underway and its final results and related documentation is expected to be complete in 2020.

RP6-5   SUMMARY

The value of the diaphragm design force reduction factor, R_s, for concrete on metal deck diaphragms was investigated using three approaches including (a) using past test data to quantify ductility and overstrength, (b) application of the same approach used for cast-in-place concrete diaphragm systems, and (c) validation of the selected R_s using the FEMA P695 methodology. Approaches (a) and (b) resulted in a shear-controlled R_s=2.0, and approach (c) is currently underway to verify this value. A flexure-controlled R_s value is not calculated and not considered applicable for concrete on metal deck diaphragms.

RP6-6   REFERENCES

AISI (2016) North American standard for the design of profiled steel diaphragm panels, AISI S310-16, American Iron and Steel Institute.

ASCE (2016) ASCE 7-16: Minimum design loads for buildings and other structures, American Society of Civil Engineers

ATC (1995) ATC-19: Structural response modification factors, Applied Technology Council.

Avellaneda, R.E., Easterling, W.S., Schafer, B.W., Hajjar, J.F., and Eatherton, M.R. (2019) Cyclic Testing of Composite Concrete on Metal Deck Diaphragms Undergoing Diagonal Tension Cracking, 12th Canadian Conference on Earthquake Engineering, Quebec QC, June 17-20.

FEMA (2009) Quantification of building seismic performance factors, FEMA P695. Applied Technology Council, Federal Emergency Management Agency.

Foroughi, H., Wei, G., Torabian, S., Eatherton, M.R., and Schafer, B.W. (2019) Seismic Demands on Steel Diaphragms for 3D Archetype Buildings with Concentric Braced Frames, 12th Canadian Conference on Earthquake Engineering, Quebec QC, June 17-20.

Newmark, N.M., and Hall, W.J. (1982) Earthquake Spectra and Design, Monograph Series, Earthquake Engineering Research Institute.

O'Brien, P., Eatherton, M.R., and Easterling, W.S. (2017) Characterizing the Load-Deformation Behavior of Steel Deck Diaphragms using Past Test Data, Cold-Formed Steel Research Consortium Report Series, CFSRC R-2017-02.

Porter, M., and Easterling, W. (1988) Behavior, analysis, and design of steel-deck-reinforced concrete diaphragms, Report No. ISU-ERI-Ames-88305 Project 1636, Iowa State University.

Wei, G., Foroughi, H., Torabian, S., Schafer, B.W., and Eatherton, M.R. (2019) Evaluating Different Diaphragm Design Procedures Using Nonlinear 3D Computational Models, 12th Canadian Conference on Earthquake Engineering, Quebec QC, June 17-20.

RESOURCE PAPER 7 DEVELOPMENT OF DIAPHRAGM DESIGN FORCE REDUCTION FACTORS, R$_S$

RP7-1   INTRODUCTION

Diaphragm design force reduction factors (R_s factors) were first introduced in the 2015 NEHRP Provisions (FEMA, 2015), and are currently included as part of an alternative diaphragm design procedure in ASCE 7 (ASCE, 2017) Section 12.10.3 and Table 12.10-1. Prior to inclusion of R_s factors in ASCE 7, design force demands on diaphragms were exclusively derived as a function of the R-factor of the vertical seismic force-resisting system, with upper and lower bounds imposed. The R_s factor is part of alternative diaphragm design provisions that directly recognize the effect of diaphragm overstrength and displacement capacity on diaphragm design forces. The alternative diaphragm design provisions have two basic parts. One part provides new formulas to better estimate seismic design forces for diaphragms exhibiting near elastic behavior. The second part provides reduction of this near-elastic force through the R_s factor.

The objective of this white paper is to recommend next steps towards the development of R_s factors for diaphragm systems not yet addressed. R_s factors are currently published in ASCE 7 for precast concrete diaphragms, cast-in-place concrete diaphragms, and wood structural panel diaphragms on wood framing. R_s factors have just been developed for bare steel deck diaphragms, which are intended to be included in the 2020 NEHRP Provisions and ASCE 7-22. Studies are currently under way to address concrete topped metal deck diaphragms. Not yet addressed are a few common diaphragm systems such as wood structural panel diaphragms on cold-formed steel (CFS) framing, wood structural panel diaphragms stapled to wood framing, steel truss diaphragms, and cross-laminated timber (CLT) diaphragms. Also not yet addressed are a wide range of proprietary diaphragms for which development of R_s factors may be desired. This white paper summarizes background information, identifies methods used for development of the R_s factors already available, discusses considerations important for future development of R_s factors, and makes recommendations for next steps.

Since the alternative diaphragm design procedure includes explicit consideration of diaphragm ductility through the R_s factor, inelastic diaphragm deformations may be expected during the design earthquake for some diaphragm systems. In some cases (e.g. seismic separation), it may be desirable to calculate total diaphragm deflection including inelastic deformations. However, approaches for calculating total diaphragm deflection (i.e. C_d factors), for use with the alternative diaphragm design procedure are not currently available in ASCE 7 or the NEHRP Provisions. This issue is discussed in the section on recommended next steps.

RP7-2   BACKGROUND

The following general discussion of the alternative diaphragm design provisions is largely taken from the commentary to the 2015 NEHRP Provisions, Section C12.10.3.5 Diaphragm Design Force Reduction Factor.

Despite the fact that analytical and shake table studies indicate higher diaphragm accelerations than currently used in diaphragm design, many commonly used diaphragm systems, including diaphragms designed under a number of U.S. building codes and editions, have a history of excellent earthquake performance. With limited exceptions, diaphragms have not been reported to have performed below the life-safety intent of building code seismic design provisions in past earthquakes. It is noted, however, that in some cases, failure of other parts of the building (e.g. wall anchorage) may have occurred which protected the diaphragm from experiencing larger demands.

Based on this history, it is felt that, for many diaphragm systems, no broad revision is required to the balance between demand and capacity used for design of diaphragms under current ASCE 7 provisions. In view of this observation, it was recognized that the analytical studies and diaphragm testing from which the

higher accelerations and design forces were being estimated used diaphragms that were elastic or near-elastic in their response. Commonly used diaphragm systems are recognized to have a wide range of overstrength, and inelastic displacement capacity (ductility). In ASCE 7 Section 12.10.3, alternative design provision for diaphragms, the diaphragm overstrength and inelastic displacement capacity are recognized through the use of the diaphragm force reduction factor, R_s. This factor is most directly based on the global ductility capacity of the diaphragm system; however, the derivation of the global ductility capacity inherently also captures the effect of diaphragm overstrength.

For diaphragm systems with inelastic deformation capacity sufficient to permit inelastic response under the design earthquake, the diaphragm design force reduction factor, R_s, is typically greater than 1.0, so that the design force demand, F_{px}, is reduced relative to the force demand for a diaphragm that remains linear elastic under the design earthquake. For diaphragm systems that do not have sufficient inelastic deformation capacity or overstrength, R_s should be less than 1.0, or even two-thirds (assumed factor between the design earthquake (DE) and maximum considered earthquake (MCE)), so that linear-elastic force-deformation response can be expected at the MCE.

RP7-2.1   Objective of R_s Factor

The objective of the R_s factor is to produce diaphragm design forces that will lead to acceptable seismic performance of the structure. In considering the development of R_s factors, the simplified nature of methods currently used to develop seismic design forces and to model diaphragm behavior need to be taken into account. For this reason, it is desired to confirm that the design resulting from R_s factors and simplified design tools can be demonstrated to result in adequate performance.

RP7-2.2   Interaction between R_s and R

Although the design approach using a response modification factor, R, for the vertical seismic system and a separate diaphragm design force reduction factor, R_s, for the horizontal seismic system implicitly treats the vertical and horizontal systems as acting independently in terms of dynamic behavior and inelastic deformation demands, both systems act together as one building system. A parametric computational study was recently conducted using an assembly of simplified elastic-plastic springs as shown in Figure 1(a) to represent a building with vertical seismic force resisting system (stiffness K_h) and diaphragm system (stiffness K_d)(Fisher and Schafer 2018). The yield strength of the elastic-plastic springs was set equal to the maximum force experienced in the springs during response history analysis when the springs were elastic, divided by a ductility factor, R_d, for the springs in the vertical seismic force resisting system and a ductility factor, R_{sd}, for the springs in the diaphragm system.

Figure 1(b) through 1(e) show average results from a set of 22 ground motions for a number of variations in the ductility factor, R_d, for the vertical springs and the ductility factor, R_{sd}, for the horizontal springs. The vertical axis in these plots is the average peak force in the spring normalized by the total elastic inertial force expected in the short-period region (short period spectral acceleration used in ground motion scaling multiplied by the total mass). Some key observations include:

- When both the vertical and horizontal systems are kept elastic, as shown in Figure 1(b), the vertical system experiences forces consistent with the elastic response spectrum that was used for ground motion scaling. The horizontal system can experience similar force levels if the diaphragm is extremely stiff relative to the vertical system (i.e. see the T_d/T_h=0.5 line in Figure 1(b)), or substantially smaller forces if the diaphragm is relatively flexible (i.e. see the T_d/T_h=10 line in Figure 1(b) and definition of T_d and T_h in Figure 1(a)).

- Figure 1(c) shows that inelasticity in the vertical system not only caps the forces the vertical system can experience, but also leads to a significant reduction in the forces in the horizontal system (i.e. see the T_d/T_h=0.5 line and the T_d/T_h=10 line in Figure 1(c)).

- However, the inverse is not as true; Figure 1(d) shows that inelasticity in the horizontal system caps

the forces the diaphragm can experience, but the forces in the vertical system are not reduced as much.

- Finally, Figure 1(e) shows that inelasticity in both the vertical and horizontal systems leads to further reduction in diaphragm forces, especially when the diaphragm is flexible compared to the vertical system (i.e see the T_d/T_h=10 line in Figure 1(e)).

Two conclusions from this study include 1) inelasticity in the vertical system is better at reducing the diaphragm forces than inelasticity in the diaphragm is at reducing forces in the vertical system, and 2) there is an interaction between inelasticity in the vertical and horizontal systems that can lead to further reduction in diaphragm forces. The implications of these conclusions for the analytical calculation or validation of R_s factors can be summarized as follows:

1. For justification of an R_s factor, the most conservative validation check would involve use of the lowest applicable vertical system R factor and highest vertical system overstrength (least amount of inelasticity in the vertical system), as illustrated in Figure 1(b) and 7-1(d), combined with the lowest ratio of diaphragm to vertical system periods, as seen in the T_d/T_h=0.5 data in Figure 1(d).

2. The calculation of R_s factors that would lead to the most economical structures would be specific to the amount of ductility provided by each type of vertical seismic force resisting system (SFRS).

3. It would be conservative to assume the vertical system is elastic in the determination of an R_s factor as evidenced by larger diaphragm forces in Figure 1(d) as compared to those in Figure 1(e). In some cases, this may be an overly conservative assumption, but in others (e.g. low-rise shear wall buildings) there may be significant overstrength leading to elastic response of the vertical SFRS.
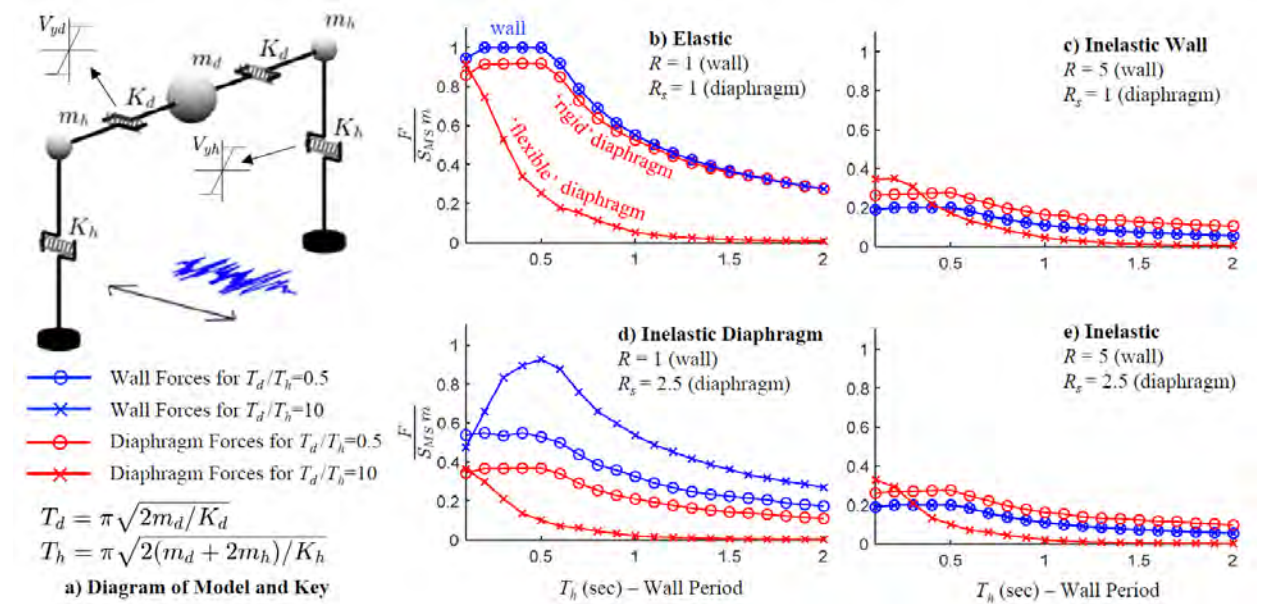

Figure 1 Interaction between inelasticity in the vertical SFRS and the diaphragm [from (Fischer et al. 2018)]

RP7-3　　METHODS USED TO DERIVE RS FACTORS FOR 2015 NEHRP AND ASCE 7

The alternative diaphragm design provisions of Section 12.10.4 of the NEHRP Provisions and Section 12.10.3 of ASCE 7 included R_s factors for precast concrete diaphragms, cast-in-place concrete diaphragms, and wood structural panel diaphragms on wood framing. These R_s factors were drawn from the best available information at the time, and the methods used to derive them varied between the materials. Detailed discussion of the basis is provided in the commentaries to both the NEHRP Provisions and ASCE 7. This section provides a very brief overview of the methods used.

RP7-3.1　　Precast Concrete Diaphragms

The diaphragm force reduction factor, R_s, in ASCE 7 Table 12.10-1 for precast concrete diaphragms was established based on the results of analytical earthquake simulation studies conducted within a multi-university project: Development of a Seismic Design Methodology (DSDM) for Precast Concrete Diaphragms (Fleischman et al. 2013). In this research effort, diaphragm design force levels have been aligned with the diaphragm deformation capacities specifically for precast concrete diaphragms. Three different design options were proposed according to different design performance targets, as indicated in ASCE 7 Table C12.10-1. The relationships between diaphragm design force levels and diaphragm local/global ductility demands have been established in the DSDM research project. These relationships have been used to derive the R_s factors for precast concrete diaphragms in Table 12.10-1.

Extensive analytical studies have been performed (Fleischman et al. 2013) to develop the relationship of R_{dia}-μ_{global}-μ_{local}. R_{dia} is the diaphragm force reduction factor (similar to the R_s in Table 12.10-1) measured from the required elastic diaphragm design force at MCE level. μ_{global} is the diaphragm global ductility demand and μ_{local} is the diaphragm local connector ductility demand measured at MCE level. ASCE 7 Figure C12.10-9 shows the μ_{global}-μ_{local} and R_{dia}-μ_{global} analytical results for different diaphragm aspect ratios and proposed linear equations fit to the data. Then, using the local ductility for three types of connectors (low, moderate, and high deformability), associated global ductility and R_s factors were calculated using the linear equations.

RP7-3.2 Cast-in-Place Concrete Diaphragms

The following provides an overview of the method used to develop R_s factors for cast-in-place concrete diaphragms, as included in ASCE 7. Flexural yielding is the preferred yield mechanism for a reinforced concrete diaphragm because flexure is a more ductile limit state for reinforced concrete than shear. There are many circumstances, however, where the development of a well-defined flexural yielding mechanism is not possible due to diaphragm geometry (aspect ratio or complex diaphragm configuration), in which case, an additional designation as a shear-controlled diaphragm and use of a lower R_s factor is required.

Test results for cast-in-place reinforced concrete diaphragms are not available in the literature. Test results for reinforced concrete shear walls subjected to cyclic lateral loading were considered to provide the best available guidance for determination of an R_s factor. The critical regions of shear wall test specimens usually have high levels of shear force and moment while being subjected to drift demands; high levels of shear force have been shown to degrade the flexural ductility capacity. The flexural ductility capacity of shear wall test specimens subjected to cyclic lateral loading was used to estimate the flexural ductility capacity of reinforced concrete diaphragms, using the method described in Section RP 1-4.2 of this document based on Newmark and Hall (1982), and illustrated in Figure 2.
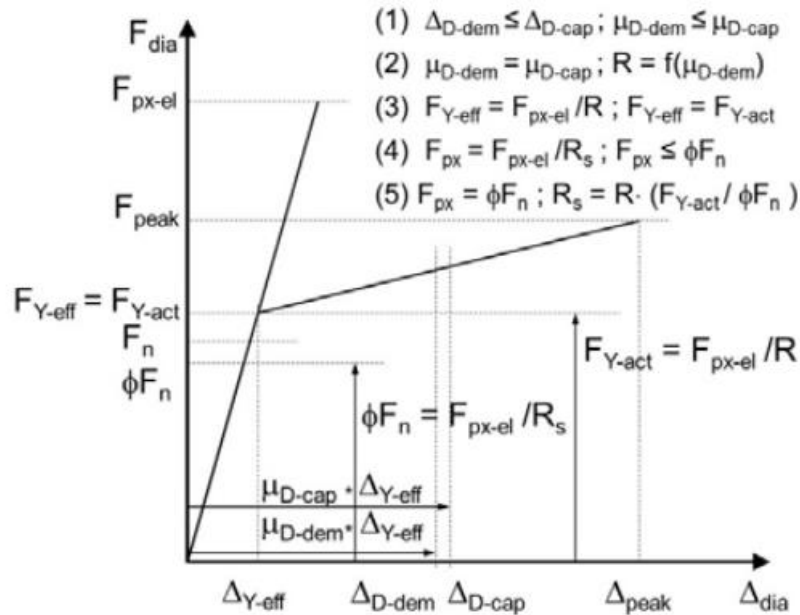
Figure 2. Diaphragm inelastic response model for a diaphragm system that exhibits a distinct yield point [Figure credit: 2015 NEHRP Provisions].

Based on shear wall test results, the global flexural ductility capacity of a reinforced concrete diaphragm has been estimated to be 3. Based on judgement the design ductility capacity is taken as two-thirds of the estimated global ductility capacity, so the design ductility capacity ($\mu_{D\text{-}cap}$) is 2.

Setting the ductility demand (μ_{dem}) equal to the design ductility capacity ($\mu_{D\text{-}cap}$) and using the equal energy rule, the ductility part of the force reduction factor R_μ is: $R_\mu = (2\mu_{dem} - 1)^{0.5} = 1.73$.

R_s is set equal to R_μ multiplied by the ratio $F_{Y\text{-}eff}/\phi F_n$. $F_{Y\text{-}eff}$ is taken equal to $F_{Y\text{-}actual}$ which is assumed to be $1.1F_n$ and ϕ equals 0.9[symbols $F_{Y\text{-}eff}$, $F_{Y\text{-}actual}$, and F_n *need to be explained*]. Therefore $R_s = 2.11$, which is rounded to be 2 for flexure-controlled cast-in-place reinforced concrete diaphragms.

Due to the geometric characteristics of a building, or other factors such as minimum reinforcement requirements, it will not be possible to design some reinforced concrete diaphragms to yield in flexure. Such diaphragms are termed as "shear-controlled" to indicate that they are expected to yield in shear. Since test data are not available to prove otherwise, the ductility of shear-controlled reinforced concrete diaphragms is taken as 1.0.

For shear-controlled reinforced concrete diaphragms, R_s has been specified as 1.5 because of expected overstrength. ACI-318 specifies a resistance factor, ϕ of 0.75 or 0.6 for diaphragm shear strength and limits the concrete contribution to the shear strength to only $2(f'_c)^{0.5}$. The ratio $F_{Y\text{-}eff}/\phi F_n$ for a reinforced concrete diaphragm, where $F_{Y\text{-}eff}$ is taken equal to $F_{Y\text{-}actual}$, is expected to exceed 1.5, which is the rationale for $R_s = 1.5$, even though μ_{dem} is assumed to be 1 for the design earthquake.

RP7-3.3 Wood Structural Panel Diaphragms

Wood-sheathed diaphragms are shear-controlled, with design strength determined in accordance with the Special Design Provisions for Wind and Seismic (SDPWS) (AWC, 2015) and the shear behavior based primarily on the sheathing-to-framing fastening. Wood diaphragm chord members are unlikely to form flexural mechanisms (ductile or otherwise), due to the overstrength inherent in axially loaded members designed in accordance with applicable standards.

The wood structural panel diaphragm R_s factor was derived using nonlinear response history analysis (NRHA) studies of a group of archetype light-frame buildings, conducted by Zhang and Cobeen (2014). The archetype buildings were braced with wood structural panel shear walls and had diaphragm spans ranging from 24 to 64 feet. Seismic design was provided in accordance with ASCE/SEI 7-10 (ASCE, 2010). The NRHA used a suite of ten earthquake ground motions. Pinching and degrading hysteretic models of the shear wall and diaphragm systems were developed. The model properties for the diaphragms addressed nine groups of diaphragm types for which seismic testing data were available, including consideration of: rated sheathing and Structural I sheathing, blocked and unblocked diaphragms, diaphragms with openings and high-load diaphragms with multiple lines of edge fastening. At both design earthquake (DE) and MCE ground motion levels, the NRHA considered R_s factors of 1.5, 2, 2.5, 3, 3.5, 4 and 5 to develop a relationship between R_s and the required global diaphragm ductility, μ_{dia}. In the case of wood structural panel diaphragms, it was determined that local ductility need not be specifically investigated, as the local ductility was seen to be consistently adequate to develop the global diaphragm ductility. Next, these data were compared to the available global diaphragm ductility justified by available test data for each diaphragm group. At DE ground motions, the lowest available global ductility was identified to be approximately 2.3 for high load nailed diaphragms; this was identified to correspond to $R_s = 3.5$. The highest available global ductility factor was identified to be approximately 6 for unblocked rated sheathing diaphragms, corresponding to $R_s > 5$. $R_s = 3$ was selected to be included in ASCE 7 Table 12.10-1. This value was selected to be conservative relative to data for the nine diaphragm groups. This was noted to typically result in diaphragm forces greater than or equal to those determined in accordance with the provisions of ASCE 7 Sections 12.10.1 and 12.10.2.

RP7-3.4 Bare Steel Deck Diaphragms and Concrete-on-Metal Deck Diaphragms

The R_s factors for bare steel deck diaphragms proposed in Part 1 of the 2020 NEHRP *Provisions* were developed using a multistep approach as described in the following paragraphs. First, past experimental data were collected and mined to evaluate ductility and overstrength of the diaphragm sub assemblages. Since these sub assemblage test specimens represent a small part of a diaphragm span, a method was developed to convert sub assemblage ductility into an estimated diaphragm system level ductility. The system level ductility and overstrength were then used to estimate an R_s value. The R_s value was then validated using NRHA on archetype buildings.

A database of past cantilever diaphragm experiments was assembled (O'Brien et al., 2017) including 671 bare steel deck diaphragm specimens and 82 diaphragm specimens that had some type of concrete fill on the metal deck. Of this set of 753 total past test specimens, 108 were found to provide sufficient information and include load-displacement data extending past the point of peak load, to allow evaluation of ductility and overstrength. This set of 108 included 20 concrete-on-metal deck diaphragm specimens and 88 bare steel deck diaphragm specimens. The bare steel deck diaphragm specimens were further subdivided into groups based on the types of support and sidelap fasteners.

As summarized in O'Brien et al. (2017), ductility and overstrength were obtained for each specimen. Ductility was defined as the ratio of shear angle associated with a 20% loss of strength relative to peak strength (consistent with FEMA P695 definition) to the shear angle associated with yield (calculated as the peak strength divided by the initial stiffness). Overstrength was calculated as the measured peak strength divided by the predicted strength using AISI S310 (AISI 2016) equations and nominal geometric and material properties.

The measured sub-assemblage ductility was then converted into a diaphragm system ductility (O'Brien et al. 2017). A diaphragm span experiences seismic loads as a distributed load such that the shear demands near the ends of the diaphragm span are considerably larger than those at midspan. Large portions of the diaphragm span may remain elastic during seismic loading, so the ultimate displacement of the diaphragm (for use in calculating diaphragm system ductility) can be assumed equal to elastic deformations plus inelastic deformations of a plastic zone near the ends of the diaphragm span. Results from cantilever

diaphragm specimens represent the load-deformation behavior of a small piece of the diaphragm in this plastic zone and thus can be used to determine the amount of inelastic deformations that can be expected in the plastic zone. An equation was developed to calculate diaphragm system ductility as a function of cantilever specimen (sub-assemblage) ductility.

Methods for calculating the response modification factor (i.e. R factors) based on the ductility and overstrength of the system have been proposed in the past (ATC 19 1995). This approach, which is described below in Section 4.2, was used to estimate the R_s factors. For bare steel deck diaphragms, it was determined that diaphragms with mechanical fasteners that comply with a certain set of detailing requirements (referred to here as "special detailing"), produce higher ductility and resulting R_s factor. For that reason, two values of R_s were proposed for bare steel deck diaphragms, a larger value of R_s=2.5 for those satisfying the special detailing requirements and a value of R_s=1.0 for all others. The special detailing requirements necessary to use a value of R_s>1.0 are being proposed for inclusion in future editions of AISI S400. A computational study involving NRHA of one-story archetype buildings that were part of the development of design procedures for rigid wall-flexible diaphragm structures was used to support the resulting values of R_s.

A similar approach was used to determine an R_s factor for composite concrete-on-metal deck diaphragms. Test data from a set of 16 cantilever diaphragm tests was used to quantify the ductility and overstrength of concrete-on-metal deck diaphragm subassemblies. Global diaphragm system ductility was then computed from subassembly ductility using the derived equation described above. The component ductility method as described in Section rp7-4.2 and, separately, the approach and assumptions used in determining the R_s factor for cast-in-place reinforced concrete diaphragms were applied to concrete-on-metal deck diaphragms. Both approaches resulted in R_s=2.0. A FEMA P695 type study is underway to verify the collapse resistance of buildings designed using the proposed R_s values (Wei et al. 2019, Foroughi et al. 2019). A detailed description of the approach for determining R_s for concrete-on-metal deck diaphragms and associated results are included in a white paper in Part 3 of the 2020 NEHRP *Provisions*.

RP7-4 METHODS TO BE CONSIDERED FOR FUTURE DEVELOPMENT OF R_S FACTORS

It is recognized that there are a number of methods by which diaphragm design force reduction factors, R_s, might be developed for diaphragm systems not already addressed. In all cases, physical testing on full diaphragm systems, subassemblies of diaphragms, diaphragm components, or assemblies that represent construction similar to the diaphragm is required. In some cases, tests directly provide the global deformation capacity, but more often, tests provide only the local response, including the strength and deformation capacity of diaphragm subassemblies, components and connections.

It is also necessary to determine the deformation demands associated with some seismic performance criteria. The mapped spectral response accelerations in ASCE 7-16 are intended to provide a target risk of structural collapse equal to 1% in 50 years based upon a generic structural fragility. FEMA P695 similarly defines acceptable response modification factors based on structural collapse. It is therefore deemed appropriate to consider structural collapse performance criteria similar to those in these two documents, when determining the deformation demands on diaphragm systems and diaphragm components.

In some cases, the hysteretic behavior of the diaphragm components obtained from experimental testing can be used directly in NRHA computational simulations to evaluate whether the designed diaphragm leads to acceptable seismic performance (i.e. sufficiently small probability of structural collapse). In other cases, computational simulation may be used to determine the deformation demands in diaphragm components which can then be compared to the deformation capacity obtained from experiments. A third option uses period-based deformation demands based on Newmark and Hall (1982) to define the required system level ductility demand (See Section RP 7-4.2). However, this last approach does not explicitly control probability of collapse (which is a function of more than just the yield strength), and therefore may be more appropriate

just for initial estimates of R_s. This section describes approaches thought to provide acceptable performance and some of the challenges that should be considered for each approach.

RP7-4.1 FEMA P-695 Methodology

FEMA P695 is a methodology for quantifying design factors such as the response modification factor, R, overstrength factor, Ω_o, and deflection amplification factor, C_d, for seismic force resisting systems to produce a probability of collapse less than 10% during the MCE. The approach consists of the following general steps: 1) define detailed design procedures and detailing for the seismic system, 2) calibrate nonlinear computational models to fit experimental behavior of the system or components that follow the defined design procedures and detailing, 3) define a set of archetype buildings and create nonlinear computational models of each, 4) conduct NRHA of the buildings with increasing scale factor on the ground motions until 50% of the building models collapse, and 5) evaluate whether there was a sufficiently large scale factor compared to the MCE and if not, change the design procedures / detailing and start over.

It is noted that FEMA P695 represents the best available approach for explicitly satisfying seismic performance goals related to collapse prevention of buildings. The approach is widely accepted and applied in the assessment of design procedures for existing seismic force resisting systems and development of design factors for new seismic systems.

However, FEMA P695 is typically applied using two-dimensional models of the vertical seismic force resisting system, and in the rare cases where three-dimensional models are used, the diaphragm has been considered rigid or elastic. To apply the FEMA P695 methodology in the development of diaphragm force reduction factors, R_s, there are a number of issues that should be considered:

- A full FEMA P695 study to determine an R_s factor requires a substantial amount of effort and computational time. Compared to a typical FEMA P695 analysis, additional archetype buildings may be required (see discussion in following items), the models need to be three-dimensional, models are generally more complex, and more elements have nonlinear behavior. Because of added complexity and nonlinearity, achieving convergence in nonlinear solution algorithms for these structural models is typically more difficult.

- The set of archetype buildings should span the intended design space for the vertical seismic system and diaphragm system. FEMA P695 identifies configuration variables that can affect system behavior such as: 1) occupancy and use, 2) elevation and plan configuration, 3) building height, 4) structural component type, 5) seismic design category and 6) gravity load intensity. In addition to these configuration variables, additional variables that can affect diaphragm system behavior include: 7) type of vertical seismic system 8) diaphragm span and aspect ratio and 9) diaphragm shape and openings. Since the list of configuration variables is longer than the list for vertical SFRS (1- 6 vs. 1- 9), a larger number of archetype buildings may be necessary for the evaluation of R_s. As stated in FEMA P695: "While index archetype configurations are not intended to represent every conceivable combination of design parameters, the archetype configurations must encompass the full design space permitted by the design requirements."

- Interaction between the vertical seismic system and diaphragm system should be considered. Three approaches are identified here:
    1. The set of archetypes could include a range of vertical seismic systems with varying plan and height in combination with a range of diaphragm spans and aspect ratios.
    2. To reduce the number of archetype buildings, the configurations could use a vertical seismic system with the lowest applicable R factor, largest expected overstrength in the vertical system, and lowest ratio of diaphragm to vertical system periods (see Section 2.2 for definition of these periods). As discussed in Section 2.2, this combination should result in the largest diaphragm demands. Like this approach.]
    3. It would be conservative to assume the vertical seismic system is elastic in the determination of an R_s factor. In this case, the computational models would use elastic

material behavior for the vertical system, and nonlinear material behavior for the diaphragm only.

- FEMA P695 was not created explicitly for diaphragm inelasticity or development of R_s factors. Use of NRHA on three-dimensional models and IDAs to estimate collapse resistance of combined vertical and horizontal seismic force resisting systems is a new undertaking, and as such is still under development. Further understanding of modeling of mechanisms, implications of scaling of earthquake, and other aspects of the methodology are still needed and little or no validation of results with full building behavior is available.

- When inelastic diaphragm behavior is considered in computational models, collapse probabilities get larger than with models that only consider the vertical seismic system. The lateral drift of the vertical seismic system and the deformations of the diaphragm lead to larger P-Delta forces which tends to destabilize the building faster. Also, there are more modes (i.e. shapes) of instability. It does not make sense to have the same acceptable collapse margin ratio for 2D models of the vertical system and 3D models that also capture diaphragm inelasticity. The acceptability criteria should be reviewed for these types of models.

Because of the challenges listed above, FEMA P695 has not been applied for any of the R_s factors defined in Chapter 3. One example of the application of the FEMA P695 methodology for diaphragms was for the development of the RWFD design methodology documented in FEMA P1026.

A modified approach employed in the definition of R_s for some diaphragm systems described in Section 3 used NRHA to determine ductility demands (either global diaphragm ductility demands, or local ductility demands) which were in turn compared to ductility capacity of diaphragm assemblies or components. This approach could be used to satisfy the intent of FEMA P695, if the hazard level (ground motion scale factor) is chosen in accordance with FEMA P695 Appendix F and the ductility demands are taken as the median demand obtained from a set of response history analyses.

RP7-4.2 Component Ductility Method

The component ductility method is based on the work of Newmark & Hall (1982) and ATC 19 (ATC 1995) and is an approach for determining the R_s factor as a function of the ductility and overstrength of the diaphragm system. Figure 3 shows schematically the force-deformation (F_{dia} vs. Δ_{dia}) response of a diaphragm spanning between two vertical elements of the seismic force resisting system (e.g. shear walls, braced frames, etc.).

It is noted, that the diagrams shown in Figure 3 are for global deformation behavior of a diaphragm span, which is not the same as the deformation behavior from a cantilever diaphragm test or a test on diaphragm components. To use this approach for calculating R_s factors, it is necessary to either experimentally obtain global diaphragm system behavior or to convert test data on subassemblies / components to the expected global behavior of a full diaphragm span. When tests provide only the local deformation behavior, typical diaphragms should be analyzed to estimate the associated global deformation behavior. These analyses should consider: (1) the specified yield mechanism, (2) the local force-deformation response data from tests, (3) the typical distributions of design strength and internal force demands across the diaphragm, and (4) the potential for localization of yielding (such as concentration of inelastic deformations at the ends of the diaphragm span) and any other factors that may cause concentrated local inelastic deformations to occur when the intended yield mechanism forms.
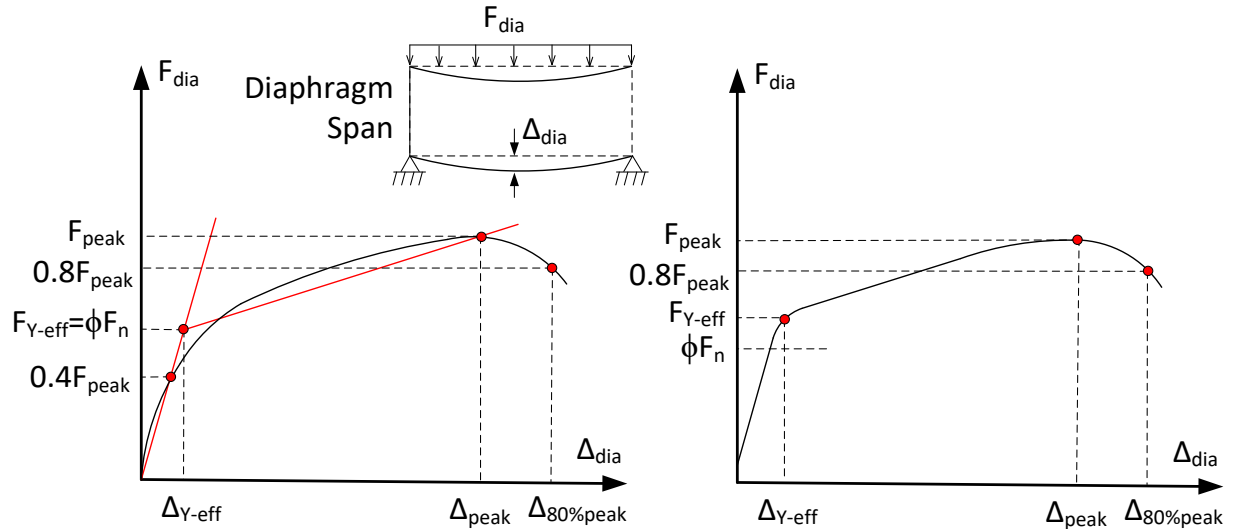
Figure 3. Diaphragm load vs. deformation response for (a) diaphragm system that does not exhibit a distinct yield point and (b) diaphragm system that does exhibit a distinct yield point.

Figure 3(a) shows the response of a diaphragm that does not exhibit a distinct yield point. In this case, the stiffness is defined by the secant stiffness through a point corresponding to 40% of the peak strength, F_{peak}, and the effective yield point is defined as the intersection of the secant stiffness and the design strength, ϕF_n. This effective yield point is used to define the effective yield strength, $F_{Y-eff} = \phi F_n$, and the effective yield displacement, Δ_{Y-eff}. Figure 3(b) shows schematically the force-deformation (F_{dia} vs. Δ_{dia}) response of a diaphragm with a well-defined yield point. For this type of a diaphragm system, the effective yield point is defined by the observed yield strength, F_{Y-eff}, and the yield displacement, Δ_{Y-eff}. In this case, the yield strength, F_{Y-eff} may be larger than the design strength ϕF_n.

Next, the design deformation capacity, Δ_{D-cap}, is determined. The ultimate deformation capacity can be taken as the displacement associated with peak load, Δ_{peak}, or for some diaphragm systems it may be acceptable to use the displacement corresponding to 80% of the peak load $\Delta_{80\%peak}$. However, only a portion of the deformation capacity of a diaphragm should be utilized for the design earthquake in recognition of two concerns: (1) the diaphragm must perform adequately under the MCE, which has a design response spectrum 50% more intense than the design earthquake response spectrum, (2) significant inelastic deformation under the design earthquake may result in undesirable damage to the diaphragm. As a rough estimate, the diaphragm deformation capacity for use with the design earthquake, Δ_{D-cap}, should be limited to approximately one-half to two-thirds of the ultimate deformation capacity. The global ductility capacity, μ_{cap}, can then be computed using Eq. (1). In Eq. (1), an example expression is given for the diaphragm deformation capacity, Δ_{D-cap}, as two-thirds the displacement corresponding to 80% of the peak load.

Previous work has shown that both ductility and overstrength contribute to the response modification factor (e.g. see ATC 1995). The contribution of ductility, R_μ, to the force reduction factor, R_s, is ideally derived from system-specific studies. Where such studies are unavailable, however, some guidance on the conversion from global ductility to force reduction is available from past investigations. Expressions that provide the ductility part of the force reduction factor, R_μ, for the seismic force-resisting system of a building corresponding to an expected ductility (μ_{cap}) have been proposed by numerous research teams (e.g. ATC 1995). Two such expressions, which are based on elasto-plastic force-deformation response under cyclic loading (Newmark & Hall, 1982), are given in Eq. (2). Eq. 2(a) for medium period structures is sometimes referred to as the equal energy rule and according to ATC (1995) is applicable for the period range 0.12 sec < T < 0.5 sec. Eq. 2(b) for long period structures is often called the equal displacement rule and ATC (1995) suggests that it is applicable for periods, T > 1.0 sec.

Overstrength can also contribute to the R_s factor. Eq. (3) defines the overstrength component, R_Ω, as the ratio of the diaphragm effective yield force to the diaphragm design strength, ϕF_n. For a diaphragm system without a distinct yield point, such as shown in Figure 3(a), the overstrength component is taken as $R_\Omega=1.0$ because the effective yield force was assumed equal to the design strength. Finally, the diaphragm response modification factor can be calculated using Eq. (4) as the product of the ductility and overstrength components.

$$\mu_{cap} = \frac{\Delta_{D-cap}}{\Delta_{Y-eff}}$$

$$\left(\Delta_{D-cap} = \frac{2}{3} \Delta_{80\% peak} \text{ for example} \right) \tag{1}$$

$$R_\mu = \sqrt{2\mu_{dem}-1}$$

valid for "medium" period systems (2a)

$$R_\mu = \mu_{dem}$$

valid for "long" period systems (2b)

$$R_\Omega = \frac{F_{Y-eff}}{\phi F_n}$$

(=1.0 for diaphragms that use $F_{Y-eff}=\phi F_n$) (3)

$$R_s = R_\Omega R_\mu \tag{4}$$

The procedure for using the component ductility method to define an R_s factor is summarized as follows:

1. Obtain the global diaphragm behavior from tests on full diaphragm spans or by converting test data from experiments on subassemblies or components to global diaphragm behavior.
2. Find the effective yield displacement, Δ_{Y-eff}, as shown in Figure 3, and the design deformation capacity, Δ_{D-cap}, as described above.
3. Calculate the diaphragm ductility capacity, μ_{cap}, using Eq. (1).
4. Calculate the ductility component, R_μ, of the response modification factor through system specific study or using Eq. (2).
5. Calculate the overstrength component, R_Ω, of the response modification factor using Eq. (3).
6. Calculate the response modification factor, R_s, using Eq. (4).

RP7-4.3 Demonstrating Equivalence to an Approved R_s

In the future, it may be desirable to develop new diaphragm connectors or diaphragm systems with similar behavior as conventional connectors or systems. As such, it may not be reasonable to conduct a large experimental or computational simulation program for every variation in a diaphragm system. It is therefore useful to create a framework whereby new diaphragm components or systems can be shown to have performance nominally equivalent to that of systems with an already approved R_s value. FEMA P795 (FEMA 2011) may be such a framework or the basis of a framework for diaphragm equivalency, but the method has not yet been applied to diaphragms and the associated challenges have not been determined.

Experience with the development of R_s values for conventional diaphragm systems has shown that there are several key aspects of the diaphragm load deformation response that affect building seismic behavior. To show that new diaphragm components or systems are equivalent to existing systems, it is necessary to show the following:

1. The new diaphragm system should have the same deformation mode, failure mechanism, and distribution of inelasticity through the diaphragm as the conventional system. For instance, if the strength and ductility of the conventional diaphragm system is associated with connectors between elastic panels (e.g. precast concrete or wood sheathed diaphragms), the new system needs to have

the same size and layout of panels and force the same failure mechanism in the connectors. This is important to keep the ductility demands similar between the new and conventional systems.

2. The new diaphragm system or diaphragm connectors need to demonstrate equal or better initial stiffness, strength, and ductility as the corresponding conventional system or connectors.

3. Other hysteretic parameters may also be important. For instance, severe pinching in the cyclic load-deformation response may lead to larger displacement demands.

Examples of this approach are available for precast concrete diaphragms, with testing standards referenced from ACI 318 (ACI 2019). Similarly, qualification testing for bare steel deck diaphragm connectors is being developed by AISI, and is anticipated to be included in AISI S400 with specified performance requirements for structural and sidelap connections.

RP7-5   RECOMMENDED NEXT STEPS

The following recommendations are made relative to the development of an accepted procedure for defining diaphragm response modification factors, R_s:

1. It is recommended that future editions of FEMA P695 and FEMA P795 be expanded to address diaphragm systems and the development of diaphragm seismic design parameters such as R_s. Alternatively, a similar effort could be pursued in separate documents, but regardless, resources will likely be required beyond a typical code committee.

2. As part of development of procedures to determine performance factors for diaphragms, consideration should be given to the interaction between the vertical and horizontal systems.

3. The specification of diaphragm deflection amplification factors or overstrength factors are absent from ASCE 7 and the 2020 NEHRP *Provisions*. Future development of diaphragm response modification factors, R_s, and the procedures to obtain R_s, should include these factors.

A more formalized procedure for computing diaphragm design factors or proving equivalence to existing diaphragm systems is needed. It is anticipated that these procedures will be used for either industry driven systems or proprietary systems through an evaluation service process.

RP7-6   REFERENCES

ACI (2019) Building Code Requirements for Structural Concrete (ACI 318-19), American Concrete Institute

ACI (2014) Building Code Requirements for Structural Concrete (ACI 318-14), American Concrete Institute

ACI (2013) Design Guide for Connections in Precast Jointed Systems (ACI 550.2R-13), American Concrete Institute

AISI (2015) AISI S400-15 North American Standard for Seismic Design of Cold-Formed Steel Structural Systems, American Iron and Steel Institute

AISI (2016) AISI S310-16 North American Standard for Design of Profiled Steel Diaphragm Panels, American Iron and Steel Institute.ASCE/SEI, 2010. Minimum Design Loads for Buildings and Other Structures, 2010 edition, American Society of Civil Engineers, Reston, Va.

ASCE/SEI, 2017. Minimum Design Loads and Associated Criteria for Buildings and Other Structures, 2016 edition, American Society of Civil Engineers, Reston, VA.

Applied Technology Council. (1995). ATC-19: Structural response modification factors. Applied Technology Council, Redwood City, California.

AWC, 2015. Special Design Provisions for Wind and Seismic (SDPWS), American Wood Council, Leesburg, VA

FEMA, 2009. Quantification of Building Seismic Performance Factors (FEMA P-695), Federal Emergency Management Agency, Washington, DC.

FEMA, 2011. Quantification of Building Seismic Performance Factors: Component Equivalency Method (FEMA P-795), Federal Emergency Management Agency, Washington, DC.

FEMA, 2015. NEHRP Recommended Seismic Provisions for Buildings and Other Structures, 2015 Edition (FEMA P-1050), Federal Emergency Management Agency, Washington, DC.

Fischer, A.W., and Schafer, B.W. (2018) "Inelastic Time History Response of Lumped Parameter Wall and Diaphragm Building", Eleventh U.S. National Conference on Earthquake Engineering, Los Angles, June 25-29.

Fleischman, R.B., Restrepo, J.I., Naito, C.J., Sause, R., Zhang, D., and Schoettler, M. (2013) "Integrated Analytical and Experimental Research to Develop a New Seismic Design Methodology for Precast Concrete Diaphragms" Journal of Structural Engineering, Vol. 139, No. 7, pp. 1192-1204.

Foroughi, H., Wei, G., Torabian, S., Eatherton, M.R., and Schafer, B.W. (2019) "Seismic Demands on Steel Diaphragms for 3D Archetype Buildings with Concentric Braced Frames", 12th Canadian Conference on Earthquake Engineering, Chateau Frontenac Quebec, QC, June 17-20.

Newmark, N.M, and Hall, W.J., (1982) Earthquake Spectra and Design, published by the Earthquake Engineering Research Institute

O'Brien, P., Eatherton, M.R., Easterling, W.S., Schafer, B.W., Hajjar, J.F. (2017) "Steel Deck Diaphragm Test Database v1.0." CFSRC Report R-2017-03, permanent link: jhir.library.jhu.edu/handle/1774.2/40634

Wei, G., Foroughi, H., Torabian, S., Schafer, B.W., and Eatherton, M.R. (2019) "Evaluating Different Diaphragm Design Procedures Using nonlinear 3d Computational Models", 12th Canadian Conference on Earthquake Engineering, Chateau Frontenac Quebec, QC, June 17-20.

Zhang, D. and Cobeen, K. (2014) "Nonlinear Response History Analyses of Light-Frame Timber Buildings", BSSC PUC Issue Team 6 (IT6) committee communications

RESOURCE PAPER 8 CALCULATION OF DIAPHRAGM DEFLECTIONS UNDER SEISMIC LOADING

RP8-1   INTRODUCTION

In ASCE 7-16, requirements relating to seismic deflection and drift limitations can be found in six locations in Chapter 12 and approximately 30 locations in Chapters 13 through 18. The 2020 NEHRP Provisions update proposal RS-1 has moved these provisions towards uniform terminology in order to provide increased clarity. Even with this increased clarity, questions have arisen regarding calculation of diaphragm deflections for use in the ASCE 7 provisions.

During the 2015 and 2020 NEHRP update cycles, a number of proposals relating to diaphragm seismic design forces were developed by the Provisions Update Committee's issue teams, resulting in the addition of two alternatives to the basic diaphragm seismic design force provisions of ASCE 7 Sections 12.10.1 and 12.10.2. New Section 12.10.3 provides an alternative seismic design procedure for diaphragms, chords and collectors using a diaphragm design force reduction factor, R_s. Section 12.10.4 provides an alternative seismic design procedure for flexible diaphragms in one-story rigid-vertical element, flexible-diaphragm structures. Sections 12.10.1, 12.10.2 and 12.10.3 are silent on determination of diaphragm deflections, deferring to other provisions in ASCE 7. Section 12.10.4 specifically identifies a $C_{d\text{-diaph}}$ factor for amplification of diaphragm deflections, consistent with the FEMA P-695 method that was used to develop the provisions.

Of the six ASCE 7-16 requirements relating to seismic deflection and drift, 2020 NEHRP proposal RS-1 has eliminated one (Section 12.12.2) and identified two (the second-order effect of Section 12.8.7 and the drift limits of Section 12.12.1), for which inclusion of diaphragm deflection is not required; as a result, these provisions are not considered further in this resource paper. The remaining three provisions for which diaphragm deflection must be considered are Section 12.12.3 structural separation, Section 12.12.4 members spanning between structures, and Section 12.12.5 deformation compatibility. Looking at these three and the Section 12.10 provisions as a group, IT9 has become aware that there is a significant lack of clarity as to how diaphragm deflections should be calculated and incorporated into building deflections and drifts. This includes both the force level at which deflections should be calculated, and the amplification of calculated deflections. Proposal RS-1 by Rafael Sabelli (Sabelli, 2019) provides clarity of intent for a number of aspects of earthquake displacement and drift calculations, but leaves determination of amplification of diaphragm deflection to the judgement of the designer.

This resource paper has been developed to document the questions that have arisen regarding calculation of design diaphragm deflections, relevant background information, and recommended further steps needed in order to provide clarification within the ASCE 7 provisions or commentary. This resource paper begins with Section RP8-2 discussion of structure types for which diaphragm deflection is of concern. Section RP8-3 discusses the need for clarity as to which force levels and amplification factors may be appropriate for the computation. Greater detail related to each of ASCE 7's three diaphragm design methods is provided in Section RP8-4 for the traditional diaphragm force procedure (ASCE 7 Section 12.10.1 and 12.10.2), Section RP8-5 for the alternative design provisions for diaphragms (ASCE 7 Section 12.10.3), and Section RP8-6 for the alternative seismic design procedure for flexible diaphragms in one-story buildings with rigid-vertical elements (ASCE 7 Section 12.10.4). Section RP8-7 discusses possible similar questions related to the Section 12.3.1.3 calculated flexible diaphragm condition. Finally, Section RP8-8 of this resource paper contains interim recommendations for designers and recommended next steps. This documentation has been developed to provide interim guidance to designers and with the hope that at a future time recommendations for next steps will be pursued in research or guideline development.

Background information relating to development of C_d factors can the found in a separate 2020 NEHRP Provisions resource paper titled "Seismic Design Story Drift Provisions: Current Questions and Needed Studies."

RP8-2 WHEN DIAPHRAGM DEFLECTION IS OF CONCERN

Diaphragm deflections can vary from near negligible in some diaphragm systems to very large in others. A few examples of diaphragm systems for which the deflection can be large and therefore potentially have a significant impact on design include:

- Rigid wall-flexible diaphragm (RWFD) structures with long-span wood structural panel or bare steel deck diaphragms. These are most often one-story structures, but can also be of two or three stories.
- Structures with long-span untopped precast concrete diaphragms, such as parking garages. These are commonly two and three story structures.
- Commercial or office buildings with long-span bare steel deck diaphragms. These structures are generally low rise, with the flexible diaphragm generally occurring at one or more roof levels.

While long spans are the predominant feature resulting in high deflection, span to depth ratios can also be contributors. Although these particularly stand out as requiring attention, the deflection in other diaphragm systems could potentially be critical for design. For this reason, the discussion of this resource paper is intended to apply to all diaphragm systems.

RP8-3 FORCE LEVELS AND AMPLIFICATION FACTORS FOR DETERMINATION OF DIAPHRAGM DEFLECTIONS

ASCE 7-16, Sections 12.10.1 and 12.10.2 provided seismic force levels for diaphragm design (F_{px}) forces. While some changes to the force level derivation have occurred, the provisions have been conceptually consistent over many editions of the ASCE 7 standard. These provisions do not make mention of calculations of seismic deflections. Provisions regarding determination of story drift are found in Sections 12.8.6, 12.9.1 and 12.9.2. These indicate use of F_x forces that are amplified by the C_d associated with the vertical seismic force-resisting system (SFRS). The structural separation, members spanning between structures and deformation compatibility provisions of Sections 12.12.3, 12.12.4, and 12.12.5 refer back to these sections and equations, suggesting use of F_x forces and tabulated C_d factors. When added into ASCE 7-16, Section 12.10.3 similarly incorporated provisions for diaphragm seismic forces without specifically addressing calculation of diaphragm deflections.

When further consideration is given to the intent of the calculated deflections, a reasonable argument can be made for using F_{px} forces for determining diaphragm deflections. The F_{px} forces are intended to identify the most critical diaphragm design forces that might occur over the duration of a design level ground motion, while the F_x forces are intended to identify the most critical shears and moments in the vertical elements. If the deflection of the diaphragm is of concern, it would best be evaluated using the F_{px} forces representing the most critical seismic forces to the diaphragm.

At this time there is thought to be a range of practice in the design community regarding force levels used for calculation of diaphragm deflections for both single-story and multi-story buildings. It appears desirable to provide recommendations or design provisions to narrow the range of practice.

In multi-story buildings the potential differential deflection between two adjacent stories adds further complexity that is of concern and interest. Several different patterns of loading could potentially be applied:

- The worst case scenario would have diaphragms at adjacent stories completely out of phase. In talking to designers, this is not currently perceived as a necessary design case.
- A second scenario would have one diaphragm deflect while diaphragms above and below have no deflection.
- A third scenario would have each diaphragm over the height of the building deflecting at F_x or F_{px} level forces, resulting in significant differential deflections between ground and second floor diaphragm, but little to no differential deflection for stories above.

The third scenario is likely what is most often implemented in design. This third scenario is important to consider in all structure designs, as it should capture the most critical relative displacement between the ground and second floor, which is often the highest drift demand in the structure. There may, however, be building configurations where a more detailed consideration of deflection patterns over the height of the structure is appropriate.

Similarly, consideration is needed regarding appropriate amplification of diaphragm deflections. With the development of Section 12.10.4 provisions based on the FEMA P-695 methodology, a $C_{d\text{-}diaph}$ factor for amplification of diaphragm deflections was specifically derived. This in turn brought up the question of what amplification might be applied to diaphragms using forces from Sections 12.10.1, 12.10.2 and 12.10.3. When the question of diaphragm deflection amplification is considered, it is logical that the deflection amplification should be a function of the diaphragm system, rather than the vertical elements of the SFRS.

RP8-4   TRADITIONAL DIAPHRAGM DESIGN APPROACH (ASCE 7 §12.10.1)

Calculation of diaphragm design forces in accordance with ASCE 7 Section 12.10.1 has been the typical approach for many decades. The diaphragm design force F_{px} is derived from the story force F_i which is derived from the base shear $V=C_sW$ (with applicable upper and lower bounds). Embedded within C_s and thus F_{px} is the SFRS's response modification coefficient, R, which reduces forces down to design levels. As such, to compute the SFRS's maximum inelastic displacements, it would generally be anticipated that design force level displacements computed based on C_s would be amplified by the deflection amplification factor C_d to obtain inelastic displacements. In a broad sense, R reduces the building's expected seismic forces down to a reasonable design level with considerations for ductility and overstrength, and C_d brings the displacements computed with those design forces back up to an expected inelastic level. Lacking other specific direction from the ASCE 7 provisions, it might be anticipated that this is a commonly used approach for calculating deflections for diaphragms as well as vertical elements of the SFRS.

Where the deflection of a diaphragm is to be calculated, Chapter 12 provisions do not currently have requirements other than implied use of F_x forces amplified by the C_d of the vertical SFRS. An important question is whether the deflection amplification factors C_d in ASCE 7 Table 12.2-1 should be used to amplify the computed design force level diaphragm deflections up to inelastic levels for the purpose of evaluating building separations, property line setbacks, structural integrity, and deformation compatibility. The use of the SFRS's C_d to obtain maximum inelastic diaphragm deflections has been illustrated in published seismic design examples (SEAOC, 2016; Lawson, 2013).

If a designer uses F_x forces amplified by C_d, some concerns are created. The deflection amplification factor C_d is used to partially offset the response modification coefficient's force reduction, however both R and C_d are related to the expect performance of the SFRS, not the diaphragm. An example that suggests that this approach is not appropriate is the comparison of two RWFD buildings with identical diaphragms: One building is comprised of a Special Reinforced Concrete Shear Wall system (R=5, C_d=5) and the other building is comprised of a Special Masonry Shear Wall system (R=5, C_d=3.5). Assuming similar building mass, both have identical base shears and identical diaphragm loading and thus diaphragm construction; however, their C_d's would seemingly predict very different inelastic diaphragm deflections.

This discussion suggests that the deflection amplification factors corresponding to the response modification coefficients of the SFRS vertical elements found in ASCE 7 Table 12.2-1 may not provide the most rational approach to computation of inelastic diaphragm deflections. An alternative approach is not currently provided by ASCE 7 when using the diaphragm design procedure in Sections 12.10.1 and 12.10.2. Development of more specific direction to the designer is recommended; interim recommendations can be found in Section RP8-8.

RP8-5 ALTERNATIVE DIAPHRAGM DESIGN PROVISIONS (ASCE 7 §12.10.3)

ASCE 7-16 Section 12.10.3 introduced an alternate design procedure for diaphragms; this procedure provides unique diaphragm design force reduction factors, R_s, as specified in Table 12.10-1. Unlike the SFRS response modification coefficients R in Table 12.2-1, R_s factors are directly related to the expected performance of the diaphragm design and construction. This alternative procedure, however, does not currently have requirements for calculation of diaphragm deflection other than use of F_x forces amplified by the C_d of the vertical SFRS.

If a designer uses F_x forces amplified by C_d, some concerns are created. To illustrate this, consider the design of a 1-story building that incorporates an intermediate precast concrete shear wall system with flexible wood structural panel diaphragm designed for $S_{DS} = 1.0$). For this example building, the building base shear V and story force F_x is 0.25W, but the diaphragm design force F_{px} is $0.208w_x$, reflecting the two different approaches taken for the building design and diaphragm design. As discussed in Section RP10-3, some suggest that F_x force levels are appropriate for the diaphragm deflection design instead of F_{px} which is used for diaphragm strength. However, in this example that approach results in 20-percent higher forces for diaphragm deflection analysis; calculation of deflections at this force level imply overstress in the wood structural panel nailing because the nail-slip shear forces exceed those permitted for diaphragm deflection computations by AWC SDPWS Table C4.2.2D.

There are no unique deflection amplification factors corresponding to R_s provided. In order to have a broader view of the alternative diaphragm design procedure's development of design forces, consider a one-story building. The diaphragm design forces are computed by starting with the actual anticipated building force levels, reduced by the SFRS's R, then increased by the SFRS's Ω_o, then reduced by the diaphragm's R_s. This process can be generalized as follows for this specific one-story building example:

$$F_{px} \approx S_{DS}I_e \left[\frac{1}{R} \times \Omega_o \times \frac{1}{R_s} \right] w_{px}$$

It is evident that a deflection amplification factor C_d that corresponds to the SFRS and R is not necessarily appropriate for the diaphragm design based on R_s. To compute the maximum expected diaphragm deflections δ_x, considering inelastic behavior, a deflection amplification factor C_d is not provided in the alternative design procedure; but it is likely appropriate to use $C_d = R_s$. Development of more specific direction to the designer is recommended; interim recommendations can be found in Section RP8-8.

RP8-6 ALTERNATIVE SEISMIC DESIGN PROCEDURE FOR FLEXIBLE DIAPHRAGMS IN ONE-STORY BUILDINGS WITH RIGID-VERTICAL ELEMENTS (ASCE 7 §12.10.4)

Newly introduced ASCE 7 Section 12.10.4 provides a design methodology that considers the seismic behavior, performance, and inelastic deflection of both the SFRS and diaphragm for one-story RWFD buildings. This procedure's development is outlined in FEMA P-1026 as well as in a previous NEHRP Part 3 resource paper (NEHRP, 2015). In this alternate design procedure, a separate response modification coefficient R_{diaph} and deflection amplification factor $C_{d\text{-}diaph}$ are provided for the diaphragm design through a two-stage analysis procedure. For diaphragms using wood structural panels fastened with nails, R_{diaph} is equal to 4.5, with a 10% wide perimeter band strengthened 1.5x to encourage distributive yielding (Koliou et al., 2016). A corresponding $C_{d\ diaph} = 4.5$ is specified for wood structural panel diaphragms. The development of R_{diaph} and $C_{d\text{-}diaph}$ followed the procedure described in FEMA P-695 (FEMA, 2009), but are only valid when the alternative design procedure with perimeter strengthening is employed. The decision to select $C_{d\ diaph} = R_{diaph}$ was based on recommendations within FEMA P-695, based on the "Newmark Rule." FEMA P-695 states, "In general, inherent damping may be assumed to be 5% of critical…. Thus, for most systems the value of C_d will be equal to the value of R."

Chapter 6 of FEMA P-1026 illustrates a design example on a 400-ft x 200-ft tilt-up concrete building with wood structural panel diaphragm in Seismic Design Category D_{max} and computes an elastic diaphragm deflection of 6.48-inches using a simplistic standard approach. Estimating the inelastic diaphragm response with $C_{d-diaph} = 4.5$, maximum inelastic deflection is reported at 29.1-inches. However, as outlined in Lawson (2019), this deflection is based on very conservative assumptions, and a separate analysis using more refined assumptions with the same $C_{d-diaph}$ factor indicates an inelastic diaphragm deflection less than 12-inches.

An update to FEMA P-1026 is underway to include untopped steel deck diaphragms with unique R_{diaph} and $C_{d\,diaph}$ parameters for design based on research work by Schafer (2019).

RP8-7   CALCULATED FLEXIBLE DIAPHRAGM CONDITION

While some designers may be concerned that a similar consideration of forces and deflection amplification is needed in order to use the calculated flexible diaphragm condition provisions of Section 12.3.1.3, such consideration is not necessary. Section 12.3.1.3 is intended as a relative check of deflection between the diaphragm and supporting vertical elements, with both δ_{MDD} and Δ_{ADVE} at similar design force levels. Thus, this comparison is calculated at F_x design level forces, with no consideration of amplification of either the diaphragm or the vertical element deflections.

Some confusion may still exist because loading from Section 12.8 is explicitly indicated, and Section 12.8.6 defines the design story drift, Δ, as determined using the building deflections amplified by C_d. Amplification of deflections when using Section 12.3.1.3 is not intended.

RP8-8   INTERIM RECOMMENDATIONS AND FURTHER STEPS

The current ASCE 7 Chapter 12 provisions do not appear to give the designer adequate direction regarding calculation of diaphragm deflections. The following are put forward as interim recommendations.

RP8-8.1   Force Level for Calculation of Diaphragm Deflection

It is recommended that diaphragm deflections be calculated using F_{px} forces. Reasons include:

- This is the current best available indicator of design forces and therefore design deflections for diaphragms,
- In a multi-story building, F_x at lower floors will underestimate diaphragm forces and therefore diaphragm deflections, and most notably the deflection of the second floor diaphragm with respect to the ground floor, and
- Use of F_{px} prevents the disparity shown in the example in Section RP8-5 where the F_x forces used to calculate the deflection can imply overstress in the diaphragm.

RP8-8.2   Amplification of Diaphragm Deflection

Four methods are suggested for determining the amplification of diaphragm deflections, based on the method used to determine the design level F_{px} forces used in diaphragm deflection calculations. These methods are recommended for use as follows:

- When using diaphragm design forces determined in accordance with Section 12.10.3, it is recommended that Method 3 be used.
- When using diaphragm design forces determined in accordance with Section 12.10.4, it is recommended and intended that Method 4 be used.
- When using diaphragm design forces determined in accordance with Sections 12.10.1 and 12.10.2, either Method 1 or Method 2 can be used, but Method 2 is recommended.

Method 1. For diaphragm deflections calculated using design level F_{px} forces determined in accordance with Sections 12.10.1 and 12.10.2, deflections are to be multiplied by 0.7R, using R in accordance with Table 12.2-1. Method 1 is roughly equivalent to multiplying by the C_d for the vertical elements of the seismic force-resisting system, but removes the concern regarding variability of C_d factors that was discussed in Section RP8-4. For purposes of this method, R might be limited to not greater than five; this will compensate for diaphragm design forces in some cases being controlled by minimum required F_{px} forces. This is the least preferred amplification method because it relies on force levels and amplifications that are representative of the vertical elements of the SFRS, and not necessarily good predictors of diaphragm response.

Method 2. For diaphragms deflections calculated using design level F_{px} forces determined in accordance with Sections 12.10.1 and 12.10.2, deflections are to be multiplied by F_{px} as calculated in Section 12.10.3 and R_s as determined in Section 12.10.3, and divided by F_{px} as determined in Sections 12.10.1 and 12.10.2. Because the R_s factor will cancel out when determining deflections with this method, it is possible to use this for any diaphragm system, whether or not it has a listed R_s-factor. Method 2 recognizes Section 12.10.3 F_{px} times R_s as the best available estimate of anticipated diaphragm forces for near-elastic behavior. By multiplying the deflection at design level forces by this ratio, a best estimate of diaphragm inelastic deflection is provided.

Method 3. For diaphragm deflections calculated using design level forces determined in accordance with Section 12.10.3, amplification of diaphragm deflections by R_s is recommended.

Method 4. For diaphragms designed in accordance with Section 12.10.4, use of the provided $C_{d\text{-diaph}}$ factor is required and appropriate.

RP8-8.3   Patterns of Diaphragm Deflection

Sections RP8-2 and RP8-3 discuss patterns of diaphragm deflection that might be of concern when considering deformation compatibility. The drift imposed on elements of the gravity load-carrying system at any point in the structure is determined by the combination of the drift of vertical elements of the SFRS and deflections of the diaphragms. It is recommended that consideration be given to likely patterns of force and deflection in vertical elements and each diaphragm when determining drift levels imposed on the gravity load-carrying system.

RP8.8-4   Further Steps

For future development, it is recommended that available information be collected from numerical studies and instrumented buildings to develop $C_{d\text{-diaph}}$ factors for all diaphragm design methods and diaphragm systems. This effort would be intended to result in guidance for designers, replacing the interim guidance provided above. It is also recommended that systematic consideration be given to the patterns of diaphragm deflection to be used in design of multi-story buildings, further pursuing the discussion in Section RP8-3. Some sources of strong motion records for flexible diaphragm can be found in the following papers: Wood and Hawkins (1998), Graf and Malley (2004), and Freeman et al. (1995).

RP8-9 REFERENCES

ASCE, 2017. *Minimum Design Loads and Associated Criteria for Buildings and Other Structures*, 2016 Edition (ANSI/ASCE 7-16), American Society of Civil Engineers, Reston, VA.

AWC, 2015. *Special Design Provisions for Wind and Seismic* (SDPWS), American Wood Council, Leesburg, VA.

BSSC, 2019. Provisions Update Committee Proposal RS-1. See BSSC ballot archives.

FEMA, 2009. *Quantification of Building Seismic Performance Factors* (FEMA P-695), Federal Emergency Management Agency, Washington, DC.

FEMA, 2015. *Seismic Design of Rigid Wall-Flexible Diaphragm Buildings: An Alternative Procedure* (FEMA P-1026), Federal Emergency Management Agency, Washington, DC.

Freeman, S.A., Gilmartin, U.A., and Searer, G.R., 1995. "Tilt-up Construction: Proposed Seismic Design Procedures Developed from Strong Motion Research." *Proceedings of the NEHRP Conference and Workshop on Research on the Northridge, California Earthquake of January 17, 1994.* Consortium of Universities for Research in Earthquake Engineering, Richmond, CA

Graf, T. and Malley, J., 2004. *Evaluation and Application of Concrete Tilt-Up Assessment Methodologies* (PEER 2004/03), Pacific Earthquake Engineering Research Center, University of California, Berkeley, CA

Koliou, M; Filiatrault, A; Kelly, D.J.; and Lawson, J, 2016. "Distributed Yielding Concept for Improved Seismic Collapse Performance of Rigid Wall – Flexible Diaphragm Buildings," *Journal of Structural Engineering*, February, 2016, American Society of Civil Engineers, Reston, VA.

Lawson, 2013. *Seismic Design of Timber Panelized Roof Structures,* WoodWorks, Wood Products Council, Washington DC.

Lawson, 2019. "Improving the Accuracy of Wood Diaphragm Deflection Computations and its Impact on ASCE 41 Pseudo-Lateral Force Estimates," *2019 SEAOC Convention Proceedings*, August, 2019, Structural Engineers Association of California, Sacramento, CA.

NEHRP, 2015. "One-Story, Flexible Diaphragm Buildings with Stiff Vertical Elements," *Recommended Seismic Provisions for New Buildings and Other Structures* (FEMA P-1050-2), 2015 Edition, Volume II: Part 3 Resource Papers, pp. 111-161, Building Seismic Safety Council and the National Institute of Building Sciences, National Earthquake Hazard Reduction Program, Washington, DC.

Schafer, 2019. Research on the Seismic Performance of Rigid Wall Flexible Diaphragm Buildings with Bare Steel Deck Diaphragms. CFSRC Report 2019-2.

SEAOC, 2016. *2015 IBC SEAOC Structural/Seismic Design Manual – Vol. 2*, Structural Engineers Association of California, Sacramento, CA.

Wood, S. and Hawkins, N., 1998. "Measured Response of Two Tilt-up Buildings," *The Loma Prieta Earthquake of October 17, 1989 – Building Structures*, United States Geological Survey Professional Paper 1552-C, United St

RESOURCE PAPER 9 MODAL RESPONSE SPECTRUM ANALYSIS METHODS

RP9-1   INTRODUCTION

During the 2020 NEHRP update cycle, Issue Team 3 (IT-3) reviewed and considered potential updates to the existing Response Spectrum Analysis (RSA) method of ASCE 7-16 Section 12.9.1. RSA is one of the recommended methods of lateral analysis of structures and has traditionally been considered superior to the Equivalent Lateral Force Analysis (ELF) of Section 12.8. RSA, (or the more advanced Linear Response History Analysis), is therefore the required elastic analysis procedure for structures that possess certain irregularities or for flexible buildings taller than 160 feet in height. The effort of the IT-3 was intended to focus on reviewing the existing state of the RSA and suggest improvements as appropriate.

RP9-2   BACKGROUND

IT-3 identified a list of tasks at the beginning of the provision update cycle. These tasks included the following:

1. Application of the response modification factor, R only to first mode response, assuming that higher mode structural response typically does not include significant nonlinear behavior.

2. Consideration (or reconsideration) of the appropriateness of current approaches for scaling to the results of ELF including drift, base shear, overturning moment, etc.

3. Application of a multi degree of freedom factor to RSA scaling.

4. Revision of triggers for RSA in ASCE 7.

Note that currently ASCE 7-16 requires RSA for the following structures in SDC D, E and F:

a. Structures exceeding 160 ft in structural height with any structural irregularity or $T > 3.5T_s$

b. Structures not exceeding 160 ft in structural height and having horizontal irregularities of Type 1a, 1b or 5 in Table 12.3-1 or vertical irregularities of Type 1a, 1b, 2 or 3 in Table 12.3-2.

As part of this study, trigger a and horizontal irregularity 1a and vertical irregularity 1a, 2 of trigger b were investigated.

Recommendations derived from the studies by the IT-3 committee for Tasks 1 through 4 are summarized at the end of the paper.

RP9-3   ANALYTICAL EFFORT

IT-3 studied a series of analytical models of archetype structures to address the tasks listed in the previous section. The various archetypes and models studies are listed below:

- Low to Mid-Rise (3-story, 6-story and 9-story) Steel Special Moment Frame study (2D Model).

- 20-Story Regular Steel Moment Frame Study (2D Model).

- Low to Mid-Rise (3-story, 6-story and 9-story) Buckling-Restrained Braced Frame Study (2D Model).

- 20-Story Steel Moment Frame Study with mass irregularities at 5th, 10th and 15th level (2D Model).

- 20-Story Steel Moment Frame Study with Stiffness Irregularity at 10th and 15th level (2D Model).

- 8-Story Reinforced Concrete Shear Wall building with (a) no plan irregularity (b) plan irregularity about one axis and (c) plan irregularity about both axes.

- Reinforced Coupled Concrete Shear Wall buildings (study conducted by UCLA).

For the purpose of the above studies, all buildings except the ductile coupled wall buildings were located in Los Angeles with S_{DS} = 1.3 and S_{D1} = 0.73. A standard RSA was first performed on all the models using ASCE 7-16. This was followed by a nonlinear response history analysis (NLRHA) using the software program PERFORM-3D (Version 7.0.0). The moment frame designs for the 3, 6 and 9-story buildings were based on Sanchez et al. (2017). Hence the same seven sets of ground motion mentioned in that paper were utilized for the NLRHA with different sets of scale factors used for the various archetypes (same scale factor was used when the periods were relatively close). These sites correspond to relatively high seismicity areas with Strike-slip, Reverse or Reverse-oblique faulting mechanisms, maximum expected moment magnitudes, M_w of 6-8 and a distance to the R_{jb} greater than 10 km, therefore, not affected by fault directivity effects. In addition, a shear wave velocity, v_{s30} of approximately 750 ft/sec corresponding to stiff soil or Site Class D was assumed for the site. The various ground motions are listed in Table 1. Note that ASCE 7-16 Site Class D specific scaling of F_v to 2.5 was not followed. However, it is our opinion that this scaling will not affect the conclusions derived at the end of this study.

Ground motions were amplitude scaled per ASCE 7 Section 16.2.3 to match the DE spectra. For each pair of ground motions, the maximum direction spectrum (ROTD100) was obtained from the PEER Database. The motions were then scaled in the period ranges of 0.2 to 1.5 times the fundamental period of the structure such that the average of the maximum direction spectrum did not fall below 90% of the target spectrum in that period range. A sample scaling for the 3, 6 and 9-story moment frames is shown in Figure 1. The fundamental periods for these three buildings are 0.41 sec, 0.77 sec and 1.26 sec respectively. The same scale factor was used for all three buildings for the sake of simplicity.

Table 1 – Characteristics of Selected Ground Motions

Earthquake	Year	RSN# *	Station Name	*Mw*	Mechanism	Scale Factor
Imperial Valley	1940	6	El Centro Array #9	6.95	Strike Slip	2.60
Kern County	1952	15	Taft Lincoln School	7.36	Reverse	2.77
Northern. California	1954	20	Ferndale City Hall	6.50	Strike Slip	2.50
San Fernando	1971	57	Castaic Old Rdg Rte	6.61	Reverse	2.19
Friuli, Italy	1976	125	Tolmezzo	6.50	Reverse	2.15
Imperial Valley	1979	164	Cerro Prieto	6.53	Reverse	2.26
Coalinga	1983	340	Parkfield-Flt Zone 16	6.36	Reverse	3.39

RSN = Record Sequence Number used in the NGA-West 2 Online Ground Motion Database
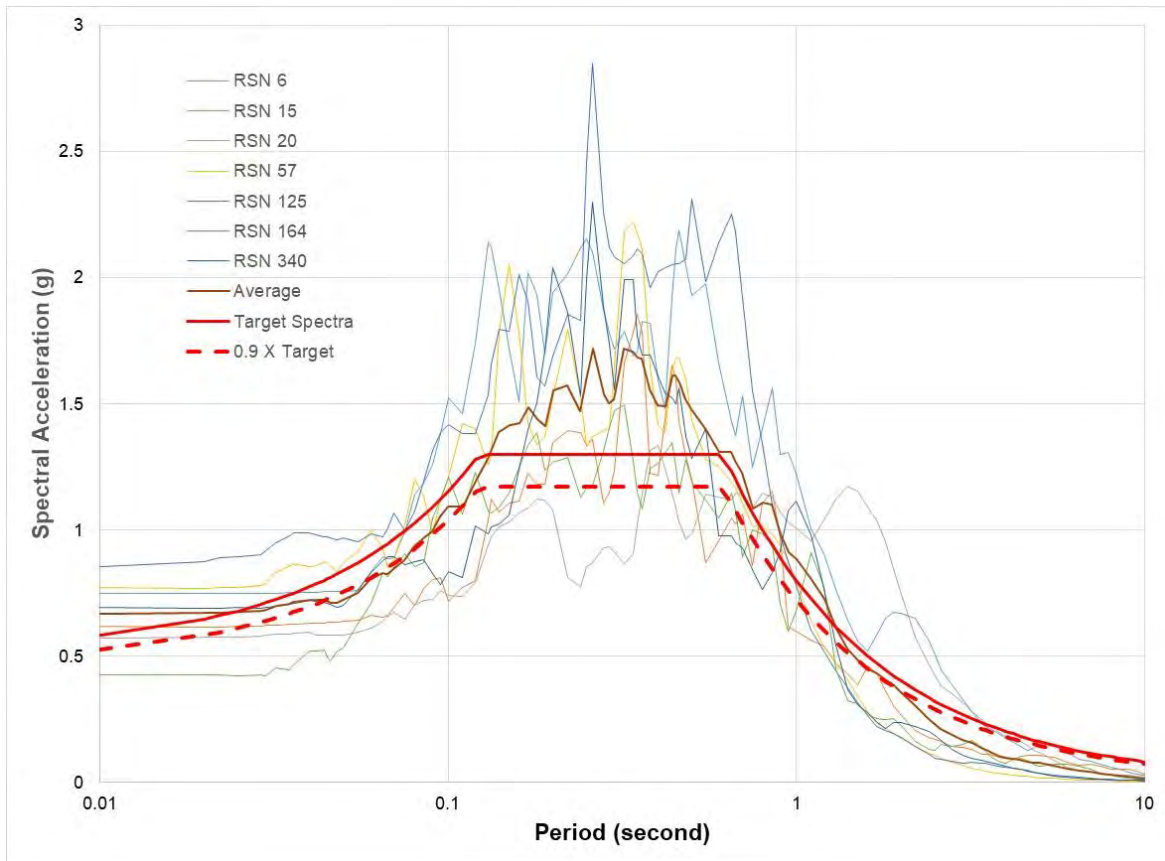
Figure 1 Maximum Direction Spectra Illustrating the ASCE 7 Scaling Procedure

Low to Mid-Rise Moment Frame Study: For the purpose of this study, the steel moment frames that were designed by Sanchez et al. (2017) were used. Typical elevations and plan view of the three frames are shown in Figure 2. To calculate the drifts for the standard case (Response Modification Coefficient (R) applied uniformly), all spectral ordinates were scaled by C_d. For the case where R was only applied at the fundamental period, only that spectral ordinate was scaled by C_d. All other ordinates were left unscaled. This was done because low to mid-rise moment frames are principally first mode governed and hence any inelastic behavior of members is more than likely to govern the first (fundamental) mode.

Recommendations of ASCE 41-13 were used to model the nonlinear beam and column hinges for the time history analysis (refer to Figure 2). All beam-to-column connections were assumed to be standard WUF-W per AISC 358-16.

Figure 3 shows the results of this study for the 9-story and 6-story moment frames. As can be seen from this Figure, the differences in drift between the models where R is only used in the first mode versus all modes, as is the current practice, is not as pronounced as the behavior of these buildings are predominantly governed by the fundamental mode. However, it is obvious from the 6-story moment frame plot that both the scaling approaches seem to under predict the drift when compared to the nonlinear analysis results illustrating the inappropriateness of C_d value. The use of $C_d = R$ is perhaps more justified in the case of the 6-story structure. Results of the 3-story building are similar to the 6-story structure.

3-bay frames
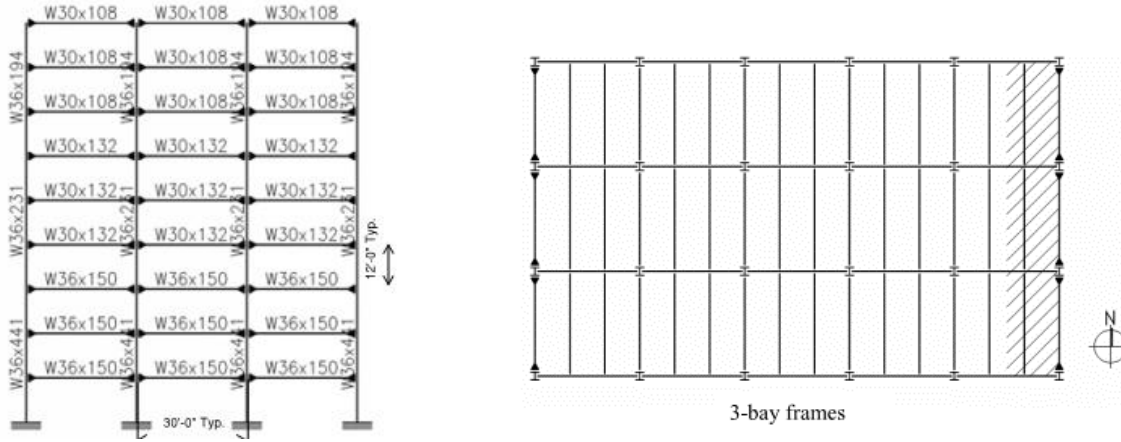
Table 9-6. Modeling Parameters and Acceptance Criteria for Nonlinear Procedures—Structural Steel Components

	Modeling Parameters			Acceptance Criteria		
	Plastic Rotation Angle, Radians		Residual Strength Ratio	Plastic Rotation Angle, Radians		
Component or Action	a	b	c	IO	LS	CP
Fully Restrained Moment Connections[f]						
WUF[g]	0.051–0.0013d	0.043–0.00060d	0.2	0.026–0.00065d	0.0323–0.00045d	0.043–0.00060d
Bottom haunch in WUF with slab	0.026	0.036	0.2	0.013	0.0270	0.036
Bottom haunch in WUF without slab	0.018	0.023	0.2	0.009	0.0180	0.023
Welded cover plate in WUF[g]	0.056–0.0011d	0.056–0.0011d	0.2	0.028–0.00055d	0.0420–0.00083d	0.056–0.0011d
Improved WUF—Bolted web[g]	0.021–0.00030d	0.050–0.00060d	0.2	0.010–0.00015d	0.0375–0.00045d	0.050–0.00060d
Improved WUF—Welded web	0.041	0.054	0.2	0.020	0.0410	0.054
Free flange[g]	0.067–0.0012d	0.094–0.0016d	0.2	0.034–0.00060d	0.0705–0.0012d	0.094–0.0016d
Reduced beam section[e]	0.050–0.00030d	0.070–0.00030d	0.2	0.025–0.00015d	0.0525–0.00023d	0.07–0.00030d

ASCE 41-13 Modeling Parameters for Beam Hinges

Figure 2 Typical Elevation, Plan View and Nonlinear Modeling Parameters for the Low-Mid Rise Moment Frame Study.
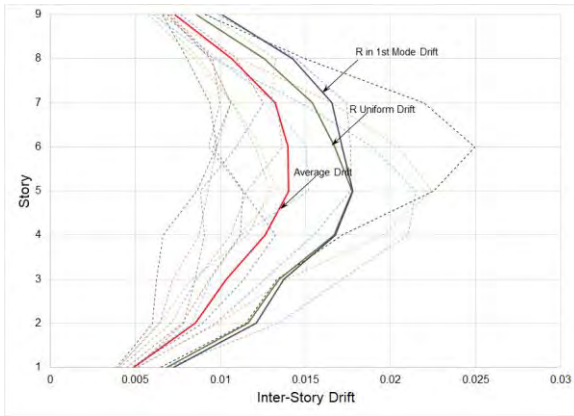
Drift Results for 9 Story Moment Frame
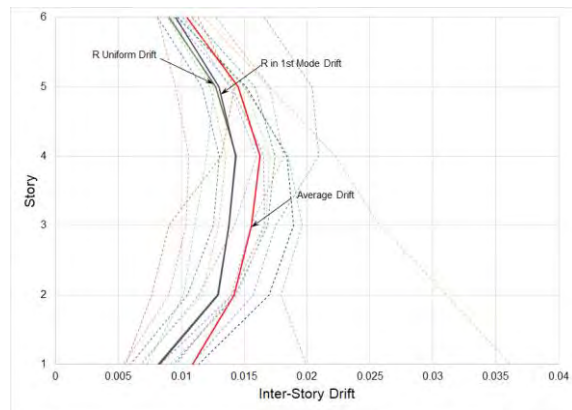
Drift Results for 6 Story Moment Frame

Figure 3 Comparison of Elastic Story Drifts Scaled to C_d/R to Drifts from NLRHA for Low to Mid Rise Steel Moment Frames.

20-Story Regular Moment Frame Study: The 20-story moment frame was analyzed following a similar procedure to the low rise moment frames. The mid-rise 20-story building was redesigned using ASCE 7-16 MRSA (base shear scaled to 100% ELF) and the subsequent nonlinear model was analyzed to the suite of seven scaled time histories. Figure 4 shows the comparison of the nonlinear story shear to the elastic response spectral story shear for the cases where the spectrum is scaled uniformly by R and when the spectrum is scaled by R only in the fundamental mode. The results indicate that the unscaled base shear (base shear not set to code specified shear) for the case where the spectrum is scaled only in the first mode exceeds the uniformly scaled spectrum results significantly. However, the drifts predicted by both the scaling approaches do not differ by the same amount. The drifts calculated using $C_d = R$ match the nonlinear drifts better than either of the individual scaling approaches.
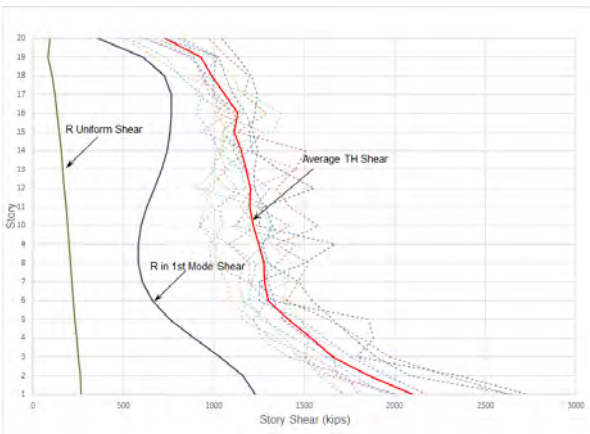
Comparison of Story Shear
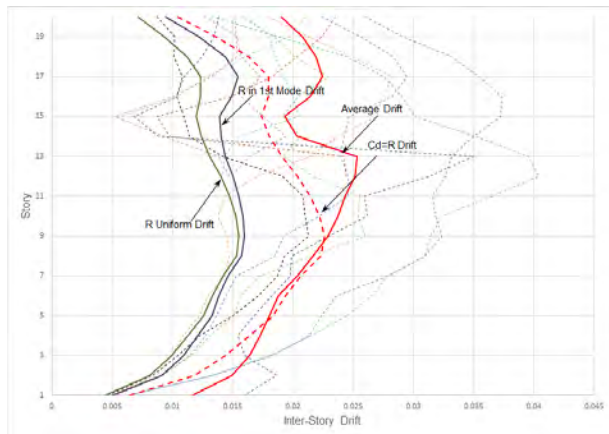
Comparison of Story Drift

Figure 4 Comparison of Story Shear and Story Drifts between RSA with Different Scaling Approaches to NLRHA.

Figure 5 shows the two RSA and nonlinear analyses compared to the ELF results for the 20-story moment frame. In these plots, the base shear of the two RSAs were scaled to the ELF base shear. The plots suggest that the uniformly scaled RSA analysis is closer to the ELF results both for prediction of story shear

at all floors. In addition, the ELF predictions of the inelastic drifts are closer to the nonlinear results and certainly better than either of the RSA approaches.

Comparison of Story Shear   Comparison of Story Drift
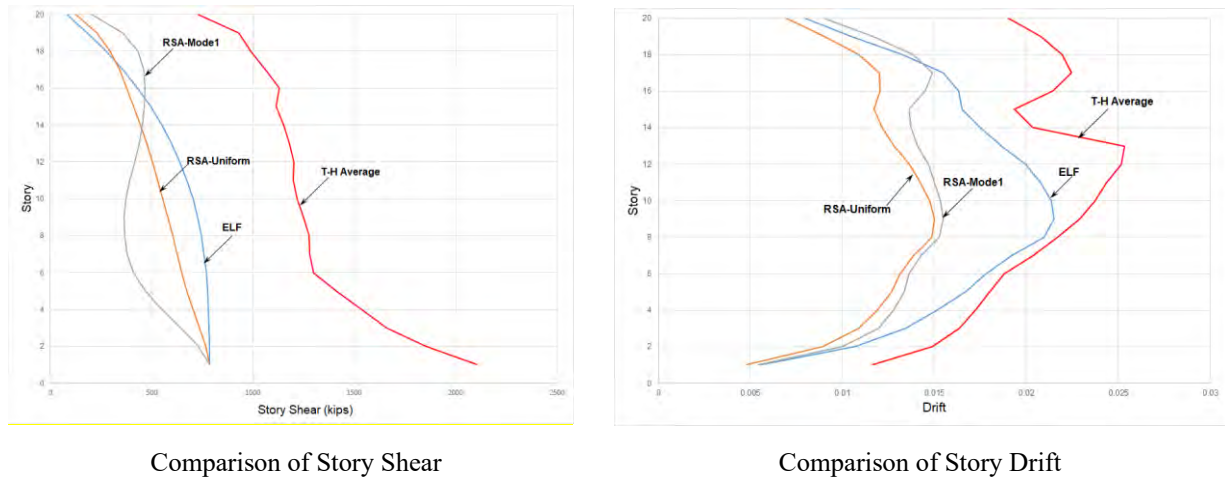
Figure 5 Story Shear and Story Drift Comparison between RSA, ELF and NLRHA for Twenty Story Moment Frame

Low to Mid-Rise (3-story, 6-story and 9-story) Buckling-Restrained Braced Frame Study: Behavior of three different heights of Buckling-Restrained Braced Frame (BRBF) structures were examined as part of this study. The same plan and mass as for the moment frame study shown in Figure 1 was used. The braces were first designed assuming the building to be located at the same location in Los Angeles with S_{DS} = 1.3 and S_{D1} = 0.73. The unscaled base shears of the two differently scaled RSA were then compared with the nonlinear time history results. These results are plotted in Figure 6. The drifts from the MRSA are also compared with the drifts from the nonlinear analysis which are presented in Figure 7.
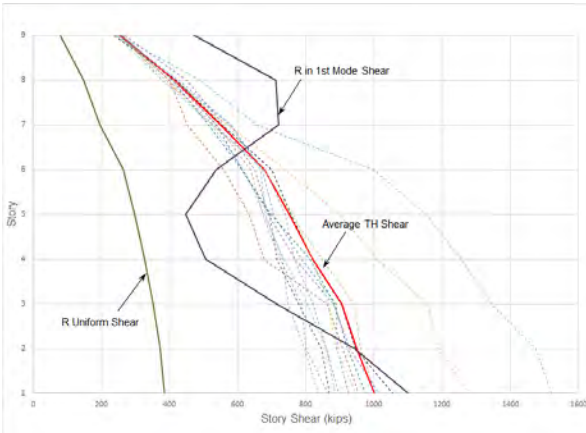
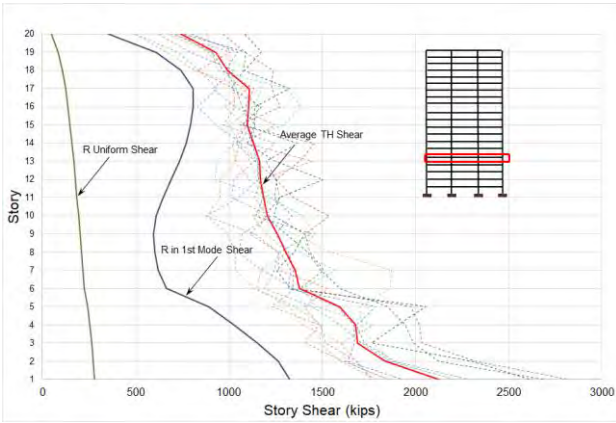Comparison of Story Shear for 9-Story BRBF
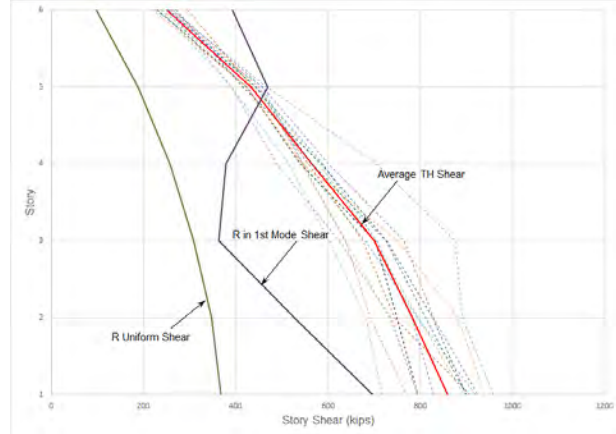
Comparison of Story Shear for 6-Story BRBF
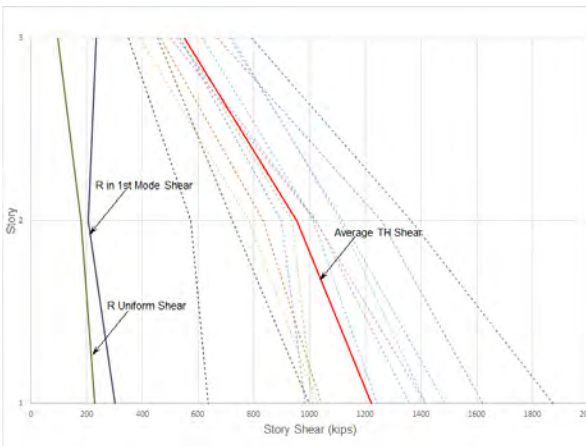
Comparison of Story Shear for 3-Story BRBF

Figure 6 Comparison of RSA and NLRHA Story Shear Plots for 9, 6 & 3-Story BRBFs.

As can be seen from Figure 6, the unscaled (not scaled to code minimum) base shears for 9-story and 6-story BRBFs exceed the uniformly scaled RSA base shears significantly. This is because of the modal participation of the higher modes are significant for the taller BRBFs. Since the responses at these modes are not scaled by the R-factor, the overall responses for the taller frames tend to exceed the uniformly scaled RSA. For the 3-story BRBF, the fundamental mode happens to have the largest participation which results in the two RSAs producing very similar results. The drift plots indicate that the results produced by the two scaling methods produce fairly similar results. It should be mentioned here that elastic drift values obtained from the response spectrum cases have been amplified by C_d for both cases. For response spectrum analysis with reduction applied in the first mode, C_d was also applied to the first mode only (since other modes are assumed to be elastic). Thus, the drift results for both the response spectrum methods appear quite similar although there is a significant difference in the unscaled base shears.
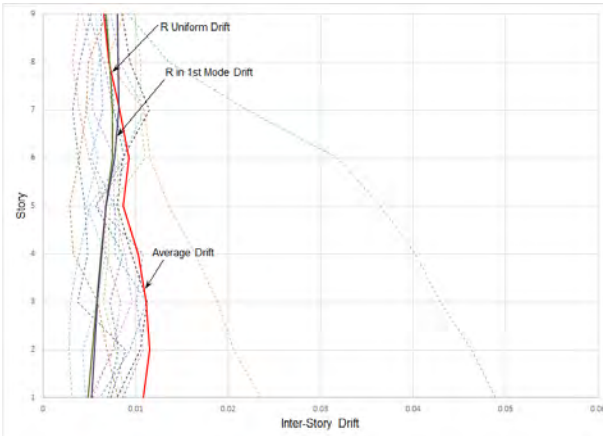
Comparison of Story Drift for 9-Story BRBF
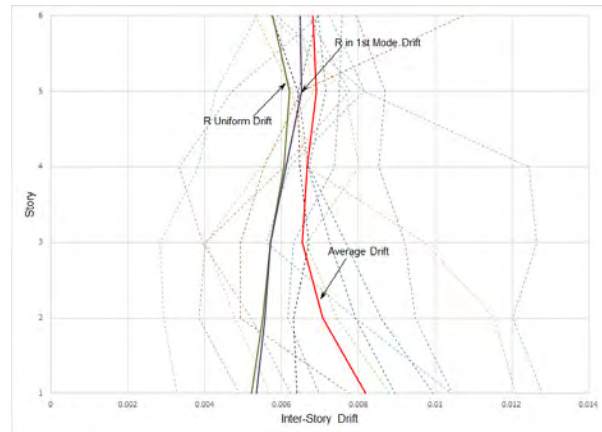
Comparison of Story Drift for 6-Story BRBF
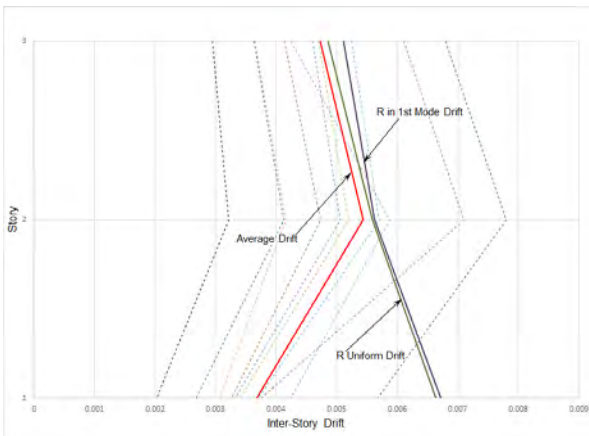
Comparison of Story Drift for 3-Story BRBF

Figure 7 Comparison of RSA and NLRHA Story Drift Plots for 9, 6 & 3-Story BRBFs.

<u>20-Story Moment Frame Study with Mass Irregularities at 5th, 10th and 15th Levels</u> (2D Model): As part of the study on mass irregular buildings, behavior of a 20-story moment frame with mass irregularities at 5th, 10th and 15th floors respectively were compared. At these floors, the mass was doubled compared to the adjacent floors immediately above and below, thereby triggering a mass irregularity per ASCE 7. Figure 8 plots the unscaled base shear (not scaled to ELF) for the three irregular buildings and compares them to two differently scaled RSA to the nonlinear analysis results. Note that the design base shear for these buildings is around 750 kips. In general, the first mode scaled RSA always produces higher base shear compared to the uniformly scaled RSA for reasons similar to the taller BRBF buildings. Figure 9 compares the results of the RSAs and ELF drifts to the nonlinear analysis. For both buildings, the ELF drifts exceed the predictions of the RSA. Figure 10 compares the RSA drift to the nonlinear drift. The drifts from the two RSAs are very similar though the drift with $C_d = R$ compares more favorably to the nonlinear analysis results than the ASCE/SEI 7-16 Table 12.2-1 value of 5.5. In addition, it is also clear from the plots that the location of the mass irregularity has no effect on the overall conclusion

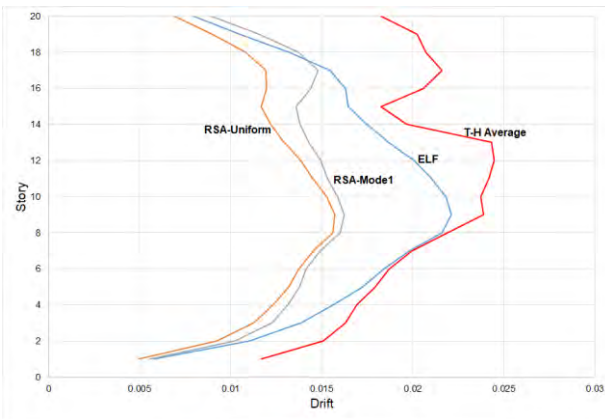Comparison of Story Shear for Irregularity at 5th Flr.
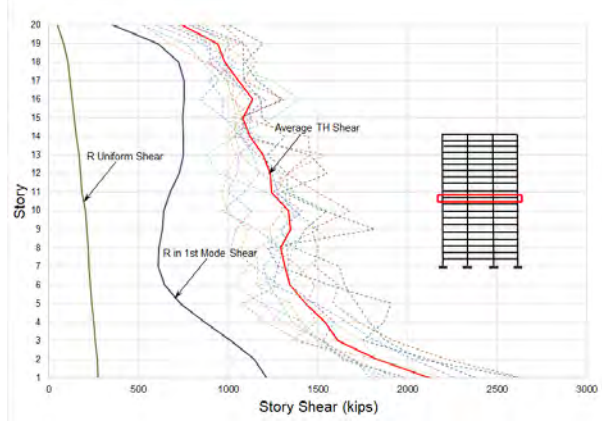
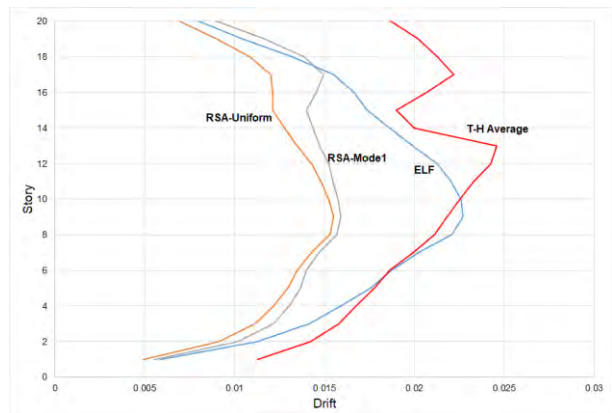Comparison of Story Shear for Irregularity at 10th Flr.
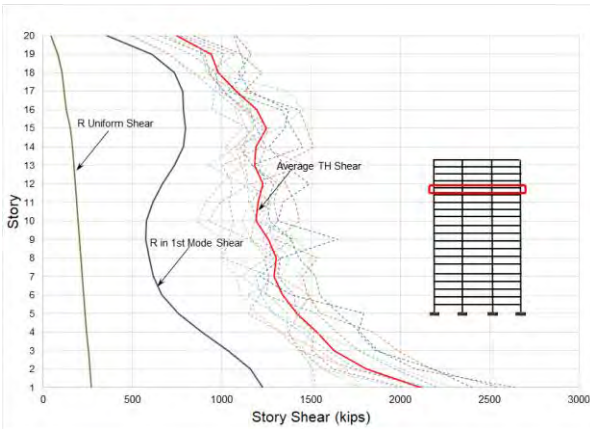
Comparison of Story Shear for Irregularity at 15th Flr.

Figure 8 Story Shear Plots for Mass-Irregular Buildings.

Mass Irregularity at 10th Floor

Mass Irregularity at 15th Floor

Figure 9 Comparison of Story Drift between RSA, ELF and NLRHA for Mass Irregularity at Levels 10 and 15.
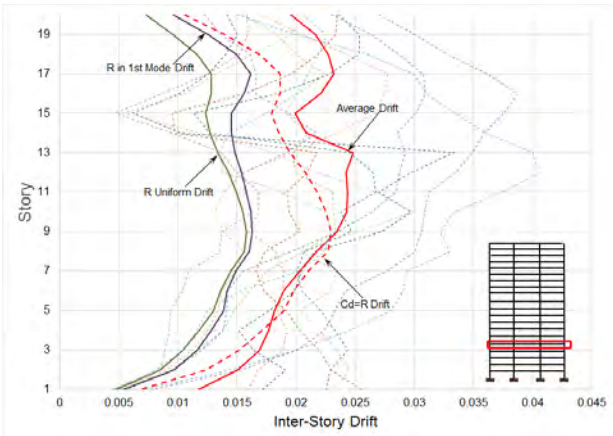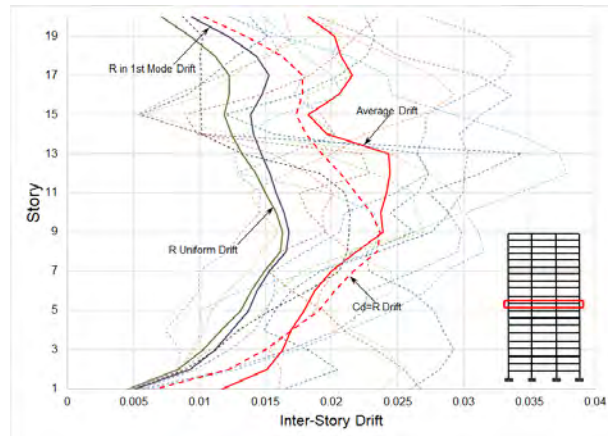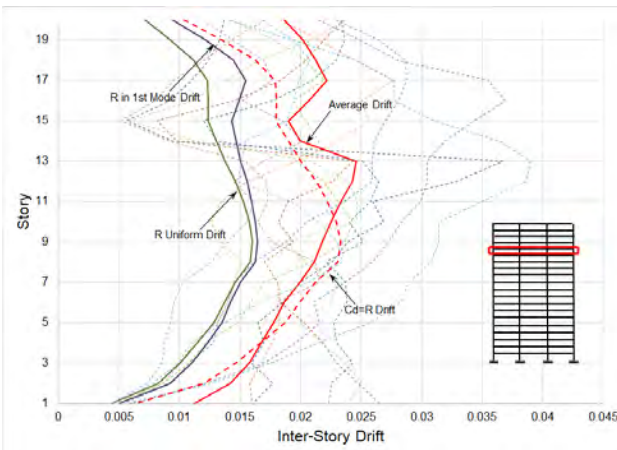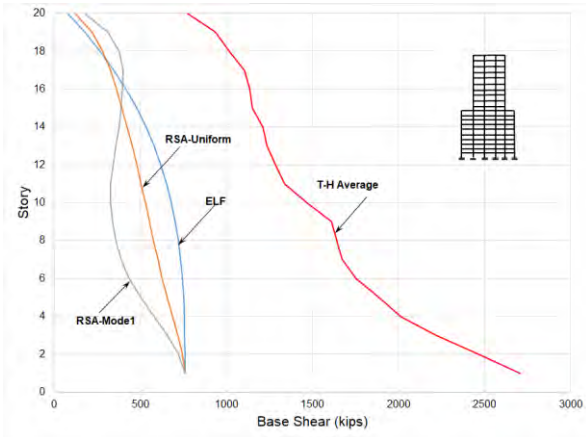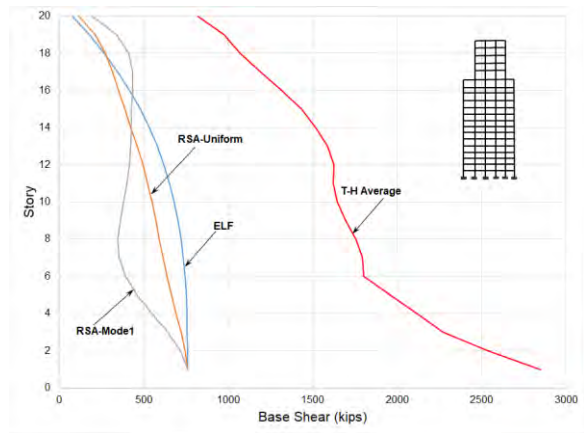
Comparison of Story Drift for Irregularity at 5th Flr.

Comparison of Story Drift for Irregularity at 10th Flr.

Comparison of Story Drift for Irregularity at 15th Flr.

Figure 10 Comparison of Story Drift between RSA and NLRHA for Mass Irregular Buildings.

20-Story Moment Frame Study with Vertical Geometric Irregularity at 10th and 15th Level: In this study the behavior of a 20-story building with vertical geometric irregularity at 10th and 15th floors were compared. The vertical geometric irregularity was created by enlarging the moment frame bays by 2 compared to the floor immediately above (the floor above has 3 bays of moment frame compared to 5 bays below). The results of the base shear distribution, overturning moment and drifts are presented in Figure 11. In these plots, the base shear for the two RSAs were scaled to 100% of the ELF base shear. As can be seen from the Figure, the overturning moment and drift prediction from ELF exceeds either of the RSA methods. The uniformly scaled RSA produces higher shear distribution over significant height of the building compared to the RSA scaled to the fundamental mode. Similarly, the overturning prediction from the uniformly RSA produces higher values compared to the RSA scaled to the first mode only. ELF drifts provide generally better match to the nonlinear results compared to either of the RSA results. The difference between the RSA and ELF drift predictions appear to be more pronounced when the irregularity is at the 15th floor. For that case, RSA uniform also provides marginally better prediction than the RSA first mode.
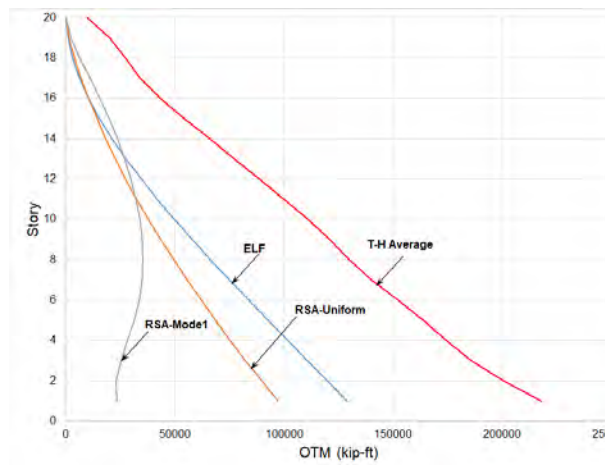
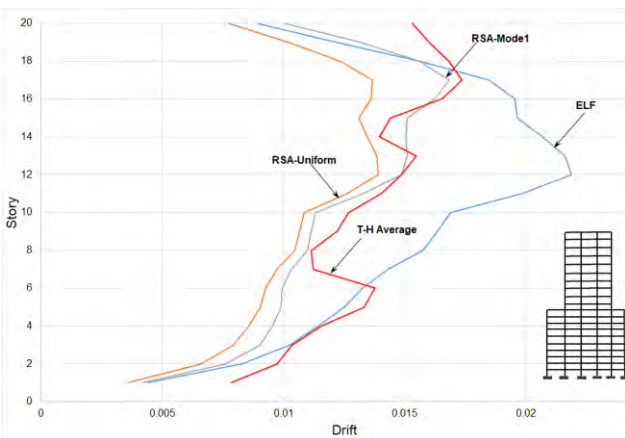Comparison of Story Shear for Geom. Irreg. 10th Flr.

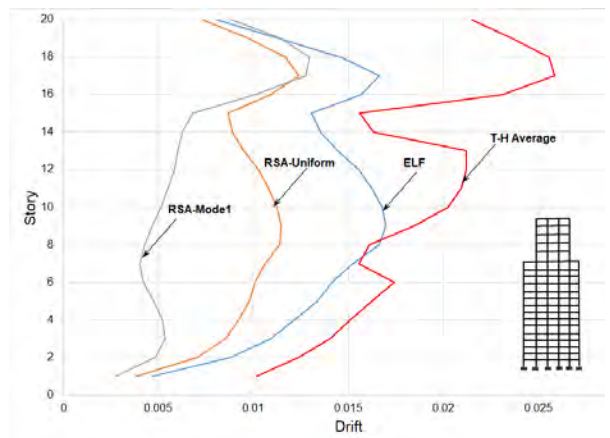Comparison of Story Shear for Geom Irreg. at 15th Flr.
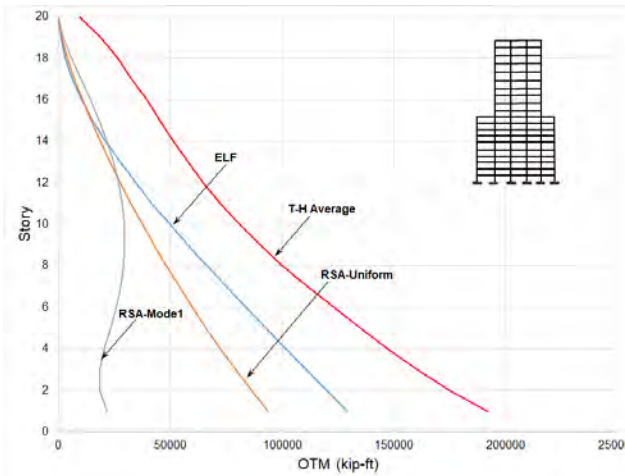
Comparison of OTM for Geom. Irreg. at 10th Flr.

Comparison of OTM for Irregularity at 15th Flr.

Comparison of Story Drift for Geom. Irreg. at 10th Flr.

Comparison of Story Drift for Irregularity at 15th Flr.

Figure 11 Comparison of Story Shear, Overturning Moment and Story Drifts between RSA, ELF and NLRHA for the Geometrically Irregular Buildings.

8-Story Concrete Shear Wall Building: In this study, the behavior of an 8-story concrete shear wall building modeled after a design used in the ATC-123 document was studied. Three design cases were considered as follows: (a) walls are symmetrically arranged in plan and there is no torsional irregularity (b) walls are arranged in plan in such a way that there is torsional irregularity about one axis and (c) walls are arranged in plan in a way that there is torsional irregularity about both axes. Please refer to Figure 12 for the three cases.
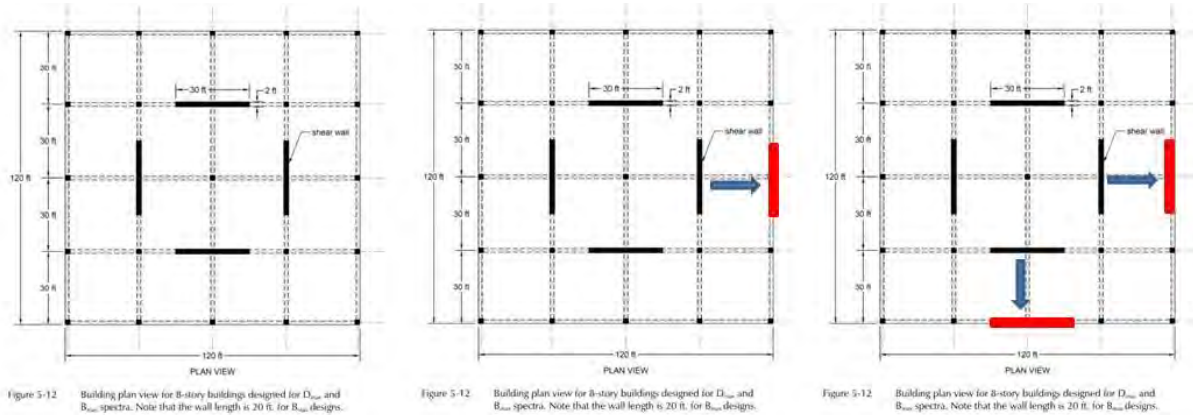

Figure 12 8-Story Shear Wall Cases

As before, it was assumed that the building would be located in Los Angeles with seismic parameters presented earlier. A code design of the building with $R = 5$ (Bearing Shear Wall Building) was performed and the wall flexural and shear reinforcement were calculated. Following this the walls were modeled in PERFORM-3D and a nonlinear analysis with appropriately scaled bidirectional ground motion was performed. Figure 13 shows a comparison of the most critical drifts (captured at the building corner producing the worst drift) for the regular building with the drifts obtained from the case where there is torsional irregularity about both axes. For both cases, the ELF approach produces a more conservative estimate of lateral drifts compared to the RSA approach. In addition ELF also produces drifts that exceed the NLRHA drifts for this case.

No Torsional Irregularity   Irregularity About both Axes
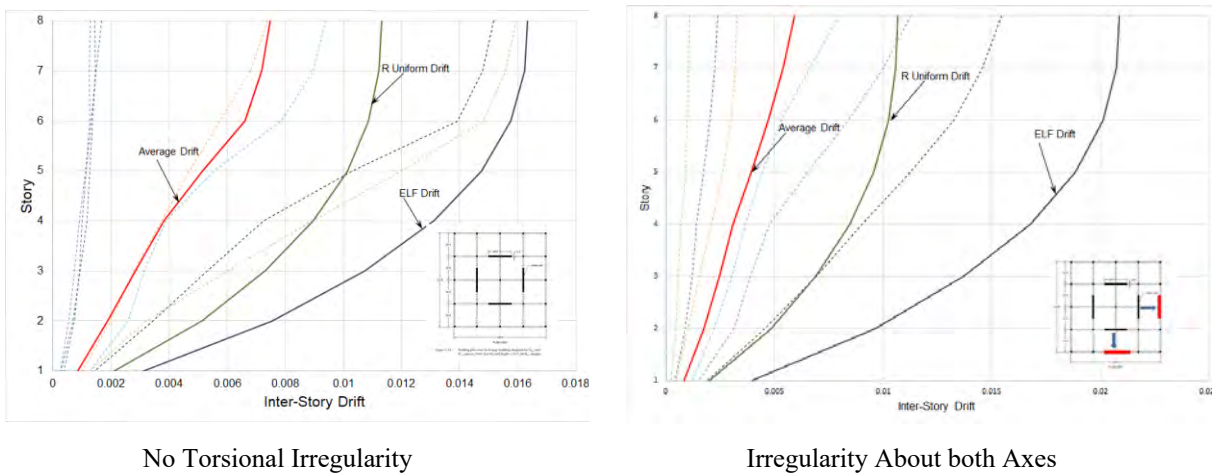
Figure 13 Comparison of Story Drifts for 8-Story Shear Wall Buildings

Reinforced Concrete Ductile Coupled Wall (RCDCW) Buildings: Results for this system was provided by Tauberg et al. (2019). In this study, they assessed the collapse potential of RC Coupled Wall Archetypes

representative of common practice according to ASCE 7-16 and ACI 318-19 provisions and then performed nonlinear pushover and incremental dynamic analyses to quantify the system overstrength and adjusted collapse margin ratios. Following the FEMA P695 methodology, values for the response modification factor $R = 8$, the deflection amplification factor $C_d = R = 8$, and the system overstrength $\Omega_0 = 2.5$ were proposed for Reinforced Concrete (RC) Ductile Coupled Walls.

A series of forty-one coupled wall buildings were designed using a range of variables expected to influence the collapse margin ratio, with primary variables of building height (i.e., 6, 8, 12, 18, 24, and 30 stories), wall cross section (i.e., planar and flanged walls), coupling beam aspect ratio (ln/h) ranging from 2.0 to 5.0, and coupling beam reinforcement arrangement (i.e., diagonally and conventionally reinforced). The range of variables are chosen considering those used to define a Ductile Coupled Wall system in ACI 318-19. The resulting designs have the minimum wall area (length and thickness) required which is governed by shear amplification and the requirement that walls sharing a common shear force not exceed a shear stress of $8\sqrt{f'_c}A_{cv}$.

The designs were for Risk Category II structures with an importance factor $I_e = 1.0$. It incorporated provisions of ASCE 7-16 and ACI 318-19, which includes new requirements for wall shear amplification (ACI 318-19 Section 18.10.3) and a drift capacity check (ACI 318-19 Section 18.10.6.2), as well as the seismic design parameters specified in FEMA P695 (importance factor, redundancy factor, and site class and spectral values). The redundancy factor ρ was taken equal to 1.0, since the use of a larger value would increase seismic loads (and capacities) and produce more conservative designs. The seismic spectral acceleration values used are summarized below for seismic hazard D_{max} as specified in FEMA P695.

$S_S = 1.5g$	$F_a = 1.0$	$S_{DS} = 1.00$ g
$S_1 = 0.6g$	$F_v = 1.5$	$S_{D1} = 0.60g$

Seismic design forces were determined using the Response Spectrum Analysis (RSA) method of ASCE 7, subject to scaling the base shear to 100% of the Equivalent Lateral Force base shear of ASCE 7 for a period $T = C_u T_a$. Modal damping ratio was assumed to be 5%, and the Complete Quadratic Combination (CQC) method was used to combine modal responses.

The story heights were taken equal to 10 feet for all designs. Building stories, the fundamental period T_1, the design period $T = C_u T_a$, the design coefficient C_s, and the design base shear V_b are summarized in Table 2 as follows:

Table 2 - Coupled Wall Archetype Design Information

# of Stories	T_1 (s)	T (s)	C_s	V_b (kips)
6	0.83	0.604	0.124	1062
8	1.27	0.749	0.100	1200
12	2.14	1.1015	.074	1360
18	3.14	1.376	.0545	1490
24	3.39	1.707	0.044	1654
30	3.62	2.018	0.044	2112

It should be noted that incorporating wall shear amplification in the design was necessary because preliminary analysis results using $R = C_d = 8$ and designed conforming to ACI 318-14 shear provisions, did

not meet the FEMA P695 acceptability criteria due to a high number of shear failures experienced during incremental dynamic analysis. The wall shear amplification requirement per the new code provision of ACI 318-19 amplifies the code level shear force (V_u) by a flexural overstrength factor (Ω_v) and a dynamic shear amplification factor (ω_v) that accounts for higher modes. The dynamic shear amplification factor (ω_v), depends on number of stories (n_s). The overstrength factor (Ω_v) is the ratio of probable moment strength M_{pr} to code required strength M_u, which shall not be taken less than 1.5 per ACI 318-19. In this study, the ratio of M_{pr} to M_u was set equal to 1.5 for all designs so that the designs would not be overdesigned for shear strength and represent the governing case for collapse analysis.

Two-dimensional nonlinear models were created for each design using the structural analysis software Open Systems for Earthquake Engineering Simulation (OpenSees), and nonlinear static pushover (NSP) and incremental dynamic analyses (IDA) were performed in accordance with FEMA P695. For the IDAs, a set of twenty-two pairs of far-field horizontal ground motion records of FEMA P695 were used.

The dynamic analyses were conducted at DE and MCE hazard levels, as well as at ground motion intensities representative of the collapse capacity of each design. The collapse capacity was determined by incrementally increasing the intensity of the 44 ground motion records until just less than half of the records cause collapse of the Archetype building as represented by the established failure modes of the model.

Figure 14 compares the story shears from the ELF, RSA, RSA design amplified shear demand (V_e), and NLRHA results for DE level shaking. In general, ELF wall shear and moment demands exceed RSA demands along the building height. The NLRHA values shown include the mean of the maximum story shears from the 44 ground motions as well as mean ± standard deviation values. The story shears represent the sum of the individual shears of the coupled wall piers. The NLRHA results highlight the effects of wall shear amplification as nonlinear shear demands range about 2 to 4 times the design shear demands at the lower levels. However, the RSA design amplified demand (V_e) exceeds the NLRHA mean + standard deviation shears at almost all levels.

Figure 15 compares the story drifts including the drifts at the center of mass from the RSA designs using $C_d = R = 8$, the 2% drift limit, and the mean as well as mean ± standard deviation of the nonlinear story drift results from 44 ground motions scaled to the DE level shaking. The resulting ELF drifts using $C_d = R = 8$ have also been added for reference. However, it is important to note that the Archetypes were designed using RSA, and a different building design would have been required had ELF been used.

Mean nonlinear story drifts match closely with design drifts for the shorter 6, 8, and 12-story coupled wall designs. However, the design story drifts for the taller 24- and 30-story designs exceed the drift values determined from NLRHA.

The design drifts in this study were obtained using a wall flexural effective stiffness $I_{eff} = 0.75I_g$ based on input from our advisory panel for effective stiffness values commonly used in practice for RC coupled walls. This effective stiffness assumption results in lower design drifts than if, for example, $I_{eff} = 0.5I_g$ were used in design. However, since the designs have been for amplified shear demands and conform to the drift capacity check per the new provisions of ACI 318-19, the designs were not drift-governed and the wall piers were thicker and stiffer than if designed per ACI 318-14. The maximum design drifts observed at the center of mass among any of the Archetypes was less than 1.6% when using $I_{eff} = 0.75I_g$ and less than 2% when using $I_{eff} = 0.5I_g$ (per ACI 318-14 where this value is permitted to compute drifts).
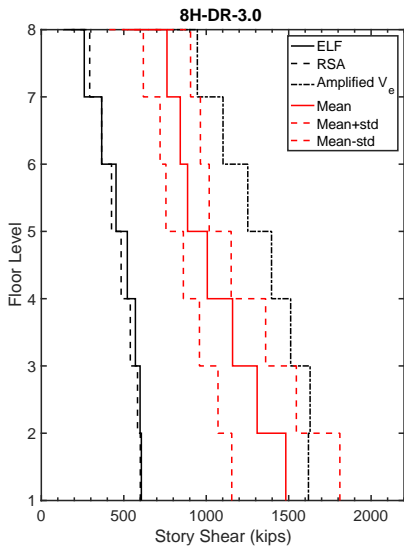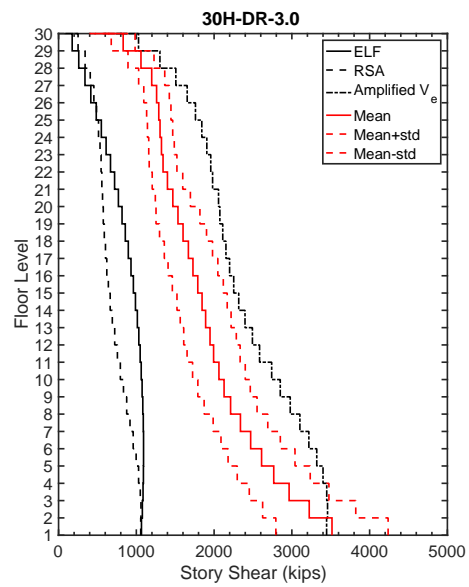
Comparison of Story Shear for 8-Story RCDCW
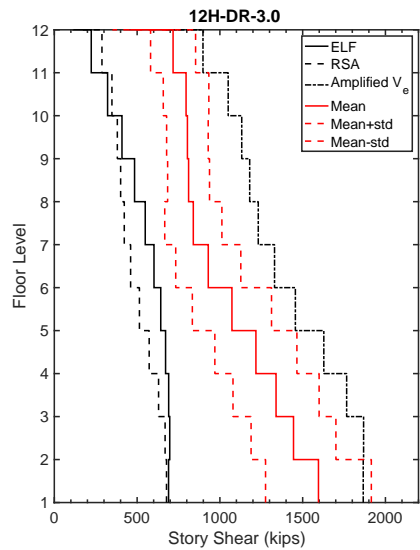
Comparison of Story Shear for 12-Story RCDCW
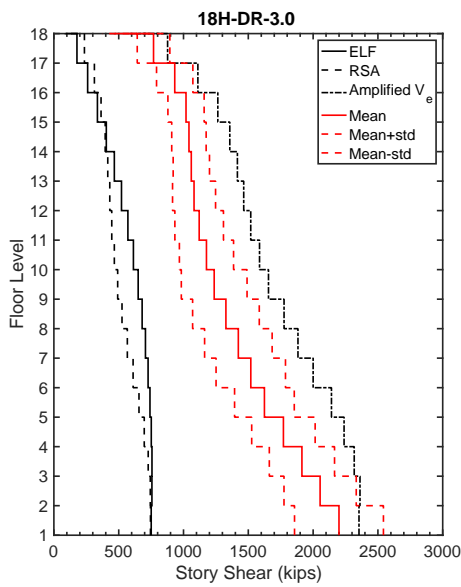
Comparison of Story Shear for 18-Story RCDCW

Comparison of Story Shear for 30-Story RCDCW

Figure 14 Comparison of Story Shears for Reinforced Concrete Ductile Coupled Wall Buildings.
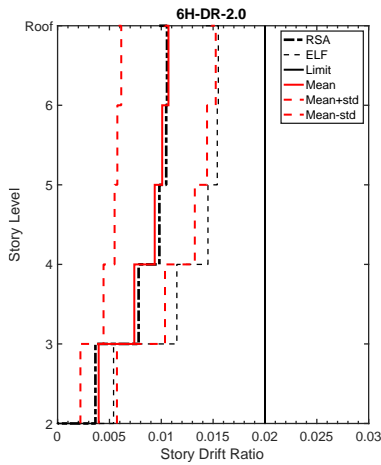
Story Drift Ratio of 6-Story RCDCW
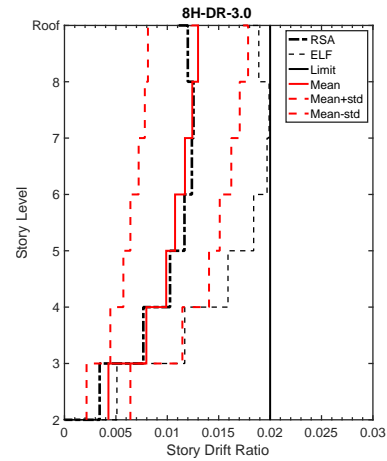
Story Drift Ratio of 8-Story RCDCW

Story Drift Ratio of 12-Story RCDCW

Story Drift Ratio of 18-Story RCDCW

Story Drift Ratio of 24-Story RCDCW

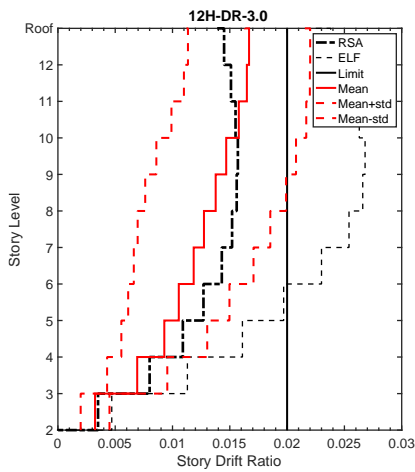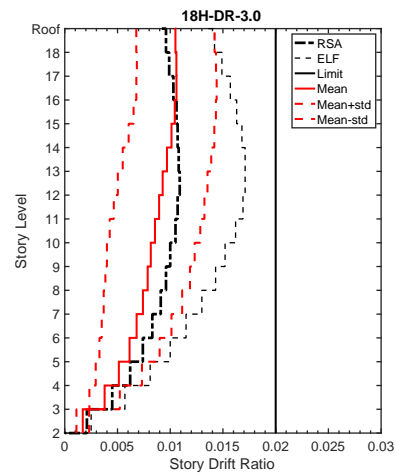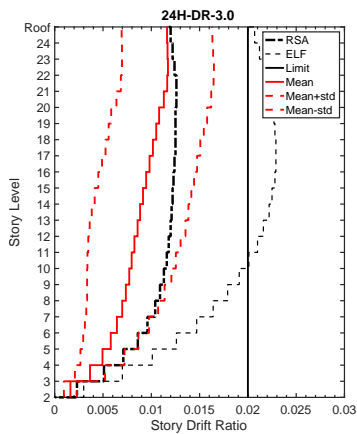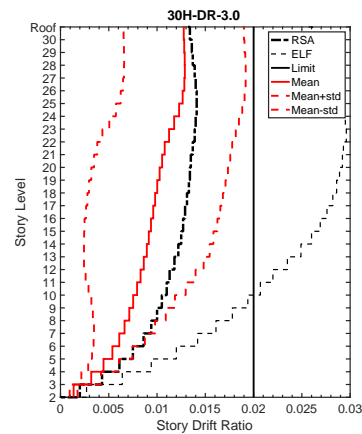Story Drift Ratio of 30-Story RCDCW

Figure 15 Comparison of Story Drift Ratio for Reinforced Concrete Ductile Coupled Wall Buildings.

The C_d factor for RC Ductile Coupled Walls was assessed using the ratio of a median value of nonlinear inelastic roof drifts (δ) from 44 records at DE level shaking to the design level drifts (δ_E/R). Table 2 summarizes the drifts and resulting C_d values for a subset of Archetypes. The computed C_d values for these archetypes result in a median value of $C_d = 8.8$ (cov = 0.13). For the subset of Archetypes listed in Table 3, adjusting the nonlinear RHA roof drift values for 5% damping results in a median C_d value of 8.4. Therefore, a deflection amplification factor of $C_d = R = 8$ was proposed and approved by the BSSC PUC at the April 18, 2019 meeting in San Francisco for RC Ductile Coupled Walls.

Table 3 - Assessment of C_d based on drifts from a Subset of Archetypes

Archetype	# stories	h_n (ft.)	Design $(\delta_E/R)/h_n$ (%)	Median RHA δ / h_n (%)	C_d $\delta / (\delta_E/R)$
30H-DR-3	30	300	0.145	1.14	**7.9**
18H-DR-3	18	180	0.111	1.22	**10.9**
12H-DR-3	12	120	0.161	1.58	**9.8**
8H-DR-3	8	80	0.127	1.14	**9.0**
6H-DR-2	6	60	0.109	0.94	**8.6**
6H-CR-5	6	60	0.130	1.05	**8.1**

RP9-4   CONCLUSIONS AND RECOMMENDATIONS

Following are the conclusions and recommendations obtained from the study:

1. A change to use *R* only in the first mode rather than in all modes as in current practice is not justified. If *R* is used in the first mode only, the resultant design base shear will be significantly higher than the ELF base shear.
2. The range of buildings studied as part of this effort include:

   - Structures exceeding 160 ft in height with Vertical Structural Irregularity 1a and 2 per Table 12.3-2 of ASCE 7-16

   - Structures exceeding 160 ft with $T>3.5T_s$

   - Structures lower than 160 ft in height with Horizontal Structural Irregularity Type 1a per Table 12.3-1 and Vertical Structural Irregularity Type 1a and 2 per Table 12.3-2.

   For the above buildings ELF provides more consistent story shear, overturning moment and story drift results than MRSA when compared to nonlinear dynamic response at design level earthquake. Based on these studies and evidence from existing literature, it is recommended that ELF be allowed for all building types irrespective of irregularities and building height. Other irregularities and combinations in Tables 12.3-1 and 12.3-2 were not studied. There may exist a class of buildings (such as one with highly irregular mass distribution, certain long span dynamically sensitive structures etc.) where ELF might yield un-conservative design forces. The engineer is expected to use his/her judgement regarding the use of appropriate analysis methodology under those circumstances.

3. For large majority of buildings use of Cd = R provides a better estimate of the nonlinear dynamic story drift response than the current Cd values in ASCE/SEI 7-16 for the buildings in this study. However, it is important to conduct a more exhaustive study before Cd = R is adopted by ASCE 7. The reader is referred to the Part 3 Resource Paper authored by Issue Team 2 of the 2020 NEHRP Provisions Update Committee for further information.

RP9-5   REFERENCES

ATC 123 Preliminary Phase III Report (2017). "Improving Seismic Design of Buildings with Configuration Irregularities", Applied Technology Council, 201 Redwood Shores Parkway, Suite 240, Redwood City, California 94065.

Part 3 Resource Paper (2020); "Seismic Design Story Drift Provisions-Current Questions and Needed Studies", Issue Team 2, 2020 NEHRP Provisions Update Committee.

Sanchez, J., Mohr, B., Harris, S., Aviram, A., and Goings, C. (2017). "Parametric Study of Steel Moment Frames Considering Foundation Rocking." Proceedings of the 16th World Conference on Earthquake Engineering, Santiago, Chile, January, 2017.

Tauberg, N.A., Kolozvari, K., and Wallace, J.W. (2019). "Ductile Reinforced Concrete Coupled Walls – FEMA P695 Study". Report No. *SEERL 2019/01*, University of California, Los Angeles, Department of Civil and Environmental Engineering.

2020 NEHRP RECOMMENDED SEISMIC PROVISIONS FOR NEW BUILDINGS AND OTHER STRUCTURES

VOLUME II

APPENDIX RESOURCE PAPER PARTICIPANTS

This appendix includes all the contributors who are involved in the development of the Volume II Resource Papers. All the papers have been evaluated and approved for inclusion in this volume by the Provisions Update Committee and the BSSC member organizations, which are listed in Volume I Appendix.

RP1 RESILIENCE-BASED DESIGN AND THE NEHRP PROVISIONS	
Ibrahim Almufti	Arup
David Bonowitz	David Bonowitz, S.E.
Nicolas Luco	U.S. Geological Survey
Robert Pekelnicky	Degenklob Engineers
Jeffrey Soulages	Intel Corporation
RP2 RISK-BASED ALTERNATIVES TO DETERMINISTIC GROUND MOTION CAPS	
C.B. Crouse	AECOM
John Hooper	Magnusson Klemencic Associates
Nicolas Luco	U.S. Geological Survey
Jonathan Stewart	University of California, Los Angeles
RP3 DESIGN OF ISOLATED AND COUPLED SHEAR WALLS OF CONCRETE, MASONRY, STRUCTURAL STEEL, COLD-FORMED STEEL AND WOOD	
Richard Bennett	University of Tennessee
Jeffrey Berman	University of Washington
Michel Bruneau	University of Buffalo
Jon-Paul Cardin	American Institute of Steel Construction
Jason Collins	PCS Structural Solutions
Kelly Cobeen	Wiss, Janney, Elstner Associates
David Fields	Magnusson Klemencic Associates
Larry Fahnestock	University of Illinois, Urbana-Champaign
Joe Ferzli	Cary Kopczynski & Company
S. K. Ghosh	S. K. Ghosh Associates
John Hooper	Magnusson Klemencic Associates
Gino Kurama	University of Notre Dame
Dawn Lehman	University of Washington
Philip Line	American Wood Council
Laura Lowes	University of Washington
Rafael Sabelli	Walter P. Moore
Andrew Taylor	KPFF Consulting Engineers
Amit Varma	Purdue University
John Wallace	University of California, Los Angeles
Tom Xia	DCI Engineers

RP4 SEISMIC LATERAL EARTH PRESSURES	
Scott J. Brandenberg	University of California, Los Angeles
Maria Giovanna Durante	University of Texas, Austin
Jonathan Stewart	University of California, Los Angeles
RP5 SEISMIC DESIGN STORY DRIFT PROVISIONS – CURRENT QUESTIONS AND NEEDED STUDIES	
David Bonneville	Degenkolb Engineers
Kelly Cobeen	Wiss, Janney, Elstner Associates
John Gillengerten	SE, Retired OSHPD
John Harris	National Institute of Standards and Technology
Jim Harris	James Harris & Associates
Jon Heintz	Applied Technology Council
Conrad "Sandy" Hohener	Degenkolb Engineers
John Hooper	Magnusson Klemencic Associates
Edwin Huston	Smith & Huston
Charlie Kircher	Charles Kircher & Associates
Dawn Lehman	University of Washington
Philip Line	American Wood Council
Bonnie Manley	American Iron and Steel Institute
Robert Pekelnicky	Degenkolb Engineers
Benjamin Schafer	Johns Hopkins University
RP6 DIAPHRAGM DESIGN FORCE REDUCTION FACTOR, R_s, FOR COMPOSITE CONCRETE ON METAL DECK DIAPHRAGMS	
Kelly Cobeen	Wiss, Janney, Elstner Associates
John Lawson	Cal Poly San Luis Obispo
S.K. Ghosh	S. K. Ghosh Associates
Ron La Plante	California Division of the State Arch
Ben Schafer	Johns Hopkins University
Tom Sabol	Engelkirk & Sabol
Patrick Bodwell	Vulcraft/ Verco Group
Dan Dolan	Washington State Universtiy
Matt Eatherton	Virginia Tech
Andre Filiatrault	SUNY University at Buffalo
Christopher Gill	Hilti North America
Dave Golden	ASC Steel Deck Div. of ASC Profiles
Jerome (Jerry) Hajjar	Northeastern University
Steve Hobbs	Vulcraft
Maria Koliou	Colorado State University
William Holmes	Rutherford + Chekene
Philip Line	American Wood Council
Bonnie Manley	American Iron and Steel Institute
Walt Schultz	Nucor

Andrew Shuck	Wiss, Janney, Elstner Associates
Robert Tremblay	Polytechnique Montreal
Tom Xia	DCI Engineers
RP7 DEVELOPMENT OF DIAPHRAGM DESIGN FORCE REDUCTION FACTORS, R$_S$	
Kelly Cobeen	Wiss, Janney, Elstner Associates
John Lawson	Cal Poly San Luis Obispo
S.K. Ghosh	S. K. Ghosh Associates
Ron La Plante	California Division of the State Arch
Ben Schafer	Johns Hopkins University
Tom Sabol	Engelkirk & Sabol
Patrick Bodwell	Vulcraft/ Verco Group
Dan Dolan	Washington State Universtiy
Matt Eatherton	Virginia Tech
Andre Filiatrault	SUNY University at Buffalo
Christopher Gill	Hilti North America
Dave Golden	ASC Steel Deck Div. of ASC Profiles
Jerome (Jerry) Hajjar	Northeastern University
Steve Hobbs	Vulcraft
Maria Koliou	Colorado State University
William Holmes	Rutherford + Chekene
Philip Line	American Wood Council
Bonnie Manley	American Iron and Steel Institute
Walt Schultz	Nucor
Andrew Shuck	Wiss, Janney, Elstner Associates
Robert Tremblay	Polytechnique Montreal
Tom Xia	DCI Engineers
RP8 CALCULATION OF DIAPHRAGM DEFLECTIONS UNDER SEISMIC LOADING	
Kelly Cobeen	Wiss, Janney, Elstner Associates
John Lawson	Cal Poly San Luis Obispo

RP9 MODAL RESPONSE SPECTRUM ANALYSIS METHODS	
Kelly Cobeen	Wiss, Janney, Elstner Associates
John Lawson	Cal Poly San Luis Obispo
S.K. Ghosh	S. K. Ghosh Associates
Ron La Plante	California Division of the State Arch
Ben Schafer	Johns Hopkins University
Tom Sabol	Engelkirk & Sabol
Patrick Bodwell	Vulcraft/ Verco Group
Dan Dolan	Washington State Universtiy
Matt Eatherton	Virginia Tech
Andre Filiatrault	SUNY University at Buffalo
Christopher Gill	Hilti North America
Dave Golden	ASC Steel Deck Div. of ASC Profiles
Jerome (Jerry) Hajjar	Northeastern University
Steve Hobbs	Vulcraft
Maria Koliou	Colorado State University
William Holmes	Rutherford + Chekene
Philip Line	American Wood Council
Bonnie Manley	American Iron and Steel Institute
Walt Schultz	Nucor
Andrew Shuck	Wiss, Janney, Elstner Associates
Robert Tremblay	Polytechnique Montreal
Tom Xia	DCI Engineers